Jonas Sjolte

Marine renewable energy conversion

Grid and off-grid modeling, design and operation

Thesis for the degree of Philosophiae Doctor

Trondheim, July 2014

Norwegian University of Science and Technology
Faculty of Information Technology, Mathematics
and Electrical Engineering
Department of Electric Power Engineering

NTNU – Trondheim
Norwegian University of
Science and Technology

NTNU
Norwegian University of Science and Technology

Thesis for the degree of Philosophiae Doctor

Faculty of Information Technology, Mathematics and Electrical Engineering
Department of Electric Power Engineering

ISBN 978-82-326-0350-3 (printed ver.)
ISBN 978-82-326-0351-0 (electronic ver.)
ISSN 1503-8181

Doctoral theses at NTNU, 2014:214

Printed by NTNU-trykk

Abstract

The global energy production from renewable sources is increasing, with high penetration of both wind and solar in key regions. Ocean Wave Energy is projected to contribute with an increasing share of the future power supply, and the focus of this work is to investigate the requirements for connecting wave energy to the power grid, in context of the *Fred. Olsen* (FO) Wave Energy Project.

Most *Wave Energy Converters* (WECs) produce highly distorted power due to the reciprocal motion induced by the ocean waves. Some WEC systems have integrated energy storage that overcomes this limitation, but adds significant expenses. As an alternative approach, this work investigates direct power export that relies on aggregate smoothing among several WECs. By optimizing the position of the WEC devices with respect to the incoming waves, fluctuations may be mutually canceled out between the devices.

FO has closely monitored the global development within wave energy for about two decades, and has worked actively on developing WECs since 2002. The latest WEC system, named *Lifesaver*, has been in operation since April 2012 and is the basis of this thesis work. The *Lifesaver* system is described in detail, and comprehensive data on operational performance is presented.

The major cost driver for grid integration is the peak to average power ratio, which can be as high as 20 in the early power conversion stages. Thus, it is crucial to improve the power quality early in the conversion chain so that the downstream power system is efficiently utilized. The simulations undertaken in this work indicate that a high quality power output can be achieved at the farm level, but that significant oversize factors will be required in the intermediate power systems within the farm.

Cost-benefit analysis of the system show that a grid connected system at the current technology level will return marginal profitability. Therefore, several alternative approaches are investigated that could serve as a bridge towards future large scale systems. This includes autonomous systems that could supply power to remote ocean based units such as measurement and surveillance buoys, aquaculture facilities and support systems for the off-shore oil and gas industry.

In general, the findings show that the WEC system is well suited for grid integration, although it becomes clear that significant development remains before wave energy can become an important supplement in the energy mix. Moreover, there seems to be a market for autonomous systems that is economically viable at the current technology level that could allow for immediate deployment of commercial systems.

Structured Contents

Chapter 1

Introduction

Synopsis

The introduction explains the document structure and lists the contributions provided by this doctoral thesis. The subject at hand is introduced and presented, including the general principles of wave energy power conversion, the global wave energy potential and the history of the Fred. Olsen Wave Energy Project.

Contents

1.1 About this work

This Ph.D thesis investigates electricity production from marine renewable energy sources, with focus on *Wave Energy Converters* (WECs). The thesis consist of the main part of 107 pages, and 11 publications that are attached in Appendix A-K. The main part is written as a complete and continuous document, and can be read without referencing the attached publications.

The Ph.D program has been organized as a collaboration between the privately owned company Fred. Olsen (FO), which is actively developing WEC systems, and the Norwegian University of Science and Technology (NTNU). The program is funded by the Norwegian Research Council through the *Næringsphd* program.
Main contributions by this work:

- Design, build and operation of medium sized WECs based on non-resonant point absorbers
  (Chapter 1, 2, 3, Appendix B, G, K)
- PTO and generator optimization, mechanical and electrical configuration, high overspeed operation
  (Chapter 2, Appendix A, C)
- PTO force control and power control optimization
  (Chapter 2, 3, Appendix B, C, J)
- Active and reactive power control optimization for point absorber systems
  (Chapter 3, Appendix J)
- Design and simulation of multi-body systems, arrays and farms
  (Chapter 4, Appendix D, E,F,F,I)
- Power management for WEC farms and power export to grid
  (Chapter 4, Appendix F, I)
- WECs as power source for autonomous systems
  (Chapter 5)
- Energy storage design, operation and control
  (Chapter 3, Appendix B, K)
- Experience with cost optimization of WECs
  (Chapter 7)
- Definition of the power rating of a general WEC system
  (Chapter 1)

A detailed description of the thesis outline is presentetd in the Structured Contents on page iv.

1.2 Global wave energy potential

According to the Intergovernmental Panel on Climate Change (IPCC) [28] and the International Energy Agency (IEA) [18], an increasing amount of the future global energy demand will have to be supplied by renewable sources to avoid dangerous global warming. Ocean waves represent an untapped source of energy that could be an important contribution to the future energy mix. The global gross wave energy resource is estimated to 3.7 TW [26], which is similar to the global electricity consumption of approximately 2.7 TW [44]. However, most of the available energy

is located in remote areas, and only a small fraction of the total wave energy potential can be considered as useful energy.

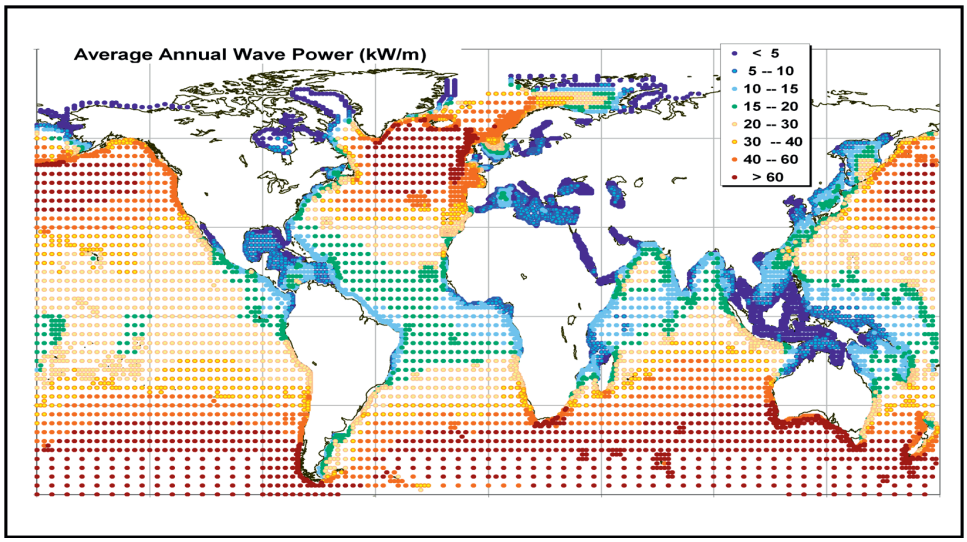

Figure 1.1: Global wave energy potential. Source: WorldWaves data/OCEANOR/ECMWF

The power flux of ocean waves is described in kW/m, and refers to the average power that passes a cross section of one meter width and infinite depth, perpendicular to the wavelength. An analogy is the power exerted per meter by waves breaking onto a beach. Fig.1.1 displays the global wave energy potential in kW/m. The power flux P can be calculated from the significant wave height H_s and period T_p by Equation 1.1, where ρ represents the density of sea water and g is the gravitational constant. Usually, the simplified equation to the right is used, which gives the power directly in kW/m.

$$P = \frac{\rho g^2}{64\pi} \cdot {H_s}^2 \cdot T_p \Rightarrow P \approx 0.5 \cdot {H_s}^2 \cdot T_p \tag{1.1}$$

1.3 Wave energy conversion principles and power export

Fig. 1.2 shows the main conversion methods for wave energy, and illustrates the large variety of systems, as many of these systems also have subcategories. The Fred. Olsen system is based on the point absorber principle shown in Fig. 1.2(a), which is thought to be one of the simplest and most effective concepts, and is also used by competing companies such as *Ocean Power Technologies* (OPT) [36], Seabased [5, 9] and Wavestar [15]. One interesting property of the point absorber is the ability to resonate with the incoming wave field, much like a dipole antenna. This gives the point absorber a theoretical power capture of $6{\cdot}\pi$ times its width with respect to the incoming energy [10].

The attenuator principle illustrated in Fig. 1.2(b) is used by *Pelamis Wave power* [16] and is well suited for slack moored configuration. The gyroscopic device pictured in Fig. 1.2(c) is explored by *SeaRev* [40]. Fig 1.2(d) shows an underwater buoyant device that utilizes differential

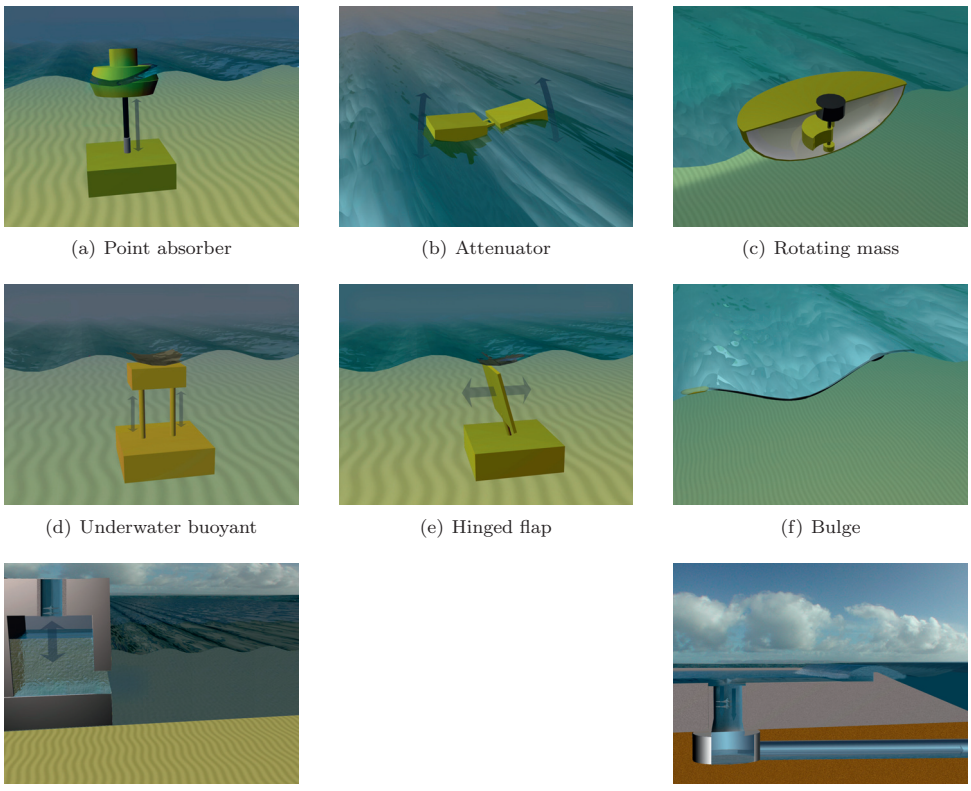

(a) Point absorber (b) Attenuator (c) Rotating mass

(d) Underwater buoyant (e) Hinged flap (f) Bulge

(g) Oscillating Water Column (h) Overtopping

Figure 1.2: General wave energy conversion principles. Source:Aquaret

pressure in a submersed air volume and is tested in the *Carnegie* system [6]. The Bulge system shown in Fig. 1.2(f) is based on floating rubber hoses that pumps water, and is believed to be in an early development phase. Common to these systems is that they are flexible with respect to location and depth. The remaining systems, the hinged flap (Fig. 1.2(e)), the oscillating water column (Fig. 1.2(g)) and the overtopping device (Fig. 1.2(h)), are typically fixed structures that are mounted on the sea floor or along the shore line, although some floating versions of these systems also exists.

In addition to being an alternative energy source, wave energy also supplies a different power profile than the other renewable sources. This can be very valuable for power systems with high share of renewable energy, as the availability of the source will influence heavily on the electricity price. This can help to lift wave energy into the market as some of the increased cost can be displaced by increased total availability of the renewable power system. This is illustrated in Fig. 1.3, which shows a simulation of several renewable sources feeding to a common power system.

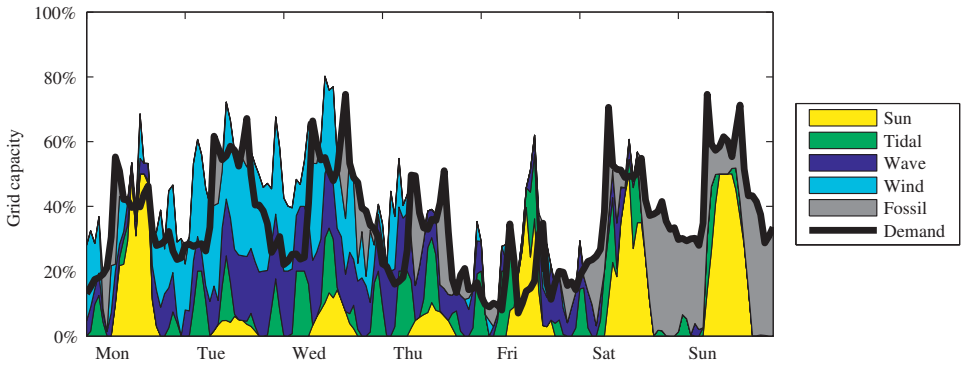

Figure 1.3: Simulated energy balance with high penetration of renewable energy

Although wind and wave have strong correlation, it is clear that the combination of these helps the overall power balance. This is mainly because wind turbines only can produce power from weather systems surrounding the wind park, while wave energy converters can produce power from weather systems far away. The situation simulated in Fig. 1.3 shows a typical situation where a low pressure system is building up (Mon-Tue). When the weather system reaches its apex (Tue-Wed), both wind and wave produce at full power. As the weather system drifts off (Thu), the wind production quickly drops, while the WECs maintain production at a moderate decay. In this example, there are two occasions, Thursday night and Friday night, where wave is the sole renewable energy producer. Thus, for a region aiming for full renewable energy coverage, wave energy will be valuable to the power system.

Solar power output is directly linked to the solar influx and typically has a strong negative correlation with wind and wave. Low pressures that carry strong winds usually also bring a thick cloud cover. Thus, solar is very effective in combination with wave and wind. Although solar systems have a low capacity factor of only 10-20% [45], most of the power production takes place during day at peak demand, which helps making solar and attractive renewable resource.

Tidal power systems are directly influenced by the lunar cycle, and have little correlation with the local weather, which makes tidal power an excellent contributor to the power system. Tidal power fluctuates with mixed patterns of 12-hour cycles and 24-hour cycles due to earth's

rotation, and has underlying 14 and 28-day cycles due to the moons rotation around the earth. This makes the tidal power output highly predictable, but also results in some of the production occurring out of pace with demand. Like wave, tidal is still in early development with few systems in commercial operation.

1.4 Challenges with Wave Energy Converters

Although WEC systems have been under development for more than two hundred years [8], no commercial system have been developed yet. The problems are multifaceted, being of both practical and physical nature. FO has identified five main challenges:

- **High force, low speed**
  The average effective surface elevation speed of good production waves is typically less than 0.5 m/s, and can be found by direct calculation of the wave height and period. Thus, a WEC that shall produce 100 kW will require a production force of at least $P = F \cdot v$ 200 kN, as given by the general definition of work in Equation 1.2 and 1.3. This is equivalent to 20 tons and results in large production machinery, referred to as the Power Take-Off (PTO), to produce a limited amount of power. As comparison, an average sports car with a 100 kW engine would only weigh around 1 ton, while the 100 kW wave energy converter would require the ability to effectively and efficiently lift 20 such cars, and also cost less than a single car. Thus, the challenge of the PTO is to produce high force at low cost, which is covered in Chapter 2.

$$W = F \cdot s \tag{1.2}$$

$$\dot{W} = F \cdot \dot{s} \;\Leftrightarrow\; P = F \cdot v \tag{1.3}$$

- **Cost of design iterations**
  Testing and developing WECs requires access to real ocean waves, either by going offshore, or by testing in a wave tank. Both options are costly and make design iterations expensive. The former option is also limited by strict weather windows restricting maintenance, repair and rebuild.

- **Harsh environment**
  The ocean is a harsh environment with rough conditions. Unlike ships, a WEC system cannot divert from bad weather, and has to be designed for the worst-case weather situation on the site. The extreme mooring loads are many multiples higher than the average loads, and the worst-case weather situation will be a major cost driver.

- **High power fluctuations**
  WECs have to extract power from the reciprocal motion of the waves. This varying speed directly causes reduced output power quality of the PTO, as the machinery cannot run constantly at its optimal speed. In addition to affecting the cost of the PTO, this also transfers to the downstream power system and requires installed overcapacity.

- **Limited power rating**
  The incoming waves have limited wavelength, which limits the maximum size of most of the WEC technologies. As presented in section 7.3, the FO system is limited to a maximum rated power capacity of around 1 MW.

1.5 Electrical output power quality

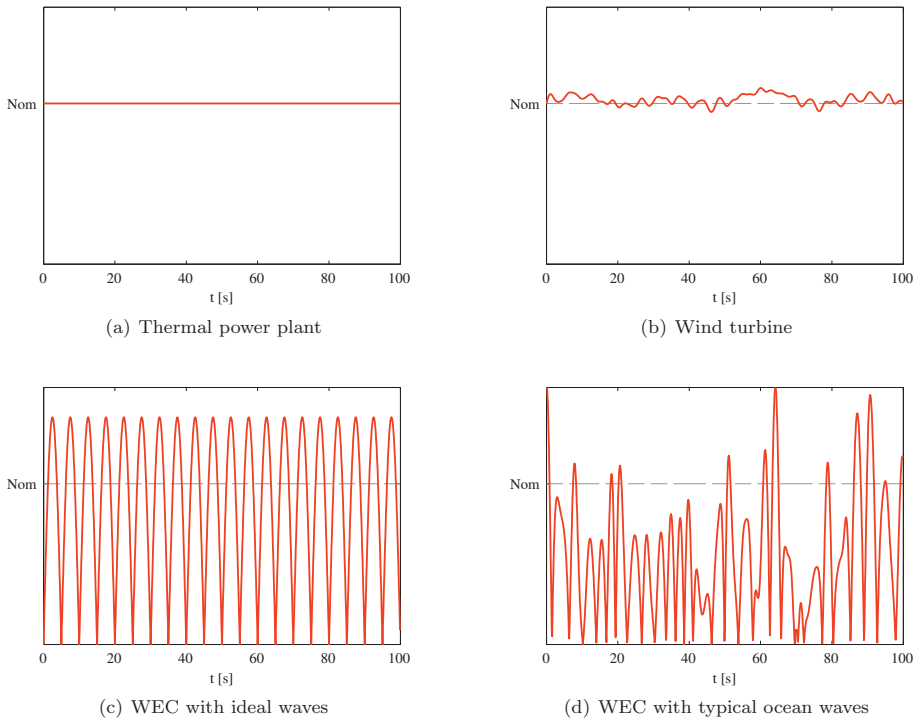

(a) Thermal power plant

(b) Wind turbine

(c) WEC with ideal waves

(d) WEC with typical ocean waves

Figure 1.4: Power output from various power sources when operated in optimal conditions

Most power plants have the capability to produce the nominal output power specified by the rated generator capacity. This is valid for wind turbines, hydro power stations and thermal power stations, and is due to the ability to obtain close to nominal speed on the generator during production. Most WECs however, have generators that operate with varying speed, which reduces the average output power below the rated power. Depending on the mode of operation, the generator may also be allowed occasionally to exceed the nominal power rating. This is illustrated in Fig. 1.4, and makes wave energy converters very different from other types of power plants in its export power quality.

The challenge is how the power shall be managed to reach the high power quality required for export to grid. As illustrated in Fig. 1.5, there are two origins of the disturbances, the first is the regular wave to wave fluctuation plotted in Fig. 1.5(a). Secondly, waves tend to gather in groups to form sub harmonic fluctuations with respect to the wave period. Fig. 1.5(b) illustrates that this effect requires power smoothing over a period far beyond the regular wave period, required smoothing periods up to 200 seconds has been suggested [32]. To avoid heavy investments in energy storage, the main concept pursued in this work is to level out the power by natural smoothing within a farm of multiple converters. Fig. 1.6 shows the improvement in power quality that is believed to be required through the power chain for a commercially attractive system.

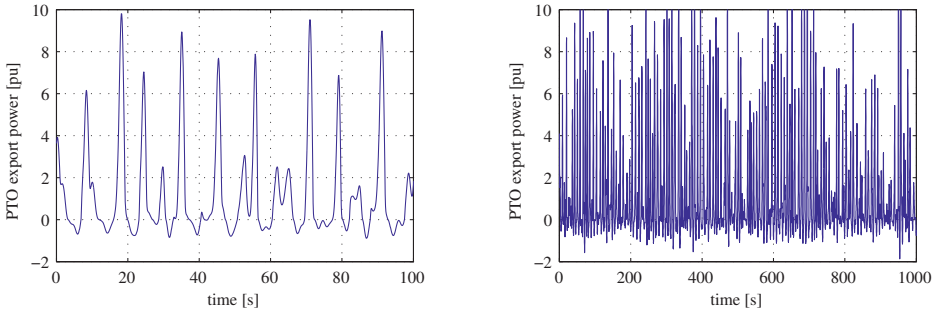

(a) Wave to wave fluctuations

(b) Wave group fluctuations

Figure 1.5: Typical power output fluctuation measured at Lifesaver

The colored fields illustrates the power quality where the red color represents peak power and the green color represents rated power. The light green color indicates the allowed short-term overrun at rated power. Several methods are explored to meet this target including optimal positioning of devices, utilization of energy storage in various segments of the power system and forcing peak shaving through power dumping. Each segment of the power system is analyzed individually through Chapters 2, 3 and 4.

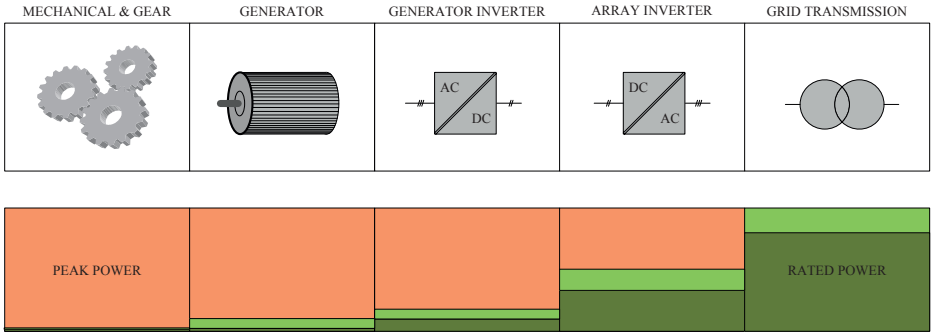

Figure 1.6: Possible power quality improvement through the power transfer chain

1.6 Conventions for rating WECs

As of today, there is no agreed convention on how to rate the power capacity of a WEC, and several figures are used interchangeably. This causes confusion about the real energy export capability and makes it difficult to compare WECs

The wind industry has many of the same issues as WECs, and the rated power for a wind turbine has to be accompanied by a figure for the lowest wind speed that can produce rated power, typically between 11-13 m/s wind speed. To describe the quality of a wind site, the number of full load hours that can be obtained with the specified wind turbine is given. This

cause a natural balance between rated capacity and load hours, as an overrated turbine would result in poor load hour rating.

FO has adopted this method for WEC rating, and propose to implement this as an international standard. The approach consists of three steps:

- **Design wave state**
  Firstly, the design wave state must be chosen, which serve as the design target for optimal WEC performance. For most WEC sites the design wave state is likely to be in the range 2.0-3.0 m Hs.

- **Rated power**
  The average power output in the design wave state defines the rated power for the device.

- **Annual load hours**
  The annual energy output divided by rated power gives the annual load hours and describe the power quality from the WEC system. This parameter is site specific, and a realistic interval for typical sites should be presented for the device.

This method was applied on *Lifesaver*, which was initially targeted for the Wavehub test site. The wave state that delivers most energy per year on Wavehub is 2.75 m H_s / 6.5 s T_z, and this was selected as design wave state. *Lifesaver* was simulated to produce 75 kW in this wave state, which then becomes *rated power*. Simulating a full year of production at Wavehub resulted in approximately 5 000 annual full load hours, and the three rating parameters have thus been defined. Lifesaver can then easily be compared with other renewable resources.

This method has a few shortcomings compared to the wind turbine case, mainly related to power quality. While a 2 MW wind turbine would only require 2 MW of export capacity, a 100 kW WEC would require significantly more than 100 kW of export capacity. Thus, the WEC rating could be accompanied by numbers for RMS power rating and peak power rating, which would say more about the required export infrastructure. These numbers are, however, less important for drawing the larger picture, and implementing only the three initially listed parameters would provide a powerful tool for comparing WECs, and for comparison to other energy sources.

1.7 Fred. Olsen Wave Energy Project

FO started with Wave Energy around 2000 with the development of the WEC system FO^3, which consisted of a matrix of point absorbers fixed to a semi-submersible platform of the Aker H3 type, pictured in Fig. 1.7(a). Model tests were performed in a test tank in collaboration with Marintek, Trondheim, and both survival capabilities and power production capabilities were verified. However, due to the high level of uncertainty with such a system, it was decided to build a 1:3 scale system for initial sea trials. This resulted in the test platform *Buldra* which were equipped with five individual PTOs. Buldra is pictured in Fig. 1.7(b) on site outside *Jomfruland, Norway*, where it was installed during the winter of 2005.

The Buldra tests uncovered some important differences between the real sea environment and the test tank. The actual power output was lower than anticipated, and the total cost of the system was too high. However, the test period also gave significant experience and resulted in new ideas on how the system could be improved. System cost was identified as the key factor, and the FO team investigated extensively on cost down strategies, which led to the design guide lines listed in section 1.8. The conclusion was to cancel the FO^3 project and pursue an alternative system path.

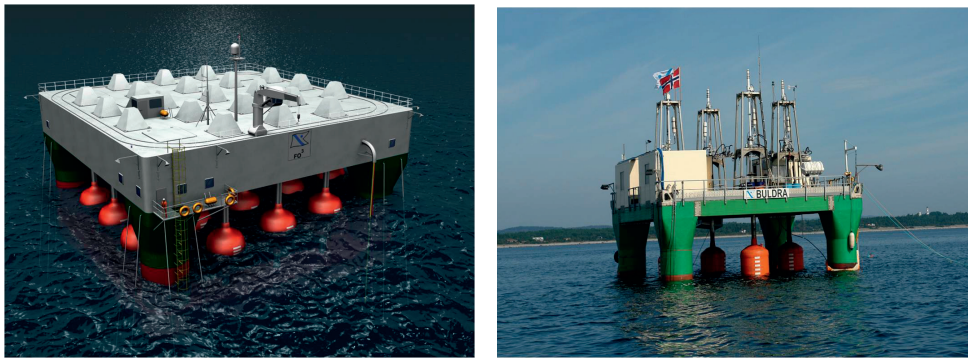

(a) Full scale device (b) Buldra

Figure 1.7: The FO^3 project

The next stage started with the attempt of removing all components and structure from the FO^3 system that was not absolutely necessary. It was decided to stay with the point absorber concept since it had demonstrated good performance, and since it was viewed as one of the simplest systems due to its directional insensitivity. One of the great challenges with the platform, in addition to the high cost, was the strong guides and structures required to absorb the lateral forces between the point absorbers and the platform. The FO team concluded on dropping the platform concept entirely, and instead pursue free-floating point absorbers.

The small-scale test device *B33* was designed as a proof-of-concept device, and was quickly assembled out of polystyrene. It measured ca 1x1 m, weighed less than 100 kg and was fitted with a simple gearbox and induction motor PTO. The system was manually operated and tested close to shore outside Risør, Norway during the autumn 2007 and winter 2008, and was operated from a land based observation post. The PTO and instruments were directly connected to the control box on shore through a short sea cable. The control box contained the motor drive to control the PTO and data logger equipment. B33 demonstrated the viability of the concept, and gave valuable learning on operating systems in real sea conditions. However, B33 was not accurate enough, and had several limitations that prevented accurate measurements of the produced power. Also, the location close to shore caused strong wave reflections that distorted the power output. It was decided to proceed with a more thoroughly designed prototype.

The next step was the *B22* system, which was designed as an autonomous offshore device. It was equipped with a complete control and communication system, and had a well-designed PTO system that could accurately produce and measure a realistic power output. However, as the project saw the opportunity for fast advancement to a full scale prototype, the B22 program deviated from the original plan, and was instead used to provide design inputs into the full scale project *Bolt*®. B22 was operated outside Risør, Norway from the summer of 2008 until the spring of 2009.

In parallel with the internal R&D work performed by FO, a European research project named *SEEWEC* [29] was established to investigate the FO^3 system. The *SEEWEC* project consisted of several European companies and universities and was EU funded. This collaborative work led to the full-scale system *Bolt*®, which was a hydraulic-electric hybrid system developed in close collaboration with BoschRexroth®. Bolt® was installed outside Risør, Norway in June 2009 and had, per December 22, 2010, produced 3 360 kWh of energy [17]. The system is pictured on site

(a) B33

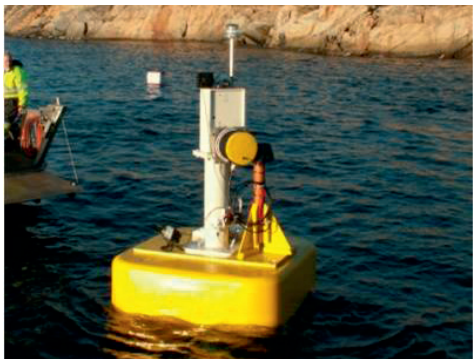

(b) B22

(c) Bolt®

(d) Lifesaver

Figure 1.8: Single point absorber systems developed by FO in the period 2006-2012

outside Risør in Fig. 1.8(c).

Based on the success with Bolt®, FO decided to use the knowledge and experience gained so far to proceed to the next generation design. An agreement with several UK companies was made with funding from the UK *Technology Strategy Board* (TSB). The goal of the project was to improve the Bolt® concept towards a commercial level where it could be launched at the Wavehub test site [43], and hence the project name *Bolt2Wavehub*. The project resulted in the full-scale system *Lifesaver*, consisting of a 16 m toroidal floater with up to five individual all-electric PTO systems. Lifesaver was installed on the test site *Fabtest* in April 2012 and is planned to stay in operation until March 2014. The *Bolt2Wavehub* project and the *Lifesaver* system is explained in detail in Chapter 3.

Until now, FO has not had a single serious event with any of the WEC systems, which has allowed for continuous long term testing in real sea conditions. This has proved invaluable for building experience with wave energy.

1.8 FO design guide lines

Through many years of design and operation of WEC systems, FO has developed a set of design guidelines to work towards a commercially attractive system. The guidelines are focused on the

FO technology, but are believed to be valid for most WEC systems.

- **All floating structure should contribute to energy production**
  This is a lesson learned from the FO^3 system, were an expensive support structure held the absorbers. This structure was quite large compared to the point absorber structures, while it did not contribute to energy production. It was decided that as a first cost down move, all inactive structure had to be removed.

- **Light-weight system**
  Although ballast in a floating system can be inexpensive, the secondary effects of heavy systems can significantly drive up cost. The system mass is directly proportional to the submersed volume, which in turn drives the drift forces on the system. Hence, cost of the storm moorings will be directly affected, in addition to the required extra support structure, and the cost of structure itself. Mass should be regarded an expensive commodity, and should be kept as low as possible. FO has made it a common practice to evaluate the system on a rated kW/kg basis.

- **Tight-moored system**
  Floating systems have to react against some sort of fixed body to produce force, and hence power. The options are to react against a stiff mooring tied to the sea floor, or to have a dual body or multi-body system where body elements react against each other. A common example is to use a heave plate, which is a large viscous friction plate, below the point absorber. Such solutions require the fixed body to have a mass of at least $\frac{1}{2}F_0 g$, where F_0 is the production force and g is the gravity constant. This extra mass must be offset with an equal amount additional buoyancy, which add yet more mass. FO has decided on a path toward tight moored systems to improved the kW/kg rating.

- **All mooring forces must contribute to energy production**
  Moorings contribute significantly to the total system cost and the required mooring forces should be kept as low as possible. Moreover, the mooring system should be designed to utilize the force effectively for energy production, and all moorings should be PTO production moorings. However, while in the developing phase, all WEC systems should be equipped with strong secondary mooring systems until the system behavior is fully understood. Backup moorings have proven to be crucial on several occasions in the FO project.

- **Electro-mechanical PTO**
  FO initially experimented with hydraulic PTO systems as they perform well with high force and low speed. However, when evaluating cost, efficiency and controllability, hydraulic systems show performance issues due to the large variation in speed, and the low average speed of WECs. Hydraulics also has limited ability to perform active filtering to damp unwanted system behavior, which is common in WECs due to the large speed variations. FO has achieved far better performance with electro-mechanical systems that are based on mechanical gear and variable speed drive, as described Chapter 2.

- **Unlimited stroke length**
  The WEC has to be designed with a given stroke, which is the length it can follow the wave motion. The difference between the ultimate stroke, often statistically calculated from the 10-year wave, the average stroke during normal production is very large, and it is tempting to design the WEC with a limited stroke that is optimized for production performance. However, this requires the system to handle the impulse that occurs when end of stroke

is reached. The maximum impulse J_{max} can be calculated by Equation 1.4, where v_{max} is the maximum WEC speed, m is the WEC mass, m_i is the mass equivalent of the PTO rotational inertia and m_a is the added mass of the surrounding sea water. The shock absorber systems absorbing such an impulse showed to be extensive and FO has chosen to avoid end stops, and instead ensure enough stroke length to accommodate for the extreme waves.

$$J_{max} = v_{max}\left(m + m_i + m_a\right) \tag{1.4}$$

- **Early saturation in PTO force**
  There are large variations in speed and force between the largest waves and the most common waves. When designing the PTO, a force saturation threshold must be selected, from where some of the wave power is left untapped. A strong PTO has the possibility to extract more power through advanced reactive control, described in Appendix J, however, when cost optimizing the system, it becomes evident that the PTO machinery is more expensive than the floater, and that the PTO should be designed to reach nominal production already in low waves. An example of this kind of cost optimization is shown in section 7.3, and demonstrates very clearly the importance of early saturation of the PTO force.

- **Above surface device**
  WECs may benefit from being mounted subsurface, or to use submersion as a survival strategy in bad weather. However, having subsurface system components complicates access and design, and conflicts with the rapid prototyping principle [30], which calls for fast development iteration cycles. Until the WEC systems are fully developed and matured, the WECs should be above surface.

- **KISS - Keep it simple stupid**
  A Wave energy device requires a high level of complexity just to maintain basic functions, and any unnecessary added complexity should be avoided. Especially for the early stages it is much more important to develop the robustness and reliability of the WEC system rather than maximizing energy output.

1.9 Concluding remarks

This chapter has presented the problem description for this doctoral thesis. In addition, the FO Wave Energy Project has been described with focus on the history of WEC development, and the general experience gained by FO on WEC development has been presented. The next chapters will originate from this problem description and experience, and Chapter 2 and 3 will give a detailed presentation of the existing *Lifesaver* system and the technology behind it. Chapter 4 and 5 attacks the stated issues with power quality and power control, Chapter 6 presents the theoretical modeling work behind the system and Chapter 7 and 8 wraps up the thesis by presenting the economical performance figures for the system, future possibilities and finally, the conclusion of the thesis.

Chapter 2

Power Take-Off system design

Synopsis

This chapter describes the Power Take-Off machinery used by Fred. Olsen and goes through the practical aspects and the experience gained during pre-testing and sea trials of the *Lifesaver* system. Generator design, configuration and rating is addressed in detail, and a method to reduce the required power rating by high overspeed is presented. The generator is powered through a frequency converter, and the configuration and applied control model is demonstrated.

Contents

Related publications

2.1 Introduction

The purpose of the *Power Take-Off* (PTO) system is to convert linear motion into electrical power. Although the PTO ultimately is defined by its output power, it is more sensible to evaluate and rate the PTO based on the available damping force. As established by Equations 1.2 and 1.3, produced power equals wave force wave times speed. Since the wave speed is too low to impose any restrictions on the drive train, the PTO cost is mainly force driven. The rated force defines the dimensions of shafts, bearings and pulleys. The gearbox gives flexibility to utilize the speed capability of the generator, thus, power becomes and important factor for the high-speed components. However, the selected gear ratio also has strong impact on the moment of inertia, which may restrict the gearing. FO therefore uses force as the main parameter for PTO rating with the cost performance indicator N/€.

Linear reference frame

The PTO operates with both linear and rotational motion, and FO has selected linear motion as reference frame. The total gear ratio n is introduced to describe the relationship between generator rotational speed and the PTO linear speed, and is defined by Equation 2.1. Here, ω_{gen} refers to the generator speed in rad/s, and v_{pto} refers to the PTO linear speed in m/s. M_{gen} is the generator torque and F_{pto} is the linear PTO force, while n_{gear} and r_{drum} refers to the rotational drive train gear ratio and the radius of the winch drum, as illustrated in Fig. 2.1.

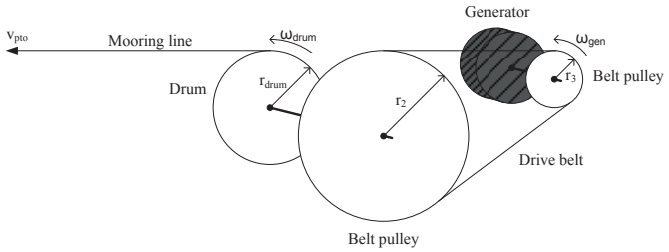

Figure 2.1: Illustration of the linear to rotational gear ratio

$$n = \frac{n_{gear}}{r_{drum}} = \frac{\omega_{gen}}{v_{pto}} = \frac{F_{pto}}{M_{gen}} \tag{2.1}$$

The effect of inertia is included by introducing the inertia mass equivalent parameter m_i, which is found by using the kinetic energy comparison described by Equations 2.2 and 2.3, where I denotes the rotational moment of inertia of the generator. By substituting $\frac{\omega_{gen}}{v_{pto}}$ by n, according to Equation 2.3, Equation 2.4 is found. The equation can be used for all parts of the drive train by using the correct inertia and gear ratio.

$$E_{k-lin} = E_{k-rot} \tag{2.2}$$

$$\frac{1}{2} m_i \cdot {v_{pto}}^2 = \frac{1}{2} I \cdot {\omega_{gen}}^2 \tag{2.3}$$

$$m_i = n^2 \cdot I \tag{2.4}$$

2.2 Mechanical configuration

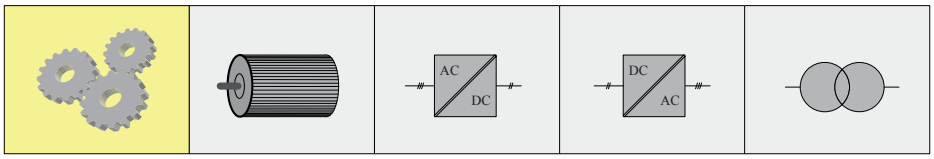

Figure 2.2: Power chain: Mechanical conversion

The FO PTO system is realized as a winch and rope system, as illustrated in Fig. 2.3. The generator can only produce power during upwards motion, and has to operate in motoring mode during downwards motion to wind the rope back on to the drum. The target force for the Bolt2Wavehub project was ten tons and resulted in the PTO configuration parameters listed in Table 2.1.

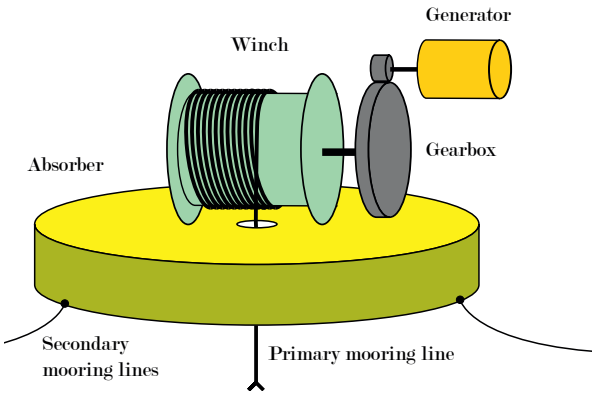

Figure 2.3: Principal sketch of the PTO and WEC

The PTO gearbox is realized as a belt drive system based on Gates® carbon fiber timing belts. The belt drive is very robust against shock loads and operates well with reciprocating motion. The belts are coated with polyurethane and are resistant against the highly corrosive environment at sea. FO has used the belt drive system for all the single body systems, and the gear concept has demonstrated excellent performance. The belt drive is also very flexible as belts and pulleys can be easily replaced. This is a highly valuable property for a prototype, since there is high risk of accidentally subjecting the drive train to excessive internal or external loads.

The Bolt2Wavehub drive train has been further developed from the original concept, and the balanced split drive configuration is a new design for the Bolt2Wavehub project developed and patented by FO. This has the advantage of better utilizing the first step, as torque is created on both sides. Secondly, it balances the forces over the main pulley and the generator so that the bearing loads are minimized. This allows the generator to be mounted with the pulley directly on the shaft, which avoids a complex setup with flexible coupling. The actual drive train design is shown in Fig. 2.4.

Property	Value	
Maximum production force	100	kN
Nominal generator speed	400	rpm
Maximum generator speed	1 800	rpm
PTO nominal production power	15	kW
Generator nominal power	80	kW
Inverter nominal power	120	kW
Gear ratio	38.5	1/m
Equivalent inertia (m_i)	3 000	kg

Table 2.1: PTO specifications

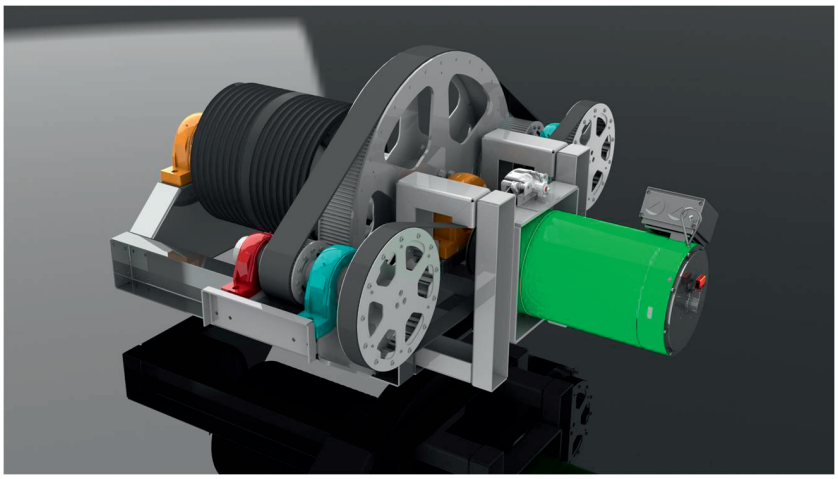

Figure 2.4: Actual PTO design

The total gear ratio of the drive train is 38.5, which is limited by the generator capacity and the resulting inertia. It has been found in simulations that a maximum speed of 6 m/s must be allowed. Since the drive train can carry full load at this speed, the power capacity is 600 kW, which leads to a very poor power utilization factor of 1/40 when compared to the nominal power output of 15 kW. This is the result of the large speed variations, and is exaggerated by the rope winch system that only allows for unidirectional production force. Bottom fixed or multi-body systems may operate with bi-directional damping force, which would double the PTO utilization factor. The FO system selection is based on total cost evaluation and concludes in favor of the unidirectional solution.

2.3 Generator selection

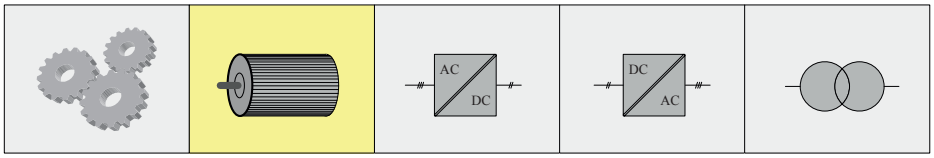

Figure 2.5: Power chain: Generator

For a dynamic drive system like the PTO, finding a suitable generator becomes very hard as there are many parameters that must be optimized. In this section, only the mechanical properties are discussed, as the electrical parameters are closely linked with the inverter configuration discussed in section 2.4. The main parameters are:

- Maximum mechanical speed
- Maximum torque
- Rotational inertia
- Efficiency
- Torque precision
- Cost

The maximum speed and torque must be matched with the PTO rating, and is typically an iterative process of finding a match between the drive train gear ratio and a specific generator system. Since this is a dynamic application, it is also important to keep the rotational inertia as low as possible. Fig 2.6 shows the linear equivalent of the drive system. To simplify the system, the PTO is used as the fixed reference frame, and the sea floor is thought to be moving as the equivalent of wave motion. On leftward motion, the PTO produces power, and on rightward motion, the PTO has to supply pullback force to rewind the PTO and maintain rope tension. As illustrated in the drawing, the major part of the dynamic mass will be in the generator, and is a significant challenge to the system. Firstly, the dynamic mass must be accelerated back and forth in each wave, causing unwanted power cycling in the drive train. This leads to reduced generator efficiency and utilization, and requires electric power to be cycled against the grid or an on-board energy storage. Secondly, high dynamic mass complicates the pull back regulation and

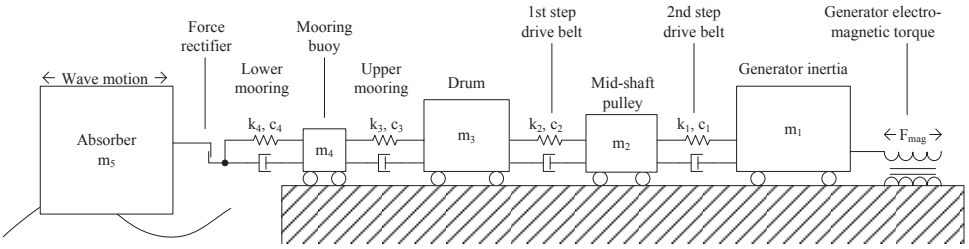

Figure 2.6: PTO dynamic model

makes the system more vulnerable to unwanted dynamic behavior, which will increase the risk of slack rope situations and require larger regulation margin. Thirdly, in slack rope situations, the impulse force that occurs during re-tensioning will be proportional to the dynamic mass. Hence, generator inertia is a crucial parameter that must be kept as low as possible.

The standard induction machine, which is the typical workhorse of industrial processes, is designed with little attention to inertia. It typically has a massive iron rotor, and is therefore unsuited for dynamic control applications. Machines that are optimized for this type of operation utilize other materials and clever design to reduce the rotor mass, and are usually based on permanent magnets since these provide higher torque density and lower inertia. Hence, the requirements seem to push toward servo machines, as opposed to standard generators.

Efficiency is also an important parameter, and although it is closely linked with the electrical configuration, the major parameters inflicting on efficiency are determined early in the design phase. The major loss factors in the generator are resistive loss in the windings, hysteresis loss and eddy currents in the iron, both due to stator and rotor magnetic field and bearing loss. It proved difficult to find generator systems that were designed with good dynamic performance that also showed good efficiency, but a suitable system were finally found in the extensive Siemens portfolio, that also allowed for customization to the customer needs. Siemens also supplied a detailed efficiency map, showed in Fig. 2.16, which also indicates the control boundaries, as discussed in section 2.5. Since the Siemens machine is optimized for accurate servo control it delivers much higher torque precision than would be required for a bulk power producer like the WEC, which results in an unnecessarily costly system.

2.4 Inverter and Generator configuration

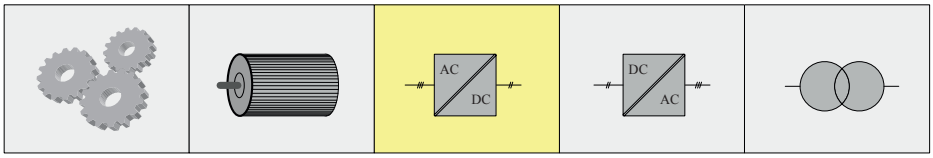

Figure 2.7: Power chain: Inverter

The mechanical properties of the generator were found in the previous section. The electrical parameters are given by the pole count, rotor configuration and winding properties. The electrical

properties result in the torque/current relationship and the speed/voltage relationship, which links the mechanical and electrical properties.

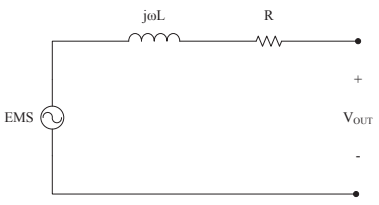

Figure 2.8: Equivalent circuit for PM generator

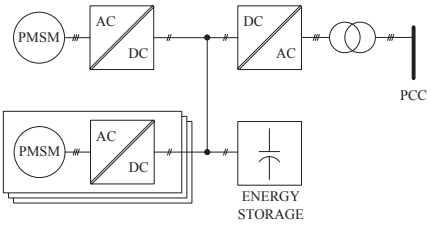

Figure 2.9: Principal diagram for BOLT2

Faradays' law of induction, as given in Equation 2.5 defines the relationship between the induced voltage ϵ, and rate of change in magnetic flux φ through a conductive loop. From this, Equation 2.6 can be derived which gives the induced voltage in n loops with area A that rotates with speed ω in magnetic field with constant flux density B. This shows the relationship between open circuit voltage and speed of a PMSM. Since the magnetic flux generated by the permanent magnets and the geometrical properties are constant, Equation 2.6 can be simplified into Equation 2.7 where v_{out} is the open circuit voltage and k is a constant. The equivalent circuit of the generator is shown in Fig. 2.8.

From this, and by including the electrical impedance of the machine, the nominal conditions can be expressed as given by Equation 2.8, where I_n is the nominal current and V_n is the nominal voltage. This shows that the number of pole windings works as a scaling factor between nominal current and voltage. However, the inverter that powers the machine has a fixed nominal voltage, and as shown in Equation 2.9, where P_n is the nominal power, ω_n is the nominal speed and M_n is the nominal torque, the pole winding count defines the nominal power and the nominal speed of the machine. Higher number of windings leads to lower nominal speed. The nominal torque is defined by the physical size and properties of the machine that were defined in the previous stage of the design process.

$$\epsilon = -\frac{d\varphi}{dt} \tag{2.5}$$

$$\epsilon\,(t) = n \cdot \omega \cdot B \cdot A \cdot \sin\,(\omega t) \tag{2.6}$$

$$v_{out}\,(t) = k \cdot n \cdot \sin\,(\omega t) \tag{2.7}$$

$$\frac{V_n}{I_n} = k \cdot n \tag{2.8}$$

$$P_n = V_n \cdot I_n = \omega_n \cdot M_n \tag{2.9}$$

Above nominal speed, the output voltage must be kept within limits by field weakening. For PMSMs, this leads to a reduction in available torque that is inversely proportional to the speed, and works as a constant power limit. Figure 2.10(a) illustrates this for a typical PMSM that

allows for running with a mechanical speed of twice the nominal electrical speed. A more extreme design with ten times overspeed range is plotted in Fig. 2.10(b) and illustrates the power limiting effect with this approach. These plots show the ideal conditions, real systems would typically show less power for higher speeds due to reduced efficiency and limitations on the field-weakening control.

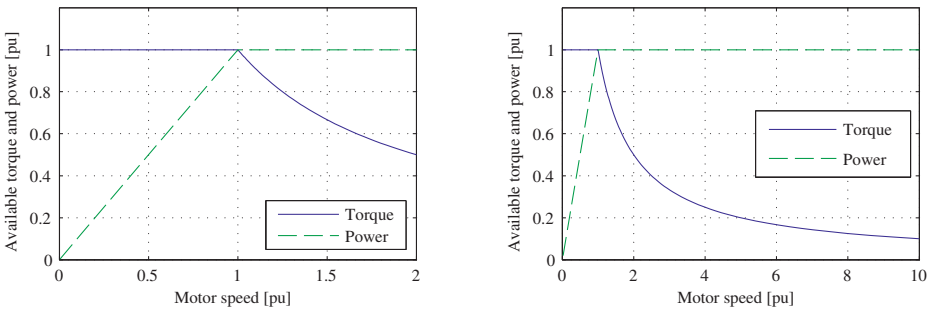

(a) Normal overspeed range

(b) High overspeed range

Figure 2.10: Ideal torque and power curves for PMSM

In context of the rather extreme peak to average speed ratio of the WECs it would be interesting to explore an extreme overspeed ratio of the generator. Bolt®, for instance, was operating with an average speed of 0.3 m/s in the most common wave state, but had to handle above 5 m/s in the most extreme wave state, which leads to a peak-to-average speed ratio of 16.7. The generator overspeed ratio is inversely proportional to installed power, and an increased overspeed ratio will therefore lead to cost reductions through the entire power chain and improve the capacity factor. Reduced installed power will also lead to lower power absorption from the high waves, and systems with very high maximum to nominal speed ratios are investigated to identify the optimal system configuration.

The overspeed optimization is performed by creating generator models for a list of different overspeed ratios. These models are then implemented into the simulation model described in Chapter 6, and a full simulation run for all the wave states in the scatter is performed for each of the generator models. The resulting annual energy production for the different overspeed ratios is listed in Table 2.2. Annual energy and load hours are shown in Fig. 2.13 and 2.12 respectively. The basis for the power normalization is 75 kW, which is the rated power for Lifesaver.

A first important observation is that the overspeed ratio can be raised to five without significant loss of annual production. This corresponds to a five times reduction in installed power. Further increase must be done as part of an economical optimization, and Fig. 2.11 shows the average power production for every hour through a year sorted in descending order, where each line represents a generator configuration with a given overspeed ratio. The figure is a good tool for sizing of the export system and clearly shows the effect of the overspeed ratio. A higher overspeed ratio results in a lower peak power rating, less fluctuation in power production and more load hours. This is mostly achieved by reducing production from the high sea states, but some energy is also lost in the low sea states due to the high irregularities of the waves.

It can be seen from Fig. 2.11 that the overspeed ratio does not appear as a constant power limit, but instead leads to a continuous reduction. This is because the overspeed ratio defines the peak instantaneous power while the exported energy is given by the average power over 20

Overspeed ratio	Annual energy [pu · hours]	Load hours [hours]	Peak power [pu]
1	5093	1840	2.77
3	5081	1928	2.64
5	5017	2180	2.3
7	4878	2511	1.94
10	4593	3026	1.52
15	4070	3690	1.1
20	3547	4128	0.859
30	2832	4773	0.593
40	2368	5244	0.452
50	2041	5611	0.364

Table 2.2: WEC performance with different overspeed ratios

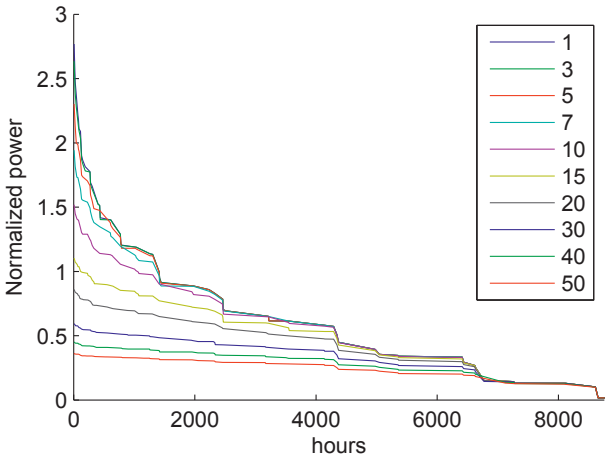

Figure 2.11: Annual power distribution per hour

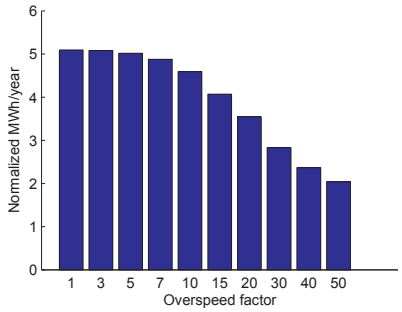

Figure 2.12: Annual energy production with different overspeed ratios

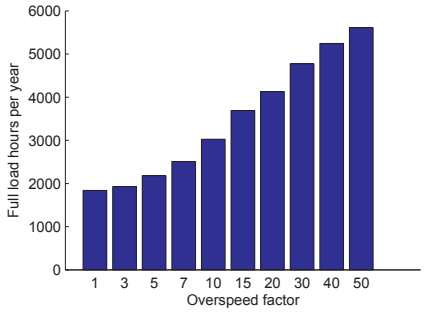

Figure 2.13: Annual load hours with different overspeed ratios

minutes. The goal is maximum utilization of the export capacity, and it is likely that other measures such as energy storage and averaging between groups of WECs also will be required.

There are, however, practical and physical limits to how high the overspeed ratio can be. The most important limitation for the Bolt2Wavehub system is that enough torque must be reserved to ensure adequate pull back force. For PM machines, the active field-weakening control also becomes very demanding for high speeds, and is limited by the magnetic properties of the machine. The Bolt2Wavehub generator is wound for a nominal speed of 400 rpm, while the maximum mechanical speed is 1800 rpm, which gives an overspeed ratio of 4.5. This generator has demonstrated very good performance, but has also suffered from minor issues at high speed. Hence, an overspeed ratio of five seems sensible for the Lifesaver system.

An important side effect of operating PMSM beyond nominal speed is that the natural electromotive force of the machine, V_{EMF}, exceeds the nominal voltage rating. This relationship is linear with speed, with potential to cause damage at high overspeed. To overcome this, a *Voltage Protection Module* (VPM) is mounted directly on the generator terminals to short-circuit the generator in case of excessive voltage, as shown in Fig 2.14. This protects against failures in the electrical system and is important to avoid dangerous power surges into the electrical system. However, it should be noted that as long as the power circuitry is intact, the terminal voltage would be kept within range, even if active field-weakening control fails, since the generator will be short-circuited through the rectifier. Hence, the VPM module will only react against physical failures in the system.

2.5 Control principle

The amount of absorbed power from a point absorber is given by the control strategy applied on the PTO. In general, the optimal energy extraction is achieved when the point absorber is moving with a 90° phase shift to the waves. Several methods of approaching this production mode are described, the best known being *reactive control* [37–39] and *latching control* [19]. Fig. 2.15 shows an electrical equivalent circuit for the WEC where the dynamic behavior is modeled as an RLC circuit. The PTO is represented by a power extracting element (resistance) and a reactive element (reactance). The goal of reactive control is to tune the reactive element of the PTO so that it compensates for the reactive elements of the WEC to maximizes power extraction.

However, with the current design of Lifesaver, the PTO is too weak to have significant impact

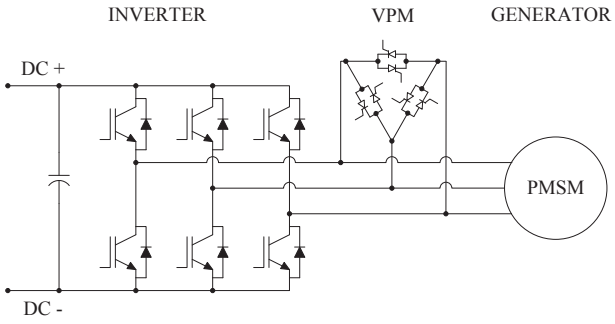

Figure 2.14: Generator frequency converter power circuit

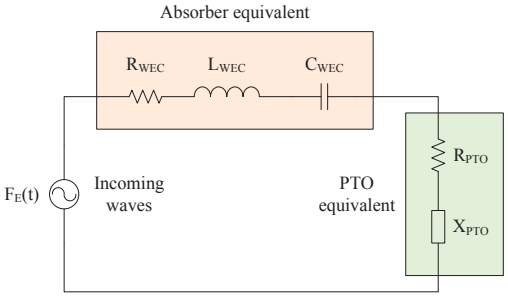

Figure 2.15: Equivalent circuit for Wave Energy Converter and Power Take Off

by advanced control, as demonstrated in Appendix J. This is a result of following the design guide lines specified in section 1.8. Passive damping therefore serves as the primary power extraction method. Nevertheless, in the lowest sea states, advanced control algorithms may improve output [37], but is not currently implemented on Lifesaver.

The PTO damping force F_{PTO} is defined in Equation 2.10 for the PTO speed v and implements passive damping with the damping coefficient B, while respecting the selected force limit F_{Lim} and the intrinsic generator power limit given by the nominal speed v_{nom} and the maximum force F_{Max}. The equation is referred to the linear reference frame with positive direction defined upwards. Thus, the damping coefficient B must be negative to extract power, and is optimized towards the highest efficiency region of the machine to produce the highest possible net power output. F_0 represents the pretension force required for pullback, and the damping function is limited to only react on positive motion. The resulting force and speed characteristics are plotted in Fig. 2.16, where the thick line shows the optimal force that results in maximum net power from the generator. Two saturation mechanisms limits the damping force, the first is the mechanical force limit of the gearbox and is reached already at 0.27 m/s. The second is the power limit of the generator, which is reached at 1.55 m/s. The linear region from 0 - 0.27 m/s corresponds to a damping coefficient of ca -350 kNs/m, which is the selected damping coefficient for Lifesaver.

$$F_{PTO}(v) = \begin{cases} \min\left(F_0 + Bv,\ F_{Max} \cdot v / v_{nom}\right) & : \quad v \geq v_{nom} \\ \min\left(F_0 + Bv,\ F_{Lim}\right) & : \quad v_{nom} \geq v \geq 0 \\ F_0 & : \quad v < 0 \end{cases} \tag{2.10}$$

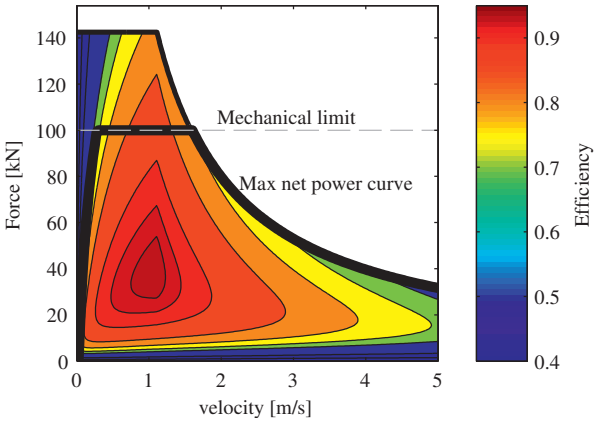

Figure 2.16: Efficiency plot for the generator used at Bolt2Wavehub

2.6 Drive train verification tests

As most of the uncertainty in the Bolt2Wavehub project was related to the PTO function, operation and control, two PTOs were built and assembled ahead of the WEC system. The two PTOs were connected against each other in a back-to-back configuration so that one could drive the other. The first PTO, referred to as the *driver*, was set to replicate the expected wave motions, while the second PTO, referred to as the *driven*, was operating according to its normal

wave production program. Continuous tests for several days were performed at full load to verify the PTO function. Several issues emerged, both in the mechanical system and in the control system, which would cause damage if left unattended. It is much easier to perform repairs and system tests in a controlled environment, and this illustrates the importance of performing a thorough commissioning before launching sea trials. After the errors were corrected the PTOs showed excellent operation.

In addition to the wave production tests, a complete mapping of the drive train loss properties was also performed. This was done by running fixed speed runs with constant speed and torque. To allow for continuous unidirectional running, the drum and rope were replaced with a chain drive that connected the two PTOs together. Thus, the power transfer chain consisted of five gear steps when the chain drive was added to the two gear steps of each PTO. To estimate the loss on a single PTO, the loss was assumed to be evenly distributed over the gear steps, so that the PTO loss was 2/5 of the total loss. The chain drive was expected to have lower efficiency than the carbon belts, however, some friction is also introduced by the generator bearings, and these effects were expected cancel out to some extent.

$$M_{loss} = M_0 + c_M \cdot M_a + c_n \cdot n_a \tag{2.11}$$

The resulting torque loss and power efficiency is plotted in Table 2.3 and 2.4. The tables indicates three loss mechanisms, which is expressed in Equation 2.11, where M_0 denotes the static friction, c_M denotes friction constant due to torque load, c_n denotes the viscous friction and other loss effects linked to speed. M_a and n_a is the actual torque and speed.

The test plan also called for dynamic tests of the drive train to investigate the frequency response of the drive train. This was mainly planned by running frequency sweeps, where the driver set speed is super-positioned with a small fluctuating speed. The frequency of the fluctuating speed can then be gradually shifted to scan the drive train response to a range of frequencies. However, due to time constraints and concerns that the chain drive would not handle the dynamic behavior, these tests were omitted. The chain drive actually broke down later in the test program, which strengthened this view. However, in retrospect, it is clear that more time should have been spent on dynamic effects, as demonstrated in the next section.

2.7 Experience from sea trials

The PTOs have demonstrated successful operation through the sea trials, and have survived rough wave states up to 5.1 m Hs, with maximum waves of ca ten meters. However, several dynamic issues have been discovered that cause oscillations in the system and will lead to reduced lifetime if left unattended. Fig. 2.17 shows a typical case during normal production. In this example, the PTO is limited to 50 kN of damping force, and the pullback force is set to 10 kN. The figure shows how the PTO force follows the production force function on upward motion and maintains the pullback force on downward motion.

The concern is the oscillations that occur when the control model switches from a damped system to a saturated system. This cause a step response in the system behavior that leads to the observed ringing. Some distortion at this switchover was expected, but the measured fluctuations showed to be much more pronounced than anticipated, and must be caused by dynamic spring effects somewhere in the system. To further investigate this issue a research project was established in collaboration with NTNU to analyze the dynamic response of the system. The work concluded that spring effects in the primary mooring is the main contributor to the oscillations, and that the problem can be mitigated thorough active compensation control [24].

Torque [Nm] \ Speed [rpm]	50	100	150	200	250	300	350	400	450	500
0	42	48	49	49	54	58	58	58	57	57
125	40	46	44	41	50	62	57	61	57	49
250	48	52	52	50	49	61	57	59	62	63
375	47	55	55	50	67	44	53	72	59	80
500	54	56	59	61	45	64	68	73	52	71
625	55	61	58	51	52	67	70	66	74	73
750	54	63	51	54	54	77	65	72	82	73
875	62	67	58	73	73	72	69	54	79	60
1000	60	64	56	78	77	70	83	86	77	77
1125	67	52	76	63	67	85	95	82	98	70
1250	65	77	82	61	63	88	81	89	92	95
1375	58	79	60	84	86	88	82	93	96	87
1500	75	80	82	114	126	81	87	135	93	120
1625	78	89	89	129	123	85	119	151	108	125
1750	83	96	108	112	111	93	143	123	143	130
1875	87	96	97	100	89	145	133	108	126	-
2000	87	105	103	101	119	152	91	127	148	-

Table 2.3: Drive train torque loss [Nm]

Torque [Nm] \ Speed [rpm]	50	100	150	200	250	300	350	400	450	500
0	-	-	-	-	-	-	-	-	-	-
125	81.8	79.6	79.7	81.1	77.8	74.6	75.7	74.2	75.1	76.8
250	87.8	86.1	85.8	86.1	86.5	83.8	84.3	84.4	83.3	83.2
375	91.8	89.8	89.1	90.3	87.2	91.2	89.2	86.1	88.1	84.8
500	92.9	92	91	90.7	93.3	90.2	89.6	88.9	91.5	89.3
625	93.8	93.1	93	94.2	93.5	91.7	91.2	91.7	90.7	90.7
750	95	93.9	94.8	94.8	94.4	91.9	93	92	91	92
875	95	94.4	95	93.4	93.6	93.7	93.6	94.9	92.7	94.3
1000	96.7	95.6	96.6	93.9	93.8	94.4	93.1	93.1	93.8	93.5
1125	96.3	97.7	94.7	96.2	95.4	93.9	93	94	92.9	94.9
1250	96.7	95.5	94.8	96.5	95.9	94.5	94.9	94.1	93.9	93.5
1375	98.7	95.8	97.5	95.3	95.1	94.9	95	94.5	94	94.7
1500	97.3	96.2	96.2	94.1	93.4	95.5	95.1	92.6	94.6	93.3
1625	97.6	96.1	96.1	93.6	94.4	95.9	94	92.4	94.3	93.5
1750	98.5	96.2	95.3	95	95.1	95.6	93.3	94	93.2	93.9
1875	97.7	97.5	96.4	95.8	96.1	93.6	94	95.2	94.3	-
2000	98.3	96.4	96.3	96	95	93.7	96.2	94.6	93.8	-

Table 2.4: Drive train power efficiency [%]

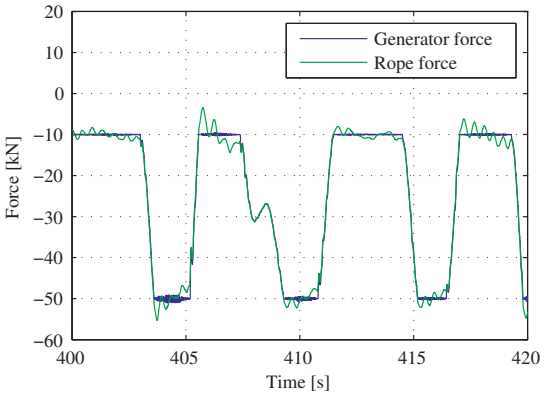

Figure 2.17: Force vibrations observed on mooring during normal operation

Another result of the same problem arises in high-speed cases. When the PTO reaches the nominal speed and has to saturate the production power due to field weakening, a system condition occurs where the damping coefficient becomes negative. This has a destabilizing effect on the system, and causes the PTO to accelerate due to positive feedback. This was expected during system design, as the force ramp down will reduce the floater submersion, but the effect was expected to decay as soon as the floater had reached its maximum speed. However, due to the dynamical softness of the system, this effect causes violent oscillations that have caused the PTO to trip on overspeed on a few occasions. This problem is believed to be easier to solve, as these occurrences are quite infrequent, so that more drastic approaches can be used without significantly affecting annual produced energy.

2.8 Concluding remarks

This chapter has described the PTO design in detail, and has addressed the many mechanisms affecting PTO performance. Important findings are the importance of inertia in the PTO system, both on dynamic behavior and on energy expenditure during pullback. It was also demonstrated that significant expenses can be saved on the inverter and power system by configuring the generator with nominal speed far below the maximum allowed speed. An overspeed ratio of around five has been found to be beneficial.

Chapter 3

Wave Energy Converter design and operation

Synopsis

This chapter presents Fred. Olsens latest WEC system *Lifesaver*, which is a 16 m toroidal point absorber with 75 kW rated power capacity. The mechanical and electrical system configuration is explained in detail, and results and experience from the sea trials at the *Fab Test* test site outside Falmouth, England is presented. This includes a complete production scatter diagram for *Lifesaver*.

Contents

Related publications

3.1 System description

The purpose of the *Bolt2Wavehub* project was improve the power output from the Bolt® system, and the initial goal was to achieve 100 kW average power output in the design wave state Hs = 2.75m / Tz = 6.5s. Bolt had a damping force of 40 kN, and it quickly became evident that it would not be possible at that technology level to achieve 100 kW with a single PTO, thus several multi-PTO solutions were investigated, and the configuration with five PTOs positioned along the edge of the buoy showed to be most promising. This configuration allowed the PTO force to be kept within 100 kN, which was believed to be a maximum limit for the winch system at the time. An important outcome of the multi-PTO configuration is the ability to produce from both heave, pitch and roll motion, as opposed to the single PTO configuration, which only produces from heave. In total, this resulted in a rated power expectation of 75 kW, which was considered to be satisfactory, the additional damping force and floater size required to obtain 100 kW was viewed as to much risk at this level.

In the SEEWEC project [29], it was found that the shape of the floater was of less importance, especially when the system is not operated with reactive control, the important parameter is the submersed cross-section area. Hence, FO had great flexibility on designing the hull, both with respect to production method and transport requirements. The team also discovered that, due to the pitch and roll-damping capability, the hull would produce more power with a ring design than a compact design, as the improved diameter would lead to a longer arm on the rotational movements. This led to the characteristic toroidal WEC system *Lifesaver*, pictured in Fig 3.1 which name is inspired by its rescue buoy like proportions.

Figure 3.1: *Lifesaver* on site outside Falmouth, England.

As can be seen from the picture, *Lifesaver* was only installed with three of the five PTOs, as this was believed to be satisfactory for understanding the system, and also allow for experience to be gained on the first PTOs so that the remaining PTOs could be built to a higher standard. The PTOs are designed to be modular and independent so that the WEC system can maintain operation in case of failure of one or more of the PTOs. This also allows for simplified service, as a failing PTO could be brought to shore while maintaining power production on the remaining

PTOs. The basic properties of the Lifesaver system are listed in Table 3.1.

Table 3.1: Lifesaver key parameters

Floater outer diameter	16	m
Floater inner diameter	10	m
Floater height	1.0	m
Mass	55	tons
Water depth	55	m
Number of PTO slots	5	
Currently installed number of PTOs	3	
Damping force per PTO	100	kN
WEC rated export power	75	kW
Total installed generator capacity	400	kW

Lifesaver is a flat absorber with low mass that gives a high resonance frequency and thus a *Response amplitude operator*, RAO, [11] close to one for most of the relevant wave states. This gives a stiff system that is well suited for passive damping and less suitable for reactive control. The absorber is tightly moored to the sea floor by a winch and connects to the generator through a gearbox, as shown in Fig 2.3. This point-absorber principle is a well known conversion system that has been extensively researched and tested [20]. Pre-tension in the mooring line is supplied either by a spring equivalent system or by the main generator itself.

3.2 Power system

Lifesaver has an advanced power system that allows for operating standardized industrial power equipment without grid connection, while still keeping the option of grid connection open. Electrically, all PTOs are connected to a common DC-bus that serves as the backbone of the power system. This allows for natural power exchange between the PTOs and the power components, and ensures a natural balance in the power flow. As can be seen in Fig. 3.2 this configuration is the same for both the stand-alone and the grid connected solution. In the grid connected option the available power surplus on the DC-Link is converted to AC and transformed to grid. The capacitor bank indicated on the schematics could serve as intermediate energy storage before transfer to grid, however recent studies have shown that this is not required and that capacitor bank only needs to be sized for the control stability of the inverters.

In the stand-alone solution on the other hand, a significant energy storage is required to make up for the negative power periods caused by pullback. Several options were considered, pointing towards the ultracapacitor bank as the most suitable solution for the system. The ultracapacitor bank is connected directly on the DC-link, and is backed by a battery bank through a bi-directional DC/DC converter. In addition, a power dump system is required to handle excess energy. Fig. 3.2(b) shows the detailed schematics for the stand-alone system, and the specific system components and solutions are explained in detail in the following paragraphs.

Capacitor bank

The requirement for the capacitor bank is to supply the required energy for winding in 10 m of rope on each PTO with 10 kN of pull force. It must also handle wind-in speeds of several meters per second. With a system efficiency of 0.8, and taking into account all five PTOs, the required energy can be calculated to 625 kJ by Equation (1.2), while Equation (1.3) indicates a required

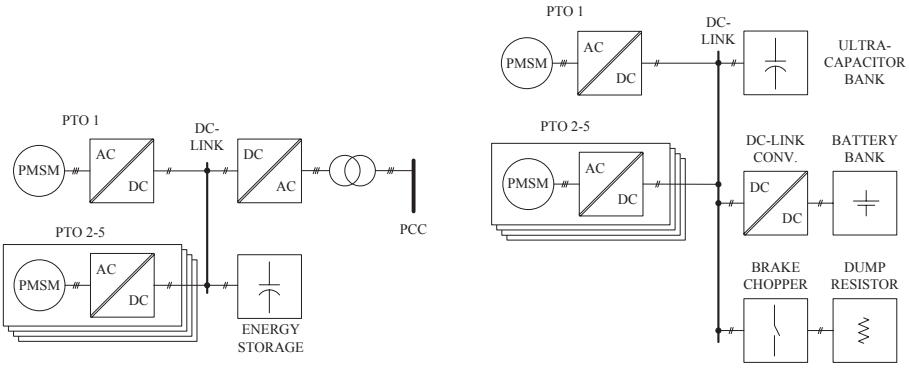

(a) Topology for grid connected system

(b) Topology for stand-alone system

Figure 3.2: Lifesaver topology

Figure 3.3: Maxwell technologies® 48V ultracapacitor bank module with active cell balancing

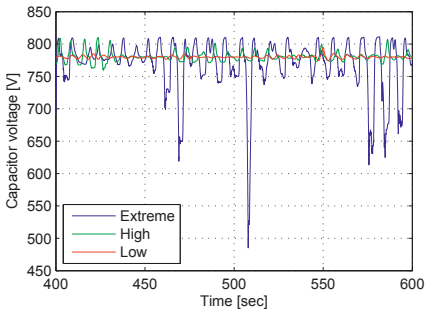

Figure 3.4: Simulated capacitor bank voltage for three wave states, Low: hs=1.25 m / Tz=5.5 sec, High: hs=2.75 m / Tz=6.5 sec and Extreme: hs=8.0 m / tz=10.0 sec

power of several hundred kilowatts. Equation (3.3) shows the energy storage capacity W_e of a capacitor based on capacitance C and nominal voltage V_n.

$$W_m = F \cdot s \tag{3.1}$$

$$P_m = F \cdot v \tag{3.2}$$

$$W_e = \frac{1}{2} C \cdot {V_n}^2 \tag{3.3}$$

A third requirement for the capacitor bank is that it must handle peak voltages up to 830 V. A configuration of 17 serial connected modules of the Maxwell technologies® 48 V module [35] fulfill all these requirements, and is the selected configuration. The module is shown in Fig. 3.3. Each module contains 18 serial connected ultracapacitors that are conditioned by an active balancing network. The balancing network allows for bypassing some of the charging current on each cell and is controlled so that all the cells are at equal voltage. If the nominal voltage on the entire module is exceeded, some current is by-passed to ensure balance between modules. Some technical parameters for the capacitor bank is listed in Table 3.2.

A drawback with direct connection to the DC-Link is that capacitor voltage will have to stay within the operational limits of the DC-Link components. Thus, the full energy potential for the capacitor cannot be utilized as it cannot be allowed to fluctuate between zero and nominal voltage. However, for the ultracapacitors to maintain the specified lifetime, discharge below $\frac{1}{2}V_{nom}$ is not permitted during normal operation. Since the Siemens inverters used allow for high fluctuations on the DC-Link, this problem can be mitigated somewhat. On Lifesaver the system is allowed to fluctuate between 500 V and 760 V in normal operation, which corresponds to 65% of the available energy. Hence, only 35% more energy could cycled through the energy storage if a separate converter were used for the ultracapacitor bank.

Property	Value	
Nominal voltage	816	V
Capacitance	4.88	F
Nominal energy	1.63	MJ
Useful energy (400V-776V)	1.08	MJ
Max continuous current	100	A
Max peak current	1 100	A
Short circuit current	4 800	A
Nominal power at 600V	60	kW
Peak power at 600V	660	kW
Modules in bank	17	
Cells per module	18	
Cell capacitance	1.5	kF
Cell voltage	2.70	V
Cycle life	10^6	

Table 3.2: Ultracapacitor bank specifications

The capacitor module has a specified cycle life of 10^6 cycles. If every charge/discharge cycle during power production is counted, this number will be reached in less than one year of operation due to the wave frequency. However, most of the cycles are caused by low waves with low energy. Maxwell technologies® offered to simulate the expected life time of the capacitor system

specifically for Lifesaver. The simulation inputs are plotted in Fig. 3.4 and shows capacitor bank voltage profiles from three different wave states, low, high and extreme. The three wave states have a defined probability of 0.4, 0.1 and 1/365 respectively. The remaining probability of approximately 0.5 is the down time expected during calm weather, and is quite high due to the sheltered conditions on the *Fab Test* site. Based on these inputs Maxwell technologies® has estimated the lifetime to 15 years.

DC-Link charger

The DC-Link charger converts energy from the battery bank to the capacitor bank. This is mainly required for three purposes:

- During startup when the capacitor bank have to be pre-charged and the PTOs have to pull in and tension the ropes.
- During service when the PTO winches have to be maneuvered.
- In extreme wave states when the required pullback energy might exceed the available energy in the capacitor bank. The pullback process and energy balance is described in section 3.2.

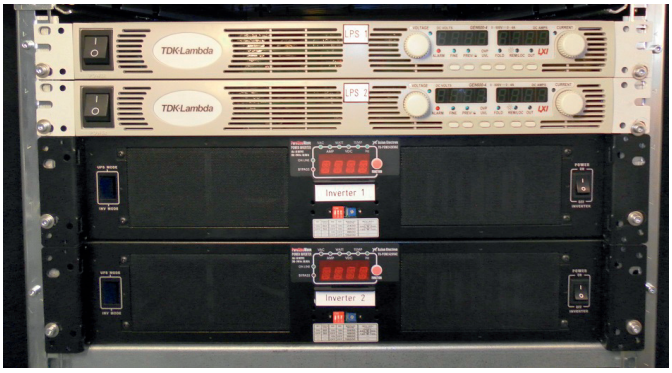

Figure 3.5: DC-Link charger: Inverters and laboratory power supplies in 19" rack configuration.

The specifications for the DC-Link charger are as follows:

- Supply up to 5kW of power
- Supply output voltage in the range 0-600VDC
- Handle voltage on the output terminals in the range 0-830VDC
- Handle input voltage in the range 22.0-29.0VDC
- Allow for current limited operation
- Controllable over LAN

From a power electronics point of view the best solution would be to use a DC/DC boost converter that directly converts the battery voltage to 600 VDC. An even more interesting solution would be to merge the DC-charger and the battery charger, which will be described in the next section, into a single bi-directional converter. A possible solution for this is the *Reduced Matrix Converter*, which is based on bi-directional RB-IGBTs. This concept has been explored in detail and has for instance been proposed for off-shore wind turbines [14]. However, no off-the-shelf converters based on these topologies that meet all the requirements could be found. Development of such a system from scratch is costly and time consuming, especially when taking into account the required support for maintenance and service. This approach was therefore rejected.

Instead a modular two-step solution based on a standard 24 VDC to 230 VAC inverter and a 230 VAC to 600 VDC laboratory power supply is selected. This takes the power via 230 VAC, which is a drawback, but greatly increases the number of off-the-shelf components available. The power supply selected is controllable by LAN, it can supply any voltage in the range 0-630VDC and can operate in current limited mode with set currents in the range 0-4.2 A. This leads to a maximum supply power of 2650 W. However, it cannot handle more than 660 VDC on the output terminals and have to be shield from the voltages on the DC-Link by a reverse blocking diode. The inverter and power supplies are 19" rack modules and can be seen in Fig. 3.5.

Battery charger

On board systems such as communication, data logging and monitoring equipment consume a considerable amount of power from the 24V battery bank. This power must be generated by some means, and the obvious solution is to use the generated wave energy. This is not straightforward however, given the high- and fluctuating voltage level on the DC-Link. A solution based on off-the-shelf wind turbines or PV cells would seem easier to implement. Nevertheless, FO decided that it was worth the extra effort to develop the system, as the purpose of the prototype is to prove the viability of wave energy. Moreover, an external power system with the required power rating would be large and potentially fragile to the extreme weather conditions experienced at sea. The battery charger has the following requirement specification:

- Handle input voltage in the range 0-830 VDC
- Operate with input voltage in the range 600-830 VDC
- Supply output voltage in the range 20-29 VDC
- Supply up to 125 A of charging current
- Control charging current based on input voltage
- Comply with 3-stage battery charging principle
- Controllable by field-bus (Profibus)

FO decided that the easiest approach to meet these requirements was to base the battery charger on the same motor drive inverter that powers the PTO generators. They can naturally handle the input voltage range, they are programmable, they natively support closed-loop control and FO already has the required knowledge to operate and program them.

The concept is illustrated in Fig. 3.6 and is based on an inverter that powers a three-phase 400/24 V transformer to supply a 3-phase bridge rectifier. Finally, the output power is smoothed through an inductive filter and fed into the battery bank. To simplify the configuration, the

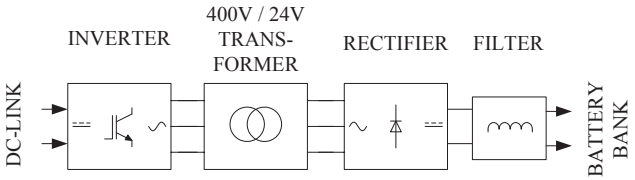

Figure 3.6: Battery charger topology

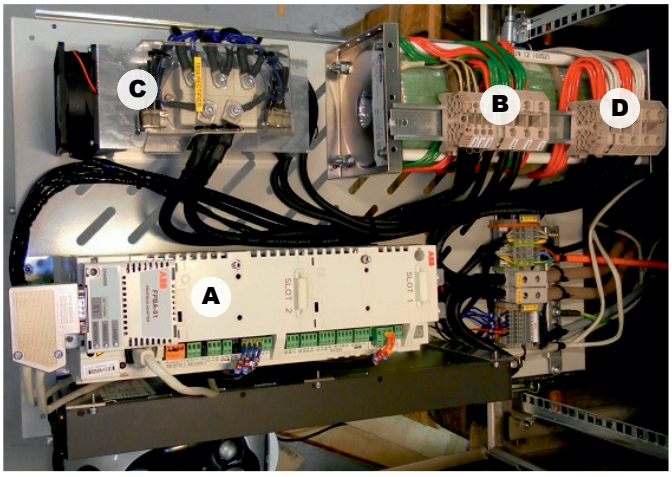

Figure 3.7: Implemented battery charger configuration: A) Inverter, B) Transformer, C) Rectifier, D) Choke

transformer and chokes are designed with the same cores and fixed in a common frame. The actual implemented system can be seen in Fig. 3.7.

The inverter is operated in scalar mode, which allows for controlling the output frequency directly. The output voltage is regulated proportional to the output frequency to adapt to the constant motor inductance to operate at nominal current. This principle is directly transferable to the transformer and gives a system where the output voltage of the transformer can be controlled without risk of excessive magnetizing currents. The nominal output frequency of the inverter is set to 200 Hz as this reduces the transformer size, while still allowing for standard 50/60 Hz transformer design methods to be applied.

The charger program is implemented as a closed-loop feedback control with an inner current control loop and an outer voltage control loop, as shown in Fig. 3.8. The current loop uses the inverter output current as feedback while the voltage loop regulates on the actual battery voltage, which is measured by an external sensor. The three-stage battery charger program is implemented by controlling the current and voltage references. The maximum allowed charging current is set to 125 A, the maximum charging voltage is set to 28.8 V and the trickle charging voltage is set to 27.6 V. The trickle charging stage triggers when the charging current falls below 10% of the nominal charging current.

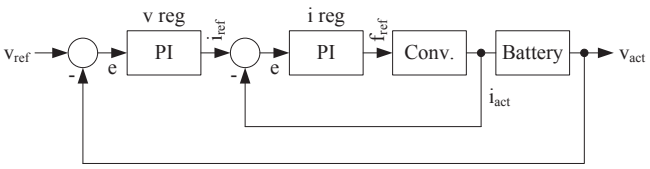

Figure 3.8: Battery charger control principle

The battery charger must adjust the charger power to the DC-Link voltage to ensure stable behavior for all WEC production levels. This is implemented by setting maximum allowed charging current as a linear function with zero power at 650 VDC and full power at 720 VDC. This prevents the battery charger from draining the capacitor bank at low power production levels.

Brake chopper

The WEC is expected to produce a power surplus in all wave states above cut-off. This excess energy will cause the DC-Link voltage to rise and must be taken away to balance the system. This is normally done by switching in a resistor that dissipates the excess energy. For good controllability, the system is typically controlled by *Pulse Width Modulation* (PWM) at around 1 kHz. This setup is usually referred to as a *brake chopper* and is very common in motor drive systems.

On *Lifesaver* a standard brake chopper system supplied by Siemens is used, which will start dumping energy at 776 V. The brake chopper has a linear PWM region where the duty cycle is increased proportional to the voltage until saturation occurs around 790 V and the resistor bank is constantly switched on. The resistor bank is a large array of air-cooled heating elements that is placed on top of the power system box on Lifesaver. It is visible on Fig. 3.1 on page 34 as the gray structure to the upper-right. Air-cooling was selected in favor of water-cooling for simplified access and maintenance.

The brake choppers operate as stand-alone units and only monitor the DC-Link voltage.

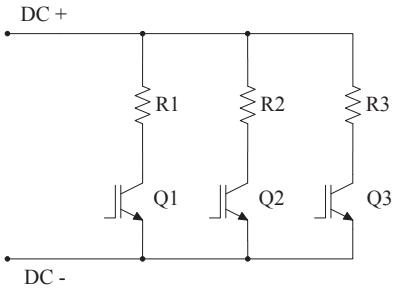

Figure 3.9: Brake chopper system

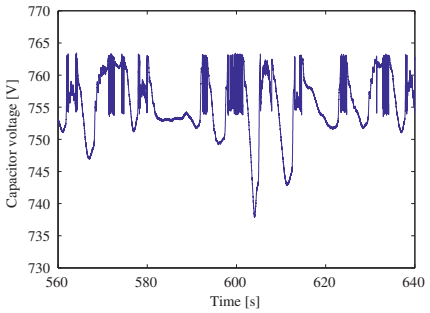

Figure 3.10: Measured DC-Link voltage during brake chopper operation

They do not require any external regulation or control. Three brake choppers are installed in parallel with individual resistors as shown in Fig. 3.9. Each brake chopper has a nominal power of 50 kW and a peak power of 250 kW, which leads to a total braking power of 150 kW nominal and 750 kW in peak, and a fully redundant system.

Lifesaver is not expected to go beyond the nominal power on average as the production will be curtailed in high to extreme wave states. However, the peak power limit of 750 kW may occasionally be breached by single large waves appearing in high sea states. This requires active power control and is described in the next section. Fig. 3.10 shows the actual response of the DC-Link system during brake chopper operation. The rapid fluctuation around 760 V is caused by the startup and shutdown of the brake chopper and not the actual PWM during operation. The issue is believed to be caused by inaccurate control of the brake chopper at low power levels and could be eliminated by improved control. Since this does not cause problems for the general operation, and since the voltage fluctuations are relatively low, it has been decided to leave it as it is.

DC-Link power control

The purpose of the DC-Link power control is to keep the capacitor bank and the DC-Link voltage within the allowed range, and to ensure required energy for pullback. The DC-Link power control is not a centralized control function, but is accomplished as the sum of several components and functions operating together. The DC-Link conditioning can be divided into three levels, green, yellow and red, as illustrated in Fig. 3.11. Within the green region, the capacitor bank voltage is conditioned by the DC-charger in the low voltage end and the brake chopper in the high voltage end. The PTOs are allowed to operate with optimal generation and motoring force. If the production exceeds the brake chopper capacity or the consumption exceeds the DC-charger capacity the yellow region is entered. Operation of all PTOs is then progressively constrained to counteract further aggravation. In the unlikely event that the absolute limits are breached and the DC-Link voltage enters the red region, all PTOs immediately shut down. For the high voltage case, the VPMs also fires to protect the DC-system and to bring the generators to a controlled stop.

The battery charger will start charging the batteries at 650V and will ramp up to full charging power of 125A / 3.6kW at 720V. These thresholds are set to optimize for production in low waves

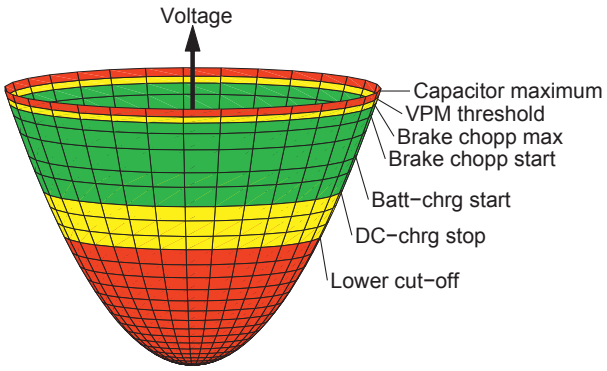

Figure 3.11: Capacitor bank energy illustrated as a volume.

to maintain an untouched reserve of pullback energy between 650V and 540V. In the higher wave states, the capacitor bank is expected to maintain close to fully charged condition with voltage above 720V most of the time. It is important to include blanking voltage between the DC-charger shutdown threshold and the battery charger startup threshold to avoid circulation of power between the two converters. The DC-charger can supply a maximum voltage of 630VDC, and the startup threshold of 650VDC ensures adequate safety margin.

In the extreme wave states the capacitor bank is completely cycled in each wave, which can be seen in Fig. 3.4 at 510 sec. This will cause cyclic charging between the battery bank and capacitor bank as the missing pullback energy must be borrowed from the battery bank. This is only expected occasionally during worst-case conditions and should not affect battery life significantly.

The DC-Link charger will normally operate whenever the DC-Link voltage is below 540V. However, if the WEC is in a low production state, the 540V level is instead used as a trigger for cut-off and causes the entire WEC to shutdown. The WEC will then go into power save mode and measure the waves periodically to determine when power production can start up again. This is handled by the top-level WEC control.

3.3 Sea Trials in Falmouth Bay

Lifesaver was launched for sea trials in April 2012 at *FaB Test*, which is a UK test site for pre-commercial WEC concepts. FaB Test is located in Falmouth bay outside Cornwall, England, as shown in Fig. 3.12, and is envisioned to be a preparation site for WECs planned for commercial operation at the Wavehub site [43], and has a moderate wave climate with good balance between production hours and availability for maintenance. Moreover, Falmouth bay has several large dock yards capable of doing advanced mechanical work and heavy lifts that are suitable for supporting WEC deployment. The tidal range in the Falmouth area can be as high as six meters which pose no problem for the *Lifesaver* system, but could be a limitation for other WEC devices. The water depth at the test site is around 50 m. Hence, Fab Test is an excellent test site for performing the initial sea trials on *Lifesaver*.

The *Lifesaver* system is designed with focus on modularity, maintainability and reliability. All mechanical and electrical parts are placed above surface for easy access, and the modular

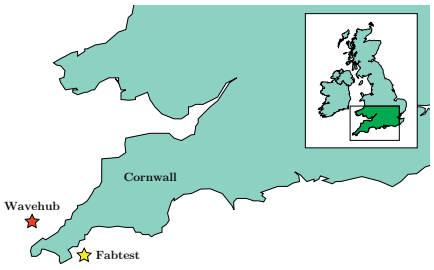

Figure 3.12: Location of the UK test sites *Wavehub* and *FaB Test*

Figure 3.13: *Lifesaver* during PTO lifting operation

and autonomous PTO configuration allows for maintaining system operation and power export with one or more PTOs out of service. Fig. 3.13 shows an example of maintenance work at *Lifesaver*, where one of the PTOs were lifted off for on-shore repairs. Over the past year a large amount of operational experience and data has been acquired. All signals and measurements are logged continuously at 200 Hz while in operation, and gives a comprehensive database for analysis. Together with the advanced simulation model, this helps build a detailed understanding of the system, and complements the theoretical model of the system. Based on this experience, a detailed power export scatter diagram has been assembled and is presented in Table 3.3. The diagram lists the average electrical power exported to the DC-bus for all wave states with the current control settings. A more detailed version of the scatter diagram is available in Appendix G. Thus, the presented figures in Table 3.3 are about 30 % lower than the theoretical production potential with optimal control parameters. The scatter diagram is based on a five PTO configuration.

Table 3.3: Exportable power [kW] from *Lifesaver* for various wave states

		Wave period (Tz) - [s]												
		4	4.5	5	5.5	6	6.5	7	7.5	8	9	10	11	12
Wave height (hs) - [m]	0.25													
	0.5	1.4	1.5	1.6	1.6	1.4	1.3	1.1	1.0	0.9	0.7	0.6	0.4	0.4
	0.75	4.0	4.2	4.5	4.4	4.0	3.8	3.3	3.1	2.9	2.4	2.1	1.7	1.5
	1	7.6	8.0	8.5	8.3	7.7	7.3	6.5	6.1	5.7	4.8	4.2	3.3	2.9
	1.25	12.4	12.9	13.6	13.5	12.4	11.8	10.5	9.9	9.2	7.8	6.4	5.4	4.4
	1.5	18.1	18.8	19.7	19.7	18.0	17.1	15.4	14.4	13.3	11.0	9.1	7.7	6.5
	2	31.8	32.7	34.0	33.2	31.3	29.5	26.6	24.7	22.9	19.5	15.8	13.8	12.3
	2.5	47.9	48.3	49.5	48.5	45.6	42.9	38.7	36.4	33.5	28.3	23.5	21.0	20.3
	3		63.9	65.3	63.0	59.9	56.5	51.1	48.2	44.8	37.3	33.6	30.2	28.6
	3.5			80.0	76.8	72.8	69.1	62.7	59.6	56.1	48.3	45.1	41.4	37.7
	4			92.9	89.2	84.4	80.3	73.7	70.2	66.3	58.9	54.9	49.6	46.3
	5				109	104	98.9	92.9	88.5	84.8	78.3	72.7	67.1	61.6
	6						113	107	103	99.4	93.5	86.7	81.4	75.6
	7						123	119	115	111	105	98.2	93.2	86.5
	8							127	124	119	114	107	103	96.3
	9								129	126	121	114	110	103
	10									130	125	120	116	109

Lifesaver is planned to stay in operation at *Fab Test* until June 2014. After a thorough inspection and refurbishment, the device will be moved to a more energetic WEC site at a non-disclosed location for continued testing and demonstration. This is expected to commence during

spring 2015. In the new test site, a grid cable will also be available to demonstrate power export to shore.

3.4 Measured power production

The actual measured power production from *Lifesaver* for the entire test period is plotted against the wave state in Fig. 3.14(a). The wave measurements are taken from a wave measurement buoy situated 1 km from the location of *Lifesaver*. Qualitatively, the measured response shows good correlation to the simulated results, and shows performance equal to similar tests performed by others [42]. However, when comparing directly to the simulated results presented in Table 3.3, it can be seen that the measured power production is somewhat lower, and also that there is a large spread in output power for the the same wave state. There are several reasons for these power differences, some are related to the selected control parameters and some are related to the system:

- **Number of PTOs**
  The simulations are performed on a system consisting of five PTOs, while *Lifesaver* currently only has three PTOs installed.

- **Sub-optimal control parameters**
  After installation, much time was spent on verifying system operation through stepwise parameter changes. This has caused a large amount of production data with sub-optimal parameter settings, and is the cause of many of the poor production series close to the design wave state.

- **Unwanted system behavior**
  In higher production states, the winch and floater system occasionally showed rapid vibrations in the primary mooring force, as plotted in Fig. 3.14(b). This is believed to be caused by the dynamic response of the primary mooring, which results in an unforeseen aggregate system response. Similar behavior has been described in related systems [41], and pose a challenge to tight moored WEC systems. On *Lifesaver*, the oscillations are mainly excited when the generator shifts from damping control to saturation control, and can be reduced by smoothing this shift. Until the issue with oscillations is managed, conservative control parameters are set for the high wave states. This is the cause for the low production in the high wave states.

- **Secondary mooring system**
  Due to the strict regulations on FaB Test, *Lifesaver* is equipped with a strong five-point catenary mooring system, in addition to the regular production moorings. This is undesired from an energy point of view and is expected to cause some reduction in production. An example of the mooring forces experienced in the secondary mooring lines is plotted in Fig. 3.14(d). The effects of the moorings are currently not taken into consideration in the simulation model. To get a better understanding, this should be included in the model, and could for instance be implemented as described in reference [12].

- **Floater height**
  The floater was intentionally designed shallow to reduce the system cost and the horizontal forces, and to gain experience with required height and draft in an optimized system. Data from on-board draft sensors show that the waves are frequently over-topping the device already in the design wave state. Some power production is believed to be lost to this

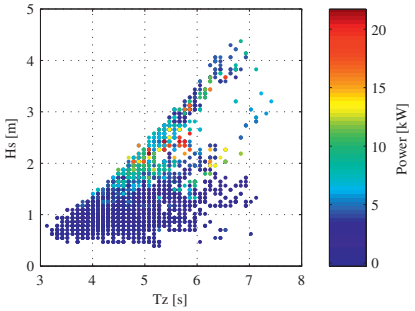

(a) Exportable electrical power for various sea states measured through one year on FaB Test

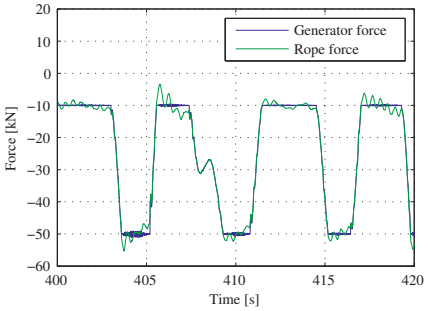

(b) Oscillations encountered in primary moorings due to system dynamics

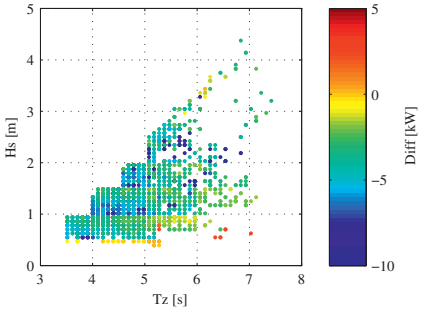

(c) Difference between actual produced power and simulated produced power for various sea states. Simulations are performed with actual parameters and configuration used at FaB Test.

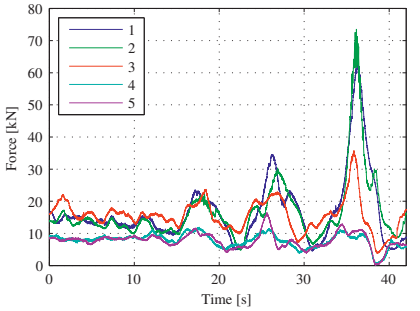

(d) Forces encountered in secondary moorings during normal production in a high sea state. The mooring lines are evenly distributed along the floater circumference in counter-clockwise order.

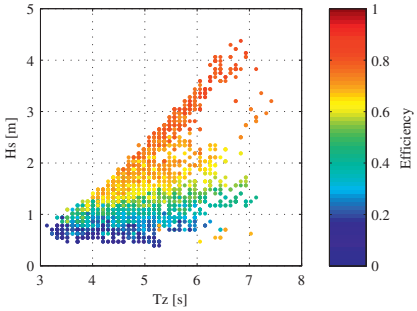

(e) Conversion efficiency: Ratio between actual exported electrical power and actual absorbed mechanical energy for various sea states experienced at FaB Test.

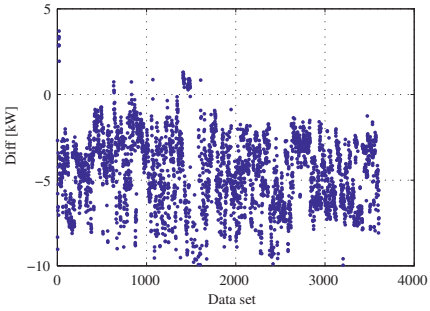

(f) Difference between actual produced power and simulated produced power for all logged data sets. Each data set lasts for 20 min. Simulations are performed with actual parameters and configuration used at FaB Test.

Figure 3.14: Measurement results from FaB Test

due to reduced buoyancy and stability. In the simulation model, the buoy is modeled with infinite height. The effect of over-topping is difficult to model and the impact of this on production output is unknown.

To investigate further on these effects, the simulation model was adjusted to match the number of PTOs and the control parameters used in the measured production series. Fig. 3.14(c) shows the difference between simulated produced power and actual produced power for all production series. The figure shows a good correlation between measured production and simulated production, but with a clear tendency of the measured production being lower than the simulated production. This is most likely caused by the combination of the secondary mooring damping and the unwanted over-topping of the device.

Upon close study of Fig. 3.14(c), several non-conform measurements point out. The steps observed to the left in the plot are caused by wave states that where not simulated, and the corresponding measurements are removed from the plot. The horizontal lines are caused by merging the observed wave states into the simulated windows of wave height and period, and there is an obvious trend of improved production towards the top of the wave height window. There is also a trend towards lower power deficit at higher periods, but the cause of this is currently not identified. Some groups of data points show large deviations from the general trend, mainly the lower row of orange to red dots and the band of dark blue dots at 2-3 m H_s. The former is believed to caused by a measurement problem in the wave rider buoy where long swells with high period and low amplitude is sometimes missed in mixed wave patterns. The latter group is probably caused by manual intervention causing startup or shutdown, which leads to lower average power for the measurement series. In an attempt to investigate further on the deviation between simulated and measured production, Fig. 3.14(f) was produced, and shows all production series up to date in chronological order. The figure could reveal time dependent effects on the measured production, such as degrading or improving friction in the PTOs, but the figure does not give any clear trend towards this.

The generator system at *Lifesaver* estimates the actual torque on the generator shaft with high precision, and also measures the exported electrical power. This opens for accurate measurement of the generator efficiency and can be used to verify the figures obtained through simulations. The actual conversion efficiency is calculated and presented in Fig. 3.14(e), and includes the measured generator and inverter loss, in addition to the estimated mechanical loss. The figure shows that there is a strong dependency between system efficiency and wave height, which is supported by the theoretical work, and is mainly linked to the generator speed. As the damping force follows the thick black line drawn in Fig. 2.16, it can be seen that the speed has to go beyond the 0.3 m/s threshold to enter force saturation before the efficiency starts to move towards an acceptable level.

As *Lifesaver* is currently not grid connected, the system has to produce net positive power to stay in operation. When the net production drops below zero, the system automatically shuts down and enters a power save mode with minimum power consumption. Shutdown typically occurs between 0.5 m and 0.6 m H_s, but has been measured as low as 0.4 m H_s for higher periods. This ability to maintain net power production at such low levels is unique for *Lifesaver* when compared to FO's earlier devices, and is made possible by the electro-mechanical PTO configuration, as opposed to the earlier systems that relied on hydraulics, either directly or indirectly. This allows for high uptime, and may result in continuous production on high energy sites. High uptime results in more load hours and is good for the energy balance as the WEC will always consume some power for monitoring purposes.

3.5 System operation and availability

Lifesaver has been in operation for more than two years and has given significant experience on how to operate and maintain a WEC system over time. The key performance indicators up to date are listed in Table 3.4 and shows that the system has been available for production for the majority of the deployment time. A graphical presentation of the KPIs is plotted in Fig. 3.15 and gives an impression of the of accessibility of the device, and the WEC production state. As FO gained experience with the system, it was discovered that *Lifesaver* could maintain net positive power production down to $H_s = 0.5$ m, and subsequently the wave height threshold for production startup was lowered in September 2012. This contributed to a significant share of the increased production availability seen in Fig. 3.15 after this date, together with rougher weather as the autumn season set in. The accumulated energy production for the first year of the test period is plotted in Fig. 3.16.

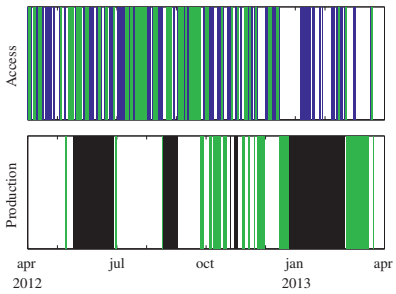

Figure 3.15: **Upper plot:** *Lifesaver* accessibility (Green = accessible for heavy lift, Blue = accessible for maintenance). **Lower plot:** *Lifesaver* production state (Green = production, White = ready for production, Black = Planned or unexpected downtime).

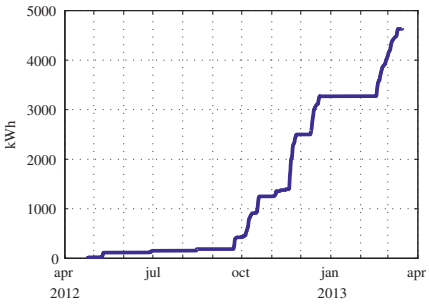

Figure 3.16: Accumulated electrical energy produced at *Lifesaver*

It is important to note that the goal of the *Bolt2Wavehub* project is not to maximize power output, but to gain experience with all the operational aspects of running a wave energy power plant. The FaB Test site was selected for its high availability for maintenance and moderate wave climate, which allows for close monitoring of the device, and is crucial for providing practical feedback into the design process, and to understand the operational expenditures (OpEx) of operating the device. Moreover, the device has been used as a test bench for testing out different maintenance methods. In one instance, when a mechanical component had to be replaced in all three PTOs early in the test period, two different maintenance approaches were tested out. The first PTO was lifted off and brought ashore for maintenance, as shown in Fig. 3.13, while the second PTO was serviced on site. It became clear that heavy-lift operations between two moving objects demanded much calmer weather than on-board maintenance, and the latter method was chosen for the remaining PTO, and has later been adopted as the preferred approach. Except for the heavy-lift trial, all maintenance during the test period has been performed on site.

The most critical component on *Lifesaver* for reliable power production is the production mooring, usually referred to as *primary mooring*, due to the high wear on the winch. FO has put serious effort towards investigating alternative line types and winch mechanisms. Most of the

Table 3.4: Key performance indicators

Production hours	1 468	h
Electrical energy produced	4 644	kWh
Mechanical energy absorbed	7 192	kWh
Overall efficiency	64.6	%
Average power during production	3.2	kW
Time on site	376	days
One or more PTOs ready for production	234	days
All PTOs ready for production	23	days
Longest continuous production period	24	days
Time available for maintenance	211	days
Availability hull	100	%
Availability communication	98	%
Availability scientific instrumentation	79	%
Availability control dependent instrumentation	100	%
Availability storm moorings	100	%
Availability cooling system	99	%

downtime on *Lifesaver* is related to the primary moorings, either due to planned maintenance for switching winch components, or due to unexpected failures in the primary mooring. The winch concept currently pursued is a high performance system with high potential lifetime, but is more fragile to abnormal loads and wear mechanisms, which has caused problems in the early stages of testing. The issues with the primary moorings are not yet solved, but significant steps have been taken towards a reliable system in close collaboration with with the manufacturer, and we have reason to believe that the reliability will be improved to a level suitable for commercial operation within the remainder of the *Bolt2Wavehub* project.

3.6 Concluding remarks

Lifesaver has showed good performance at FaB Test with no major incidents or problems, and has demonstrated acceptable power production and reliability. The FaB Test test site has a moderate wave climate with good availability for maintenance, and has proved to be a valuable test site for gaining operational experience and testing out various maintenance methods. The practical work has shown a clear advantage towards on-board maintenance, as opposed to bringing heavy equipment ashore. The main failure mode causing downtime on *Lifesaver* is failing primary moorings. This is a well-known challenge with this kind of device, and FO is pursuing several paths towards solving this issue. Although the primary moorings are not yet performing flawlessly, significant steps have been taken in the right direction, and there is reason to believe that the problem will be solved within the remainder for the test period. Thus, *Lifesaver* should soon be ready to operate on a commercial level, although elevated monitoring and maintenance must be expected for still some time.

Chapter 4

Wave farm design

Synopsis

In Chapter 4, a wave farm consisting of multiple *Lifesaver* devices is analyzed with focus on optimal positioning with respect to output power quality and accumulated power output. The detailed power system layout required for grid code conformity is described and the amount of produced power that can be exported is evaluated. The ratings of the power components are found by optimizing the component cost versus the value of the transferred energy.

Contents

Related publications

4.1 Introduction

As demonstrated in Chapter 1, the power level and power quality from a single WEC is to low to efficiently utilize installed grid export capacity. In a grid connected wave energy system, power must be leveled, either by storing energy or through aggregate power smoothing, which takes advantage of the natural wave propagation through a series of WECs. Substantial work has previously been performed within this topic, and the articles [4, 22, 40] demonstrate successful integration of WECs into farm systems.

The main goal with respect to power quality is to reduce the required rating on the power transfer system to reduce cost. The focus in this chapter is the specific integration of multiple Lifesavers into a WEC farm system, and the potential for economical optimization of the power transfer chain from wave to wire. It is convenient to split the system into three system levels for the analysis:

- **WEC**
  The WEC represents a single buoy equipped with one or more PTOs. The PTOs produce power at low voltage DC (approximately 600 VDC).

- **Array**
  Several WECs are mechanically and electrically interconnected into an array. The array is equipped with a DC/AC converter and step-up transformer for power export.

- **Farm**
  The farm us built up by several arrays to meet the required rated output power capacity. The exported power from the arrays is collected in the farm hub and exported to grid.

The function, configuration and design of these system levels are described in the next sections.

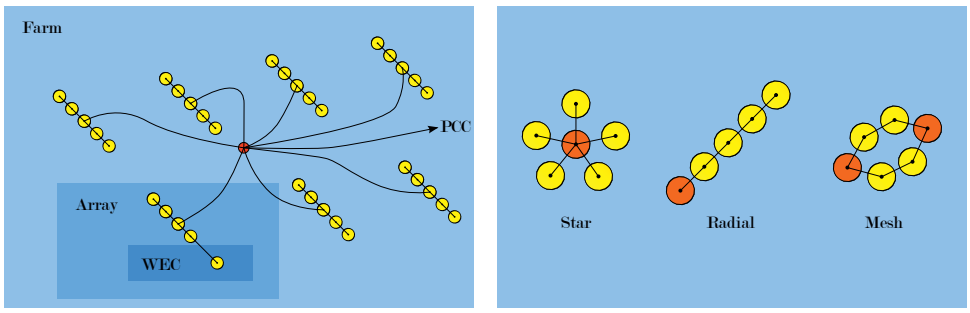

(a) System levels (b) Network types

Figure 4.1: Wave farm configuration

4.2 Array topology

The arrays are practically sized groups of closely spaced WECs. FO's current design philosophy is to mechanically link the buoys together, as indicated in Fig. 4.3. This allows for running the electrical cables directly between the buoys, and makes it possible to share parts of the mooring

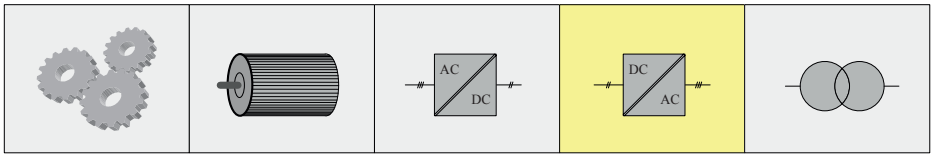

Figure 4.2: Power chain: Array inverter

system. Moreover, the mechanical interconnection can make it possible to handle an array as a single unit during tow out and installation. Although such a closely spaced configuration would attract strong lateral forces, the savings on moorings, cables and installation is expected to outweigh the cost of added mechanical reinforcement.

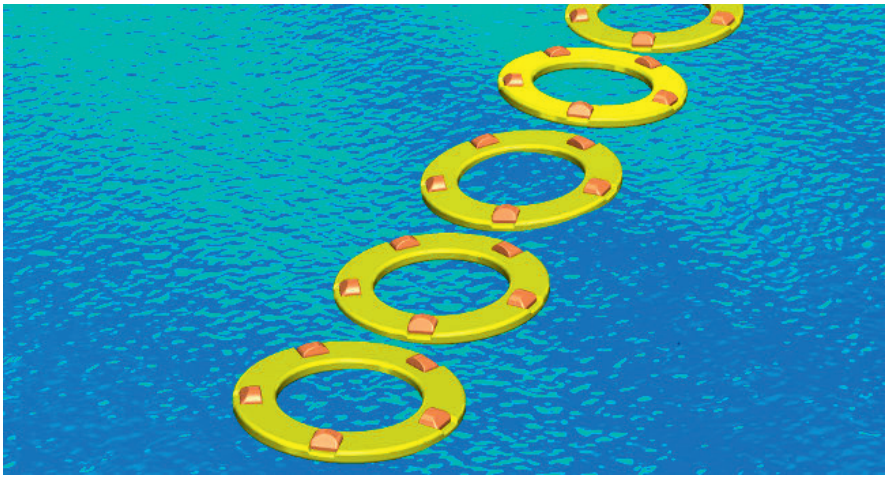

Figure 4.3: Artistic impression of an array of Lifesavers

The WECs interconnects on the DC-bus of the PTO inverters and has a bus voltage of approximately 600 VDC. A guide line current limit of 1 000 A is selected to avoid impractically large and complex cable systems on the flexible interconnectors between the WECs, which leads to a total power capacity of 600 kW on the array bus radials. The total array capacity may be increased further by using alternative network configurations with several parallel arms, as illustrated in Fig. 4.1(b).

The power produced within the array is collected in the array power hub, and is converted to medium voltage AC for export. The array power hub holds a DC/AC converter and step-up transformer, as illustrated in Fig. 4.4. The power hub may also hold an energy storage to reduce the fluctuations in power output, which can reduce the required export capacity. The balance between energy storage capacity and power transfer capacity must be optimized from an economical view point, and is investigated in section 4.6.

The array can also be configured to improve the array output power quality with clever positioning of the individual WECs, and the idea is to ensure that the incoming waves interferes sequentially with the WECs, which requires the array to be oriented along the incoming wave

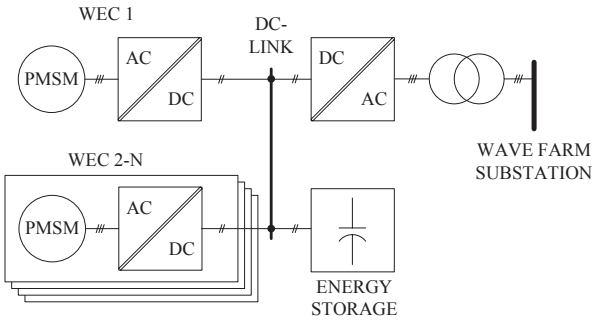

Figure 4.4: Electrical configuration of an array

direction. However, this causes shadowing effects where the rear absorbers operate in the wake for anterior absorbers, which reduces power output. Maximized power capture is obtained when the array is oriented with the broadside against the waves, so that no shadowing effect occurs. This problem is illustrated in Fig. 4.5, and was extensively studied in the articles attached in Appendices C,D and E.

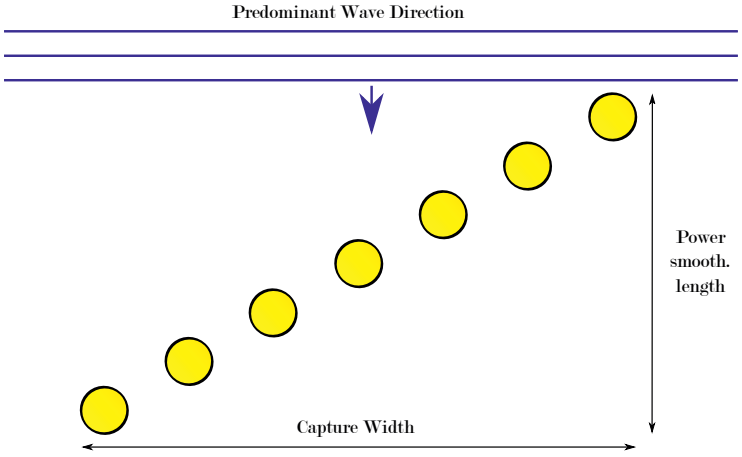

Figure 4.5: Array configuration

Appendix C shows that the array should have a size that corresponds to at least one wavelength along the predominant wave direction to ensure sufficient power smoothing. This is equivalent to a row of about seven devices of the Lifesaver type, and this is used as array size in this analysis. The effect of interference between the WECs is studied by using the methodology established in section 6.2, and significant reduction in production output power is demonstrated as the devices moves into the shadow of anterior devices. A complete simulation scan of all array-to-wave angles between 0° and 90° where performed, which covers all possible wave directions and array installation angles due to symmetry. The typical interference patterns found by the

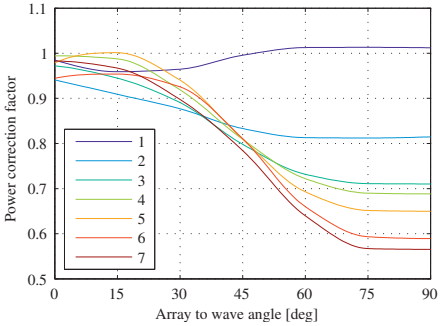

(a) Power output factor for seven individual WECs in an array as function of installation angle. At 0° the array is oriented with the broadside against the waves.

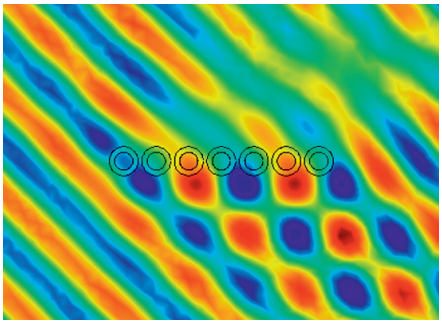

(b) Hydrodynamic interference between WECs in an array due to diffraction and radiation. The waves originate from the lower left corner.

Figure 4.6: Interference within the array

simulation model is shown in Fig. 4.6(b), and the results plotted in Fig. 4.6(a) shows the power correction factor for each of the seven absorbers for different array-to-wave angles. The simulated output power from a WEC in an array is multiplied with the corresponding correction factor to calculate the actual power output including interference effects. The array-to-wave angle is defined as zero when the waves hit the array on the broad side. The plot demonstrates the effect of shadowing, and indicates a reduction in power output of almost 50% for the rear devices in the 90° case. Based on this analysis, an installation angle of 45° is found to be optimal and is used as basis for this work.

The selection of seven absorbers in the array leads to a total installed power of 525 kW in the array, and fits quite well with the earlier established limit of 600 kW per branch. One of the absorbers must house as the array power hub, and while one of the end absorbers would have easiest access for both the export cable and personnel for inspection, placing it in the middle of the array would half the required cable rating between the absorbers. The centralized alternative could possibly allow for doubling the array size to 14-16 absorbers.

4.3 Farm topology

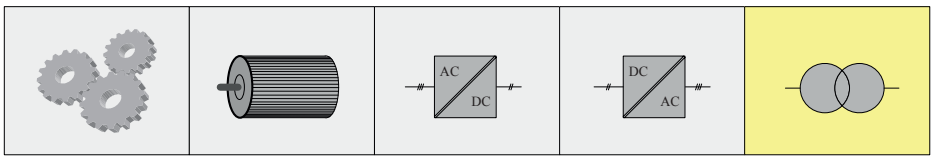

Figure 4.7: Power chain: Grid transmission

Several arrays can be interconnected to form a wave farm. There is virtually no limit to how large a wave farm can be, however large farms could require additional substations and voltage levels to improve the power transfer capacity within the internal farm network. Positioning of the individual arrays must follow the same guidelines as for the WECs, the goal is to minimize the

shadowing effects and to maximize the power smoothing effect. The farm configuration shown in Fig. 4.8 seeks to achieve this by following the diagonal principle established in section 4.2. In an attempt to increase the absorbed power, the arrays are organized into two main arms to form a wedge profile that should focus the waves and increase the total power output. This effect is hoped to compensate for some of the lost power due to negative interference between the WECs and will subject to detailed analysis.

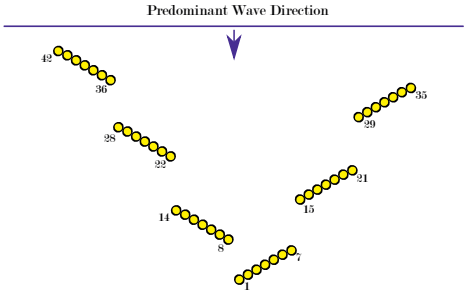

Figure 4.8: Depiction of anticipated WEC farm consisting of 42 buoys

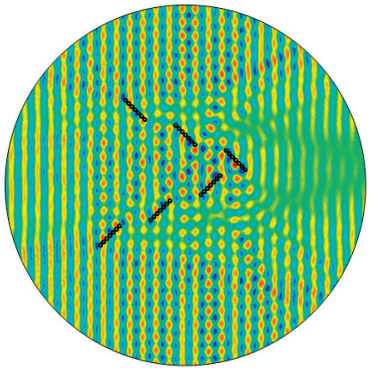

Figure 4.9: Illustration of interactions between absorbers in farm

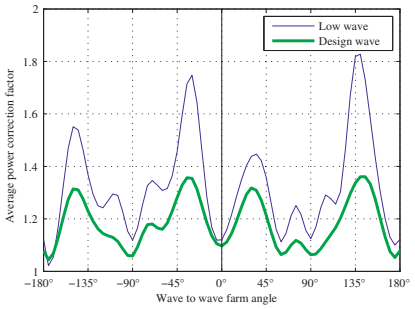

Figure 4.10: Average correction factors for the farm

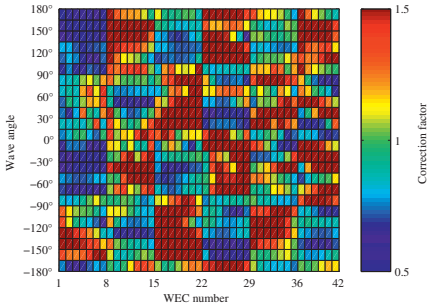

Figure 4.11: Contour plot of compensation factors at design wave state

The entire farm configuration was programmed into to the multi-body simulation model to evaluate the farm layout and to analyze the aggregate interaction within the farm. A typical interference pattern produced by the simulation is pictured in Fig. 4.9. The farm setup was based on the configuration shown in Fig. 4.8, which consists of six arrays of seven absorbers, which leads to a total of 42 absorbers. Since the system is no longer symmetrical, all directions from 0° to 360° must be simulated. Fig. 4.11 shows the resulting correction factors for the design wave state, and demonstrates that several of the absorbers actually achieve power amplification from this setup. The WEC numbers correspond to Fig. 4.8, where the bottom WEC is number one, and the WEC numbers ascends along the y-axis. The total power factor for the entire farm

is plotted in Fig. 4.10, and verifies the positive effect of the wedge profile as each WEC produce more power on average in the farm than in stand-alone configuration. As expected, the effect is stronger for shorter waves, as these are influenced more by the WECs. The figure demonstrates the success of the wedge profile as the average correction factor is above unity. However, it must be taken into account that this kind of analysis is very sensitive to small changes in wave direction and frequency, and actual performance could deviate significantly from the simulated results. These results should therefore be used with care.

The farm electrical power system topology is illustrated in Fig. 4.12. The power cables from the arrays are brought together in the farm power hub for transmission to grid at medium voltage AC. The farm power hub may hold a transformer to further step-up the voltage before transfer, depending on the voltage at the *Point of Common Coupling* (PCC). The farm could also hold extra power conditioning equipment and energy storage, if necessary, and is discussed with respect to grid code requirements in section 4.7.

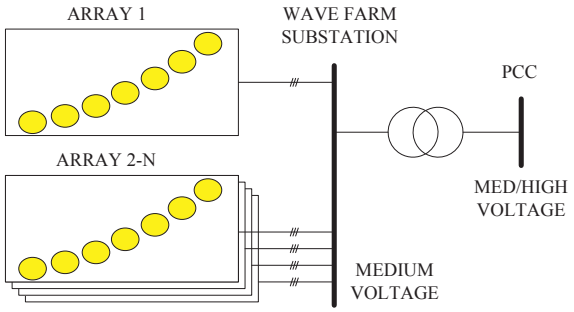

Figure 4.12: Electrical configuration of a farm

4.4 Instant power output

To take the high variability of the incident waves into consideration, the instant power output of the farm is calculated based on the time domain simulation model described in Chapter 6. Each WEC is simulated individually by calculating the incident waves for the specific WEC location, and the power output time series of one hour with 10 Hz resolution is returned for each WEC. Fig. 4.13(a) plots the power output from all 42 WECs individually, and demonstrates the power output delay between the devices as the waves propagates through the farm. The figure also shows how the shape of the wave changes as it propagates, which is caused by the different frequency components of the wave traveling at different speeds.

As previously discussed in section 1.5, and illustrated in Fig. 1.5 on page 10, the WEC output power fluctuations are caused by two different mechanisms, the fluctuation within a single wave, and fluctuations between wave groups. The main purpose of the array is to even out the fluctuations within a single wave so that the array produces a stable and positive output. This effect is demonstrated in Fig. 4.13(b), which plots the individual power output of the seven WECs within one array. If the waves were perfectly regular, this could ideally lead to constant power output for an array that was designed to perfectly fit to the wave length. However, due wave group effects, the power output from an array is quite distorted. The purpose of the farm

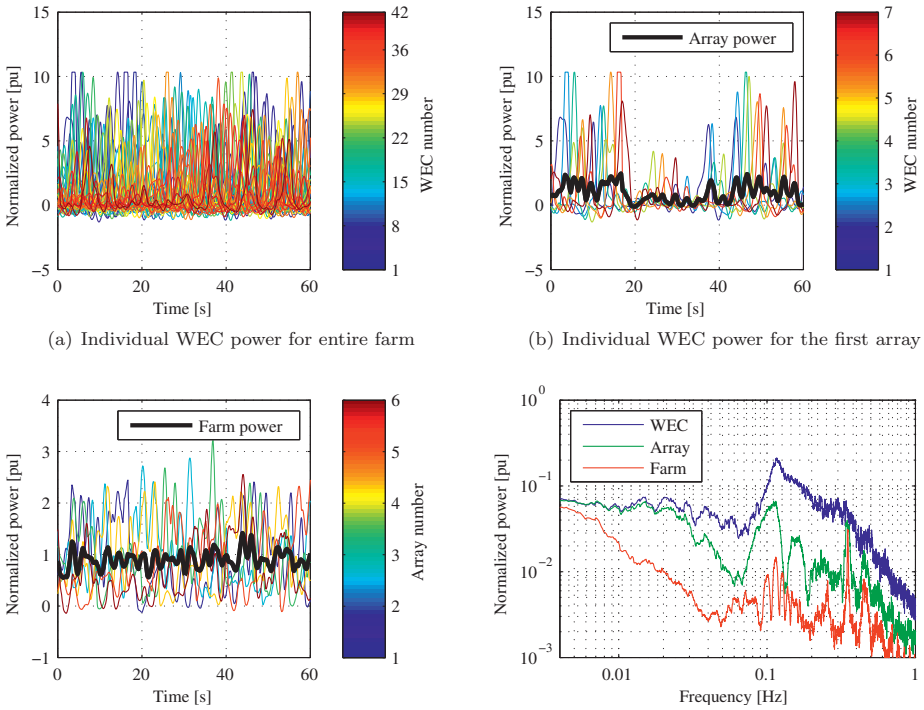

(a) Individual WEC power for entire farm

(b) Individual WEC power for the first array

(c) Average power from each array in a farm

(d) Frequency plot of power output

Figure 4.13: Farm behavior at design wave state with optimal wave direction

is to provide smoothing in the wave group domain, and Fig. 4.13(c) shows the aggregate output of the six arrays in the farm. The smoothing effect is clearly demonstrated, and also indicates that larger farms with additional arrays spatially distributed would further improve the power output quality.

Since most of the described wave effects are frequency driven, it is interesting to also evaluate the frequency response of the system. Fig. 4.13(d) shows the power output curves in the frequency domain, and demonstrates that the farm to some extent works as a low pass filter. Most of the high frequency fluctuations are effectively damped, while the lower frequencies pass with less attenuation. In general, the figure demonstrates the success of the farm configuration, in that the slow fluctuations in the 10-100 sec domain are effectively damped. However, the figure also demonstrates that some of the high frequency fluctuations pass virtually undamped. There is for instance a strong peak around 0.35 Hz that shows little attenuation. This disturbance is most likely caused by interference patters within the farm, and such side effects must be expected in a system of this complexity level. High frequency fluctuations are of less concern since they can be smoothed out with a small energy storage. Nevertheless, these effects will increase the complexity of the control system, and may reduce the output power quality, especially with respect to flicker, which is discussed in section 4.7.

4.5 Annual power output

The instant power simulation in the previous section gives a good understanding of the exported energy and the power system behavior for a specific wave state. The next step is to estimate the annual power output of the farm so that the system performance can be evaluated in economical terms. This will have to take into account the changing wave states and the actual wave directions for a specific site, and the natural choice is to use the Wavehub site that has been closely monitored for several years. FO has access to most of these data and a detailed wave scatter diagram has been established that takes into account wave height, period and direction. The process of establishing these wave data is described in section 6.3.

Based on the wave climate details, an extensive database was built that contains production data for all the individual buoys in the farm for all the wave states and directions in the wave scatter. In total this amounts to ca 12 000 individual WEC simulations, which required about four weeks of CPU time on a normal desktop computer. However, by using three multi-core computers running multiple processes in parallel, the entire simulation set was completed in less than five days. Each wave state was simulated for one hour with a resolution of 0.25 m on wave height, 0.5 s on period and 15° on direction. This totaled 10 GB of simulation data, and must be viewed as a *brute force* method, as several steps could have been taken reduce the simulation task. Nevertheless, with the easy access to processing power, there was no reason to optimize the simulation, which would have added complexity.

A full year of wave production from the entire farm was created by concatenating the required wave states from the database based on the probability given in the wave scatter diagram. The time series were expanded or trimmed to match the actual number of annual hours for each wave state. Since the wave climate scatter only holds statistical data that gives the probability of a wave state, it was not possible to create an annual time series that replicates the actual weather patterns, instead the time series consists of wave states in ascending order. This does not affect power output or the power system in this case, but becomes important for long term storage solutions, which is covered in Chapter 5.

The annual output from the farm amounts to 16.73 GWh, which equals 5 312 annual full load hours, according to the simulation. This is the gross production from the farm and does not take into consideration losses or power capping in the farm power collection system. To find the actual load and utilization of the power transfer components, annual distribution diagrams are created that shows the power distribution over the year. These diagrams are made by sorting all the samples from the power time series in descending order. This shows the number of hours per year each power level occurs and gives a good impression of the system utilization and provides useful input to the power system optimization performed in the next section. Several power distribution diagrams are plotted in Fig. 4.14 with corresponding time series examples to demonstrate the relationship between time series data and the annual distribution. Fig. 4.14(a) and 4.14(b) shows the raw output from WECs without taking into consideration the interference between the absorbers. The WEC power output has power peaks up to 10 pu, but is capped in the figure to better show the array and farm response. In Fig. 4.14(c) and 4.14(d) the output power is corrected for interference between the absorbers. Fig. 4.14(e) and 4.14(f) shows an example including power capping and storage in the power system. The figures show that the installed power capacity above unity is poorly utilized, and methods to improve this are addressed in the next section.

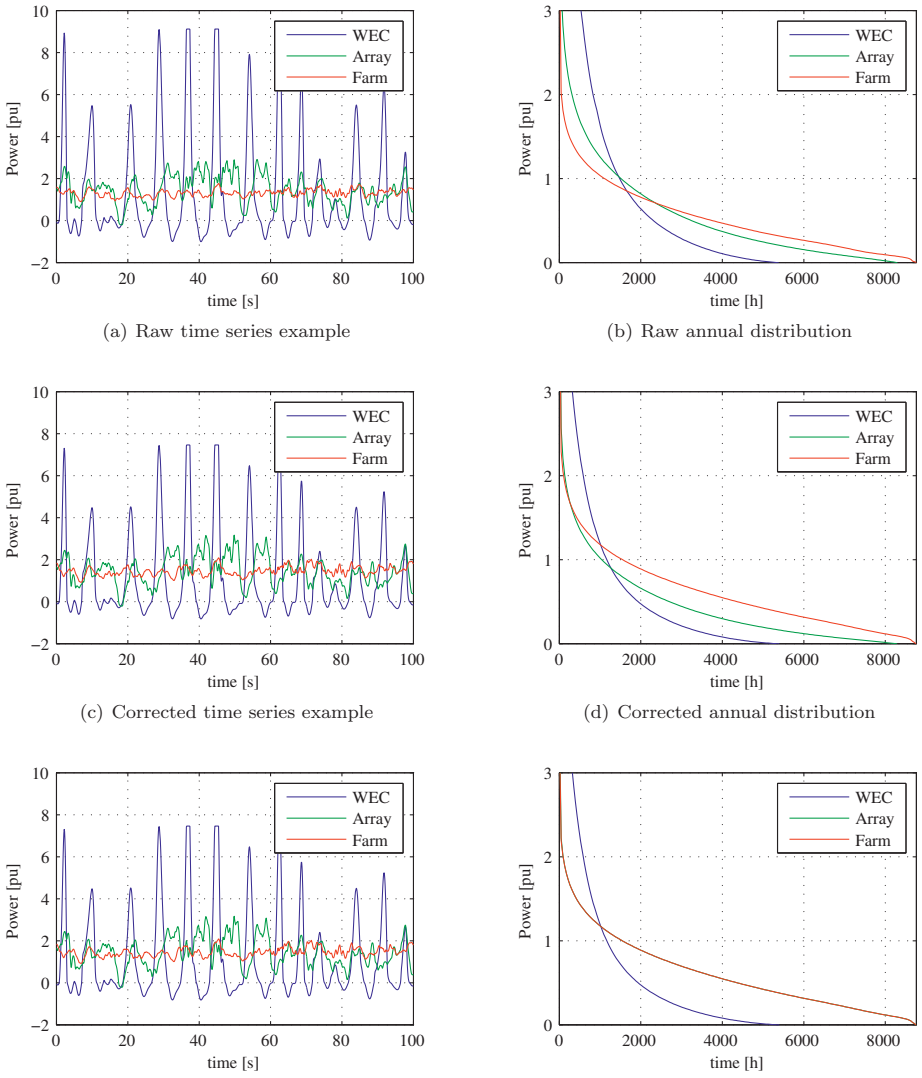

(a) Raw time series example

(b) Raw annual distribution

(c) Corrected time series example

(d) Corrected annual distribution

(e) Cap and stored time series example

(f) Cap and stored annual distribution

Figure 4.14: Annual power output distribution

4.6 Power system optimization

The next step is to size the power system in more detail by evaluating the cost of installed transfer capacity versus the revenue of exported power. The mechanisms have already been described and are based on limiting the power transfer capacity, and possibly using energy storage. The goal is to find the power system sizing that maximizes revenue. Table 4.1 lists the economical input data used for the optimization, and are very rough figures based on general experience gained through the FO wave energy project. Thus, the results from this analysis should be viewed as guidelines; the merit is to draw the general picture on what an economically optimized system would look like.

System	Unit cost	
DC/AC inverter	80	€/kW
AC/AC transformer	45	€/kW
Energy storage (U.cap)	25	€/kJ
Cable cost	100	€/kW
Array converter	125	€/kW
Farm converter	145	€/kW
WEC device (75 kW)	500	k€/unit
Energy export income*	360	€/MWh

*Energy income based on UK strike price of 305 £/MWh

Table 4.1: System economics

To achieve optimal operation of the power system, complete understanding of the loss mechanisms and limitations must be established so that the system can be pushed to its limit. Power components are usually rated for a nominal current I_n that can be safely transferred during normal operation. For a power system operating with fluctuating power output, calculating the actual component load becomes more complex as several mechanisms come into play. The major limitation for most components is the heat dissipation due to resistive loss, which is given by Equation 4.1 where P_L is the power loss, I_n is the RMS current and R is the component electrical resistance. To obtain the actual temperature of the component, a thermal model comprising heat conductivity and heat capacity could be applied, as described in Appendix H, however a much simpler approach used here is to set the RMS integration time to match the thermal time constant of the component. Equation 4.2 defines the RMS current, where i is the instant current, I is the RMS current and T is the integration time. Equation 4.3 shows the discrete implementation of the RMS calculation used on the simulation data, which calculates the moving RMS value for the sample p with the integration time equal to k samples.

$$P_L = {I_n}^2 \cdot R \tag{4.1}$$

$$I = \sqrt{\frac{1}{T}\int_0^T i\,(t)^2\ \mathrm{d}t} \tag{4.2}$$

$$I_p = \sqrt{\frac{1}{k}\sum_{j=p}^{p+k} {i_j}^2} \tag{4.3}$$

The RMS calculation covers the majority of the component power loss, although there are other important mechanisms that must be considered. The power electronics components are

Entity	**Property**	**Value**	**Unit**
Array			
	RMS current limit	I_n	A
	Peak current limit	$2 \cdot I_n$	A
	RMS integration time	60	s
	Energy storage capacity	E_n	J
Farm			
	RMS current limit	I_n	A
	Peak current limit	$1.4 \cdot I_n$	A
	RMS integration time	600	s
	Energy storage capacity	E_n	J

Table 4.2: Input parameters for the Cap and Store function

based on semiconductors that have fixed voltage drops when they are forward biased, which causes non-resistive losses in addition to the resistive loss. This is the case for both the IGBTs and the diodes in both the generator drive inverter and the DC/AC inverter in the array. Since this analysis relates to the maximum ratings of the components, these non-resistive effects will not affect the boundaries of the *Safe Operating Area* (SOA) , but will cause non-linear effects in the load model. Since this will have little effect in this analysis, the non-resistive effects are not handled separately. A second important factor is non-linear effects that may appear above nominal load. Magnetic circuits may go into saturation, and internal thermal stress may be excessive. Thus, a peak current limit independent of the RMS limit must be defined. Table 4.2 lists the defined parameters used in the cap and store model.

The table defines separate properties for the farm power collection point and the array converter. Since the array converter is a part of the wave power system, an allowed peak power of double the nominal is allowed, as it is believed that the surrounding switchgear and protection equipment can be specified towards this. The DC/AC inverter is expected to have low thermal mass, and the thermal time constant is estimated to 60 seconds. Due to the effect of thermal cycling in power electronic components, pushing the power components towards the nominal operating temperature may be disadvantageous. The effects of thermal cycling due to the wave power fluctuations are studied in Appendix H. The farm power system on the other hand, is expected to consist mainly of transformers and cables with high thermal mass. Therefore, a higher integration time of 600 s is selected. However, since the power must stay within the grid-code requirements, the peak current is set to 1.4 I_n, which is believed to be an acceptable short-term over-current in most systems.

The energy storage incorporated in the simulation model is considered ideal, hence no model related to this is included. However, based on the good experience with the ultracapacitor bank used on Lifesaver, which was described in section 3.2 on page 35, the natural choice would be to use the same system as a starting point. The ultracapacitor bank has demonstrated close to ideal behavior and is compatible with the stated approach. The installed capacity of the energy storage is normalized to $pu \cdot s$, which is relates to the number of seconds the energy storage can supply or absorb the nominal power output, referred to as 1 pu.

Fig. 4.15 shows an example of the cap and store function in action. In the start of the plot, all produced power is exported directly, and the green export curve perfectly covers the blue production curve. Installed transfer capacity in this case is 1.5 pu, which allows the peak power to go up to 3 pu in short periods. However, as the power components heat up, represented by the raising RMS power, the peak power rating must be cut back to nominal, which cause power production in excess of the transfer capacity. This overproduction is initially absorbed by the

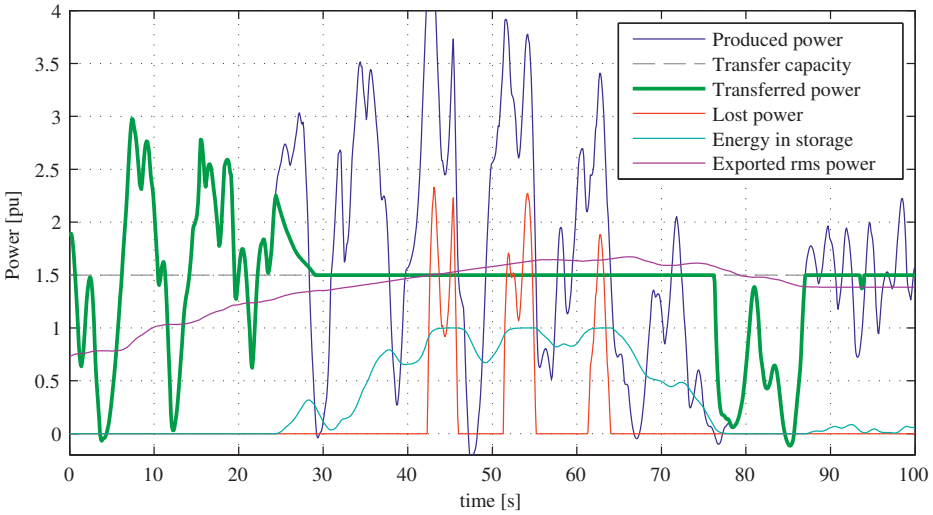

Figure 4.15: Illustration of the cap and store function

energy storage, which starts to charge at t=25 s. At t=43 s the energy storage is full and power production must be curtailed, the lost power is represented by the red curve. It can also be seen that the RMS power actually overshoots the maximum limit of 1.5 pu, which is due to shortcomings in the selected control model and should not be allowed in a real system.

Performing dynamic control of the RMS power actually showed to be quite challenging, as information about the future waves is required to optimize the control. For instance, if the controller knows that there is only a few large waves coming in, it can chose export at maximum power as there will be time for the converter to cool off after the waves has passed. However, if there is a long sequence of waves coming, the converter would quickly become exhausted, and would be forced to reduce to nominal export rating. In this case, the controller should export at a more modest level, and accept some power loss already from the start. This would allow more power to be transferred. There is large potential for improvement for the case shown in Fig. 4.15, but the current configuration is believed to be sufficient for this study.

The power system optimization is performed in two stages. Firstly the array converter power rating and energy storage capacity rating is evaluated based on transferred power and component cost. Secondly, the total power transfer system for the farm is evaluated, taking into consideration the array power system definition. The purpose of the optimization is to maximize the economic performance, and economic indicators for the system must be defined. This analysis is based on calculation of *Levelized Cost of Energy* (LCoE), which take into account the net present value of current and future cash flows for the power plant. LCoE describes the required revenue from electricity sales for the power plant to reach breakeven over its projected life time. Equation (4.4) defines the LCoE calculation where I_t, M_t and F_t denotes the expenditure for investment, maintenance and fuel for the year t. The electricity generation in year t is expressed as E_t, r denotes the discount rate and n is the projected lifetime. In this simulation the discount rate is set to 4 %.

$$LCoE = \frac{\sum_{t=0}^{n} \frac{I_t + M_t + F_t}{(1+r)^t}}{\sum_{t=1}^{n} \frac{E_t}{(1+r)^t}} \tag{4.4}$$

		P_n [pu]							
		1.5	2	2.5	2.75	3	3.5	4	5
E_n [pu·s]	0	185.4	176.5	173.8	173.4	**173.4**	173.8	174.6	176.3
	1	183.0	175.7	173.7	173.5	173.6	174.1	174.9	176.6
	2	181.8	175.4	173.8	173.7	173.8	174.5	175.3	177.0
	3	180.9	175.3	174.0	173.9	174.1	174.8	175.6	177.3
	5	180.1	175.3	174.4	174.5	174.7	175.5	176.3	178.0
	7	180.0	175.6	174.9	175.1	175.4	176.1	177.0	178.7
	10	180.2	176.3	175.8	176.0	176.4	177.2	178.0	179.8

Table 4.3: Levelized cost of energy at array level [€/MWh]

Table 4.3 lists the result of a complete scan of several configuration pairs of installed transfer capacity and energy storage. For each case, the actual revenue of the power that is transported to grid is compared with the cost of the power system. The goal is to find the optimum where any added transfer capacity does not produce additional revenue. The table shows an optimum for installed capacity of three times the average power output and is highlighted in the table. It is also interesting to note that the economical evaluation does not recommend including energy storage, as it seems that additional transfer capacity is less costly.

		P_n [pu]							
		1.5	2	2.5	2.75	3	3.5	4	5
E_n [pu·s]	0	591	788	984	1083	**1181**	1378	1575	1969
	1	669	866	1063	1162	1260	1457	1654	2048
	2	748	945	1142	1240	1339	1536	1733	2126
	3	827	1024	1221	1319	1418	1614	1811	2205
	5	984	1181	1378	1477	1575	1772	1969	2363
	7	1142	1339	1536	1634	1733	1929	2126	2520
	10	1378	1575	1772	1870	1969	2166	2363	2756

Table 4.4: Cost of array converter power system [k€]

		P_n [pu]							
		1.5	2	2.5	2.75	3	3.5	4	5
E_n [pu·s]	0	8.20%	3.06%	1.04%	0.58%	**0.31%**	0.08%	0.02%	0.00%
	1	6.78%	2.44%	0.80%	0.44%	0.23%	0.06%	0.01%	0.00%
	2	5.96%	2.08%	0.66%	0.36%	0.18%	0.04%	0.01%	0.00%
	3	5.33%	1.79%	0.55%	0.29%	0.15%	0.03%	0.01%	0.00%
	5	4.53%	1.40%	0.39%	0.19%	0.09%	0.02%	0.01%	0.00%
	7	4.05%	1.17%	0.29%	0.14%	0.06%	0.01%	0.00%	0.00%
	10	3.61%	0.96%	0.20%	0.09%	0.04%	0.01%	0.00%	0.00%

Table 4.5: Annual lost energy due to power capping in array converter

Table 4.4 lists the actual cost of the power system for the different configuration pairs. Since the cost of the entire WEC farm is 21 million euros, the array power system costs are relatively small at around 5% of the total. Table 4.5 lists the lost power due to the restrictions in the power system. The results demonstrate that an efficient system configuration must allow for some lost power production, nevertheless, the optimal case shows that only 0.3% of the annual energy is lost.

		P_n [pu]					
		1	1.2	1.4	1.6	1.8	2
E_n [pu·s]	0	194.4	185.2	180.5	178.4	**177.9**	178.2
	1	191.1	183.1	179.6	178.4	178.2	178.6
	2	190.6	182.6	179.3	178.5	178.5	178.9
	3	190.6	182.6	179.3	178.6	178.8	179.3
	5	191.0	183.0	179.8	179.2	179.5	180.0

Table 4.6: Levelized cost of energy at farm level [€/MWh]

So far the analysis has only calculated the cost including the array converters. The same procedure must be repeated for the farm converter, and Table 4.6 lists the resulting LCoE obtained by performing the same analysis for the entire farm and shows an optimal configuration of 1.8 times overcapacity and no energy storage. The actual grid cost capacity could be significantly higher depending on the distance from the connection point and the additional requirements for equipment. This would lead the system design towards less installed capacity, and as can be seen from Table 4.7, the loss of production is marginal also for lower capacity alternatives. Higher cost could also favor solutions including energy storage, and as illustrated in Table 4.6, the cost differences between energy storage and additional transfer capacity is quite small. The cost of the power system components is listed for reference in Table 4.8.

Referred to the rated power of the WEC devices, the farm produces 5 290 annual full load hours. However when the exported power is referred to the installed export capacity, the installed overcapacity significantly reduces the amount, as listed in Table 4.9, which yet again demonstrates the difference between wave energy and wind energy. Due to the more stable long-term power flux from the ocean waves, the wave farm produce more full load hours on average than wind turbines, but when the short-term fluctuations are taken into consideration, most of this advantage is displaced by the need for oversized power components.

		P_n [pu]					
		1	1.2	1.4	1.6	1.8	2
E_n [pu·s]	0	9.83%	5.12%	2.37%	0.96%	**0.41%**	0.31%
	1	8.09%	3.82%	1.70%	0.75%	0.36%	0.31%
	2	7.67%	3.35%	1.34%	0.59%	0.34%	0.31%
	3	7.51%	3.17%	1.16%	0.50%	0.32%	0.31%
	5	7.34%	3.02%	1.03%	0.42%	0.31%	0.31%

Table 4.7: Annual lost energy due to power capping in farm converter

		P_n [pu]					
		1	1.2	1.4	1.6	1.8	2
E_n [pu·s]	0	551	662	772	882	**992**	1103
	1	630	740	850	961	1071	1181
	2	709	819	929	1040	1150	1260
	3	788	898	1008	1118	1229	1339
	5	945	1055	1166	1276	1386	1496

Table 4.8: Cost of farm converter power system [k€]

		P_n [pu]					
		1	1.2	1.4	1.6	1.8	2
E_n [pu·s]	0	4790	4200	3705	3288	**2939**	2648
	1	4883	4258	3730	3295	2940	2648
	2	4905	4278	3744	3300	2941	2648
	3	4913	4286	3750	3304	2942	2648
	5	4922	4293	3756	3306	2942	2648

Table 4.9: Annual full load hours referred to installed power capacity

4.7 Grid codes

The wave farm will have to comply with the grid codes in the hosting country, which is a set of rules and specifications on how the power system shall operate. Many of the grid code requirements can be handled at the connection point by installing the correct equipment and protection devices, but some of the requirements may have consequences that reach deeper into the system. This section will explore some of the typical grid codes that may have impact on the wave energy farm.

Flicker

Flicker refers to rapid fluctuations in grid voltage and is defined in the international flicker standard IEC 61000-4-15 [1]. The principle is based on luminosity of an incadecent bulb and the perception to the human eye. The model defines the main property *short term flicker*, denoted P_{st}, that defines the flicker level of a signal over ten minutes. The threshold value of accepted flicker is defined as unity. The flicker model is integrated into power quality meters and used as a standard factor for grid power quality measurements. Another parameter, *long term flicker*, P_{lt}, is based on the short term flicker and is defined as the cubic average of the short term flicker over two hours. The threshold value for P_{lt} is 0.65. Since WEC systems generate fluctuating output power, flicker contribution must be expected. The work of Tissandier et al. [40] shows that flicker can be an issue for WEC systems, hence it is important to analyze the FO system in detail with respect to flicker. The flicker estimates calculated in this work are based on an open source model for flicker provided by *Solcept* [33], and calculates the actual flicker for a given input signal. The Solcept model is based on the work of Mombauer [25] and is in accordance with the international flicker standard.

Flicker is calculated based on line voltage fluctuations, and there is a linear relationship between flicker value and voltage fluctuation. Thus, the impedance of the connection point of the WEC farm becomes very important and may be the limiting factor with respect to flicker. To avoid linking this analysis to a specific grid configuration, a value of the required grid impedance

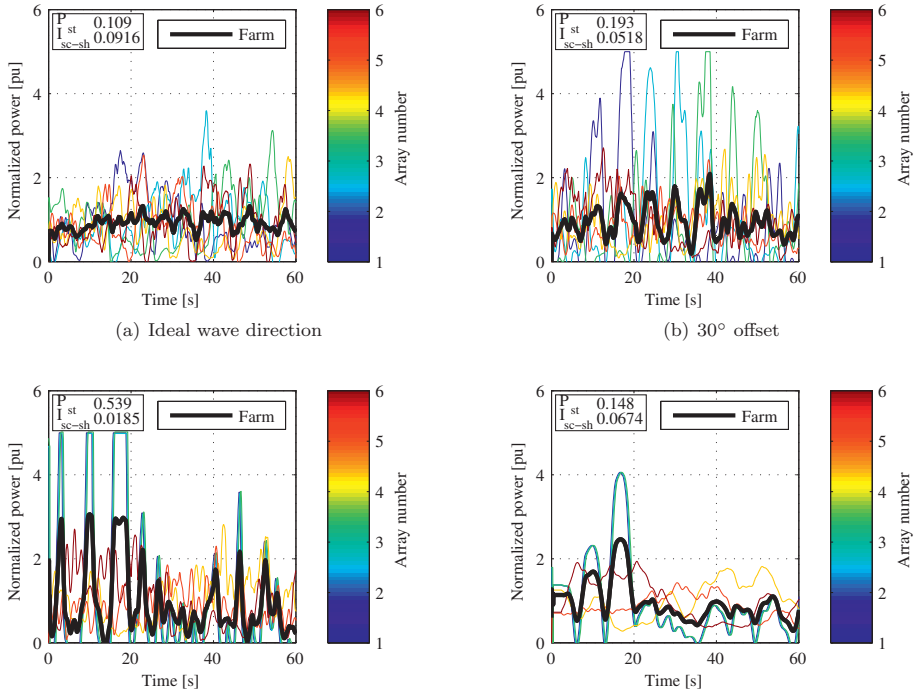

(a) Ideal wave direction

(b) 30° offset

(c) 45° offset

(d) 5 seconds moving average

Figure 4.16: Flicker analysis for different wave directions

is included that shows the required stiffness of the grid connection. The value I_{sc-sh} is defined as the *share* of the available *short-circuit* capacity that can be used wave power export. A value of $I_{sc-sh} = 0.1$ would for instance indicate that the rated output current from the WEC system must be less than 10% of the short-circuit capacity at PCC.

There will also be large differences in flicker due to changing wave climate. The output power level will affect the flicker directly thorough increased amplitude. Moreover, changes in wave direction will change the excitation pattern of the farm and will strongly affect the power smoothing effect, and hence cause more flicker. The analysis presented in Fig. 4.16 are based on the design wave state, which results in power production at rated power. Each subfigure lists the resulting flicker level P_{st} for a grid connection with an impedance of 0.01 pu related to rated power of the WEC farm, and the resulting I_{sc-sh} ratio.

Fig. 4.16(a) shows the ideal case where the waves are entering the farm from the ideal direction. This results in a moderate flicker level that can utilize ca 10% of the short-circuit capacity of the grid for electricity production. However, as the wave direction deviates significantly from the preferred direction, the flicker level rises drastically as shown in Fig. 4.16(b). Fig. 4.16(c) shows the worst case direction where one of the two arms of the farm hits the incident wave with the broad side. This causes severe flicker and only allows the WEC farm to utilize 1.9 % of the short-circuit capacity. Nevertheless, as demonstrated in Fig. 4.16(d), the flicker can be significantly reduced by filtering. The figure shows the resulting flicker after application of a

5 second moving average filter on the power output of the case presented in Fig. 4.16(c).

This analysis shows that the WEC farm will produce significant flicker that will have to be taken into consideration. The flicker levels presented here are very high, but it is also important to take the size of the wave farm into consideration. The system modeled here has a rated power of 3.15 MW, which could be insignificant for a strong grid connection point. An important aspect is how the flicker would aggregate from a larger farm. It is expected to decrease due to increased smoothing effect, but this is not verified. There are also large possibilities for actively reducing the flicker through system regulation and/or control of the energy storages. However, this initial analysis demonstrates that flicker evaluation must be an important parameter in wave farm design, and that some cost elements related to flicker reduction must be expected, either by managed power shedding or by filtering equipment.

Fault ride-through

Fault ride-through is a principle that asks for continued power export from the power plant during a low voltage fault at the PCC. This is important in situations where a fault occurs somewhere in the grid that causes the grid voltage to drop below accepted voltage. The fault can typically be power line failure, loss of production capacity or sudden increase in load. The natural response of a connected power plant would be to perform safety shutdown and wait for grid balance to be restored. However, if all generation capacity followed this principle, the power deficit could be rapidly aggravated, causing cascading black outs through the grid. Thus, the grid code calls for fault ride-through, which means that the power producers shall continue to deliver power during such an event to help restore grid balance. Since the DC-system for each array will be separated from the AC grid, this requirement will only influence the DC/AC inverters in the array hubs. To be fault-ride-through compliant, the inverters would have to be designed to operate in a wider voltage range. In theory this should not be a problem, but the actual configuration of the available hardware could be incompatible. Fault ride-through must therefore be included as a part of the requirement specification.

Reactive power

The wave power station can be asked by the utility to consume or supply reactive power, or alternatively to be supporting various voltage regulation strategies that involves transferring reactive power. This also influences the array hub DC/AC inverters, but should be relatively straight forward as many converter systems natively support reactive control regulation. However, significant transfer of reactive power will displace capacity for active power and will increase the required power rating of the transfer equipment. This is not investigated further in this work.

Advanced reactive/harmonic correction

The inverters used to convert DC to AC in the array converters are full bridge IGBT converters, which gives high flexibility and accuracy on controlling the output current flow. This capacity could be utilized to improve the grid power quality by stabilizing the power flow. Equation (4.5) and (4.6) shows a technique described by S.Fryze [13] that allows for instant power correction, that can compensate both imbalanced power flow between phases, fluctuations in power flow and harmonic distortion [3]. The amount of energy that can be stored to balance the power flow is adjusted by setting the integration time constant T, i and v refers to the instant current and voltage indexed by the phase indices a, b and c. The index $\bar{q}$ refers to the resulting phase compensation current.

$$\begin{bmatrix} i_{\bar{q}a} \\ i_{\bar{q}b} \\ i_{\bar{q}c} \end{bmatrix} = \begin{bmatrix} i_a \\ i_b \\ i_c \end{bmatrix} - G_e \begin{bmatrix} v_a \\ v_b \\ v_c \end{bmatrix} \tag{4.5}$$

$$G_e = \frac{1}{T}\int_0^T g_e(t)\,\mathrm{d}t = \frac{1}{T}\int_0^T \left(\frac{v_a i_a + v_b i_b + v_c i_c}{{v_a}^2 + {v_b}^2 + {v_c}^2}\right)\mathrm{d}t \tag{4.6}$$

The wave energy farm is ideally suited to perform such compensation tasks since it already has the required power system to do so, both in respect of energy storage and converter capacity. The best solution would be to perform such tasks when the wave energy production is below nominal so that the spare converter capacity could be utilized. Unfortunately, regulations for economically compensating such services are not in place today, and it will be difficult to gain revenue from performing such action. However, for utilities that experience high distortion in the grid that violates the grid codes could install a WEC farm under the premise that such correction is performed. Hence, this extra functionality could benefit the system, and help wave energy to market entry.

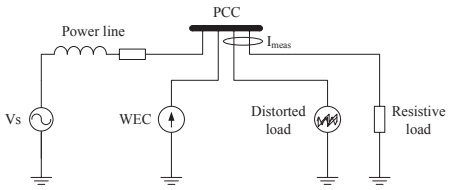

Figure 4.17: Simulation model for instantaneous power quality analysis

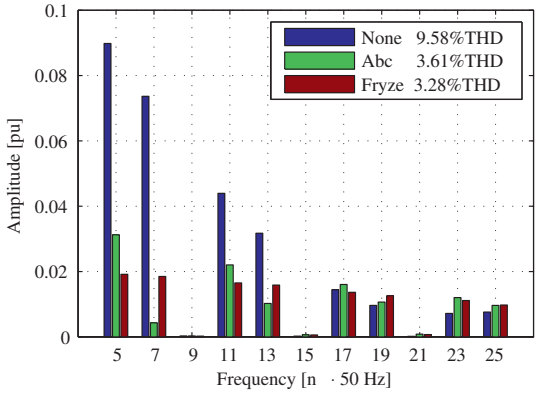

Figure 4.18: Harmonic distortion of the PCC voltage

Fig. 4.17 and 4.18 presents the system setup and results from a simulation with a wave farm compensating a distorted power system. The simulation case is based on a weak grid scenario where local distortions cause poor power quality in the system, described by the *Total Harmomic Distortion* (THD) referred in Fig. 4.18. As illustrated in the figure, the WEC farm has strong

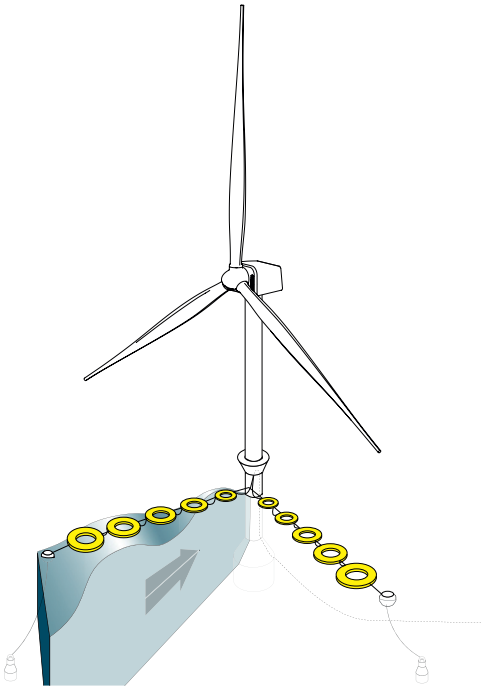

Figure 4.19: Combined wave and wind installation.

impact on the low harmonic frequencies that would otherwise be hard handle by passive filters. Detailed method and results are described in Appendix G.

4.8 Wave and wind integration

One of the major cost barriers for wave farms is the high cost of installing the power cable to grid. Offsetting the cable costs would require a very large wave farm, causing a large and risky investment. This poses an investment barrier for wave energy, as investors would like to take small steps, gaining experience while revenue is generated. One option that could reduce this problem is co-locating the wave farm with off-shore wind farms. Many of the good wind sites are also good wave sites, and wind turbines and WECs could share service and maintenance crews and equipment.

The easiest approach would be to treat the wave and wind farms as separate systems, where the only point of integration is the power cable. However, there could be large benefits from doing closer integration where the wind and wave farms also share some of the structure and/or infrastructure. Fig. 4.19 shows an artistic impression of two WEC arrays directly tied to the monopile foundation of a wind turbine. This could help saving most of the costs related to inter-array connections, and could also allow for having the array converter equipment placed in the wind turbine foundation. Obviously, no wind turbines operators would normally allow wave farms to tie on to their structures; however, this could be pursued as a partnership with

a foundation manufacturer, which could supply monopiles with integrated WEC production capacity.

Some benefit could also be gained in the power system, since the fluctuations caused by the WECs would be diluted by the power production from the wind turbine. However, the major cabling cost is related to the shore cable, and since high correlation between wind an wave must be expected, the power cable to shore must have the capacity to transfer the nominal power from both wind and wave farms. Nevertheless, as illustrated in section 1.3, there is a benefit on power quality from combining the wind and wave production.

4.9 Concluding remarks

This chapter has demonstrated the feasibility of the wave farm system, and has showed that the initial high distortion from the WEC to a large extent can be smoothed out by the spatial distribution of the WECs. The peak to average power ratio for the analyzed farm seems to be in the range 1.3 - 1.8, depending on the selection of installed capacity, which is highly dependent on the cost of the shore cable. In this analysis energy storage showed not to be economically beneficial, which results in losing approximately 1% of the annual production. However, the cost gap for energy storage is narrow, and in cases with high cost of the shore cable, energy storage is likely to be beneficial. Referred to rated power of the wave farm, 5 250 annual full load hours are produced. However, when referred to the installed transmission capacity this is reduced to 3 000 - 4 000 hours per year, depending on the selected configuration. Nevertheless, for larger farms, or for combinations with other systems, the required peak to average ratio is expected to sink towards unity, allowing for more than 5 000 annual full load hours to be transferred to grid. This will make wave energy one of the most stable renewable resources, despite of the high level of distortion at the PTO. It is also clear that flicker will be an important factor for system design that could incur significant cost on the system. The effect of flicker is very dependent on the grid capacity and must be evaluated on a site-by-site basis. However, it is also demonstrated that the flicker issue can be managed, and that existing power equipment could be sufficient. Other grid code requirements, such as fault ride-through and reactive power control seems to be easily manageable due to the powerful DC/AC converter used and it was also showed that this capacity could be utilized to perform active correction of existing grid distortions as an extra service to the grid operator.

Chapter 5

Autonomous operation

Synopsis

Wave energy converters can potentially open a new area of applications as it allows for large amounts of power to be produced at sea. This could be utilized in autonomous systems, which are investigated in this chapter, and places high requirements on the power system to deliver stable power from the fluctuating power output from the WEC. Moreover, power must be supplied to the load 24/7, which requires additional on-demand power sources for calm weather. The general requirements for such systems are discussed and a case with a 100 kW continuous load requirement is analyzed.

Contents

5.1 Introduction

Wave energy converters produce electrical power at sea, and since the oceans cover approximately 70% of the Earth's surface, this opens the possibility to operate power consuming systems in remote locations far from shore. Many such systems exist today, and are mostly powered by solar panels. For low power systems that requires less than 50 W continuous power, solar is likely to be the preferred energy source since PV-cells are reliable, light-weight, modular and simple to operate.

However, devices that require more power becomes very hard to operate with available technology, as there are few alternatives to PV. Wind turbines can supply additional power, but places strict requirements on the buoy design and stability, and are vulnerable in rough weather. Therefore, WECs could show to be very interesting for ocean based autonomous systems with its ability to tap into the high power density of ocean waves. Moreover, the ability to utilize existing floater structure and moorings for energy production can make wave energy a low cost option for autonomous power systems at sea. The following sections explore the requirements and possibilities for such systems, and discuss the required power system configuration for high power autonomous system.

5.2 Required power system

The autonomous system must be expected to be demand driven, in this analysis a constant load is defined, and the produced wave energy will have to be stored and conditioned to supply the load. The power system must both handle the large power fluctuations during normal operation due to the incident waves, and the long-term fluctuations due to changing weather. These two domains of fluctuations are very different and will have to be handled separately. Lifesaver is designed and operated as an autonomous system with a power system that is centered around an ultracapacitor bank, as described in Chapter 3. The capacitor bank handles the wave-to-wave fluctuations and ensures stable power flow to the control and monitoring system. This has proved to be a successful configuration and is the natural point of origin for designing the autonomous system.

While the capacitor bank ensures adequate power quality during WEC operation, the challenge is to handle the weather variations. Fig. 5.1 shows a possible autonomous power system configuration with wave energy as the primary source and a large battery bank to absorb the larger power fluctuations. Since the battery bank must be expected to have limited capacity, an additional power source is required for maintaining the load when the battery bank is empty. In this case, a diesel generator is selected.

The sizing of the power and energy system components should be the result of economic optimization. A configuration with wave, battery and diesel is very flexible as these power systems have very different cost properties. The WEC cost is mainly driven by installed power capacity, and the cost scales almost linearly with power rating. Since the WEC supplies renewable energy, the energy itself can be considered free of charge. The WEC total cost is to very little extent affected by the number of hours it is operated per year. Thus, the WEC should be regarded as a power scaled component.

The diesel generator has almost the opposite economical properties of the WEC as diesel generators are inexpensive per installed kW, but are expensive to operate due to the high fuel cost. Over the lifetime of a diesel generator, the majority of the life cycle cost will be diesel fuel, and the diesel generator can be considered an energy scaled component.

The battery system serves as the bridge between the renewable source and the diesel system as it allows for utilizing excess production from the WEC to save fuel. The wave energy that

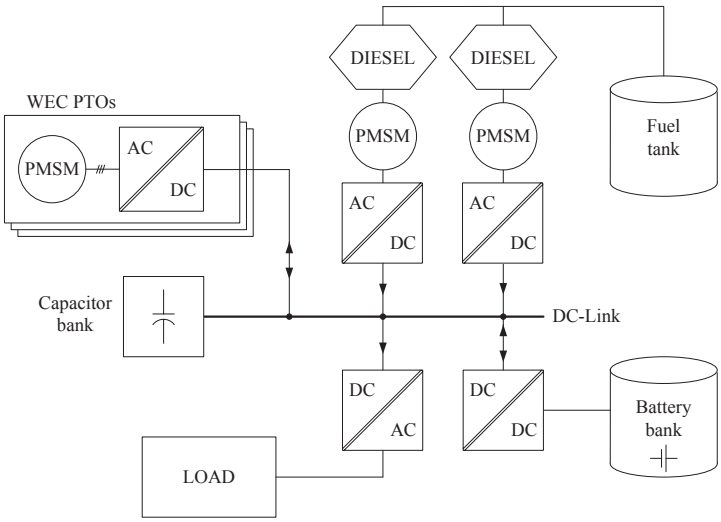

Figure 5.1: Autonomous WEC power system

passes through the battery was obtained free of charge, but saves an equal amount of costly diesel. Thus, the cost savings from the battery is calculated as the total amount of energy that has passed through the battery multiplied by the energy cost of diesel.

Battery cost is directly linked to the energy storage capacity. In addition, it is important to consider the battery lifetime, which typically lies in the range 200-2 000 full charge cycles, depending on battery technology. Since the base cost of a battery is high, it is important to ensure good utilization of the battery lifetime. Table 5.1 lists a conservative battery cost of 310 €/kWh. If this is considered to be a lithium battery with 1 000 cycles life time, the cost of energy supplied from the battery over the battery life would be 0.310 €/kWh, which is marginally less than the listed cost of diesel power. Thus, more than 850 full charge cycles is required on the battery to return profit.

This push for high battery utilization poses a challenge to WECs since the weather fluctuations are slow and infrequent. Thus, battery systems are unsuitable for providing cost efficient long-term storage unless the alternative energy cost is very high. The battery bank should therefore have limited storage capacity, and the main purpose of the battery should be to even out rapid weather fluctuations, and to supply stable power when wave power production is marginal, which would otherwise cause poor utilization of the diesel generator and frequent starting and stopping.

The combination of renewable energy, diesel and batteries makes a powerful and efficient system where the renewable source supplies most of the energy. The batteries package enhances the renewable power system and the diesel system supply the remaining energy needed in calm periods. Diesel generators are also suitable for adding redundancy due to the low cost, and provides excellent backup for the renewable power system.

The main design challenge is to find the exact sizing of the WEC and the battery bank. This should be done by optimization towards a specific load system at a given site so that the required power output can be matched with the wave energy resource and the typical distribution

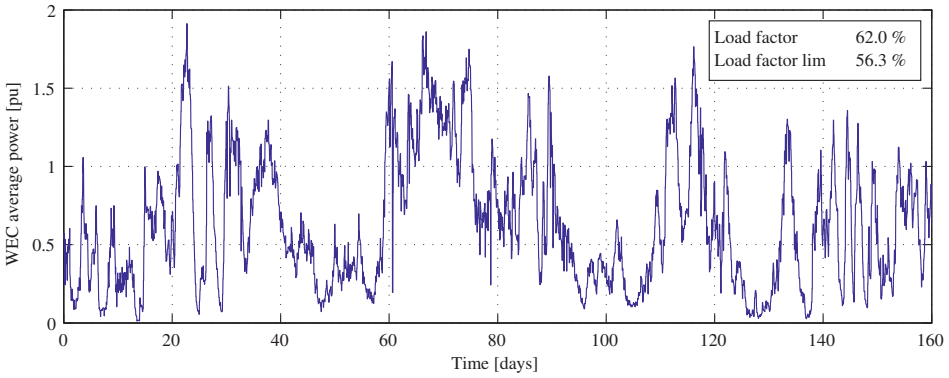

Figure 5.2: Wave time series measured at Wavehub. Converted to actual power output from WEC [pu].

of weather patterns. Fig. 5.2 shows actual wave data measured at Wavehub, which has been converted to normalized WEC power output. Unfortunately, FO does not possess a complete dataset covering a full year of continuous observations, and several datasets have been combined to produce a full year of data. Seasonal variations are therefore not correctly represented and the results should be treated with care, however as the focus of this work is to demonstrate the methodology rather than the exact results, these adaptations are believed to be adequate.

Fig 5.2 shows typical power fluctuations that must be expected due to changing weather. The stated load factor of 62% refers to the annual energy production divided by rated power. This number includes energy delivered above rated power, however if power is capped at rated power, which would correspond to 1 pu in Fig 5.2, the load factor would equal 56.3%. In addition to the annual load hours, the distribution and length of calm periods, plotted in Fig. 5.3, becomes very important for the sizing of the energy storage and the consumption of diesel fuel. The calm periods are calculated by dividing the full year time series into consecutive periods of n days. All periods with average power output less than the load demand are counted as calm periods. Rated WEC capacity in this example is three times the load demand. Since the batteries will require at least 100 full load cycles per year to yield profit, this plot gives a good impression of the possible battery size.

The WEC can also be oversized to cover the load for an additional days per year, and Fig. 5.4 plots the exact relationship based on the Wavehub data. The figure shows the progressive nature of the system, added overcapacity results in fewer and fewer added supported days as the overcapacity increases. The relationship seems to be close to linear up to ca two times overcapacity, and the optimal system must be expected to be found in vicinity to this.

So far, a complete system for continuous power delivery has been designed and discussed. Only diesel and batteries has been discussed as alternative power sources to the WEC, however many alternative technologies for energy storage and energy production exists, for instance could methanol based fuel cells be applied as an alternative to diesel for low power applications. For small systems, these considerations are more of practical nature than related to the actual cost of energy and energy efficiency. Thus, to get a better understanding of the real energy cost, a large power system will be analyzed in the next section.

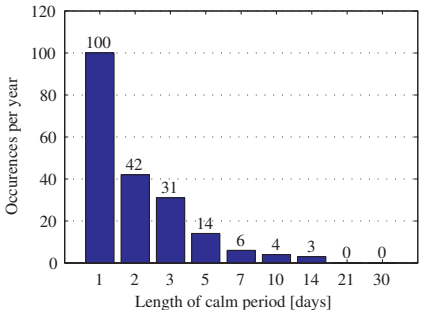

Figure 5.3: Number and length of calm periods with energy shortage. Rated power of the WEC is three times the load.

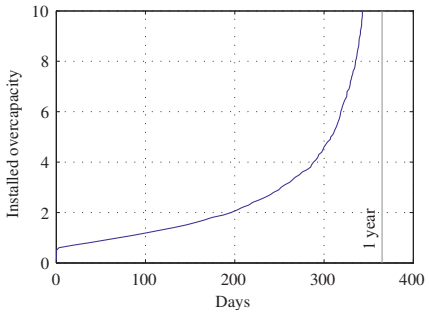

Figure 5.4: Required overcapacity to serve the load for n days per year

5.3 High power system example

While the realistic power level of a first commercial system for the FO WEC technology would most likely be in the range of a few kW continuous power, the real benefit and potential for the WEC system is expected to emerge for significantly higher power levels. Therefore, a system case with a continuous load requirement of 100 kW is defined and used in the following analysis. This is within reach of the portfolio of devices that FO can deliver, as addressed in Chapter 7. Three different cases for deployment are defined, named *Near-shore*, *Off-shore* and *Ocean*. These cases have different cost properties attached, mainly influenced by cost of maintenance and refueling due to the distance from the nearest port, and the cost parameters are listed in Table 5.1.

- Near-shore
- Off-shore
- Ocean

Property	Value	Unit
WEC, cost of power capacity	6 000	€/kW
Diesel, near-shore case, cost of energy	0.375	€/kWh
Diesel, off-shore case, cost of energy	1.0	€/kWh
Diesel, ocean case, cost of energy	10	€/kWh
Battery, conservative, cost of energy capacity	310	€/kWh
Battery, optimistic, cost of energy capacity	125	€/kWh
Hydrogen electrolyzer, cost of power capacity	363	€/kW
Hydrogen fuel cell, cost of power capacity	508	€/kW
Hydrogen storage, cost of energy capacity	16	€/kWh

Table 5.1: Cost properties for hydrogen hybrid WEC system

Table 5.1 also lists cost for the other system components, where the WEC cost is estimated based on Lifesaver and expected improvements for future systems. Two figures are presented for battery cost; the conservative case represents existing battery technology and is based on

estimates for total system cost of a battery system. The optimistic case is based on presented numbers from the automotive industry and represents expected battery cost for electric vehicles in five years time. This figure must therefore be considered very optimistic in this context.

It was previously argued that batteries are unsuitable to cover long-term fluctuations in power, especially for a large system. A 100 kW system would consume an energy amount equivalent to several hundred kg of batteries every hour, and a system that is able to cover for instance a week of consumption would be extremely heavy and expensive. This study therefore introduces hydrogen as alternative energy storage. Hydrogen has some of the same benefits as fuel oil, while also having the possibility to be produced on site. The hydrogen system consists of an electrolyzer that can produce hydrogen when excess power is available and pressure vessels that can store hydrogen as compressed gas. During calm periods, fuel cells will convert hydrogen back into electricity. In addition, an option of producing electricity from hydrogen by a standard heat engine was evaluated, but showed very poor cycle efficiency. A similar concept has been tested out at the island Utsira, Norway [46], where two wind turbines and a hydrogen storage system were used to supply stable renewable power to the island. In general, the concept showed good performance, but the fuel cells showed poor reliability. However, with recent advances on fuel cell performance in the automotive industry there is reason to believe that reliable fuel cells will be available in the near future.

The key properties for the hydrogen system is listed in Table 5.2, and are used as basis for the hydrogen storage analysis. The cost and efficiencies of the hydrogen systems listed in Table 5.1 and 5.2 are based on an analysis by the *National Renewable Energy Laboratory* [34] and results in a cycle efficiency of only 30%. The poor cycle efficiency is one of the major barriers against large-scale implementation of hydrogen as energy carrier and energy storage. However, for the autonomous WEC application, hydrogen may offer the required energy density for sustained operation. The low efficiency could have less impact since the WEC is likely to be installed with significant over capacity, hence it will produce excess energy that can be converted to hydrogen.

Property	Value	Unit
Specific energy hydrogen	123	MJ/kg
Specific energy hydrogen	34.17	kWh/kg
Density of hydrogen	0.08988	kg/m^3
Energy density @ atmospheric pressure	3.071	kWh/m^3
Energy density @ 200 bar	614.2	kWh/m^3
Energy density @ 700 bar	2 150	kWh/m^3
Nominal load	100	kW
Electrolytic cell efficiency (PEM)	57	%
Fuel cell (fc) efficiency (PEMFC)	53	%
Gas motor (gm) efficiency	≈ 35	%
Cycle efficiency (fc)	30	%
Cycle efficiency (gm)	17	%
Selected storage pressure	200	bar
Required volume per load hour (fc)	0.54	m^3
Required volume per load week (fc)	91.2	m^3

Table 5.2: Physical properties for hydrogen storage system

Fig. 5.5 shows the proposed power system for the hydrogen hybrid WEC system, which is designed around the ultracapacitor stabilized DC-Link. The diesel generator is connected to the DC-Link through a full bridge converter to handle the large voltage fluctuations that occurs on the DC-Link as the ultracapacitor bank stores and supplies energy. This was discussed in

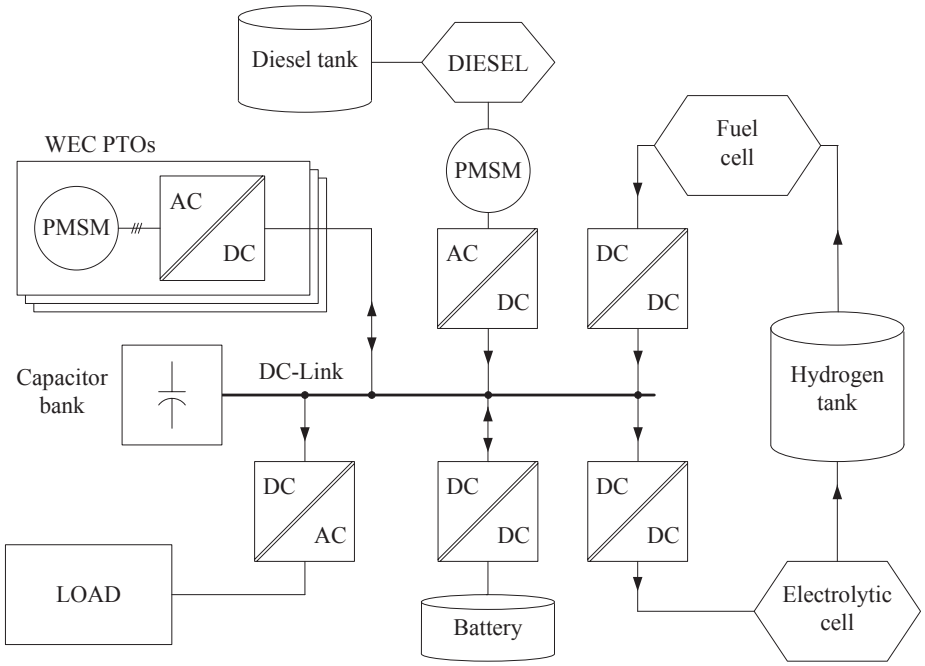

Figure 5.5: Autonomous power system with hydrogen storage

Chapter 3. This also allows for active speed control of the diesel generator, which can improve the efficiency at reduced load. The hydrogen electrolyzer and fuel cell can be thought of as battery like systems and must be operated at a controlled DC-voltage for optimal power transfer. Thus, DC/DC converters are required for the electrolyzer, the fuel cell and the battery. Finally, the load converter will supply stabilized power to the load, most likely as standard AC voltage.

As significant costs will be attached to the power system, and especially the WEC system, a thorough system optimization with respect to power component sizing is important. The analysis is performed by running multidimensional scans spanning installed WEC capacity, battery storage capacity, hydrogen storage capacity and hydrogen power capacity. The total capital expenditure (CAPEX) and operational expenditure (OPEX) over five years is calculated for each case so that the optimal solution is identified. Due to the short project lifetime selected, no discount rate was included in the calculation. The short lifetime is selected since these kind of autonomous systems are likely to have shorter horizons. Longer lifetime would strongly favor the WEC system as the operational cost of diesel is much higher than the running costs of the WEC system, thus the project life of five years can be viewed as a worst-case scenario.

The analysis has been performed for the three cases *Near-shore*, *Off-shore* and *Ocean*. The only difference between the cases is the cost of diesel, as defined in Table 5.1, which has great impact on the system design. The optimized configurations found are listed in Table 5.3, and the resulting annual energy balance is plotted in Fig. 5.6. Each case is addressed and discussed separately in the next paragraphs.

Property	Unit	Near-shore	Off-shore	Ocean
Total system capex and opex	k€	1 317	2 010	2 597
Cost of energy	€/MWh	301	459	593
WEC rated power	pu	1.0	2.0	3.0
Battery storage capacity	pu·h	0.0	1.0	5.0
H_2 storage capacity	pu	0	50	200
H_2 rated power	pu·h	0.0	0.5	1.0

Table 5.3: Optimal system configuration

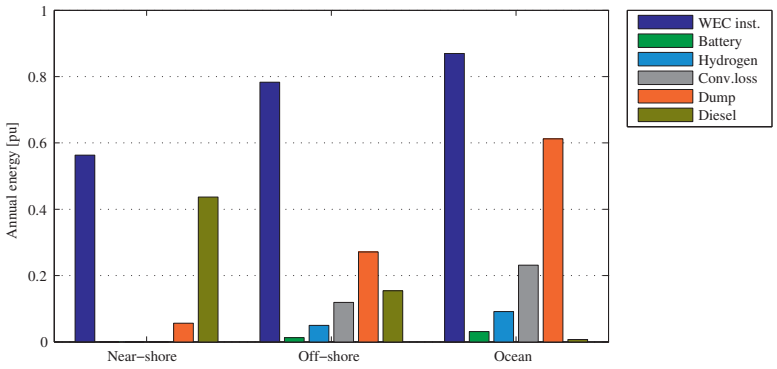

Figure 5.6: Annual energy distribution

Near-shore case

Near-shore refers to systems around or closer than 20 km to the nearest port and are viewed as easily accessible for maintenance and re-fueling. This leads to a cost of diesel marginally higher than the base cost, and when optimizing the near-shore case it quickly becomes evident that neither battery storage nor the hydrogen storage can compete with diesel. Hence, the optimal system consists only of wave and diesel, where the WEC is sized to produce the optimal amount of energy, and the calm periods are covered with diesel. An example with operation of this power system is plotted in Fig. 5.7 and shows 50 days of typical operation in Wavehub climate. As listed in Table 5.3, the optimal system configuration showed to result in a WEC with rated power equal to the load. This setup results in an annual energy balance of 57% wave energy versus 43% diesel energy. Approximately 8% of the annual produced wave energy has to be dumped due to overproduction.

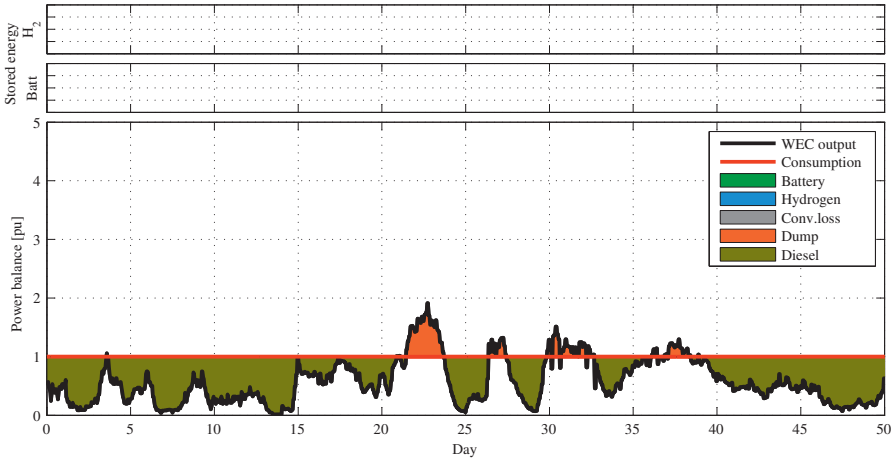

Figure 5.7: Power and Energy balance for Near-Shore case

Off-shore case

The off-shore case is defined as a remotely located systems within 100 km of the nearest port. The wave climate for such a location will typically be harsh and would require larger vessels for maintenance and refueling. This will add significantly to the diesel cost and will make alternative energy sources more attractive. In this case, hydrogen storage becomes economically attractive with power capacity sufficient to cover half the load and storage capacity sufficient to support the full load for 50 hours. As the cost of hydrogen storage capacity is significantly lower than batteries, one could expect batteries to be unfeasible when the hydrogen infrastructure already is in place; however, as batteries are significantly more efficient, they are more suitable for covering the frequent load fluctuations that appear in marginal wave states. While the hydrogen system would waste 2/3 of the cycled energy, the battery bank can deliver cycle efficiency in excess of 90% and would help maintain full energy coverage from the WEC in less energetic wave states. Nevertheless, the analysis only worked out in favor for batteries for the optimistic cost level.

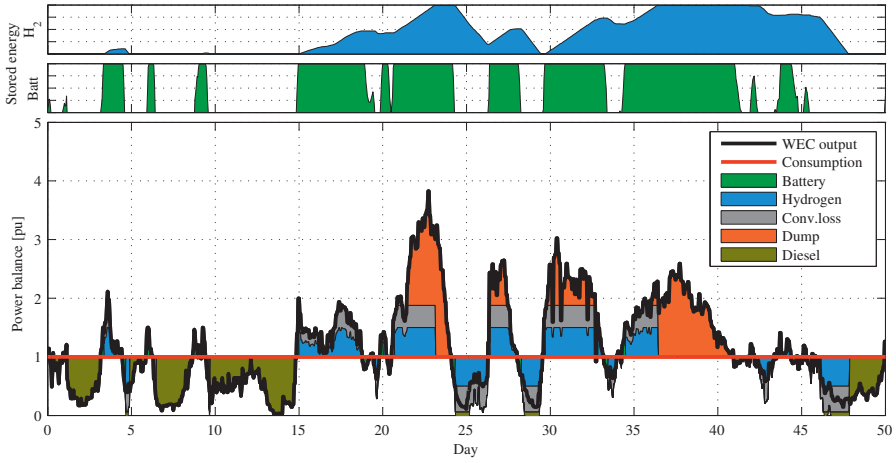

Figure 5.8: Power and Energy balance for Off-Shore case

With conservative battery cost, batteries turned out to be unprofitable in all three cases. In the off-shore case, the optimum battery size turned out to be one full load hour, which would equal 100 kWh, or a little more than a standard battery package for the Tesla Model S sports car.

Fig. 5.8 shows the power balance for the off-shore case. The two upper bands show the state of charge of both the battery storage and the hydrogen storage, from empty to full. The plot illustrates the power flows that occur when cycling the energy storages, and illustrate the amount of energy that is lost through the hydrogen conversion chain. In the offshore case, the optimal WEC rating is two times the load rating, hence significant overcapacity is installed to reduce diesel consumption. This results in annual load coverage of 78% directly from the WEC, and only 15% coverage from diesel. In addition, 1.5% of the annual energy is indirectly covered by the WEC through battery storage, and 5% is covered through hydrogen storage. An amount equal to 11% of the annual load is lost due to hydrogen and battery conversion loss, and 28% is dumped due to excessive WEC output.

Ocean case

The ocean case is defined as locations beyond 100 km from the nearest port. These systems could be very remotely located in areas such as the arctic or the oceans and would be difficult to maintain. It could be that the devices would have to be designed to sustain the entire project lifetime without maintenance. This result in very high cost of diesel, and the renewable power and storage system must be designed with abundant capacity to supply as much as possible of the annual energy. The optimal design results are listen in Table 5.1 and results in a WEC rated power of three times the load, 200 full load hours of hydrogen storage and five full load hours of battery storage. The hydrogen system must have full power capacity. This leads to annual energy coverage from diesel of only 0.75%, all the remaining energy is directly or indirectly delivered by the WEC. This is demonstrated in Fig. 5.6, which shows the distribution of annual energy from the different power components. When compared to the offshore case, the major difference is the amount of dumped energy. The high installed power capacity of the WEC results in 87% of the

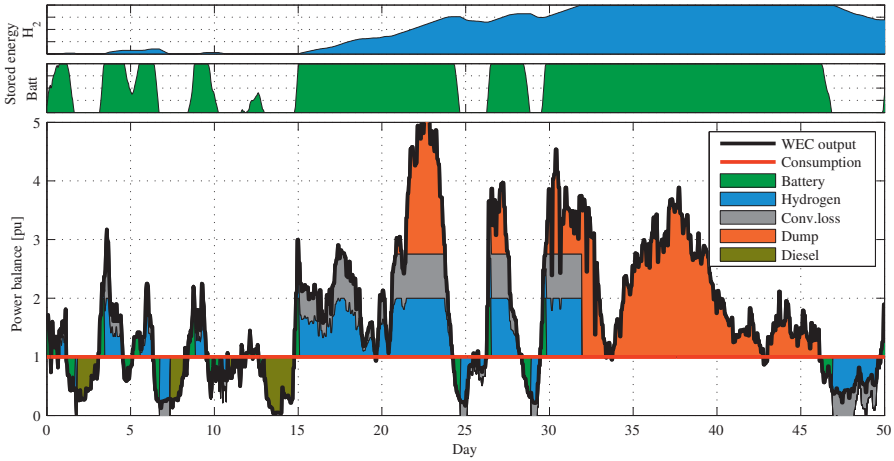

Figure 5.9: Power and Energy balance for Ocean case

annual energy to be delivered directly from the WEC. Of the remaining gap of 13%, 3% is covered from battery storage and 9% is covered from hydrogen storage. This proves the shortcomings of the energy storage system as it to a large extent is more profitable to install excess production capacity than to use storage.

Fig 5.9 shows the time series example for the ocean case. The large amount of diesel consumption in the start of the plot is due to the initial condition of the analysis that starts with empty energy storages at day zero. The figure illustrates the large installed power capacity compared to the load, as the WEC production in one instance reaches five times the load consumption in average power output. Nevertheless, the system proves stable operation within the defined limits and demonstrates the ability to supply continuous power in a remote location.

Hydrogen storage

A very large pressure vessel would be required to provide the required energy storage for the ocean case. 200 full load hours at 100 kW amounts to 20 000 kWh and equals 13 200 m^3 of H_2 at atmospheric pressure. The maximum pressure that is commonly used for hydrogen storage is 700 bar, and would lead to a total required storage volume of 19 m^3. This would likely have to be implemented as several smaller pressure vessels and would have large impact on the system design. Since the WEC absorber most likely would be designed and built specifically for the application, it could be possible to integrate the pressure vessels as a part of the hull, possibly in the load bearing structures so that structure serves dual purposes. Fig. 5.10 illustrates a configuration built around steel pipes, where the PTOs would be located at the tip of the arms. The steel pipes will carry the loads exerted on the buoy, and can act as hydrogen pressure vessels. With a length of 20 m and diameter of 0.7 m, they would deliver a storage volume of 70 m^3, hence an operating pressure of 190 bar would be required to meet the specified storage capacity. Such a pressure level would place stringent requirements on the pipe design, but could potentially lead to a cost efficient system with good integration and high material utilization. This suggestion of integration is inspired by Peugeot Citroën which are exploring an automotive hybrid system

based on compressed air [7].

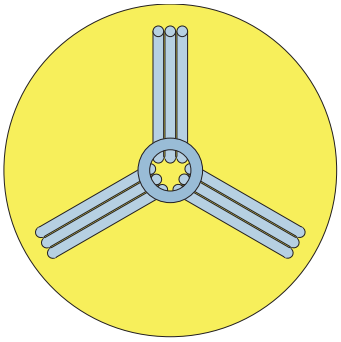

Figure 5.10: Hull integrated pressure vessels with load bearing capability

5.4 Concluding remarks

The analysis of autonomous systems shows that wave energy can be applied successfully as a power source for remote ocean based power systems. Since the wave energy resource is supply driven, an alternate source of power is required for calm weather; the typical solution would be diesel generators. The wave resource will typically be more stable than alternative renewable sources, and has demonstrated the ability to fully supply the load up to 7 500 hours per year. This is possible by overrating the WEC with respect to the load, and up to three times overrating has shown beneficial.

Two energy storage solutions was also investigated, batteries and hydrogen storage. Both solutions have high cost of energy, and turned out to be unprofitable in many of the cases. The main barriers are the high cost of batteries and the poor cycle efficiency of the hydrogen storage. The storage solutions were to a large extent penalized by the short project lifetime of 5 years selected for the analysis, nevertheless, the different cases studied demonstrated that the energy storage would only supply a small fraction of the annual energy.

Chapter 6

Modeling and simulation

Synopsis

In this chapter the theoretical models used to simulate the Wave Energy Converter systems are described. The models cover forces on the system due to incident waves and hydrodynamical effects, forces from PTOs, efficiency and power output of the system and interference between absorbers in multi-body systems.

Contents

Related publications

6.1 General buoy model

Good simulation models are essential for the wave energy industry to minimize the need for offshore testing and deployment. They can also raise the understanding of the system and provide valuable information since states and properties that are difficult or impossible to measure in real life usually are easily extracted from the model. Several simulation models have been developed within the wave energy project to simulate different parts of the system. The most advanced and important model is the general buoy model that simulates the operation of Lifesaver and other WECs in real sea conditions. The model takes into consideration the ocean properties with realistic waves, hydrodynamic properties of the WEC, actual WEC motion in six *Degrees Of Freedom* (DOF) and PTO behavior, including realistic power output.

$$\begin{bmatrix} \boldsymbol{f} \\ \boldsymbol{\tau} \end{bmatrix} = \boldsymbol{M} \begin{bmatrix} \ddot{\boldsymbol{r}} \\ \ddot{\boldsymbol{\theta}} \end{bmatrix} \tag{6.1}$$

The body motion is governed by Equation (6.1), which is derived from Newtons second law of motion. The symbols and definitions used in the equations in this section are listed in Table 6.1. The equation of motion is the backbone of the simulation model, and is implemented with six degrees of freedom, which covers the x,y,z translations surge, sway and heave, and the rotations around the local x,y,z axis named roll, pitch and yaw, which are defined in Fig. 6.1. The local axis system is referred to as R,P,Y axis since they are used to describe the roll, pitch and yaw rotations, so that these are not confused with the global x,y,z coordinate system that is independent of the WEC. By using these indices, Equation (6.1) is written on scalar form in Equation (6.2). Center of gravity is located at the origin of the local axis system, hence there are only diagonal mass elements in the mass matrix. The linear masses also include the added mass of the floater at infinite frequency, which explains the differentiation of mass on the linear axes.

$$\begin{bmatrix} F_x \\ F_y \\ F_z \\ \tau_R \\ \tau_P \\ \tau_Y \end{bmatrix} = \begin{bmatrix} m_x & 0 & 0 & 0 & 0 & 0 \\ 0 & m_y & 0 & 0 & 0 & 0 \\ 0 & 0 & m_z & 0 & 0 & 0 \\ 0 & 0 & 0 & i_{RR} & i_{PR} & i_{YR} \\ 0 & 0 & 0 & i_{RP} & i_{PP} & i_{YP} \\ 0 & 0 & 0 & i_{RY} & i_{PY} & i_{YY} \end{bmatrix} \cdot \frac{d^2}{dt^2} \begin{bmatrix} r_x \\ r_y \\ r_z \\ \theta_R \\ \theta_P \\ \theta_Y \end{bmatrix} \tag{6.2}$$

The model is converted to the standard state space form shown in Equation (6.3), which translates to Equation (6.4) on scalar form. The equation is solved as an initial value problem, using the *Ordinary Differential Equation* solver in *Matlab*. To reduce complexity and save computation time, some degrees of freedom are locked out, and most of the simulation work is performed with the three degrees of freedom surge, heave and pitch. However, to maintain order and flexibility in the equations, all equations are always described with six DOF indices.

$$\dot{\boldsymbol{x}} = \boldsymbol{A}\boldsymbol{x} + \boldsymbol{b}u \tag{6.3}$$

$$\begin{bmatrix} \dot{r_x} \\ \ddot{r_x} \\ \dot{r_y} \\ \vdots \\ \ddot{\theta_Y} \end{bmatrix} = \begin{bmatrix} a_{11} & a_{12} & a_{13} & \cdots & a_{112} \\ a_{21} & a_{22} & a_{23} & \cdots & a_{212} \\ a_{31} & a_{32} & a_{33} & \cdots & a_{312} \\ & \vdots & & \ddots & \\ a_{121} & a_{122} & a_{123} & \cdots & a_{1212} \end{bmatrix} \begin{bmatrix} r_x \\ \dot{r_x} \\ r_y \\ \vdots \\ \dot{\theta_Y} \end{bmatrix} + \begin{bmatrix} b_1 \\ b_2 \\ b_3 \\ \vdots \\ b_12 \end{bmatrix} u \tag{6.4}$$

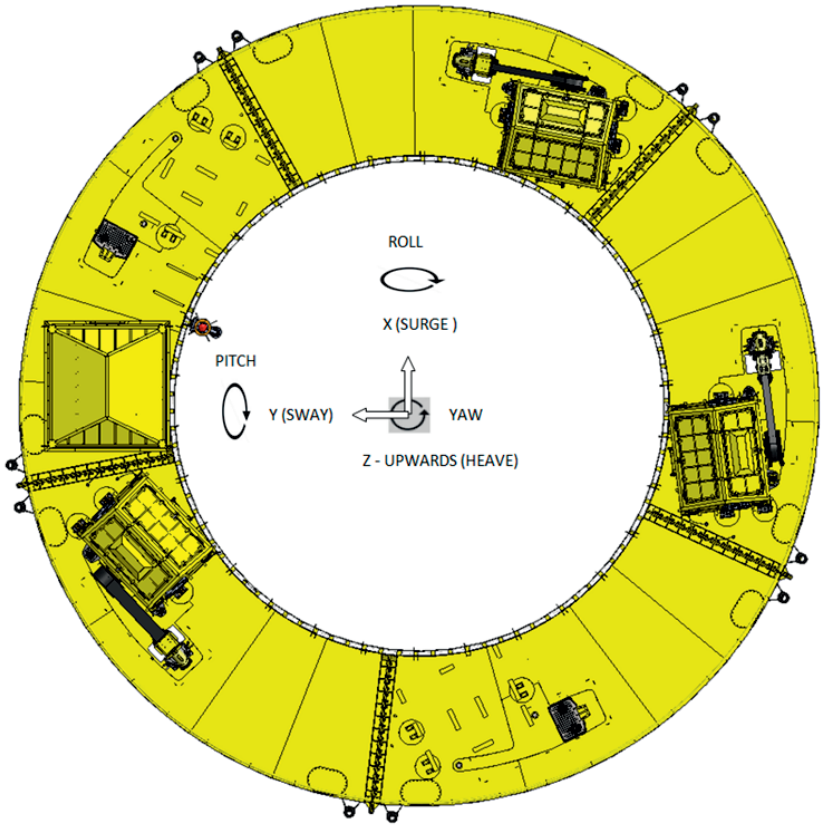

Figure 6.1: Local coordinate system on Lifesaver

The sum of forces and moments on the system is defined according to Equation (6.5) and (6.6), and are based on sub-models that are defined and implemented separately to form a modular simulation system that can be rebuilt according to need. The sub-models and the resulting forces and moments are defined in the next sections.

$$\Sigma \boldsymbol{f} = \Sigma \boldsymbol{f}_{pto} + \boldsymbol{f}_c + \boldsymbol{f}_e + \boldsymbol{f}_f + \boldsymbol{f}_r + \boldsymbol{f}_d + m_z g \cdot -\boldsymbol{k} \tag{6.5}$$

$$\Sigma \boldsymbol{\tau} = \Sigma \boldsymbol{\tau}_{pto} + \boldsymbol{\tau}_c + \boldsymbol{\tau}_e + \boldsymbol{\tau}_f + \boldsymbol{\tau}_r + \boldsymbol{\tau}_d \tag{6.6}$$

PTO forces

The PTO forces are modeled based on Equation (2.10) defined on page 28, thus they are time invariant and only depends on the drum speed. The PTO force vector is found by multiplying the scalar PTO force with the normal vector from the PTO to the mooring point. However, finding the drum speeds and force vectors is not straight forward due to the rotation of the local

Group	Property	Symbol	Unit
Notation			
	Scalar	a	
	Vector	$\boldsymbol{a}$	
	Matrix	$\boldsymbol{A}$	
	Time derivative	$\dot{a}$	da/dt
	Normal vector to $\boldsymbol{a}$	$\boldsymbol{a}_N$	
	Vector for the i-th mode of motion	$\boldsymbol{a}_i$	
	Complex operator	$i\omega$	
Constants			
	Gravity	g	9.81 m/s^2
	Density of sea water	ρ	1025 kg/m^3
Properties			
	Mass	m	kg
	Inertia	i	kgm^2
Geometry			
	Global position of the WEC	$\boldsymbol{r}_{wec}$	[m, m, m]
	Global position of the i-th mooring	$\boldsymbol{r}_{mi}$	[m, m, m]
	Local position of the i-th PTO	$\boldsymbol{r}_{ptoi}{}^*$	[m, m, m]
	Global position of the i-th PTO	$\boldsymbol{r}_{ptoi}$	[m, m, m]
	Mooring-PTO vector for the i-th PTO	$\boldsymbol{r}_{mptoi}$	[m, m, m]
	WEC rotation	$\boldsymbol{\theta}_{wec}$	[1, 1, 1]
	Rotation matrix	$\boldsymbol{R}$	$[3 \times 3]$
Forces and Moments			
	Force or Moment from the i-th PTO	$\boldsymbol{f}_{ptoi}/\boldsymbol{\tau}_{ptoi}$	$[3 \times 1]$
	Resultant PTO forces	$\Sigma\boldsymbol{f}_{pto}/\Sigma\boldsymbol{\tau}_{pto}$	$[3 \times 1]$
	Hydrostatic buoyancy force	$\boldsymbol{f}_c/\boldsymbol{\tau}_c$	$[3 \times 1]$
	Wave excitation force	$\boldsymbol{f}_e/\boldsymbol{\tau}_e$	$[3 \times 1]$
	Hydrodynamic friction damping	$\boldsymbol{f}_f/\boldsymbol{\tau}_f$	$[3 \times 1]$
	Hydrodynamic radiation	$\boldsymbol{f}_r/\boldsymbol{\tau}_r$	$[3 \times 1]$
	Hydrodynamic diffraction	$\boldsymbol{f}_d/\boldsymbol{\tau}_d$	$[3 \times 1]$
	Resultant force on WEC	$\Sigma\boldsymbol{f}/\Sigma\boldsymbol{\tau}$	$[3 \times 1]$
Hydrodyamics			
	Frequency	ω	rad/s
	Wave surface elevation	η	m
	Wave state energy spectrum	S	
	Incident wave amplitude spectrum	A_i	
	Hydrodynamic force operator	χ	
	Incident wave function	ϕ	
	Impulse response matrix	$\boldsymbol{K}$	

Table 6.1: Equation symbols

axis system, and the global coordinates has to be transformed to the local coordinates by the rotation matrix $\boldsymbol{R}$ defined in Equation (6.7).

$$\boldsymbol{R}\left(\theta_Y, \theta_P, \theta_R\right) = \boldsymbol{R_Y}\left(\theta_Y\right)\boldsymbol{R_P}\left(\theta_P\right)\boldsymbol{R_R}\left(\theta_R\right) =$$

$$\begin{bmatrix} \cos\theta_Y & -\sin\theta_Y & 0 \\ \sin\theta_Y & \cos\theta_Y & 0 \\ 0 & 0 & 1 \end{bmatrix} \begin{bmatrix} \cos\theta_P & 0 & \sin\theta_P \\ 0 & 1 & 0 \\ -\sin\theta_P & 0 & \cos\theta_P \end{bmatrix} \begin{bmatrix} 1 & 0 & 0 \\ 0 & \cos\theta_R & -\sin\theta_R \\ 0 & \sin\theta_R & \cos\theta_R \end{bmatrix} \tag{6.7}$$

The PTO to mooring vector, and the corresponding normal vector is found in Equation (6.8) and (6.9), by adding the translation of the local coordinate system and multiplying the local PTO position by the rotation matrix. The actual PTO velocity is found as the cross product given in Equation (6.10) and the resulting velocity along the PTO to mooring vector is found in Equation (6.11). By applying the PTO model, which was previously defined in Equation (6.12) on page 28, the actual rope force is found, and the resulting forces and moments for all five PTOs are found in Equations (6.13), (6.14) and (6.15).

$$\boldsymbol{r}_{mptoi} = \boldsymbol{r}_{wec} + \boldsymbol{R}\,{\boldsymbol{r}_{ptoi}}^{*} - \boldsymbol{r}_{mi} \tag{6.8}$$

$$\boldsymbol{r}_{mptoiN} = \frac{\boldsymbol{r}_{mptoi}}{|\boldsymbol{r}_{mptoi}|} \tag{6.9}$$

$$\dot{\boldsymbol{r}}_{ptoi} = \dot{\boldsymbol{r}}_{wec} + \boldsymbol{r}^{*}_{ptoi} \times \dot{\boldsymbol{\theta}}_{wec} \tag{6.10}$$

$$\dot{\boldsymbol{r}}_{mptoi} = \dot{\boldsymbol{\theta}}_{wec} \cdot \boldsymbol{r}_{mptoiN} \tag{6.11}$$

$$\boldsymbol{f}_{ptoi} = F_{PTO}\left(|\dot{\boldsymbol{r}}_{mptoi}|\right) \cdot \boldsymbol{r}_{mptoiN} \tag{6.12}$$

$$\boldsymbol{\tau}_{ptoi} = \boldsymbol{f}_{ptoi} \times \boldsymbol{r}^{*}_{ptoi} \tag{6.13}$$

$$\Sigma\boldsymbol{f}_{pto} = \sum_{i=1}^{5} \boldsymbol{f}_{ptoi} \tag{6.14}$$

$$\Sigma\boldsymbol{\tau}_{pto} = \sum_{i=1}^{5} \boldsymbol{\tau}_{ptoi} \tag{6.15}$$

Hydrodynamic forces

This section describes the method for finding the hydrodynamic forces on the body. Realistic waves are generated based on the JONSWAP spectrum which is representative for the North Sea [21]. The energy spectrum $S(\omega)$ as function of the frequency ω is calculated based on the JONSWAP definition, and can be converted to the wave amplitude spectrum $A_i(\omega)$ by Equation (6.16). Time series data for the wave surface elevation η is found by the inverse Fourier transform of the amplitude spectrum $A_i(\omega)$, as shown in Equation (6.17), where φ refers to randomly added phase for each frequency step and $\Re$ represents the real part of the expression. The simulation model is discrete and operates with a sampling rate of ca 10 Hz, and the inverse

Fourier transform is performed for each time step so that the coupled effects of the simulation model, such as surge movement, can be taken into consideration.

$$A_i(\omega) = \sqrt{2 \cdot S(\omega)\ d\omega} \tag{6.16}$$

$$\eta(t) = \Re \int_{-\infty}^{\infty} A_i(\omega)\ e^{i(\omega t + \varphi(\omega))}\, d\omega \tag{6.17}$$

The hydrodynamic forces from the waves can be divided into excitation forces and radiation forces [27]. The excitation forces are a combination of hydrostatic forces due to surface elevation on a fixed body and diffraction forces because of interactions of incident waves with the fixed body. The radiation forces appear because the body radiates waves due to body movement. For the point absorber, this causes ring waves propagating away from the absorber. The $\boldsymbol{\chi}$ operator is the excitation coefficient and describes all the forces mentioned here for all degrees of freedom. Equation (6.18) describes the relationship between the wave surface elevation η and the amplitude spectrum $A(\omega)$. The $\boldsymbol{\chi}$ operator is the link between surface elevation and hydrodynamical forces, as described by Equation (6.18). The direct link between the $\boldsymbol{\chi}$ operator and the hydrodynamical forces are shown in Equation (6.19).

$$\begin{bmatrix} \boldsymbol{f}(t) \\ \boldsymbol{\tau}(t) \end{bmatrix} = \Re \int_{-\infty}^{\infty} \chi(\omega) \cdot A_i(\omega)\ e^{i(\omega t + \varphi(\omega))}\, d\omega \tag{6.18}$$

$$\begin{bmatrix} \boldsymbol{f}(\omega) \\ \boldsymbol{\tau}(\omega) \end{bmatrix} = A_i(\omega) \cdot \boldsymbol{\chi}(\omega) \tag{6.19}$$

$$\chi_i(\omega) = \iint_{S_B} \phi_0 \frac{d\phi_i}{d\boldsymbol{n}_i} - \phi_i \frac{d\phi_i}{d\boldsymbol{n}_i}\, dS \tag{6.20}$$

The incident waves are described for all frequencies by the function ϕ_0, and the radiated and diffracted waves are described by the function ϕ_i for all frequencies and the i-th mode of motion. By integration over the area cross section of the body surface S_B, the force operator χ is found, as described in Equation (6.20). The surface normal vector for each mode of motion is denoted as $\boldsymbol{n}_i$. The radiation forces are calculated by integrating the radiation potential on the body surface, as showed in Equation (6.21).

$$F_k(\omega) = \sum_{i=1}^{6} -\rho \iint_S \frac{\partial \phi_i}{\partial \boldsymbol{n}_i} \boldsymbol{n}_k \,\mathrm{d}S \tag{6.21}$$

When solved, this force can be separated in two parts, as showed in Equation (6.22). One part is proportional to the acceleration, the radiation added mass a_{ki}, and one part is proportional to the velocity, the radiation damping b_{ki}. The radiation force contribution in a given mode of motion is the sum of the added mass and radiation contribution in that mode of motion due to forced oscillation in any mode of motion.

$$F_k(\omega) = -\sum_{i=1}^{6} \dot{U}_i a_{ki} + U_i b_{ki} \tag{6.22}$$

However, memory effects in radiation cause time variant behavior that cannot be directly transformed into a time domain equation. The conventional method is to apply the convolution integral shown in Equation (6.23), which is computationally hard.

$$\begin{bmatrix} \boldsymbol{f}(t) \\ \boldsymbol{\tau}(t) \end{bmatrix} = \int_{-\infty}^{t} \boldsymbol{K}(t-T) \begin{bmatrix} \dot{\boldsymbol{r}}(T) \\ \dot{\boldsymbol{\theta}}(T) \end{bmatrix} dT \tag{6.23}$$

An alternative approach, as described by Kristian et al. [23] is to make a separate state space model for the radiation forces. First the added mass at infinite frequency is separated out and added to the system mass matrix $\boldsymbol{M}$, described in Equation (6.1). Secondly, the new state space model is created by evaluating the impulse response $\boldsymbol{K}$ of the system. An example of the system impulse response is plotted in Fig. 6.2.

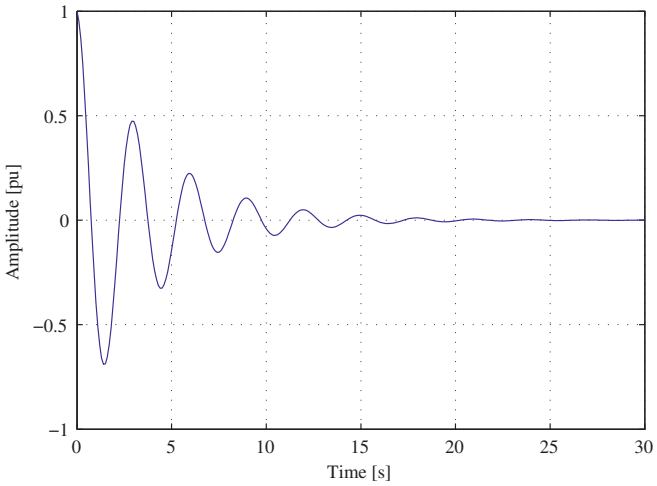

Figure 6.2: Example of system impulse response

The added mass and damping coefficients are ordered into the standard state space model described by Equation (6.26). Equation (6.24) describes the radiation forces as the sum of added mass and damping of the system in the frequency domain. In Equation (6.25) the added mass at infinite frequency is separated out. This opens for utilizing the method described by Kristiansen et al. [23] and rewrite the radiation forces on a state space form where the radiation force is only a function of the velocity $\dot{r}$. The properties are found numerically through *Computational Fluid Dynamics* (CFD) by using the *Finite Element Method* (FEM). For this study, COMSOL was used to find the hydrodynamic properties.

$$\begin{bmatrix} \boldsymbol{f}(\omega) \\ \boldsymbol{\tau}(\omega) \end{bmatrix} = -\left(\boldsymbol{A_0}(\omega) \begin{bmatrix} \ddot{\boldsymbol{r}}(\omega) \\ \ddot{\boldsymbol{\theta}}(\omega) \end{bmatrix} + \boldsymbol{B}(\omega) \begin{bmatrix} \dot{\boldsymbol{r}}(\omega) \\ \dot{\boldsymbol{\theta}}(\omega) \end{bmatrix} \right) \tag{6.24}$$

$$\begin{bmatrix} \boldsymbol{f}(\omega) \\ \boldsymbol{\tau}(\omega) \end{bmatrix} = -\left((\boldsymbol{A}(\omega) - \boldsymbol{A}(\infty)) \begin{bmatrix} \ddot{\boldsymbol{r}}(\omega) \\ \ddot{\boldsymbol{\theta}}(\omega) \end{bmatrix} + \boldsymbol{B}(\omega) \begin{bmatrix} \dot{\boldsymbol{r}}(\omega) \\ \dot{\boldsymbol{\theta}}(\omega) \end{bmatrix} \right) \tag{6.25}$$

$$\begin{aligned} \dot{\boldsymbol{x}}_i &= \boldsymbol{A}_i \boldsymbol{x}_i + \boldsymbol{b}_i \dot{r}_i \\ f_r\, i &= \boldsymbol{c}_i \boldsymbol{x}_i + d_i \dot{r}_i \end{aligned} \tag{6.26}$$

Hydrodynamic drag

The methods used so far to compute the hydrodynamic properties are based on the assumption of no drag on the system. The actual drag is marginal compared to the damping force applied by the PTOs, and this approach is believed to be accurate. However, operating the model without damping is likely to cause adverse effects such as oscillations. In the Lifesaver case, the problem is mostly related to the surge movement, since the PTOs have little influence on these movements.

Equation (6.27) shows the standard expression for hydrodynamic drag, where F_d is the drag force, A is the cross section surface area, C_D is the drag coefficient and u is the velocity. This is transformed to vector form in Equation (6.28), and the complete implementation using the already established hydrodynamic functions is shown in Equation (6.29).

$$F_d = -\frac{1}{2}\rho \cdot A \cdot C_D \cdot u^2 \tag{6.27}$$

$$\boldsymbol{f}_f = -\frac{1}{2}\rho \cdot A \cdot C_D \cdot |\boldsymbol{u}|\boldsymbol{u} \tag{6.28}$$

$$\boldsymbol{f}_{f\,i} = \frac{1}{2}\rho\, S_i\, C_D \left|\frac{\partial \phi_0}{\partial \boldsymbol{n}} - \dot{\boldsymbol{r}}_{wec\,i}\right| \left(\frac{\partial \phi_0}{\partial \boldsymbol{n}} - \dot{\boldsymbol{r}}_{wec\,i}\right) \tag{6.29}$$

6.2 Multi body model

The general buoy model ignores radiation and diffraction that will occur in multi-body systems, and each WEC is simulated as if it was alone. Incorporating coupled multi-body effects in the general buoy model would add very high complexity. The largest effect of interference is expected to be reduced power output as the energy potential in the waves are reduced as power is absorbed by the early WECs in the wave field. To compensate for this, a set of correction factors are calculated in a separate interference analysis, which are multiplied with the original simulation output to give realistic power output.

The hydrodynamic problem is solved within the framework of linear potential theory, specifically the Laplace equation, resulting in the interaction field illustrated in Fig.4.9. In this paper, the theoretical basis is only gone through briefly. The work of J.N Newman's *Marine Hydrodynamics* [27] is used as basis for this simulation work.

Since the velocity potential is linear, all contributions to forces and motions are linear. As a result, the principle of superposition applies. Therefore, it is convenient to split the complex problem into a set of simpler problems. The full solution is thus the sum of several simpler solutions. The potential arising from N absorbers in a farm can thus be described as the sum of contributions defined in Equation (6.30).

$$\phi = \phi_0 + \phi_D + \phi_R \tag{6.30}$$

The total velocity potential ϕ due to the interaction of N absorbers in a farm is the sum of the excitation potential due to incident waves ϕ_0, the diffraction potential due to the interaction of the incident potential with all absorbers at rest ϕ_D, and the radiation potential ϕ_R due to the independent motion of every absorber in every mode of motion with no incident waves present.

The diffraction problem and the radiation problem are solved independently. Thus, there are $N + 1$ independent problems to solve. Further, the radiation potential from each absorber is separated in 6 independent modes of motion. The total potential ϕ_N^i acting on absorber N in mode i of motion is the sum of every other absorber's radiation and diffraction potential in addition to the diffraction and radiation potential from absorber N acting on itself in mode i

of motion. Combining the 6 modes of motions for each absorber, and allowing for all absorbers to interact, results in a total of $N \times 6$ independent linear equations to be solved for each wave frequency. With a full description of the velocity potential, it is possible to integrate solutions in the frequency domain on specific wave climates and optimize the array energy output with respect to array layout angle and power take off damping coefficient.

In order to represent the interactions within the farm in the time domain model, a set of correction factors is applied to the power output from the time domain model of an farm without interactions. Correction factors are calculated individually for each wave direction and wave period encountered. The correction factor for the individual WECs are plotted as a function of the wave angle, as illustrated in Fig. 4.5 on page 54 for the design wave period ($Tz = 6.5s$).

6.3 Wave resource estimation

The simulations are performed based on the WEC prototype test site *Wavehub* located west of Cornwall, England as shown in Fig. 3.12. The test site is funded and supported by the renewable energy program administrated by the British government. The site includes a sub-sea power substation that allows for electrically connecting the WECs to grid. Wavehub has been surveyed and monitored for an extensive period, and work is still ongoing to calculate true statistical wave data for the site. The wave scatter diagram listed in Table 6.2 shows the most current data known to FO. A directional spectrum for Wavehub is plotted in Fig. 6.3. The site is heavily dominated by waves from west, and the directional plot has logarithmic scaling to show all the directions observed.

	Period Tz [s]													
	3.25	3.75	4.25	4.75	5.25	5.75	6.25	6.75	7.25	7.75	8.25	8.75	9.25	9.75
0.25	1	66	22	9	4	1	0	0	0	0	0	0	0	0
0.75	0	42	347	350	241	178	75	21	1	0	0	0	0	0
1.25	0	0	32	591	677	347	240	143	45	8	2	0	0	0
1.75	0	0	0	32	515	573	258	153	130	46	17	3	0	0
2.25	0	0	0	0	39	397	392	173	99	87	33	5	1	0
2.75	0	0	0	0	0	47	287	234	98	63	52	15	3	0
3.25	0	0	0	0	0	1	55	247	130	55	39	23	7	1
3.75	0	0	0	0	0	0	3	65	170	68	32	17	7	2
4.25	0	0	0	0	0	0	0	4	92	97	36	16	6	2
4.75	0	0	0	0	0	0	0	0	12	89	41	12	6	1
5.25	0	0	0	0	0	0	0	0	0	28	49	12	4	1
5.75	0	0	0	0	0	0	0	0	0	3	38	17	3	1
6.25	0	0	0	0	0	0	0	0	0	0	14	19	2	1
6.75	0	0	0	0	0	0	0	0	0	0	1	12	3	0
7.25	0	0	0	0	0	0	0	0	0	0	0	4	4	0
7.75	0	0	0	0	0	0	0	0	0	0	0	1	4	1
8.25	0	0	0	0	0	0	0	0	0	0	0	0	2	0
8.75	0	0	0	0	0	0	0	0	0	0	0	0	1	1
9.25	0	0	0	0	0	0	0	0	0	0	0	0	0	1
9.75	0	0	0	0	0	0	0	0	0	0	0	0	0	0

Wave height Hs [m]

Table 6.2: Wavehub scatter diagram, hours per wave state per annum

However, it showed to be difficult to interpolate the sparse directional data base with the comprehensive non-directional data base as several data points were missing from the directional data base. Moreover, the range of the directional data did not cover the required range for the new scatter. Instead of interpolation, and approach of curve fitting was selected. The directional data were gathered into 24 separate scatters that covered all directions from 0°-360° with 15° resolution. For each of these scatters, the simplified function for calculating wave state probability given in Equation (6.31) was fitted by minimizing the sum of the residuals defined in Equation (6.32), as shown in Equation (6.33). The new probability function was then

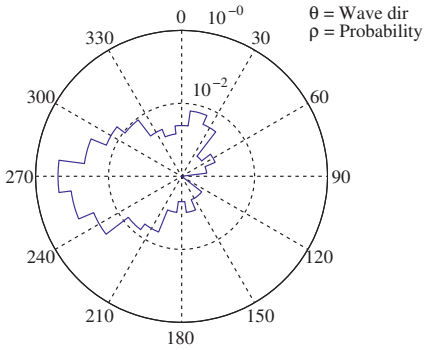

Figure 6.3: Probability distribution of wave direction on Wavehub. The plot is a logarithmic polar plot defined by the angle θ and radi ρ.

used to calculate all the wave states in the comprehensive scatter for each direction. At this moment, the new scatter is solely based on the weak directional scatter. To take advantage of the comprehensive scatter, the new scatter was normalized so that the sum of all directions on every wave state equaled the comprehensive scatter. Hence, the only information taken from the directional scatter is the distribution between the directions. An illustration of the estimated directional scatter is shown in Fig 6.4.

$$p\left(H_s, T_z, \boldsymbol{\beta}\right) = \beta_1 H_s^2 + \beta_2 H_s + \beta_3 T_z^2 + \beta_4 T_z + \beta_5 \tag{6.31}$$

$$r_i = p_i - p\left(H_s, T_z, \boldsymbol{\beta}\right) \tag{6.32}$$

$$S = \sum_{i=1}^{n} r_i^2 \tag{6.33}$$

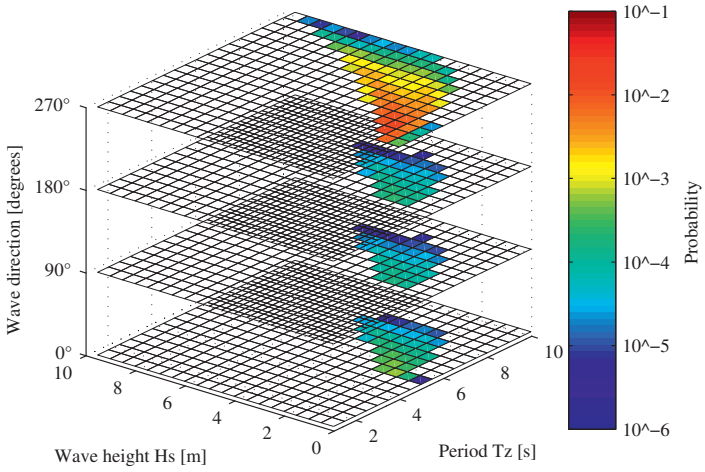

Figure 6.4: Illustration of wave scatter diagram that includes wave height, period and direction

Chapter 7

Path to commercialization

Synopsis

The major challenge for wave energy converters to enter the marked is reaching grid parity on cost of energy. In this chapter the general principles of system economics are described and the necessary steps toward profitability are pointed out. Analysis of future systems and the potential for scaling up the devices are also presented.

Contents

7.1 Current cost level

The major barrier against commercialization of wave energy today is the high cost of the systems. IEA estimates the cost of installed capacity to be in the range 3 375 - 5 250 €/kW [2], which is high compared to other renewable sources. Although several newcomers claim to have systems ready for commercialization, the general consensus among the established actors is that significant development remains before wave energy is ready to compete in the regular energy market. In this chapter, the current situation for the FO wave energy project is analyzed and possible paths forward and some general numbers for system cost are discussed and presented.

The cost of the Lifesaver system can be divided into five categories: Floater cost, PTO cost, installation cost, cost of auxiliary systems (moorings, cables, peripherals) and operational costs. Table 7.1 lists the actual cost encountered on Lifesaver according to these categories, and also present the projected cost for the next generation device. Lifesaver was primarily built as a prototype to gain operational experience, and is not optimized for low cost of energy, or low operational cost. A large portion of the operational cost is also linked to planned research activities such as system reconfiguration and maintenance training. Hence, there is a great cost reduction potential, as the cost numbers of the next generation device indicates. These projected costs are based on detailed design of the next device, and are believed to be accurate with a high level of confidence, and include realistic contingency. The operational costs are given per device, but assume a cost optimized wave farm so that operations can be shared between the devices. The operational costs include maintenance cost, full time employment for service crew and control and monitoring crew, housing, equipment, rental, insurance and logistics. Hence, these numbers are believed to be realistic and are used as basis for the economical analysis.

Item	Lifesaver	Next generation	Unit
Floater	7.7	1.6	k€/kW
PTO	8.0	2.2	k€/kW
Mooring and auxiliary	7.6	2.1	k€/kW
Installation	-	0.95	k€/kW
Operational cost	5.3	0.38	k€/(kW·yr)
Sum CapEx	23.3	5.9	k€/kW
Sum OpEx (NPV, 20 yr, 4%)	-	5.2	k€/kW
Sum CapEx + OpEx	-	11.1	k€/kW

Table 7.1: System cost for Lifesaver and estimates for next generation device

Since wave energy is an immature energy source, several political incentives exist to facilitate the development of this new resource. Several governmental subsidies and mechanisms are available, such as investment support and feed-in tariffs, the best support regime present as this work is in writing is believed to be the UK *Strike Price*, which guarantees wave energy producers a fixed income of 360 €/MWh [31], regardless of the electricity price. The design target for the next generation device is 175 kW rated capacity, which shall result in at least 700 MWh produced electricity per year at Wavehub. The performance simulations in section 7.3 indicates somewhat higher output power for the selected system, and the numbers stated here are believed to be conservative. Thus, annual electricity revenue of 250 k€per year can be expected for one device at Wavehub.

To calculate the financial viability for the project, the input data listed in Table 7.2 is used. These numbers are based on a 5 MW wave farm installed on Wavehub, and does not include cost of the cable to shore since this is already present at Wavehub. The cost of installation is heavily dependent on the farm size, and the relatively small project size of 5 MW consisting of only 28

Property	Value	Unit
System investment cost	1 029	k€
Installation cost	166	k€
Total investment cost (CapEx)	1 195	k€
Operating cost (OpEx)	67	k€/yr
Electricity price	360	€/MWh
Rated power of device	175	kW
Annual produced energy	700	MWh
Annual electricity revenue	250	k€
Lifetime	20	yr
Required IRR	15	%

Table 7.2: Cost assumptions per device for a 5 MW grid connected wave energy farm at Wavehub

WECs is heavily penalized due to the high startup cost of vessel chartering and site survey, which results in a unit cost of 166 k€ per device. The total project cost is calculated with Equation (7.1), which describes the *Net Present Value* (NPV) of an investment that involves future cash flows. The purpose of the NPV is to incorporate the effect of the interest rate i, which makes future investments R for the year t less costly than present investments. This has negative impact on renewable power systems since most of the investment occurs up front, while the revenue comes from future energy production. In comparison, most fossil-based power systems have lower investment cost and higher running cost due to fuel expenses. The *Internal Rate of Return* (IRR) is the interest rate that results in zero NPV, as shown in Equation 7.2. The IRR shows the payback rate of the investment, and must be higher than the general bankable interest rate for the project to be considered profitable. To also cover the added risk due to variable electricity prices and other unforeseen events, projects of this kind are generally expected to yield at least 15 % IRR.

$$NPV\,(i,N) = \sum_{t=0}^{N} \frac{R_t}{(1+i)^t} \tag{7.1}$$

$$NPV\,(i,N) = 0 \;\Rightarrow IRR = i \tag{7.2}$$

Table 7.3 lists the resulting cash flow through the project duration. The net present value of the project is negative, which shows that the project is not profitable with the current assumptions. However, it was found that for a larger farm, the reduction in installation cost per device was enough to turn a positive profit margin. These numbers are based on an IRR of 15%, but due to the high risk with a project of this nature, investors are likely to require higher returns. The approach of improving profitability by increasing the size of the project must also expect poor support from investors as larger investments demand lower risk. To make the project practically viable, a solution that allows for small start up investments must be found.

The high dependency of subsidies is also problematic for the future profitability, as the subsidies are scheduled to be discontinued in the future. The strike price supported by the UK government is mainly a strategic subsidy meant to boost activity in the renewable energy sector, however some parts of the subsidies can be expected to last. Firstly, clean energy is likely to be rewarded in the future and a fixed rate for renewable energy should be expected. Secondly, as more of the energy is supplied from renewable sources, regulation of the power balance will become more difficult. As argued in section 1.5, the ability of wave energy to produce a different

Year	Cash flow	NPV
0	-1 195 000 €	-1 195 000 €
1	183 000 €	159 130 €
2	183 000 €	138 374 €
3	183 000 €	120 325 €
⋮	⋮	⋮
20	183 000 €	11 181 €
Sum NPV	-	**-49 792 €**

Table 7.3: Cash flow for a single device for the project duration

power profile than the other renewable resources provides added value that should be favored by a regulatory subsidy.

7.2 Cost down process

As wave energy conversion is an immature technology compared to the existing renewable technologies such as PV and wind turbines, extensive investments over long periods must be expected for building up a wave energy industry that can compete in the energy market. It is also important to respect the fact that wave energy may show to be an unprofitable energy source in the long-term. Therefore, WEC development must be organized so that R&D can be performed through incremental steps requiring small investments. A development path must be identified that can generate income along the way so that R&D cost can be covered by revenue rather than upfront investments. Such an approach also ensures early experience from operation and early customer feedback, which is vital for efficient usage of development resources according to the *Lean startup model* [30]. Three cases for possible future project paths are defined for further investigation, which are illustrated in Fig. 7.1, where Fig. 7.1(a) shows the current status, referred to as the base case. The three cases are:

1. Grid connected system
2. Remote system
3. Integrated system

Grid connected system

The fastest way to large-scale market entry would be to perform full-scale system deployment on a site like Wavehub. Such a move could also show to be strategically important since it would be the first commercial wave farm connected to grid. This could prove the viability of wave energy as a power source, and could attract others to invest in wave energy. Many wave energy projects have failed in the past, which has created large skepticism towards wave energy.

The calculations in section 7.1 demonstrated that the project cost where on the borderline for profitability. This was based on scaling up the Lifesaver system from its current 75 kW capacity to 175 kW to meet the financial performance requirements, as illustrated in Fig. 7.1(b). This will also incur significant development costs that has not been discussed yet, these costs should be expected to be in the 10-20 M€ range. For continuing this approach, a path that can

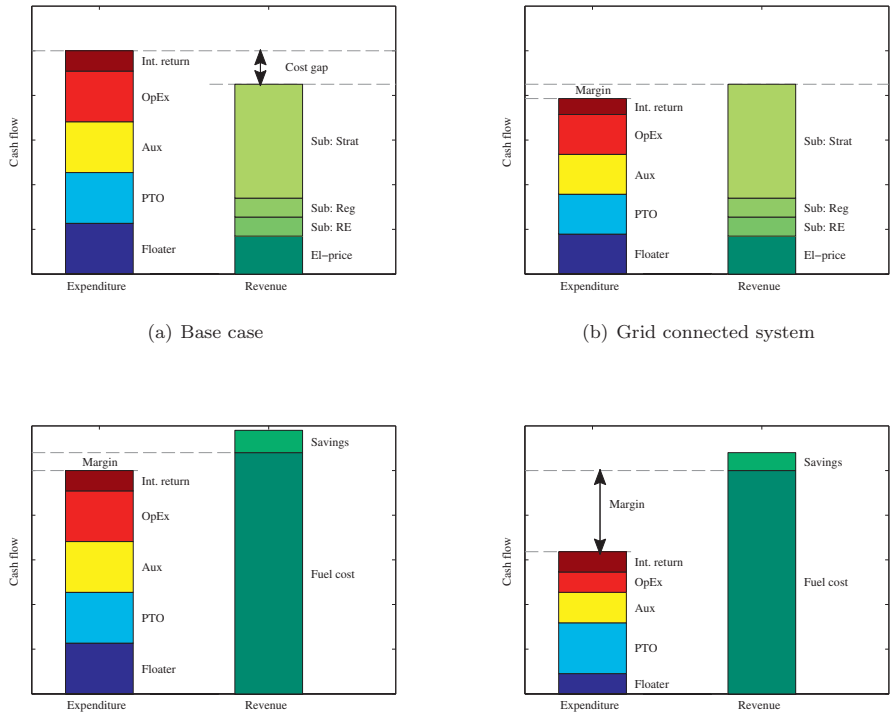

(a) Base case

(b) Grid connected system

(c) Remote systems

(d) Integrated system

Figure 7.1: Cost and revenue elements for various development paths

both demonstrate increased return from system investment and a good potential to cover the development cost must be demonstrated.

The UK strike price of 360 €/MWh is limited to the first 30 MW of installed production capacity [31], which pose a threat to the future income from wave energy. There is high uncertainty linked to the future subsidies after this threshold has been breached, and the grid approach should aim to prove profitability within the given framework of the strike price program. Hence, pursuing the grid-connected case would require investment support.

Based on the calculation presented in section 7.1, deployment of 5 MW farm would cost 33.5 M€. If 16.5 M€ of development cost are included, the project will amount to 50 M€. With an investment funding of 50%, this would result in a healthy return on investment of 20%. The availability for such funding programs has currently not been recognized, but there is strong political support in many countries for developing wave energy, and it is fully possible that such a program could be established.

Remote systems

A large portion of the global electricity production is not connected to a centralized grid. In smaller island grids, much of the power is often supplied by diesel generators, with high cost of diesel due to transportation cost and high oil price. In isolated locations where the wave resources are good, wave energy could be an attractive energy supplier, as illustrated in Fig. 7.1(c). However, for wave energy to be the preferred choice, the location must be less suitable for wind and solar power, as these sources could be more attractive alternatives.

The concept of the remote system approach is to identify customers that can benefit from the FO wave energy system at the current technology level. This could allow for rapid deployment of small farm systems and would require low investments compared to the grid case. Since the system could be deployed quickly, involving less development activity, this approach could also speed up the learning rate. The remote system approach could also be suitable for small incremental improvements, allowing a larger farm being built up based on the experience gained on the first devices.

However, as it may be difficult to find sites that can accept the current electricity cost from Lifesaver, some development effort is likely to be required to reduce the cost of electricity. Recapping this cost will take more time for a small system and could be a lengthy process. In addition, many of the possible sites will be in remote locations that will be hard to visit. This may counteract the ability for fast learning and prototyping as frequent visits to the facility for development team will be difficult.

Integrated systems

Every floating device that consumes power and is exposed to ocean waves could be a potential wave energy customer. Devices like offshore-platforms, stationary buoys/vessels and fish farms could have an integrated wave energy device that delivered power for on-board consumption. The base electricity price on such a location is likely to be high, given its remote nature. In addition, the integration of the wave energy device could significantly reduce cost of electricity since items as floater, moorings and control/communication could be shared with the existing system, as illustrated in Fig. 7.1(d). If the device is manned, or requires regular maintenance, a large portion of the operating cost can also be taken out or shared since this is related to transportation of personnel.

Such a system could be very advantageous, as it may fit very well with the wave power application and be directly competitive to alternative renewable sources with the current technology level. Although the devices are likely to be in remote locations, development, build and operation is likely to take place in a centralized facility located in an industry cluster close to suppliers. This is a large benefit to drive quick development.

7.3 Future potential

The Lifesaver system is 16 m in diameter and has a rated power output of 75 kW. It is evident through simulations that there is a large potential for further up-scaling of the system, and in an endeavor to investigate the ultimate potential for the FO concept, a comprehensive analysis has been performed for a large number of theoretical systems. The process is based on the FO simulation model described in Chapter 6, which has been developed through the entire wave energy project, and which has become very accurate for these systems.

The analysis is performed by simulating different pairs of floater sizes and PTO sizes. All configurations are simulated for the design wave state (H_s = 2.75m / T_z = 6.5s), and for a low

wave state defined as (H_s = 1.25 / T_z = 5.0). In addition, estimates for the system cost is required to give an impression of the feasibility of the designed systems, and two very simplified cost functions where established as a best guess based on experience with earlier systems. The floater cost estimate is given in Equation 7.3 and establishes the cost $C_{floater}$ as function of the floater area A in square meters. The cost curve has progressive rate, which makes each added square meter more expensive than the previous one. This is due to included volume effects that demands increased floater height and increased structural support as the area increases.

$$C_{floater} = 500 \cdot A^{1.15} \tag{7.3}$$

$$C_{PTO} = 60 \cdot F^{0.65} \tag{7.4}$$

Equation 7.4 gives the PTO cost C_{PTO} as function of the PTO production force F in Newtons. This function is regressive, as economy of scale reduces the specific cost. In addition, improved efficiency of the larger generator help increase power output. These mechanisms has been verified by comparison against similar systems developed by FO. By using these formulas, the floater cost listed in Table 7.4 and the PTO cost listed in Table 7.5 is found. Table 7.4 also lists the incoming energy on each floater size. This is defined as the wave power flux in the design wave state multiplied with the width of the floater and describes the amount of energy that interferes directly with the floater.

		Cost [k€]	Area [m^2]	Weight [ton]	Draft [m]	P_{Wave} [kW]
d [m]	LS	87.56	123	46	0.36	511
	15	114.2	177	60	0.33	479
	20	221.4	314	116	0.36	639
	25	369.9	491	194	0.39	799
	30	562.5	707	295	0.41	959
	35	801.9	962	421	0.43	1118
	40	1090	1257	572	0.44	1278
	50	1821	1963	955	0.47	1598

Table 7.4: Cost [€] of the floater with specified diameter, and incoming energy on this floater in the design wave state. (LS: Lifesaver)

		Number of PTOs				
		1	3	4	5	6
PTO force [tons]	30	217.9	320.1	354	382.8	408
	50	303.7	446.1	493.4	533.5	568.6
	75	395.3	580.7	642.2	694.4	740.1
	100	476.6	700.1	774.2	837.1	892.3
	150	620.3	911.2	1008	1090	1161
	200	747.9	1099	1215	1314	1400
	300	973.4	1430	1581	1710	1822
	400	1174	1724	1906	2061	2197
	500	1357	1993	2204	2383	2540
	650	1609	2363	2614	2826	3012
	800	1841	2705	2991	3234	3448
	1000	2129	3127	3458	3739	3986
	1250	2461	3615	3998	4323	4608

Table 7.5: Total PTO cost [€] given a total force rating and number of PTOs. (LS: Lifesaver)

The PTO costs in Table 7.5 shows high influence of the number of PTOs in the configuration. Due to economy of scale, it is beneficial to locate all the damping force in one PTO. However,

simulations with Lifesaver have shown significantly increased power output with multi-PTO systems due to the ability to produce power from roll and pitch motion in addition to heave motion. To get an overview of the production potential of multi-PTO systems, a general scan that simulated all the buoys in the simulation library was performed. The buoys are simulated with different number of PTOs, ranging from one to six. The PTO is positioned in center in the single PTO case, otherwise the PTOs are positioned evenly distributed along the outer edge 0.75 R from center, as illustrated in Fig. 7.2. The incoming wave direction is from north, referred to the figure, which is believed to be the worst-case direction for power production.

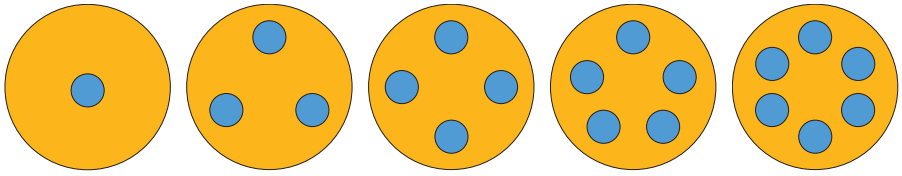

Figure 7.2: Five different configurations tested with one to six PTOs

The multi-PTO scan showed a clear preference towards three PTOs. Configurations beyond three PTOs showed slightly increased power output, but the additional produced energy did not offset the increased PTO cost. Three PTOs seems like the optimal solution as it is the smallest multi-PTO configuration that can fully exploit the pitch and roll potential, and this configuration was selected for the PTO and floater scan. Table 7.6 shows the average power production in the design wave state for the various configuration pairs, and shows a high potential for higher power output, with the average output power actually exceeding 1 MW for the largest devices simulated. However, as these numbers are far away from our current power range, they are not verified against real systems, and must be handled with care.

		Total production force [tons]												
		30	50	75	100	150	200	300	400	500	650	800	1000	1250
d [m]	LS	35	52	65	72	80	76	64	54	47	39	33	27	22
	15	46	71	95	112	132	138	126	107	92	77	66	56	46
	20	49	79	111	139	181	209	233	231	216	185	159	135	115
	25	50	82	118	150	207	252	315	348	360	353	328	284	239
	30	49	83	121	156	221	276	366	428	469	501	506	486	440
	35	48	82	120	156	224	286	391	475	539	607	646	666	654
	40	47	82	121	158	229	294	411	509	591	687	757	816	847
	50	45	79	117	154	226	295	421	536	638	773	887	1011	1126

Table 7.6: Average power [kW] in design wave state (Hs=2.75m/Tz=6.5s) (LS: Lifesaver)

All configuration pairs were also simulated for the low wave state (Hs=1.25m/Tz=5.5s), and by assuming 25% occurence of the design wave state and 50% occurence of the low wave state, the annual prodced energy could be estimated. The weight between design wave state and low wave state are based on the Wavehub scatter diagram. Table 7.7 lists the resulting annual energy production, and by incorporating the simplified cost figures calculated from Equation 7.3 and 7.4, the estimated cost of energy is found, as listed in Table 7.8. In this case, a simplified model for cost of energy is used where the running cost and revenue through the entire project life is simplified to equal 10 years of revenue. This result in very rough estimates, and the numbers should only be evaluated on a relative basis.

As expected, the results show a strong dependency between floater size and PTO force. The table point out the 600 kW device with 500 tons of damping force and 40 m circular disk floater

		Total production force [tons]												
		30	50	75	100	150	200	300	400	500	650	800	1000	1250
d [m]	LS	120	170	206	221	232	218	182	153	133	109	92	75	58
	15	173	253	319	361	399	400	357	301	259	216	186	155	128
	20	190	295	400	482	595	659	691	664	611	522	450	382	325
	25	193	310	435	544	719	847	999	1055	1056	1003	919	798	675
	30	194	317	454	578	793	967	1220	1371	1451	1484	1456	1365	1225
	35	188	312	452	583	817	1020	1344	1576	1735	1872	1926	1918	1834
	40	186	312	456	591	840	1062	1434	1725	1947	2180	2322	2410	2419
	50	173	293	433	566	818	1052	1470	1827	2132	2505	2795	3077	3300

Table 7.7: Annual energy [MWh]. Calculated as 25% occurence of design wave state and 50% occurence of low wave state. (LS: Lifesaver)

		Total production force [tons]												
		30	50	75	100	150	200	300	400	500	650	800	1000	1250
d [m]	LS	588	552	575	634	768	973	-	-	-	-	-	-	-
	15	431	386	383	399	457	541	775	-	-	-	-	-	-
	20	473	382	344	330	332	352	422	521	645	885	-	-	-
	25	577	433	365	332	304	298	313	348	394	482	593	780	-
	30	715	509	409	359	311	290	279	288	306	344	393	476	603
	35	920	628	487	415	343	308	279	272	275	291	315	357	421
	40	-	760	574	479	383	335	290	272	266	269	279	301	337
	50	-	-	846	685	521	437	354	314	292	276	269	270	278

Table 7.8: Cost of energy [€/MWh]. Calculated as device cost over 10 years of energy production. (LS: Lifesaver)

as the most profitable. However, the analysis also demonstrates that the profit gain from up-scaling is small, and that good system configurations can be found also for smaller systems. Three systems were selected for a comprehensive analysis and were simulated for all wave states occurring in the Wavehub scatter. The resulting KPIs are listed in Table 7.9, and the KPIs and units are defined in Table 7.10.

		ΣF_{pto}	A_{buoy}	P_{nom}	E_{year}	C_{buoy}	C_{pto}	C_{Σ}	C_P	C_E
Floater	LS	30	122.5	32.99	181.4	87.56	320.1	407.6	12360	321.1
	D25	150	490.9	198.8	1075	369.9	911.2	1281	6442	170.2
	D30	300	706.9	352	1884	562.5	1430	1992	5660	151.1
	D40	600	1257	633.1	3404	1090	2244	3334	5266	139.9

Table 7.9: Overview of system performance of the three selected systems plus Lifesaver (LS). Units listed in Table 7.10

All of these systems show promising cost parameters, and to get a more firm understanding of the actual profitability, a more detailed cost analysis must be performed. The 25 m buoy configuration was selected as the most realistic next step, and was used as basis for the detailed analysis. To have contingency on power output, rated power of this system were set to 175 kW, although the simulation indicate 198 kW. The system has been designed to a moderate level of detail, with selection and asking quotes for the major components. A rough design of the hull was also performed. These analysis resulted in the numbers presented in the economical analysis in section 7.1.

7.4 Concluding remarks

The analysis performed in this chapter demonstrates the possible paths forward for development of wave energy. An approach of grid connecting a medium sized farm at Wavehub seems to

Symbol	Property	Unit
ΣF_{pto}	Total production force	kN
A_{buoy}	Area of floater	m^2
P_{nom}	Rated power of device	kW
E_{year}	Annual energy production at Wavehub	MWh
C_{buoy}	Cost of floater	k€
C_{pto}	Cost of PTO	k€
C_{Σ}	Cost of device	k€
C_P	Cost of installed power	k€/kW
C_E	Cost of energy	€/MWh

Table 7.10: Units used in Table 7.9

be feasible, but it is clear that such an approach would require significant external investment support. The analysis demonstrated the feasibility of larger systems and show cost savings potential for systems up to 1 MW.

Several possibilities exists for performing development through smaller scale systems, the most lucrative solutions seems to be integration with autonomous buoy systems where structure costs and mooring costs could be shared or covered by the existing system. For such systems, wave energy could show to be directly competitive with the existing energy sources.

Chapter 8

Conclusion

This work demonstrates that, despite of the poor power quality produced from the WECs, high quality power can be delivered to grid by accumulating power from several WECs. The specific system example studied consisted of 42 WECs of the Lifesaver type, which results in a total farm capacity of 3 150 kW. Simulated operation at the *Wavehub* test site resulted in 5 312 annual load hours referred to the WEC capacity, however the simulation also showed a recommended capacity on the transmission line of 180 % of the WEC capacity, which lowers the effective performance to 2 939 annual load hours. For the base case, energy storage did not turned out to be economically viable. However, for configurations with high transmission costs, or for situations where excess transfer capacity is not available, the system can be operated towards unity power capacity. This configuration will favour energy storage to compensate for the lost transmission capacity, and the optimal case with approximately three seconds of full power storage capacity results in a loss of only 7.5 % of the annual production output, which results in 4 913 full load hours to be delivered to grid annually. This is significantly higher than most of the alternative renewable sources and demonstrates the long term power stability of wave energy.

FO's cost calculations show that the PTO is the major cost driver in the WEC system. This enforces a paradigm shift in the PTO control strategy from traditional approaches where the PTO is designed and optimized to maximize the power output from the floater. Instead, the system should be designed to maximize the PTO utilization; hence, the floater should be oversized to push the PTO up to or above rated power as much and often as possible. Simulations indicate a maximum draft as result of damping force in the range 30-45 cm for the optimal configurations. This leads to a control philosophy based on passive damping and early saturation, as the PTO will be too weak to perform effective reactive control. A large portion of the annual energy should be produced in saturation. However, experience from sea trials has also uncovered some adverse effects from saturation control that cause unwanted oscillations in the system. This has been verified by theoretical modeling and shows that there is a delicate balance between damped and saturated operation.

Several years of design iterations and sea trials has brought FO to a fully electro-mechanical PTO configuration. Although many hydraulic components show high efficiency at rated speed, the efficiency drop below rated speed is typically much more pronounced than for electrical machines, and has great impact on energy production due to the high variability in speed on WECs. An electro-mechanical configuration that also includes full inverter control of the generator shows superior control and output performance, and is one of the key factors for the successful operation demonstrated during sea trials, where net power output has been demonstrated for wave states down to 0.4 m significant wave height.

The *Lifesaver* system has demonstrated two years of successful sea trials at the *FaB Test* test site outside Falmouth, England. The only issue causing concern is related to excessive wear on the primary mooring lines, which has required *Lifesaver* to be operated at reduced power output. The situation has been greatly improved during the test period, and the FO team believes that the problem will be fixed by proper tuning of the mechanical guiding system for the primary mooring. The current configuration and component selection is expected to provide excellent performance and lifetime when properly adjusted. Except from this issue, the system has shown excellent performance and high reliability, and the sea trials demonstrate that *Lifesaver* is ready for commercial deployment in applications that can tolerate the current cost and maintenance level.

As an alternative approach to market entry, autonomous power systems has been investigated. These could typically power ocean based systems such as measurement stations and other power consumers, and demonstrates a high potential for the FO WEC system. However, to be competitive with PV and small scale wind turbines, the applications must require a moderate power level, typically in the kilowatt range, to fully benefit from wave energy and the high energy density in ocean waves. Currently, no demand for such autonomous power delivery is known, but this could be because this power capacity has not been available until now. Autonomous WEC devices could also prove advantageous in polar regions where the availability of solar energy is low. Most ocean based sites will provide a high number of annual load hours, and by oversizing the WEC with respect to the load, good coverage for the load can be provided so that only limited energy storage is required for continuous load support.

The two major hurdles for commercialization of wave energy is the high cost level of wave energy converters, and the high rate of investments and improvements on the competing renewable energy sources such as wind and solar. However, FO has demonstrated a WEC system that is close to parity with existing feed-in tariffs and current technology, and the major barrier against commercial deployment is the high investments required to cover the fixed costs of deployment, which requires a very large wave farm to return profit. Alternative approaches for development has been studied, which suggest alternative paths to commercialization through small-scale development of various niche markets.

Future work

Several work packages has been identified that should be performed as a continuation of this work, and will be required for large-scale deployment of the FO technology:

- Significant work remains on the array configuration with respect to the mechanical interconnecting between the WECs. This work is based on the presumption that the WECs can be closely spaced to form a larger integrated unit. Some work has been done to support this, but a thorough verification including practical tests is required before full-scale deployment of the FO farm system can be commenced.
- The farm analysis performed in this work is based on the *Lifesaver* system, and should be updated with a fully cost optimized next generation system based on the experience from *Lifesaver*.
- A thorough verification of the multi-body model and correction factors should be performed, including practical verification.
- The power quality assessment showed high values for flicker, which could be a challenge for grid connection. Although some solutions to the problem where suggested, a complete walk-through and verification is required with respect to flicker.

- A detailed grid connection system should be test-designed for a specific set of grid codes to demonstrate the required full scale power system.

Bibliography

[1] IEC 61000-4-15. Electromagnetic compatibility (emc), testing and measurement techniques, flickermeter, edition 1.1, Feb 2003.

[2] International Energy Agency. Annual report, ocean energy systems. `http://www.iea.org/media/openbulletin/OES2012.pdf`, 2012. [Online; accessed 8-April-2014].

[3] H. Akagi, E.H. Watanabe, and M. Aredes. *Instantaneous power theory and applications to power conditioning*. IEEE Press series on power engineering. Wiley, 2007.

[4] A. Blavette, D.L. O'Sullivan, A.W. Lewis, and M.G. Egan. Impact of a wave farm on its local grid: Voltage limits, flicker level and power fluctuations. In *OCEANS, 2012 - Yeosu*, pages 1–9, May.

[5] Cecilia Boström. *Electrical Systems for Wave Energy Conversion*. PhD thesis, Uppsala University, Electricity, 2011. Felaktigt tryckt som Digital Comprehensive Summaries of Uppsala Dissertations from the Faculty of Science and Technology 727.

[6] Carnegie. Australian wave project gets environmental approval. *Pump Industry Analyst*, 2013(1):3 – 4, 2013. `http://www.sciencedirect.com/science/article/pii/S1359612813700107` [Online; accessed 8-April-2014].

[7] PSA Peugeot Citroën. Hybrid air, an innovative full hybrid gasoline system. `http://www.psa-peugeot-citroen.com/en/featured-content/automotive-innovation/hybrid-air-engine-full-hybrid-gasoline`, 2013. [Online; accessed 18-March-2014].

[8] Alain Clément, Pat McCullen, António Falcão, Antonio Fiorentino, Fred Gardner, Karin Hammarlund, George Lemonis, Tony Lewis, Kim Nielsen, Simona Petroncini, M.-Teresa Pontes, Phillippe Schild, Bengt-Olov Sjöström, Hans Christian Sørensen, and Tom Thorpe. Wave energy in europe: current status and perspectives. *Renewable and Sustainable Energy Reviews*, 6(5):405 – 431, 2002.

[9] Jens Engström. *Hydrodynamic Modelling for a Point Absorbing Wave Energy Converter*. PhD thesis, Uppsala University, Electricity, 2011.

[10] J Falnes. Principles for capture of energy from ocean waves. phase control and optimum oscillation. *Internet Web page. http://www.phys.ntnu.no/instdef/prosjekter/bolgeenergi/phcontrl.pdf*, 1997.

[11] Johannes Falnes. *Ocean Waves and Oscillating Systems: Linear Interactions Including Wave-Energy Extraction*. Cambridge University Press, 2002.

[12] John Fitzgerald and Lars Bergdahl. Including moorings in the assessment of a generic offshore wave energy converter: A frequency domain approach. *Marine Structures*, 21(1):23 – 46, 2008. http://www.sciencedirect.com/science/article/pii/S0960148111005702.

[13] S Fryze. Wirk-, blind- und scheinleistung in elektrischen stromkreisen mit nichtsinusförmigem verlauf von strom und spannung. In *ETZ-Arch. Electrotech.*, volume 53, pages 596–599, 625–627, 700–702, 1932.

[14] A. Garces, E. Tedeschi, G. Verez, and M. Molinas. Power collection array for improved wave farm output based on reduced matrix converters. In *Control and Modeling for Power Electronics (COMPEL), 2010 IEEE 12th Workshop on*, pages 1 –6, june 2010.

[15] Rico H. Hansen, Morten M. Kramer, and Enrique Vidal. Discrete displacement hydraulic power take-off system for the wavestar wave energy converter. *Energies*, 6(8):4001–4044, 2013. http://www.mdpi.com/1996-1073/6/8/4001.

[16] Ross Henderson. Design, simulation, and testing of a novel hydraulic power take-off system for the pelamis wave energy converter. *Renewable Energy, Marine Energy*, 31(2):271 – 283, 2006. "http://www.sciencedirect.com/science/article/pii/S0960148105002259" [Online; accessed 24-Feb-2014].

[17] I.Bjerke, E.Hjetland, G.Tjensvoll, and J.Sjolte. Experiences from field testing with the bolt wave energy converter. In *Submitted to the European Wave and Tidal Energy Conference (EWTEC11)*, september 2011.

[18] International Energy Agency (IEA). Clean energy progress report. http://www.iea.org/publications/freepublications/publication/CEM_Progress_Report.pdf, 2011. [Online; accessed 23-March-2014].

[19] J.Falnes. Principles for capturie of energy from ocean waves: phase control and optimum oscillation. Technical report, NTNU, 1997. http://folk.ntnu.no/falnes/w_e/index-e.html#RAPPORTAR.

[20] J.Falnes and P.M.Lillebrekken. Budal's latching-controlled-buoy type wave-power plant. In *5th European Wave Energy Conference*, 2003.

[21] Joint North Sea Wave Observation Project (JONSWAP). http://www.wikiwaves.org/Ocean-Wave_Spectra.

[22] D. Kavanagh, A. Keane, and D. Flynn. Challenges posed by the integration of wave power onto the irish power system. In *Published at the EWTEC11 conference*, Sept. 2011.

[23] Erlend Kristiansen, Åsmund Hjulstad, and Olav Egeland. State-space representation of radiation forces in time-domain vessel models. *Ocean Engineering*, 32(17):2195–2216, 2005.

[24] Mathias Huuse Marley. Modelling and robust control of production force of a wave energy converter. 2014.

[25] W. Mombauer. *EMV: Messung von Spannungsschwankungen und Flickern mit dem IEC-Flickermeter ; Theorie, Normung nach VDE 0847 Teil 4-15 (EN 61000-4-15) - Simulation mit Turbo-Pascal*. VDE-Schriftenreihe Normen verständlich. VDE-Verlag, 2000.

[26] Gunnar Mørk, Stephen Barstow, Alina Kabuth, and M.Theresa Pontes. Assessing the global wave energy potential. In *Proceedings of OMAE2010, 29th International Conference on Ocean, Offshore Mechanics and Arctic Engineering*, June 2010.

[27] J.N. Newman. *Marine Hydrodynamics*. Mit Press, 1977.

[28] Intergovernmental Panel on Climate Change (IPCC). Assessment report 4, synthesis report. http://www.ipcc.ch/pdf/assessment-report/ar4/syr/ar4_syr.pdf, 2009. [Online; accessed 23-March-2014].

[29] SEEWEC Project. Web page. http://www.seewec.org/index.html, 2007. [Online; accessed 24-March-2014].

[30] Eric Ries. *The Lean Startup: How Today's Entrepreneurs Use Continuous Innovation to Create Radically Successful Businesses*. Crown Business, 2011.

[31] Kelvin Ross. UK reveals renewable energy strike prices. *Renewable Energy World*, http://www.renewableenergyworld.com/rea/news/article/2013/06/uk-reveals-renewable-energy-strike-prices, June 2013.

[32] S. H. Salter. World progress in wave energy 1988. *International Journal of Ambient Energy*, 10(1):3–24, 1989. http://www.tandfonline.com/doi/abs/10.1080/01430750.1989.9675119.

[33] Solcept. Flicker simulator. http://www.solcept.ch/en/embedded-tools/flickersim/, 2014. [Online; accessed 7-Apr-2014].

[34] Darlene Steward, Todd Ramsden, and Kevin Harrison. Hydrogen for energy storage analysis overview. *National Renewable Energy Laboratory. NREL/PR-560-48360*, 2010.

[35] Maxwell Technologies. http://www.maxwell.com.

[36] Ocean Power Technologies. http://www.oceanpowertechnologies.com/. [Online; accessed 8-April-2014].

[37] E. Tedeschi, M. Carraro, M. Molinas, and P. Mattavelli. Effect of control strategies and power take-off efficiency on the power capture from sea waves. *IEEE Transactions on Energy Conversion*, 26(4):1088–1098, 2011. http://www.scopus.com/inward/record.url?eid=2-s2.0-82155162473&partnerID=40&md5=8154812c8af086cfd9453f02ec99ee8d.

[38] E. Tedeschi and M. Molinas. Impact of control strategies on the rating of electric power take off for wave energy conversion. In *IEEE International Symposium on Industrial Electronics*, pages 2406–2411, 2010. http://www.scopus.com/inward/record.url?eid=2-s2.0-78650351853&partnerID=40&md5=a82865e32786f6209031b80a5811868a.

[39] E. Tedeschi, M. Molinas, M. Carraro, and P. Mattavelli. Analysis of power extraction from irregular waves by all-electric power take off. In *2010 IEEE Energy Conversion Congress and Exposition, ECCE 2010 - Proceedings*, pages 2370–2377, 2010. http://www.scopus.com/inward/record.url?eid=2-s2.0-78650080836&partnerID=40&md5=8c61000510e8fb13d631995a5d32b4c4.

[40] J. Tissandier, A. Babarit, and A.H. Clement. Study of the smoothing effect on the power production in an array of searev wave energy converters. In *Proceedings of the International Offshore and Polar Engineering Conference, 2008*, Jul. 2008.

[41] Pedro C. Vicente, António F.O. Falcão, and Paulo A.P. Justino. Nonlinear dynamics of a tightly moored point-absorber wave energy converter. *Ocean Engineering*, 59(0):20 – 36, 2013. http://www.sciencedirect.com/science/article/pii/S0029801812004179.

[42] R. Waters, M. Rahm, M. Eriksson, O. Svensson, E. Strömstedt, C. Boström, J. Sundberg, and M. Leijon. Ocean wave energy absorption in response to wave period and amplitude - offshore experiments on a wave energy converter. *IET Renewable Power Generation*, 5(6):465–469, 2011.

[43] Wavehub. The wave power climate at the wave hub site, Nov 2006. Journal: Applied Wave Research Review of Wave Power Climate.

[44] Wikipedia. Electricity generation — wikipedia, the free encyclopedia. `http://en.wikipedia.org/w/index.php?title=Electricity_generation&oldid=578105754`, 2013. [Online; accessed 29-October-2013].

[45] Wikipedia. Capacity factor — wikipedia, the free encyclopedia. `http://en.wikipedia.org/w/index.php?title=Capacity_factor&oldid=599322736`, 2014. [Online; accessed 24-March-2014].

[46] Øystein Ulleberg, Torgeir Nakken, and Arnaud Eté. The wind/hydrogen demonstration system at utsira in norway: Evaluation of system performance using operational data and updated hydrogen energy system modeling tools. *International Journal of Hydrogen Energy*, 35(5):1841 – 1852, 2010. `http://www.sciencedirect.com/science/article/pii/S0360319909016759`.

Appendix A

Conference paper 1

Title: All-Electric Wave Energy Power Take Off Generator Optimized by High Overspeed

Conference/Journal: European Wave and Tidal Energy Conference (EWTEC)

Date: 5.-9. September 2011

Location/Publisher: Southampton, UK

All-Electric Wave Energy Power Take Off Generator Optimized by High Overspeed

Jonas Sjolte*, Ida Bjerke*, Even Hjetland* and, Gaute Tjensvoll*
*Fred Olsen
Fred Olsens Gate 2, N0152 Oslo
E-mail: jonas.sjolte@fredolsen.no, ida.bjerke@fredolsen.no,
even.hjetland@fredolsen.no, gaute.tjensvoll@fredolsen.no

***Abstract*—*Wave Energy Converters* (WEC) with all electric *Power Take Off* (PTO) systems have large fluctuations in output power, and have a peak to average power ratio way beyond most other energy producers. Special care must therefore be taken when designing such systems for power export to grid. This paper focus on the electrical design of the PTO and how to optimize towards an optimum peak to average ratio for export. The optimization method is based on the possibility to design the electrical machine with a high ratio between nominal speed and maximum speed, termed the *overspeed ratio*. The design method is implemented into Fred Olsen's point absorber simulation model and ran for various overspeed ratios. A full year of production based on a given scatter diagram is simulated and the resulting annual production and load hours is presented. The simulations show that a high overspeed ratio can be beneficial for most direct driven systems.**

***Index Terms*—Wave Energy, Power take off, Electrical, Generator, Overspeed, Load hours, Export**

I. Introduction

Wave energy producers are different from most other energy producers in that the prime mover operates with a sinusoidal velocity. When such a producer is directly connected to its generator, the generator also has to operate in a sinusoidal manner where the speed is continuously fluctuating from positive to negative. This leads to a continuously fluctuating power output that has to touch zero in every wave. This behavior can be seen in figure 1 which shows the power output from Fred Olsens *Wave Energy Converter* (WEC) *Bolt* [1].

In addition to the power fluctuation in a single wave, the average power between consecutive wave groups is also fluctuating. This can also be seen in figure 1. These properties lead to a high peak power to average power ratio, often above 10 [2].

This paper focuses on how the peak to average ratio can be optimized in the *Power Take Off* (PTO) design in direct driven systems. The method pursued is based on designing the generator and converter system with a nominal speed that is less than the maximum speed. This is referred to as the *overspeed ratio* in the following. When the generator reaches its nominal speed it enter a power saturation region that help limit the peak to average power ratio

The peak to average ratio drives both the cost of the single PTO and the downstream power collection system and grid connection. This is one of the greatest challenges when designing a grid connected WEC system. The method explored in this paper allows for some reduction in the cost driving elements and should always be included in the design process for direct driven generators.

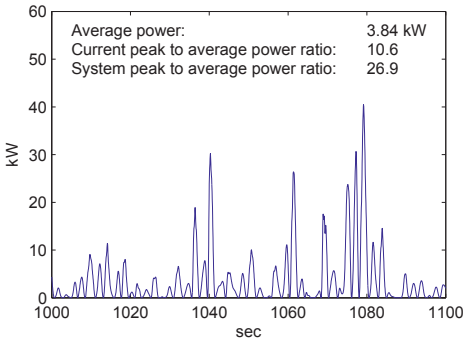

Fig. 1. Typical power output from Fred Olsen's wave energy converter Bolt

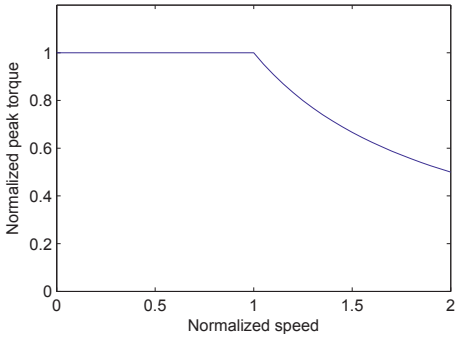

Fig. 2. Available torque from an electrical machine above and below nominal speed

There are two reasons why a high peak to average ratio is bad. The first is that the peak power is driving costs while average power is driving income. The second is the power quality at the grid connection point.

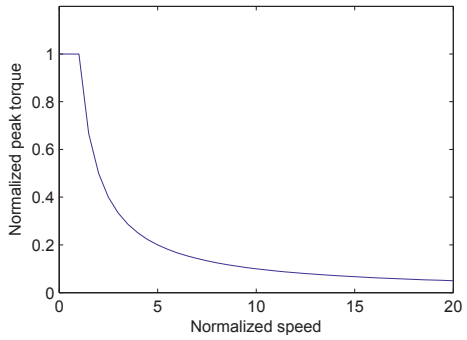

Fig. 3. Available torque from a PMSM machine with an overspeed ratio of 20

II. PTO DESIGN

The main design property for a PTO is the production force. This defines the mechanical structure and strength for most of the components. Since the velocity of WECs is low, the speed is not significant to most of the PTO. The PTO cost is therefore mostly force driven. This also applies to the generator whose size is determined by the required torque. It is not until one reaches the generator windings that the power domain is fully entered. From the generator output and all the way to the grid, power is the cost driving parameter.

A. Generator design

The generator has to be designed as part of the mechanical PTO design and has to comply with the force and speed requirements of the system. These are the mechanical properties of the generator. The electrical properties of the generator is given by its pole count, rotor configuration and winding properties. In the following, the generator system is defined as a frequency converter controlled *Permanent Magnet Synchronous Machine* (PMSM).

Faradays' law of induction, as given in equation 1 defines the relationship between the induced voltage (ϵ), and rate of change in magnetic flux (ϕ) through a conductive loop. Hence, the voltage output from a PMSM can be described by equation 2 where v_{out} is the open circuit voltage, n is the number of pole windings, ω is the electrical frequency and k is a constant comprising the remaining physical properties of the machine. From this, and by including the electrical impedance of the machine, the nominal conditions can be expressed as given by equation 3 where I_n is the nominal current and V_n is the nominal voltage. This shows that the number of pole windings works as a scaling factor between nominal current and voltage. The converter however, has a fixed nominal voltage and as shown by equation 4 where P_n is the nominal power, ω_n is the nominal speed and M_n is the nominal torque, the pole winding count defines the nominal power and the nominal speed of the machine. The nominal torque is assumed to be defined by the physical size and properties of the machine in an earlier stage of the design process.

$$\epsilon = -\frac{d\phi}{dt} \tag{1}$$

$$v_{out} = k \cdot n \cdot sin\left(\omega t\right) \tag{2}$$

$$\frac{V_n}{I_n} = k \cdot n \tag{3}$$

$$P_n = V_n \cdot I_n = \omega_n \cdot M_n \tag{4}$$

Above nominal speed, the output voltage must be kept within limits by field weakening. For PMSMs, this leads to a reduction in available torque that is inversely proportional to the speed. Figure 2 shows the speed torque curve for a common PMSM.

Now, in context of the rather extreme peak to average speed ratio it would be interesting to explore an extreme overspeed ratio of the generator. For instance, Fred Olsens energy producer "Bolt" is operating with an average speed of 0.3 m/s in the most common wave state, but has to handle above 6 m/s in the most extreme wave state. In the following it will be investigated how the nominal speed can be used as a design parameter to optimize the PTO design and power output. Systems with very high maximum to nominal speed ratios are investigated.

B. Control method

Fred Olsen has acquired a viewpoint that an economical direct driven electrical system must be designed so sparse that it is saturated on force and power already in low sea states. This result in little flexibility on doing advanced control algorithms such as reactive control or latching control, and in normal production mode, natural damping serves as the primary production model. In lower sea states however, advanced control algorithms can improve output [2]. Natural damping is defined by equation 5 where the damping coefficient B is optimized towards the highest efficiency region of the machine. M and ω is torque and speed on the generator.

$$M = -B \cdot \omega \tag{5}$$

III. SIMULATION MODEL

The simulation model used [3] [4] simulates the new point absorber system Bolt2 which is under development by Fred Olsen [5].

$$F_{e,i}\left(t\right) - F_{r,i}\left(t\right) - F_{d,i}\left(t\right) - C_i \cdot \zeta_i\left(t\right) - F_{PTO}\left(t\right) = \frac{d^2\zeta\left(t\right)}{dt^2} \tag{6}$$

The simulation model solves the differential equation 6 for $\zeta\left(t\right)$ in the time domain. The index denotes the mode of motion, given by the 6 degrees of freedom of motion for the floater. The excitation force matrix $F_{e,i}$ is now the time dependent force due to incident waves. $F_{r,i}$ accounts for the

time dependent forces on the floater due to radiation of waves. The new term $F_{d,i}$ accounts for non linear damping terms like drag forces. ζ_i is the time dependent motion of the floater, C_i is the restoring force matrix accounting for the hydrostatic pressure acting on the floater and F_{PTO} is the time dependent force applied from the PTO (power take off). The PTO is modeled as a rope and winch system that is tightly connected to the sea floor.

The simulation is based on a detailed 6DOF model of Bolt2 and Fred Olsen therefore keeps the simulation model confidential. However, the high level of complexity is not required for this study and a simplified 1DOF model would produce much the same result. It is therefore possible for a third party to verify the results published here without detailed knowledge about the simulation model used.

For each wave state a 20 minutes time series of irregular waves are generated based on the Wavehub spectrum. The subsequent excitation forces are then calculated and the simulation is run for the full length of the time series. The simulation model also takes into account PTO and generator losses, and the model outputs a 20 minutes time series of exported electrical power from the PTO. The average of this time series is then presented as produced power for that wave state (i.e in figure 4(b).

The simulation model is developed through many years of development and testing and is verified against real production data from several prototypes, among other Bolt.

A. Scatter diagram

All simulations are based on the Wavehub scatter diagram [6]. The probability scatter is shown in figure 4(a). By simulating the power production for the Bolt2 for all occurrences in the scatter, an overall performance plot of Bolt2 can be made. Figure 4(b) shows the simulated operation of Bolt2 in various sea states. The output power is normalized to the defined nominal output of Bolt2 as specified later in this section. The WEC power scatter can now be multiplied with the probability scatter to calculate annual energy production. This is shown in figure 4(c). The plot shows the amount of the annual energy production that occurs in the various sea states.

These three diagrams are an important tool for further WEC optimization. For instance it can be calculated that the most frequent wave height is hs=1.25m and occurs 25% of the time. However, less than 10% of the annual energy is produced on this wave height. The most producing wave state is hs=2.25 and tz=5.5sec and contributes to 9% of the annual energy.

It can be seen from figure 4(b) that the average power from Bolt2 increases with wave height. The theoretical maximum power produced from the PTO, which would occur at constant optimum speed, is even higher. This is typical for most WECs and complicates the definition of rated PTO power. Fred Olsen has decided that the average power in the wave state that produces most annual energy shall be defined as the nameplate power rating. Hence, the most producing wave state hs=2.25 and Tz=5.5sec defines unity in figure 4(b).

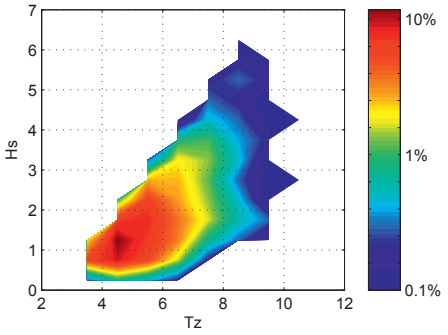

(a) Wave state scatter diagram Wavehub

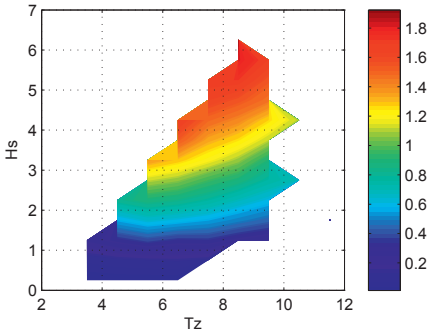

(b) Normalized exported power from Bolt2

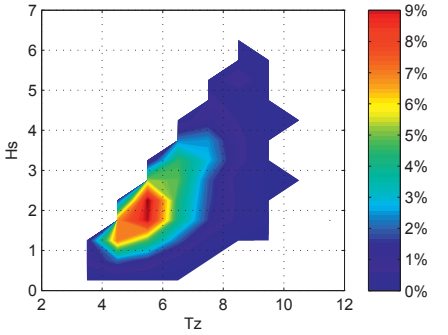

(c) Annual energy production scatter

Fig. 4.

IV. Overspeed optimization

The overspeed optimization is performed by creating generator models for a list of different overspeed ratios. These models are then implemented into the simulation model and a full simulation for all the wave states in the scatter is ran

Overspeed ratio	Annual energy [pu · hours]	Load hours [hours]	Peak power [pu]
1	5093	1840	2.77
3	5081	1928	2.64
5	5017	2180	2.3
7	4878	2511	1.94
10	4593	3026	1.52
15	4070	3690	1.1
20	3547	4128	0.859
30	2832	4773	0.593
40	2368	5244	0.452
50	2041	5611	0.364

TABLE I
WEC PERFORMANCE WITH DIFFERENT OVERSPEED RATIOS

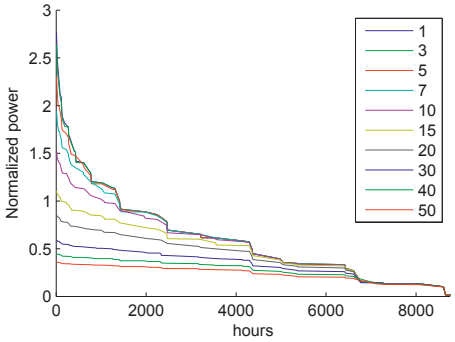

Fig. 5. Annual power distribution per hour

for each of the generator models. The resulting annual energy production for the different overspeed ratios is shown in figure I. The basis for the power normalization is the defined rated power for Bolt2 as described in section III-A. The normalized annual energy is normalized power multiplied with hours.

table I

A first important observation is that the overspeed ratio can be raised to 5 without significant loss of annual production. This corresponds to a 5 times reduction in installed power. Further increase must be done as part of an economical optimization.

For power export, the power distribution of the annual energy production is of great importance since this defines the utilization of the electrical export capacity. Figure 5 shows the average power production for every hour through a year sorted in descending order. Each line represent a generator configuration with a given overspeed ratio. The figure is a good tool for sizing of the export system and it clearly shows the effect of the overspeed ratio. A higher overspeed ratio results in a lower peak power rating, less fluctuation in power production and more load hours. This is mostly achieved by reducing production from the high sea states, but some energy is also lost in the low sea states due to the high irregularities always present.

It can be seen from figure 5 that the overspeed ratio does not appear as a constant power limit, but instead leads to a continuous reduction. This is because the overspeed ratio defines the peak instantaneous power while the exported energy is given by the average power. The goal is maximum utilization of the export capacity, and it is likely that other measures such as energy storage and averaging between groups of WECs also will be used. Another option for improvement of power quality is therefore to implement a saturation mechanism in the controller that regulates against a total defined maximum average power. This can further be improved to aim for a total export capacity from an array of WECs. This, however, is not within the scope of this paper and should be subject for further research.

V. CONCLUSION

The study shows that the overspeed factor can be increased to a factor of five without significant loss in annual energy production. Thus, the peak power rating of the converter and the power export system can be reduced to one fifth without trading away produced power. Hence, overspeed optimization should be a part of every design study that involves all electric PTOs. Further increase in overspeed factor can be done as a part of economical analysis. This study indicates an annual loss of energy production of 10% at an overspeed factor of 10. This is probably around where the lost energy production goes beyond the cost reduction of the power system. Overspeed ratios significantly higher than 10 therefore seem less likely. Further improvements may be achieved by also including power saturation in the motor controller. This will be subject to further study.

REFERENCES

[1] I.Bjerke, E.Hjetland, G.Tjensvoll, and J.Sjolte, "Experiences from field testing with the bolt wave energy converter," European Wave and Tidal Energy Conference (EWTEC11), Tech. Rep., 2011.
[2] E.Tedeschi and M.Molinas, "Impact of control strategies on the rating of electric power take off for wave energy conversion," Norwegian University of Science and Technology, Tech. Rep., 2009.
[3] M.Molinas, O.Skjervheim, P.Andreasen, T.Undeland, J.Hals, T.Moan, and B.Sorby, "Power electroncis as grid interface for actively controlled wave energy converters," International Conf. on Clean Energy Power (ICCEP07), Tech. Rep., 2007.
[4] O.Skjervheim, B.Sorby, and M.Molinas, "All electric power take off for a direct coupled point absorber," Proceedings of the 2nd International Converence on Ocean Energy (ICOE2008), Tech. Rep., 2008.
[5] I.Bjerke, E.Hjetland, G.Tjensvoll, and J.Sjolte, "A brief introduction to the bolt-2-wave project," European Wave and Tidal Energy Conference (EWTEC11), Tech. Rep., 2011.
[6] "The wave power climate at the wave hub site," November 2006, journal: Applied Wave Research Review of Wave Power Climate.

Appendix B

Conference paper 2

Title: All-Electric Wave Energy Converter with Stand-alone 600VDC Power System and Ultracapacitor Bank

Conference/Journal: Electric Vehicles and Renewable Energy conference (EVER)

Date: 27.-30. March 2012

Location/Publisher: Monte Carlo, Monaco

All-Electric Wave Energy Converter with Stand-alone 600VDC Power System and Ultracapacitor Bank

Jonas Sjolte
Fred Olsen / Norwegian University of Science and Technology (NTNU)
Fred. Olsens gate 2, 0152 Oslo, Norway
NTNU, Department of Electrical Power Engineering
Norwegian University of Science and Technology, O. S. Bragstads plass 2E, N-7034 Trondheim
e-mail: jonas.sjolte@fredolsen.no or jonas.sjolte@ntnu.no

Gaute Tjensvoll
Fred Olsen
Fred. Olsens gate 2, 0152 Oslo, Norway
e-mail: gaute.tjensvoll@fredolsen.no

Marta Molinas
Norwegian University of Science and Technology (NTNU)
NTNU, Department of Electrical Power Engineering
Norwegian University of Science and Technology, O. S. Bragstads plass 2E, N-7034 Trondheim
e-mail: marta.molinas@ntnu.no

Abstract: *Fred Olsen has developed a new Wave Energy Converter that is to be launched early 2012. The first stage of testing will be performed in a location without grid connection. The on-board energy production system consists of multiple industrial 400V motor drive inverters that are used to control the generators. Operating such a system off grid requires a complex stand-alone system that can replace the grid functions. In the following the requirements, the chosen design and the implementation of such a system is presented. The corner stone in the system is a 1MJ ultracapacitor bank that stabilizes the power flow and supplies energy for motoring operation. Results from tests up to date are presented.*

Keywords: Wave Energy, Power take off, Electrical, Generator, Export, Autonomous, Stand-alone.

1. Introduction

Fred. Olsen Wave Energy Project (FO) has developed a new *Wave Energy Converter* (WEC) which is going to be launched in Falmouth Bay, England [1] early in 2012. The prototype is equipped with a complete power production system that can export electricity to the grid. However, during the first test phase the WEC will be in a location not suitable for grid connection. Therefore, a method that also allow for operation in stand-alone mode has been developed and implemented by FO. For scientific purposes, this approach is equally relevant since the produced energy can be measured accurately. In the following the requirements for such a system, the development process and the resulting implementation is discussed and presented in detail. Because of confidentiality considerations the *Power Take Off* (PTO) system itself and exported power will only be described in qualitative terms.

1.1 F.O. Wave Energy Project

FO started with Wave Energy in 2000. In 2004 the Wave Energy Converter *Buldra*®, built as a platform with multiple point absorbers, was launched. Since then FO has tested out various concepts and built several different prototypes, all based on the point absorber concept. The series of experiences have led to the single body point absorber system Bolt® shown in figure 1. Point absorbers are not the most efficient absorber type, but has shown to be successful on total performance and cost of energy. Bolt® has been in operation outside Risør in Norway since June 2009 and has up to date performed very well with only minor issues and incidents.

Bolt® has one single PTO machine which is configured very much like the sketch shown in figure 5. It consists of a winch that is tightly connected to the sea floor. The winch drives the generator, which is connected through a gearbox. Bolt® also has a hydraulic spring system that supplies a pretension in the rope. This allows for symmetrical production on the generator. Thus, it can produce power on both upward and downward movement. Since Bolt® is a direct connected system, the generator is moving with the waves. This results in a sinusoidal-like export power that closely follows the surface movements. A typical output from BOLT® in a low wave climate can be seen in figure 2. Bolt had per December 22, 2010 produced 3 360kWh [2].

Figure 1: FO's Wave Energy Converter Bolt® located outside Risør, Norway was launched in June 2009 and is still in operation.

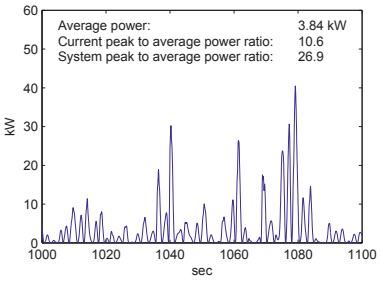

Figure 2: Typical power output from Bolt® in low waves

1.2 Bolt2Wavehub

Based on the success with Bolt®, FO decided to use the knowledge and experience gained so far and proceed to a next generation design. An agreement with several UK companies was made with funding from the UK *Technology Strategy Board* (TSB). The goal of the project is to improve the Bolt® concept to a commercial level where it can be launched at Wavehub [3], thus the project name *Bolt2Wavehub*. The first prototype WEC, which is currently being built is not named yet, but is in the following referred to as *Bolt2*.

Bolt2 is designed as an all-electric PTO system, see figure 5. Bolt2 differs from Bolt® on several points. Firstly, it has a toroidal

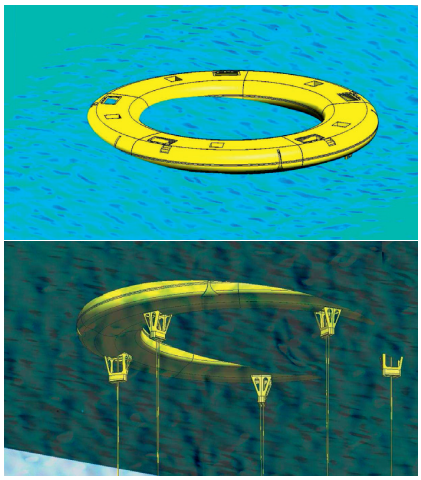

Figure 3: Artistic impression of Bolt2

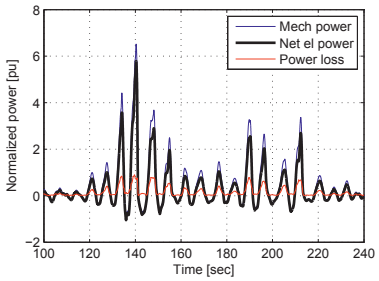

Figure 4: Simulated performance of Bolt2 at hs = 1.75m / tz = 5.5sec. The Power is normalized to the average power production at hs = 2.75m / tz = 6.5sec.

shape and 5 individual PTOs. This allows energy production also from pitch and roll motion in contrast to Bolt, which only can produce from heave motion. Combined with the larger toroidal absorber, this gives good production over a larger wave specter. In high waves, nearly all power is produced by heave motion, but as the wave length shortens and the absorber loses heave response the pitch response increases and helps to maintain a high capture ratio. Capture ratio is defined as the absorbed energy divided by the incoming wave energy through the absorber cross section.

Secondly, the hydraulic spring system from Bolt® has been removed, which includes the

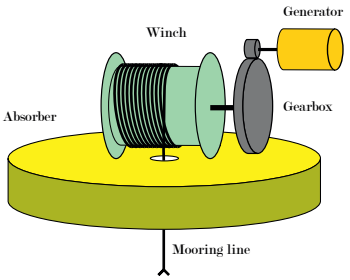

Figure 5: PTO principal sketch for Bolt2

large hydraulic energy storage that supplies the spring energy. Bolt2 is a fully electrical system, and has an electrically connected energy storage instead. This is connected directly on the DC-Link so that the generator itself can act as a motor and pull back the winch on downward movement. This significantly simplifies the PTO and becomes even simpler in a grid-connected system where the electrical energy storage may be omitted. The drawback of the solution is that the peak to average power ratio on the generator increases with at least a factor of 2 since power is produced in one direction only. This is however given by the nature of the rope/winch system. Bolt® and Bolt2 produces the same rope force characteristics, the only difference is the configuration of energy storage and motor/generator. A simulated production time series from Bolt2 is given in figure 4 and shows the bi-directional electrical power flow.

2. System description

The electrical system is based on a common DC-bus that serves as the backbone for the internal power transfer. All five PTOs can inject and extract energy as needed. As can be seen from figure 6 this configuration is the same for both the stand-alone and the grid connected solution. However, in the stand-alone solution an extra system to balance the DC-link and supply power is required to make up for the missing grid converter. This is done with the bi-directional DC-Link converter shown in figure 6(b). As discussed in section 2.3 the DC-Link charger is actually implemented as two independent uni-directional systems.

The stand-alone DC-system can only supply a very limited power, but during normal oper-

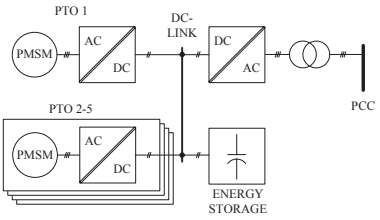

(a) Topology for grid connected system

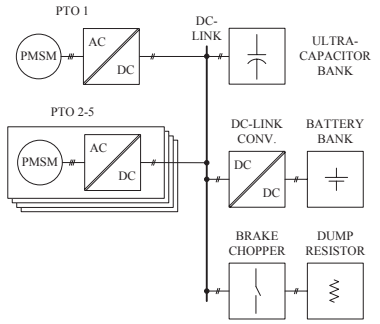

(b) Topology for stand-alone system

Figure 6: Bolt2 topology

ation the system is expected to always produce a power surplus on average. The instantaneous power consumption can be high during pullback for short periods and is supplied by the capacitor bank.

The ultracapacitor bank used as energy storage should only be discharged to half of the nominal voltage during normal cycling. The Siemens components used allow for large fluctuations on the DC-Link voltage and can actually operate with such a voltage variation. Therefore the ultracapacitor bank can be directly connected to the DC-Link and still allow for full utilization of the energy storage capacity.

2.1 Power Take-OFF system

The purpose of the *Power Take-OFF* system, (PTO), is to convert mechanical motion imposed by the waves to electrical energy. The main PTO components are the winch system, the generator and the inverter. The mechanical configuration is shown in figure 5.

A high-performance permanent magnet servo machine is selected as the generator for the system. These machines are characterized

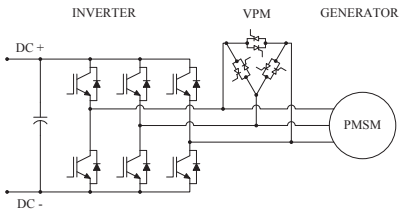

Figure 7: Electrical power take off system with *Voltage Protection Module* (VPM).

Property	Value	
Maximum production force	100	kN
Nominal generator speed	400	rpm
Maximum generator speed	1 800	rpm
PTO nominal prod. power	15	kW
Generator nominal power	80	kW
Inverter nominal power	120	kW

Table 1: PTO specifications

by low inertia, high torque density and high efficiency, which are important properties for a direct coupled wave energy device with a constantly changing speed. The machine is custom built after FO specifications to meet the requirements for Bolt2. As shown in table 1 it as high ratio between the maximum speed and the nominal speed to allow for early power saturation. The effect of this on cost and performance is described in detail in previously published articles [4], [5].

A *Permanent Magnet Synchronous Machine* that is driven by an external uncontrollable force, such as the case for a wave power plant, can be vulnerable to overspeed. If the machine is forced to exceed nominal speed while the inverter is not in operation, the system may be electrically damaged by overvoltage, even though the machine can handle the speed mechanically. Therefore, each PTO is fitted with a *Voltage Protection Module* (VPM), which will automatically short-circuit the generator in the event of uncontrolled overspeed. This will ensure that no harmful energy is allowed to enter the inverter or the downstream power system. The VPM used is a standard product supplied by Siemens and fires at 830V, which is the maximum allowed voltage for the inverter used. This defines the upper limit of the operational range of the capacitor bank as illustrated in figure 15 on page 8.

The PTO is designed as a complete system, and only requires a DC-Link connection and a field bus control connection to operate.

Figure 8: Maxwell technologies® 48V ultracapacitor bank module with active cell balancing

This leads to a flexible system where PTOs may be swapped, serviced and rebuilt without any changes to the WEC itself.

2.2 Capacitor bank

The energy storage is one of the corner stones in making the stand-alone system work. Initially, two solutions were explored: A flywheel based system and a capacitor based system. The flywheel could be implemented as an extra PTO system that rotates a mass instead of driving a winch. However, the performance and modularity offered by the off-the-shelf ultracapacitor system was thought to outperform the flywheel solution, as this would have to be custom designed.

The requirement for the capacitor bank is to supply the required energy for winding in 10m of rope on each PTO with 10kN of pull force. It must also handle wind-in speeds of several meters per second. With a system efficiency of 0.8, and taking into account all five PTOs, the required energy can be calculated to 625kJ by equation 1. Equation 2 indicates a required power of several hundred kilowatts. W_m is the mechanical energy, F is the mechanical force and s is the distance of motion parallel to the direction of force. Equation 2 is the time derivative of equation 1 where energy and distance becomes power and speed. Equation 3 shows the energy storage capacity W_e of a capacitor based on capacitance C and nominal voltage V_n.

$$W_m = F \cdot s \tag{1}$$

$$P_m = F \cdot v \tag{2}$$

$$W_e = \frac{1}{2} C \cdot {V_n}^2 \tag{3}$$

A third requirement for the capacitor bank is that it must handle peak voltages up to 830V. A configuration of 17 serial connected modules of the Maxwell technologies® 48V module [6] fulfill all these requirements, and is the selected configuration. The module is shown in figure 8.

Each module contain 18 serial connected ultracapacitors that are conditioned by an active balancing network. The balancing network allows for bypassing some of the charging current on each cell and is controlled so that all the cells are at equal voltage. If the nominal voltage on the entire module is exceeded, some current is by-passed through the entire module to ensure module balance. The technical data for the capacitor bank is given in table 2.

Property	Value	
Nominal voltage	816	V
Capacitance	4.88	F
Nominal energy	1.63	MJ
Useful energy (400V-776V)	1.08	MJ
Max continuous current	100	A
Max peak current	1 100	A
Short circuit current	4 800	A
Nominal power at 600V	60	kW
Peak power at 600V	660	kW
Modules in bank	17	
Cells per module	18	
Cell capacitance	1.5	kF
Cell voltage	2.70	V
Cycle life	10^6	

Table 2: Ultracapacitor bank specifications

The capacitor module has a specified cycle life of 10^6 cycles. If every charge/discharge cycle during production is counted this number will be reached in less than one year of operation due to the wave frequency. However, most of the cycles are caused by low waves with low energy. Maxwell technologies® offered to simulate the expected life time of the system specifically based on the expected energy profile of Bolt2. The input for the simulation is given in figure 9 and shows capacitor bank voltage profiles from three different wave states, low, high and extreme. The three wave states have a defined probability of 0.4, 0.1 and 1/365 respectively. The remaining probability of ca 0.5 is the down time expected during calm weather. The initial test site is in a sheltered area which causes the high down time.

Based on these inputs Maxwell technologies® has ensured a lifetime significantly above the base case.

2.3 DC-Link charger

The DC-Link charger converts energy from the battery bank to the capacitor bank. This is mainly required for three purposes:

- During startup when the capacitor bank have to be pre-charged and the PTOs have to pull in and tension the production ropes.
- During service when the PTO winches have to be maneuvered.
- In extreme wave states when the required pullback energy might exceed the available energy in the capacitor bank. The pullback process and energy balance is described in section 3.1.

The specifications for the DC-Link charger are as follows:

- Supply up to 5kW of power
- Supply output voltage in the range 0-600VDC
- Handle output voltage in the range 0-830VDC
- Handle input voltage in the range 22.0-29.0VDC
- Allow for current limited operation
- Controllable over LAN
- Serviceable
- Reliable with MTTF $>$ 20 000h

From a power electronics point of view the best solution would be to use a DC/DC boost converter that directly converts the battery voltage to 600VDC. An even more interesting solution would be to merge the DC-charger and the battery charger, that will be described in the next section, into a single bi-directional converter. A possible solution for this is the *Reduced Matrix Converter*, which is based on bi-directional RB-IGBTs. This concept has been explored in detail and has for instance been proposed for off-shore wind turbines [7]. However, no converters based on these topologies that meets all the requirements could be found. Development of such a system from scratch is costly and time consuming, especially when taking into account the required support for maintenance and service. This approach was therefore rejected.

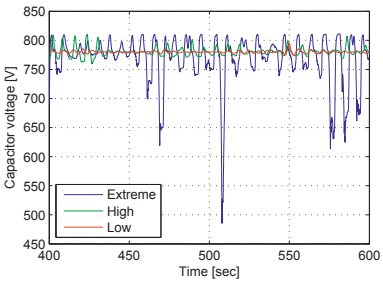

Figure 9: Capacitor voltage in three wave states, Low: hs=1.25m/tz=5.5sec, High: hs=2.75m/tz=6.5sec and Extreme: hs=8.0m/tz=10.0sec

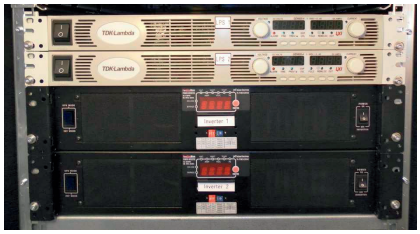

Figure 10: DC-Link charger: Inverters and laboratory power supplies in 19" rack configuration.

Instead a modular two step solution based on a standard 24VDC to 230VAC inverter and a 230VAC to 600VDC laboratory power supply is selected. This takes the power via 230VAC, which is a drawback, but greatly increases the number of off-the-shelf components available. The power supply selected is controllable by LAN, it can supply any voltage in the range 0-630VDC and can operate in current limited mode with set currents in the range 0-4.2A. This leads to a maximum supply power of 2650W. However, it cannot handle more than 660VDC on the output terminals and have to be shield from the voltages on the DC-Link by a reverse blocking diode.

The inverter and power supplies are 19" rack modules and can be seen in figure 10.

2.4 Battery charger

On board systems such as communication, data logging and monitoring equipment consume a considerable amount of power from the 24V battery bank. This power must be generated by some means, and the obvious solution is to use the generated wave energy. This is not straightforward however, given the high- and fluctuating voltage level on the DC-Link. A solution

based on off-the-shelf wind turbines or PV cells would seem easier to implement. Nonetheless, FO decided that it was worth the extra effort to develop the system, as the purpose of the prototype is to prove the viability of wave energy. Moreover, an external power system with the required power rating would be large and potentially fragile to the extreme weather conditions experienced at sea.

The battery charger has the following requirement specification:

- Handle input voltage in the range 0-830VDC
- Operate with input voltage in the range 600-830VDC
- Supply output voltage in the range 20-29VDC
- Supply up to 125A of charging current
- Control charging current based on input voltage
- Comply with 3-stage battery charging principle
- Controllable by field bus

FO decided that the easiest approach to meet these requirements was to base the battery charger on the same motor drive inverter that powers the PTO generators. They can naturally handle the input voltage range, they are programmable, they natively support closed-loop control and FO already has the required knowledge to operate and program them.

The concept is as shown in figure 11. The inverter drives a three-phase 400V/24V transformer that supplies to a 3-phase bridge rectifier. Finally, the output power is smoothed through an inductive filter and fed into the battery bank. To simplify the configuration the transformer and chokes are designed with the same cores and fixed in a common frame. The actual implemented system can be seen in figure 12.

The inverter is operated in scalar mode, which allows for controlling the output frequency directly. The output voltage is regulated proportional to the output frequency to

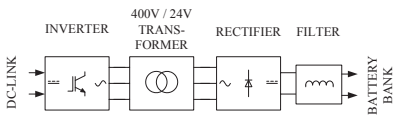

Figure 11: Battery charger topology

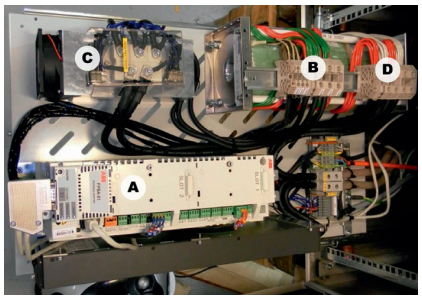

Figure 12: Implemented battery charger configuration: A) Inverter, B) Transformer, C) Rectifier, D) Choke

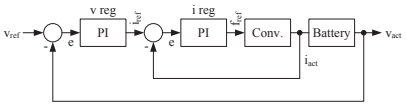

Figure 13: Battery charger control principle

keep the motor impedance constant. This principle is directly transferable to the transformer and gives a system where the output voltage of the transformer can be controlled without risk of excessive currents. The nominal frequency output frequency of the inverter is set to 200Hz as this reduces the transformer size, while still allowing for standard 50/60Hz transformer design methods to be applied.

The charger program is implemented as a closed-loop feedback control with an inner current control loop and an outer voltage control loop as shown in figure 13. The current loop uses the inverter output current as feedback while the voltage loop regulates on the actual battery voltage. This is measured by an external sensor. The three-stage battery charger program is implemented by controlling the current and voltage references. The maximum allowed charging current is set to 125A, the maximum charging voltage is set to 28.8V and the trickle charging voltage is set to 27.6V. The trickle charging stage triggers when the charging current falls below 10% of the nominal.

The battery charger shall adjust the charger power to the DC-Link voltage to allow for stable steady-state conditions for all production levels. This is implemented by setting maximum allowed charging current as a linear function with zero power at 650VDC and full power at 720VDC. This prevents the battery charger from draining the capacitor bank at low production levels.

2.5 Brake chopper

The WEC is expected to produce a power surplus, except for in the lowest wave states close to cut-off. This excess energy will cause the DC-Link voltage to rise and must be taken away to balance the system. This is normally done by switching in a resistor that dissipates the excess energy. For good controllability, the system is typically controlled by *Pulse Width Modulation* (PWM) at around 1kHz. This setup is usually referred to as a *brake chopper* and is very common in motor drive systems.

On Bolt2 a standard brake chopper system is used which will start dumping energy at 776V. The brake chopper has a linear PWM region where the duty cycle is increased proportional to the voltage until saturation occurs around 810V and the resistor bank is constantly switched on. The resistor bank is a large array of air-cooled heating elements that is placed on top of the absorber. Air-cooling was selected in favor of water-cooling for simplified access and maintenance.

The brake choppers operate as stand-alone units and only monitor the DC-Link voltage. They do not require any external regulation or control. Three brake choppers are installed in parallel with individual resistors as shown in figure 14. Each brake chopper has a nominal power of 50kW and a peak power of 250kW. This leads to a total braking power of 150kW nominal and 750kW in peak, and a fully redundant system.

Bolt2 is not expected to go beyond the nominal power on average as the production will be curtailed in high to extreme wave states. However, the peak power limit of 750kW may occasionally be breached by single large waves appearing in high sea states. This requires active production control and is described in section 3.1.

3. Control

Three layers of control are implemented to operate the system:

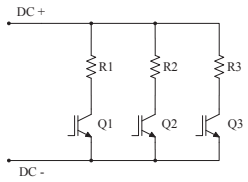

Figure 14: Brake chopper system

1. Top-level control of the WEC
2. Mid-level control of the DC-Link voltage
3. Low-level control of the PTO inverter

The top-level control mainly holds the state machine functions for the WEC and is only discussed briefly. The mid-level and low-level control is discussed in the subsequent sections.

3.1 DC-Link control

The purpose of the DC-Link control is to keep the capacitor bank and the DC-Link voltage within the allowed range, and to ensure the required energy for pullback. The DC-Link control is not a centralized control function, but is accomplished as the sum of several components and functions operating together. The DC-Link conditioning can be divided into three levels, green, yellow and red, as illustrated by figure 15. Within the green region, the capacitor bank voltage is conditioned by the DC-charger in the low voltage end and the brake chopper in the high voltage end. The PTOs are allowed to operate with optimal generation and motoring force. If the production exceeds the brake chopper capacity or the consumption exceeds the DC-charger capacity the yellow region is entered. Operation of all PTOs is then constrained to to counteract further aggravation. In the unlikely event that the absolute limits are breached and the DC-Link voltage enters the red region, all PTOs immediately shut down. In the high voltage case, the VPMs also fires to protect the DC-system and to bring the generators to a controlled stop. Since the rope tension will be lost in this case, no further extreme movements on the PTOs are to be expected.

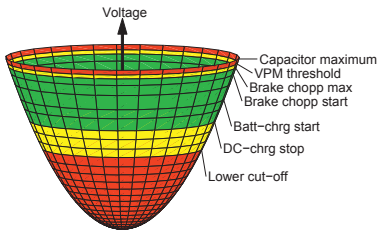

Figure 15: Capacitor bank capacity illustrated as a volume of energy. The energy is proportional to the square of the voltage, which correlates to a paraboloid

The battery charger will start charging the batteries at 650V and will ramp up to full

charging power of 125A / 3.6kW at 720V. This is optimized for production in low waves to maintain an untouched reserve of pullback energy between 650V and 540V. In the higher wave states, the capacitor bank is expected to maintain a close to fully charged state with voltage above 720V most of the time. It is also important to maintain blanking voltage between the DC-charger shutdown threshold and the battery charger startup threshold to avoid circulation of power between the two converters. The DC-charger can supply a maximum voltage of 630VDC and the startup threshold of 650VDC ensures adequate safety margin.

In the extreme wave states it is possible that the capacitor bank is completely cycled in each wave, which can be seen in figure 9 at 510sec. This will cause cyclic charging between the battery bank and capacitor bank as the missing pullback energy must be borrowed from the battery bank. This is only expected occasionally during worst-case conditions and should not significantly affect battery life.

The DC-Link charger will normally operate whenever the DC-Link voltage is below 540V. However, if the WEC is in a low production state, the 540V level is instead used as a trigger for cut-off and causes the entire WEC to shutdown. The WEC will then go into power save mode and measure the waves periodically to determine when production can start up again. This is handled by the top-level WEC control.

3.2 PTO Control

The absorbed power form a point absorber is greatly influenced by the control strategy applied by the PTO. In general the optimal energy extraction is achieved when the point absorber is moving with a 90° phase shift to the waves [8]. Several methods of approaching this production mode are described, the best known being *reactive control* [9], [10] and *latching control* [11]. Figure 16 shows an electrical equivalent

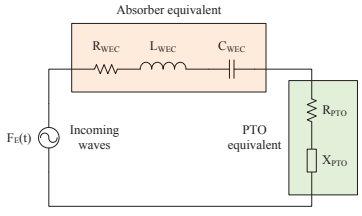

Figure 16: RLC equivalent circuit of the PTO and WEC system

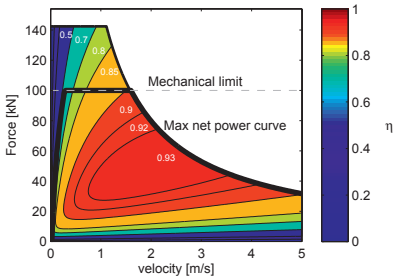

Figure 17: Efficiency plot for the generator used at Bolt2Wavehub. The thick line shows the torque that result in maximum exported power from the generator. The thin line shows maximum available torque from the generator. The dashed line shows the mechanical limit for the gearbox.

circuit for the WEC where the dynamic behavior of the WEC is modeled as an RLC circuit. The PTO is modeled as a power extraction element (resistance) in series with a reactive element (impedance). The goal of reactive control is to tune the reactive element of the PTO so that it compensates for the reactive elements of the WEC as a whole and thus maximize power extraction.

With the current design of Bolt2 the PTO force is too low to have significant impact by reactive control. This is mainly caused by the large area of the absorber that leads to a high spring constant and a high resonance frequency. Passive damping is therefore selected as the primary production model. In the lowest sea states however, advanced control algorithms may improve output [12], but is not implemented yet. A recent and ongoing study by NTNU, that specifically investigates the Bolt® project, indicates that a production boost can be expected from reactive control in wave states with low amplitude and high frequency.

The large and flat absorber shape is selected as a result of economical optimization and FO acquired viewpoint that the absorber should be large enough to push the PTO into saturation already in moderate wave states.

$$\tau = -B \cdot \omega \tag{4}$$

Passive damping is defined by equation 4. The damping coefficient B is optimized to produce the highest possible net power output. τ is the generator torque and ω is the generator speed. Figure 17 shows the torque and speed characteristics for the generator used on Bolt2. The thick line shows the optimal torque that

maximizes the generated electrical power. Two important saturation mechanisms are present; the first is the mechanical force limit of the gearbox. This is reached already at 0.27 m/s. The second is the power limit of the generator that is reached at 1.55 m/s. The linear region from 0 - 0.27 m/s corresponds to a damping coefficient of ca 350 kNs/m, which is the chosen value for B on Bolt2.

4. Discussion

The stand-alone system design presented seem to fulfill the requirement specification. Since system is meant for research only, some of the less efficient solutions are justified. However, systems like the ultracapacitor bank can also be useful in a grid connected system, but should not be adapted as is. The direct connection to the DC-Link forces the whole production system to operate with high variations on the DC-voltage, which result in lower efficiency and constrained operation. The latter is caused by the shifting of the field-weakening point and complicates high speed regulation. Therefore the energy storage should de-coupled from the DC-Link with a separate converter to improve the system efficiency.

5. Conclusion

A stand-alone power system for the wave energy converter Bolt2 has been designed and built. Most of the system components have been tested individually, but no complete system tests have been performed yet. Full system commissioning is expected during November and December 2011. Sea launch is expected early 2012 and is expected to lead to a comprehensive understanding of the system performance during 2012.

References

[1] E.Hjetland, I.Bjerke, G.Tjensvoll, and J.Sjolte, "A brief introduction to the bolt-2-wave project," in *European Wave and Tidal Energy Conference (EWTEC11)*, 2011.

[2] I.Bjerke, E.Hjetland, G.Tjensvoll, and J.Sjolte, "Experiences from field testing with the bolt wave energy converter," in *European Wave and Tidal Energy Conference (EWTEC11)*, 2011.

[3] "The wave power climate at the wave hub site," November 2006, journal: Applied Wave Research Review of Wave Power Climate.

[4] J.Sjolte, I.Bjerke, E.Hjetland, and G.Tjensvoll, "All-electric wave energy power take off generator optimized by high overspeed," in *European Wave and Tidal Energy Conference (EWTEC11)*, 2011.

[5] J. Sjolte, I. Bjerke, A. Crozier, G. Tjensvoll, and M. Molinas, "All-electric wave energy power take off system with improved power quality at the grid connection point," in *2012 IEEE PES Transmission and Distribution Conference and Exposition*, 2012, In press.

[6] "Maxwell technologies," http://www.maxwell.com.

[7] A. Garces, E. Tedeschi, G. Verez, and M. Molinas, "Power collection array for improved wave farm output based on reduced matrix converters," in *Control and Modeling for Power Electronics (COMPEL), 2010 IEEE 12th Workshop on*, june 2010, pp. 1 –6.

[8] J. Falnes, *Ocean Waves and Oscillating Systems: Linear Interactions Including Wave-Energy Extraction*. Cambridge University Press, 2002.

[9] E.Tedeschi and M.Molinas, "Effect of control strategies and power take-off efficiency on the power capture from sea waves," in *IEEE Transactions on Energy Conversion*, 2011, in Press.

[10] E. Tedeschi, M. Molinas, M. Carraro, and P. Mattavelli, "Analysis of power extraction from irregular waves by all-electric power take off," in *Energy Conversion Congress and Exposition (ECCE), 2010 IEEE*, sept. 2010, pp. 2370 –2377.

[11] J.Falnes, "Principles for capturie of energy from ocean waves: phase control and optimum oscillation," NTNU, Tech. Rep., 1997, http://folk.ntnu.no/falnes/w_e/index-e.html#RAPPORTAR.

[12] E. Tedeschi and M. Molinas, "Impact of control strategies on the rating of electric power take off for wave energy conversion," in *Industrial Electronics (ISIE), 2010 IEEE International Symposium on*, july 2010, pp. 2406 –2411.

Appendix C

Conference paper 3

Title: All-Electric Wave Energy Power Take Off System with Improved Power Quality at the Grid Connection Point

Conference/Journal: Power and Energy Society Transmission and Distribution conference (IEEE,PES T&D)

Date: 7.-10. May 2012

Location/Publisher: Orlando, FL, USA

All-Electric Wave Energy Power Take Off System with Improved Power Quality at the Grid Connection Point

Jonas Sjolte, Ida Bjerke, Aina Crozier, Gaute Tjensvoll, and Marta Molinas, *Member, IEEE*

***Abstract*—*Wave Energy Converters* (WEC) with all electric *Power Take Off* (PTO) systems have large fluctuations in output power, and have a peak to average power ratio way beyond most other energy producers. Special care must therefore be taken when designing such systems for power export to grid. This paper focuses on the electrical design of the PTO and how to optimize towards an optimum peak to average ratio for export. The optimization method is based on the possibility to design the electrical machine with a high ratio between nominal speed and maximum speed, termed the *overspeed ratio*. The design method is implemented into Fred Olsen's point absorber simulation model and run for various overspeed ratios. A full year of production based on a given scatter diagram is simulated and the resulting annual production and load hours is presented. The simulations show that a high overspeed ratio can be beneficial for most direct driven systems.**

***Index Terms*—Wave Energy, Power take off, Electrical, Generator, Overspeed, Load hours, Export**

I. Introduction

Wave energy producers are different from most other energy producers in that the prime mover operates with a sinusoidal velocity. When such a producer is directly connected to its generator, the generator also has to operate in a sinusoidal manner where the speed is continuously fluctuating from positive to negative. This leads to a continuously fluctuating power output that has to touch zero in every wave. This behavior can be seen in figure 2 which shows the power output from Fred Olsens *Wave Energy Converter* (WEC) *BOLT*® [1].

In addition to the power fluctuation in a single wave, the average power between consecutive wave groups is also fluctuating. This can also be seen in figure 2. These properties lead to a high peak power to average power ratio, often above 10 [2].

This paper focuses on how the peak to average ratio can be optimized in the *Power Take Off* (PTO) design in direct driven systems. The method pursued is based on designing the generator and converter system with a nominal speed that is less than the maximum speed. This is referred to as the *overspeed ratio* in the following. When the generator reaches its nominal speed, it enters a power saturation region that helps limit the peak to average power ratio.

Jonas Sjolte, Ida Bjerke, Aina Crozierd and Gaute Tjensvoll are with Fred Olsen Ltd, The Wave Energy Project, Fred. Olsens gate 2, 0152 Oslo, Norway e-mail: jonas.sjolte@fredolsen.no, ida.bjerke@fredolsen.no, aina.crozier@fredolsen.no and gaute.tjensvoll@fredolsen.no

Prof. Marta Molinas is with the Norwegian University og Technology and Science (NTNU).

Manuscript received September 21, 2011; revised January 11, 2007.

Fig. 1. Fred Olsens Wave Energy Converter *BOLT*® located outside Risør, Norway

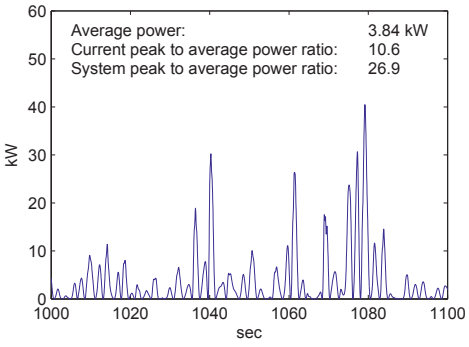

Fig. 2. Typical power output from BOLT in low waves

The peak to average ratio drives both the cost of the single PTO and the downstream power transmission system and grid connection. This is one of the greatest challenges when designing a grid connected WEC system. The method explored in this paper allows for some reduction in the cost driving elements and should always be included in the design process for direct driven generators.

There are two reasons why a high peak to average ratio is unfortunate. The first is that the peak power is driving costs while average power is driving income. The second is the power quality at the grid connection point.

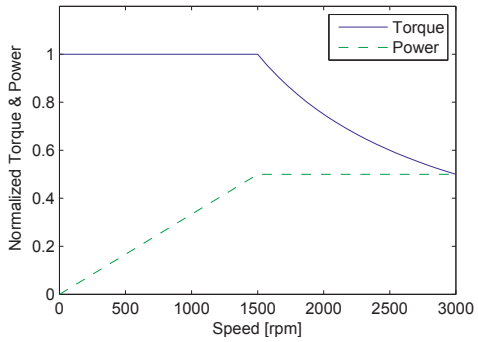

Fig. 3. Available torque from an electrical machine above and below nominal speed

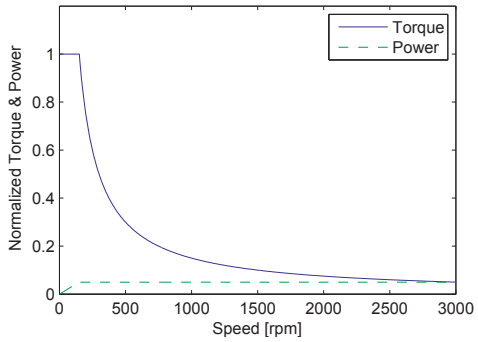

Fig. 4. Available torque from a PMSM machine with an overspeed ratio of 20

A. Fred Olsens Wave Energy Project

Fred Olsen, FO, started with Wave Energy in 2000. In 2004 FO built and launched *Buldra*®, the Wave Energy Converter based on the Aker H3 semi-submersible platform. Since then FO have tested out various concepts and built several different prototypes which have led to the the single body point absorber system *BOLT*®. This has not shown to be the most efficient wave energy absorber, but has shown to be most successful on total performance for cost of energy. *BOLT*® has been in operation outside Risør in Norway since June 2009 and is shown in figure 1. Currently FO is building the next generation of *BOLT*®, currently called *BOLT2*, through the *BOLT2Wavehub* project. This is a joint project between Fred Olsen and several UK companies funded by the UK *Techonology Strategy Board*, TSB. The goal of the project is to further develop BOLT into a commercial system that is ready for operation at the UK wave test facility *Wavehub* [3].

II. PTO DESIGN

Fred Olsen's WEC concept is based on a flat absorber with low mass that gives a high resonance frequency and thus a *Response amplitude operator*, RAO, [4] close to one for most of the relevant wave states. This gives a stiff system that is well suited for passive damping and less suitable for reactive control. The absorber is tightly moored to the sea floor by a winch. The winch connects to the generator through a gearbox. This is shown in figure 5 and is a well known conversion system that has been researched and tested by several parties [5]. Pre-tension in the mooring line is supplied either by a secondary spring equivalent system or by the main generator itself.

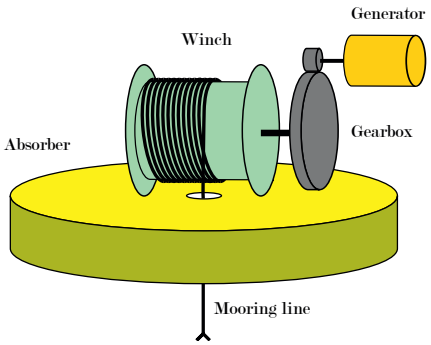

Fig. 5. Principal sketch of the WEC

The main design property for a PTO is the production force. This defines the mechanical structure and strength for most of the components. Since the WEC velocity is far below the critical speed for most of its components, speed and thus power has little impact. The PTO cost is therefore mostly force driven. This also applies to the generator where the size is determined by the required torque. It is not until one reaches the generator windings that the power domain is fully entered. From the generator output and all the way to the grid connection point, power is the main cost driving parameter.

A. Generator design

The generator has to be included in the mechanical PTO design and has to comply with the force and speed requirements of the system. These are the mechanical properties of the generator. The electrical properties of the generator is given by its pole count, rotor configuration and winding properties [6]. The electrical properties give the torque/current relation and the speed/voltage relation, which links the mechanical and electrical properties. In the following, the generator system is defined as a frequency converter controlled *Permanent Magnet Synchronous Machine* (PMSM) [7]. Figure 7 shows how the generator system is electrically integrated into the WEC system. As suggested by the figure several WECs can be connected together on the DC-Link for power smoothing before the power is transformed to AC.

Faradays' law of induction, as given in equation 1 defines the relationship between the induced voltage (ϵ), and rate of change in magnetic flux (ϕ) through a conductive loop.

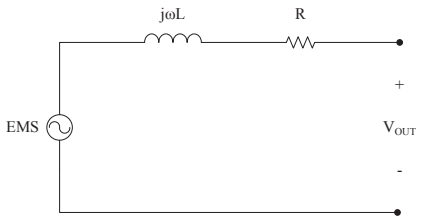

Fig. 6. Equivalent circuit for PM generator

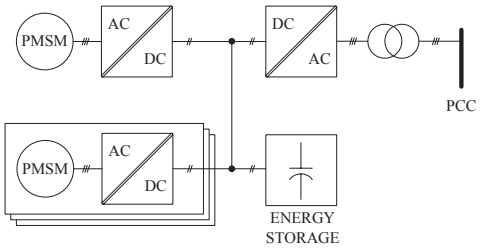

Fig. 7. Principal diagram for BOLT2

From this equation 2 can be derived which gives the induced voltage in n loops with area A that rotates with the speed ω in magnetic field with constant flux density B. This shows the relationship between open circuit voltage and speed of a PMSM. Since the magnetic flux generated by the permanent magnets and the geometrical properties are constant, equation 2 can be simplified into equation 3 where v_{out} is the open circuit voltage and k is a constant. The equivalent circuit of the generator is shown in figure 6.

From this, and by including the electrical impedance of the machine, the nominal conditions can be expressed as given by equation 4 where I_n is the nominal current and V_n is the nominal voltage. This shows that the number of pole windings works as a scaling factor between nominal current and voltage. The converter however, has a fixed nominal voltage and as shown by equation 5 where P_n is the nominal power, ω_n is the nominal speed and M_n is the nominal torque, the pole winding count defines the nominal power and the nominal speed of the machine. The nominal torque is assumed to be defined by the physical size and properties of the machine that was decided in an earlier stage of the design process.

$$\epsilon = -\frac{d\phi}{dt} \tag{1}$$

$$\epsilon\left(t\right) = n \cdot \omega \cdot B \cdot A \cdot \sin\left(\omega t\right) \tag{2}$$

$$v_{out}\left(t\right) = k \cdot n \cdot \sin\left(\omega t\right) \tag{3}$$

$$\frac{V_n}{I_n} = k \cdot n \tag{4}$$

$$P_n = V_n \cdot I_n = \omega_n \cdot M_n \tag{5}$$

Above nominal speed, the output voltage must be kept within limits by field weakening. For PMSMs, this leads to a reduction in available torque that is inversely proportional to the speed. Figure 3 shows the speed torque curve for a common PMSM.

In context of the rather extreme peak to average speed ratio it would be interesting to explore an extreme overspeed ratio of the generator. *BOLT*® for instance is operating with an average speed of 0.3 m/s in the most common wave state, but has to handle above 5 m/s in the most extreme wave state. The overspeed ratio is inversely proportional to installed power and an increased overspeed ratio will therefore reduce the cost through the power chain and improve the capacity factor. In the following systems with very high maximum to nominal speed ratio are investigated.

B. Control strategy

The absorbed power form a point absorber is greatly influenced by the control strategy applied by the PTO. In general the optimal energy extraction is achieved when the point absorber is moving with a 90° phase shift to the waves. Several methods of approaching this production mode are described, the best known being *reactive control* [8], [9] and *latching control* [10]. Figure 8 shows an electrical equivalent circuit for the WEC. The dynamic behaviour of the WEC is modeled as an RLC circuit and the PTO is modelled by a power extracting element (resitance) and a reactive element (impedance). The goal of reactive control is to tune the reactive element of the PTO so that it compensates for the reactive elements of the WEC as a whole and thus maximizes power extraction.

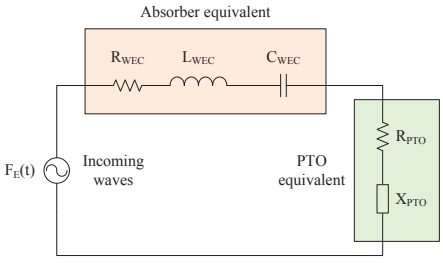

Fig. 8. Equivalent circuit for Wave Energy Converter and Power Take Off

However, with the current design of the BOLT concept the PTO is too small to have significant impact by advanced control. Passive damping therefore serves as the primary

production model. In the lowest sea states however, advanced control algorithms can improve output [2], but is not currently performed. The reason for the small PTO is the result of economical optimization and Fred Olsen acquired viewpoint that direct driven electrical PTOs should be designed so that they are saturated on force and power already in low sea states.

Passive damping is defined by equation 6 where the damping coefficient B is optimized towards the highest efficiency region of the machine to produce the highest possible net power output. M and ω is torque and speed on the generator. Figure 9 shows the torque and speed characteristics for the generator used on BOLT2 [11]. The thick line shows the optimal torque that result in maximum net power from the generator. The first saturation mechanism is the mechanical force limit of the gearbox and is reached already at 0.27 m/s. The second is the power limit of the generator, which is reached at 1.55 m/s. The linear region from 0 - 0.27 m/s corresponds to a damping coefficient of ca 350 kNs/m which is the chosen value for B on BOLT2.

$$M = -B \cdot \omega \tag{6}$$

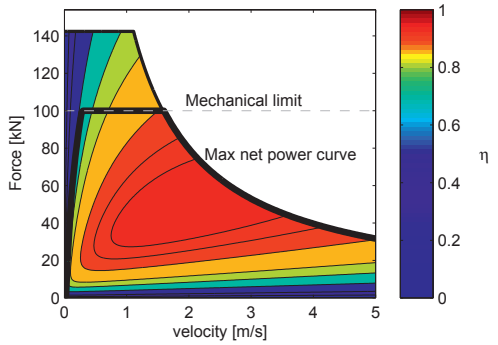

Fig. 9. Efficiency plot for the generator used at Bolt2Wavehub. The thick line shows the torque that result in maximum exported power from the generator. The thin line shows maximum available torque from the genearator. The dashed line shows the mechanical limit for the gearbox.

III. Simulation model

The simulation model used [12], [13] simulates BOLT2 (ref section I-A) for operation at Wavehub.

$$F_{e,i}(t) - F_{D,i}(t) = M\frac{d^2\zeta(t)}{dt^2} \tag{7}$$

$$F_{D,i}(t) = F_{r,i}(t) + F_{d,i}(t) + C_i \cdot \zeta_i(t) + F_{PTO}(t) \tag{8}$$

The simulation model solves the differential equation 7 for $\zeta(t)$ in the time domain. The index denotes the mode of motion, given by the 6 degrees of freedom of motion for the floater. The excitation force matrix $F_{e,i}$ is the time dependent force due to incident waves and M denotes the mass of the system. $F_{D,i}$ accounts for the sum of all the damping forces given in equation 8. Here $F_{r,i}$ accounts for the time dependent forces on the floater due to radiation of waves. The term $F_{d,i}$ accounts for non linear damping terms like drag forces. ζ_i is the time dependent motion of the floater, C_i is the restoring force matrix accounting for the hydrostatic pressure acting on the floater and F_{PTO} is the time dependent force applied from the PTO. The PTO is modeled as a rope and winch system that is tightly moored to the sea floor.

The simulation is based on a detailed 6DOF model for BOLT2 and Fred Olsen therefore keeps the simulation model confidential. However, the high level of complexity is not required for this study and a simplified 1DOF model would produce much the same result. It is therefore possible for a third party to verify the results published here without detailed knowledge about the simulation model used.

For each wave state a 20 minutes time series of irregular waves are generated based on the Wavehub spectrum. The subsequent excitation forces are then calculated and the simulation is run for the full length of the time series. The simulation model also takes into account PTO and generator losses, and the model outputs a 20 minutes time series of exported electrical power from the WEC. The average of this time series is then presented as produced power for that wave state as shown in figure 10(b).

The simulation model is developed through many years of development and testing and is verified against real production data from several prototypes, including BOLT.

A. Scatter diagram

All simulations are based on the Wavehub scatter diagram [3] shown in table I. A probability representation for the scatter is shown in figure 10(a). By simulating the power production for Bolt2Wavehub for all occurrences in the scatter, an overall performance plot can be made. Figure 10(b) shows the simulated operation of BOLT2 in various sea states. The output power is normalized to the defined nominal output of BOLT2 as specified later in this section. The WEC power scatter can now be multiplied with the probability scatter to calculate annual energy production. This is shown in figure 10(c). The plot shows the amount of the annual energy production that occurs in the various sea states.

These three diagrams are an important tool for further WEC optimization. For instance it can be calculated that the most frequent wave height is hs=1.25m and occurs 25% of the time. However, less than 10% of the annual energy is produced on this wave height. The most producing wave state is hs=2.25 and tz=5.5sec and contributes to 9% of the annual energy.

It can be seen from figure 10(b) that the average power from BOLT2 increases with wave height. The theoretical maximum power produced from the PTO, which would occur at constant optimum speed, is even higher. This is typical for most WECs and complicates the definition of rated PTO power. Fred Olsen has decided that the average power in the wave state that produces most annual energy shall be defined as the nameplate power rating. Hence, the most producing wave state hs=2.25 and Tz=5.5sec defines unity in figure 10(b).

Significant wave height hs [m]	Wave period Tz [sec]								
	3,5	4,5	5,5	6,5	7,5	8,5	9,5	10,5	11,5
0,25	26	79	44	18	0	0	0	0	0
0,75	499	832	491	140	18	0	0	0	0
1,25	184	1051	604	307	70	26	9	0	0
1,75	0	587	701	333	149	53	26	0	9
2,25	0	96	534	254	123	44	9	0	0
2,75	0	0	237	228	105	26	9	9	0
3,25	0	0	26	175	123	44	9	0	0
3,75	0	0	0	79	96	35	18	0	0
4,25	0	0	0	9	44	26	9	9	0
4,75	0	0	0	0	26	18	9	0	0
5,25	0	0	0	0	18	26	18	0	0
5,75	0	0	0	0	0	18	9	0	0
6,25	0	0	0	0	0	9	0	0	0

TABLE I
SCATTER DIAGRAM AT WAVEHUB, HOURS PER WAVE STATE

IV. OVERSPEED OPTIMIZATION

The overspeed optimization is performed by creating generator models for a list of different overspeed ratios. These models are then implemented into the simulation model and a full simulation for all the wave states in the scatter is run for each of the generator models. The resulting annual energy production for the different overspeed ratios is shown in table II. Annual energy and load hours are shown in figures 13 and 12 respectively. The basis for the power normalization is the defined rated power for BOLT2 as described in section III-A. The normalized annual energy is normalized power multiplied with hours.

A first important observation is that the overspeed ratio can be raised to 5 without significant loss of annual production. This corresponds to a 5 times reduction in installed power. Further increase must be done as part of an economical optimization.

A. Capacity factor optimization

For power export, the capacity factor is of great importance. The capacity factor is defined as the annual exported energy divided by installed power and shows how well the electrical export capacity is utilized. Capacity factor is usually expressed as the corresponding number of hours per year that the installed power is fully utilized, termed *load hours*. Figure 11 shows the average power production for every hour through a year sorted in descending order. Each line represents a generator configuration with a given overspeed ratio. The figure is a good tool for sizing of the export system and clearly shows the effect of the overspeed ratio. A higher overspeed ratio results in a lower peak power rating, less fluctuation in power production and more load hours. This is mostly achieved by reducing production from the high sea states, but some energy is also lost in the low sea states due to the high irregularities always present.

It can be seen from figure 11 that the overspeed ratio does not appear as a constant power limit, but instead leads to a continuous reduction. This is because the overspeed ratio defines the peak instantaneous power while the exported energy is given by the average power over 20 minutes. The goal is

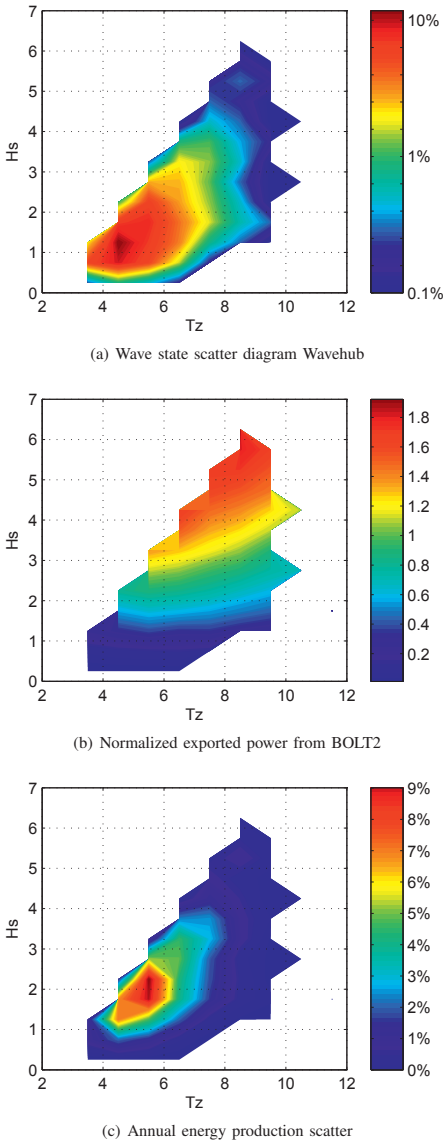

(a) Wave state scatter diagram Wavehub

(b) Normalized exported power from BOLT2

(c) Annual energy production scatter

Fig. 10. Simulated performance of BOLT2 at Wavehub

maximum utilization of the export capacity, and it is likely that other measures such as energy storage and averaging between groups of WECs also will be used. Another option for improvement of power quality is therefore to implement a saturation mechanism in the controller that regulates against a total defined maximum average power. This can further be improved to aim for a total export capacity from an array of

Overspeed ratio	Installed power [pu]	Annual energy [pu · hours]	Load hours [hours]	Max avg power [pu]
1	33.3	5093	1840	2.77
3	11.1	5081	1928	2.64
5	6.67	5017	2180	2.3
7	4.76	4878	2511	1.94
10	3.33	4593	3026	1.52
15	2.22	4070	3690	1.1
20	1.67	3547	4128	0.859
30	1.11	2832	4773	0.593
40	0.833	2368	5244	0.452
50	0.667	2041	5611	0.364

TABLE II
WEC PERFORMANCE WITH DIFFERENT OVERSPEED RATIOS

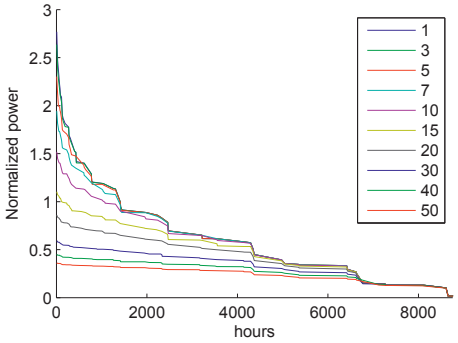

Fig. 11. Annual power distribution per hour

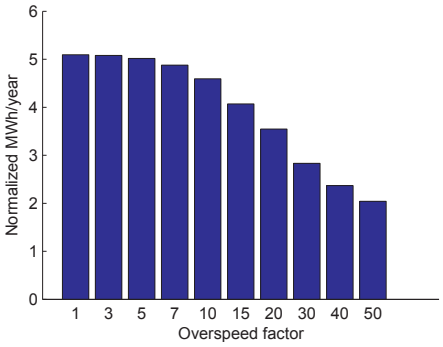

Fig. 12. Annual energy production with different overspeed ratios

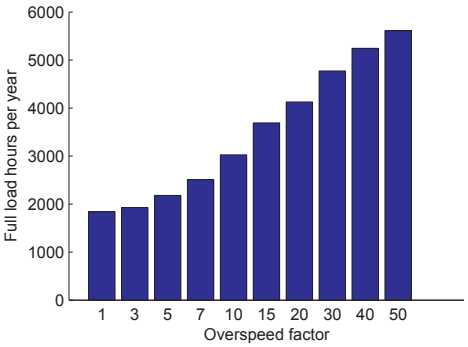

Fig. 13. Annual load hours with different overspeed ratios

WECs. This, however, is not within the scope of this paper and should be subject for further research.

V. CONCLUSION

The study shows that the overspeed factor can be increased to a factor of five without significant loss in annual energy production. Thus, the peak power rating of the that involves all-electric PTOs. Further increase in overspeed factor can be done as a part of economical analysis. This study indicates an annual loss of energy converter and the power export system can be reduced to one fifth without trading away produced power. Hence, overspeed optimization should be a part of every design study production of 10% at an overspeed factor of 10. This is probably around where the lost energy production goes beyond the cost reduction of the power system. Overspeed ratios significantly higher than 10 therefore seem less likely.

REFERENCES

[1] I.Bjerke, E.Hjetland, G.Tjensvoll, and J.Sjolte, "Experiences from field testing with the bolt wave energy converter," European Wave and Tidal Energy Conference (EWTEC11), Tech. Rep., 2011.

[2] E.Tedeschi and M.Molinas, "Impact of control strategies on the rating of electric power take off for wave energy conversion," Norwegian University of Science and Technology, Tech. Rep., 2009.

[3] "The wave power climate at the wave hub site," November 2006, journal: Applied Wave Research Review of Wave Power Climate.

[4] J. Falnes, *Ocean Waves and Oscillating Systems: Linear Interactions Including Wave-Energy Extraction*. Cambridge University Press, 2002.

[5] J.Falnes and P.M.Lillebrekken, "Budal's latching-controlled-buoy type wave-power plant," in *5th European Wave Energy Conference*, 2003.

[6] C. I. Hubert, *Electric Machines - Theory, operation, applications, adjustment and control*. Prentice Hall, 2002.

[7] N. Mohan, T. M. Undeland, and W. P. Robbins, *Power Electronics*. John Wiley & Sons, inc, 2003.

[8] E.Tedeschi and M.Molinas, "Effect of control strategies and power take-off efficiency on the power capture from sea waves," in *IEEE Transactions on Energy Conversion*, 2011, in Press.

[9] E. Tedeschi, M. Molinas, M. Carraro, and P. Mattavelli, "Analysis of power extraction from irregular waves by all-electric power take off," in *Energy Conversion Congress and Exposition (ECCE), 2010 IEEE*, sept. 2010, pp. 2370 –2377.

[10] J.Falnes, "Principles for capturie of energy from ocean waves: phase control and optimum oscillation," NTNU, Tech. Rep., 1997, http://folk.ntnu.no/falnes/w_e/index-e.html#RAPPORTAR.

[11] I.Bjerke, E.Hjetland, G.Tjensvoll, and J.Sjolte, "A brief introduction to the bolt-2-wave project," European Wave and Tidal Energy Conference (EWTEC11), Tech. Rep., 2011.

[12] M.Molinas, O.Skjervheim, P.Andreasen, T.Undeland, J.Hals, T.Moan, and B.Sorby, "Power electroncis as grid interface for actively controlled wave energy converters," International Conf. on Clean Energy Power (ICCEP07), Tech. Rep., 2007.

[13] O.Skjervheim, B.Sorby, and M.Molinas, "All electric power take off for a direct coupled point absorber," Proceedings of the 2nd International Converence on Ocean Energy (ICOE2008), Tech. Rep., 2008.

Jonas Sjolte is a project engineer with Fred Olsen and works on the Wave Energy Project. He leads the design and development of the electrical power systems within the project. He graduated from NTNU in 2007 and recieved the degree MSc in Electrical Engineering. He has also stayed at CERN, Geneava for one year where he did his master thesis within the field of High voltage pulsed power. In 2011 he started on a PhD programme in collaboration between NTNU and Fred Olsen on grid integration of Wave Energy with the goal of connecting Fred Olsens Bolt concept to Wavehub.

Ida Kathrine Bjerke has a Master of Science in Engineering Physics from the Norwegian University of Science and Technology (NTNU), Trondheim, Norway in 2008. She wrote her master thesis on the subject of control of wave energy converters at cole Centrale de Nantes in France. Since 2008 she has been employed as a project engineer for the Fred. Olsen Wave Energy Project in Oslo, Norway, where she is working with mechanical design as well as control issues related to wave energy conversion.

Aina Crozier has a Master of Science in Energy and Environmental Engineering from the Norwegian University of Science and Technology (NTNU) in Trondheim, Norway. She graduated in the spring of 2011 after spending 5 years at NTNU, including a one-year exchange to the University of British Columbia (UBC) in Vancouver, Canada. Her academic background touches on a variety of engineering fields; from Power Electronics and Control Systems to Heat and Energy Processes, Fluid Mechanics and Hydrodynamics. Her Master's thesis consisted of the design and fully-coupled simulation of a floating offshore wind turbine. Her interest lies in the renewable ocean energy industry and she is currently employed as a Project Engineer at Fred.Olsen, where she is working on developing wave power technologies.

Marta Molinas (M'94) received the Diploma of Electro-mechanical engineer from the National University of Asuncion, Paraguay in 1992; MSc from Ryukyu University, Japan, in 1997, and Doctor of Engineering from Tokyo Institute of Technology, Japan, in 2000. In 1998 she stayed at the University of Padova, Italy as a guest researcher. From 2004 to 2007 she was a Post Doctoral researcher at the Norwegian University of Science and Technology (NTNU) in Trondheim, Norway. In 2008 she became Professor at NTNU. From 2008-2009 she has been a JSPS Research Fellow at the Energy Technology Research Institute of AIST in Tsukuba, Japan. Her research interest is in wind/wave energy conversion systems, and power electronics and electrical machines in distributed energy systems. She is an active reviewer for IEEE Trans. of Industrial Electronics and Power Electronics. She is also AdCom member of IEEE Power Electronics Society and Associate editor of the IEEE Trans. of Power Electronics.

Gaute Tjensvoll is the development manager of the Fred Olsen Wave Energy project, Bolt. He got his masters degree in product development from NTNU (Norwegian University of Technology and Science) and DTU (Denmark Technical University) in 1997. He also has a master's degree in Technology Management from NTNU and MIT (Massachusetts Institute of Technology) from 2002. His professional career started in an entrepreneurial company called Think, developing an electric vehicle. His product development experience was further broadened through managerial positions in a product development consultancy called Kitron Development. For the last five years he has been dedicated to realizing wave energy concepts in Fred Olsen.

Appendix D

Conference paper 4

Title: All-Electric Wave Energy Converter Connected in Array with Common DC-Link for Improved Power Quality

Conference/Journal: Power Electronics for Distributed Generation (IEEE,PEDG)

Date: 25.-28. June 2012

Location/Publisher: Aalborg, Denmark

All-Electric Wave Energy Converter Connected in Array with Common DC-Link for Improved Power Quality

Jonas Sjolte
Fred. Olsen / NTNU
Norwegian University of
Science and Technology
Email: jonas.sjolte@fredolsen.no

Gaute Tjensvoll
Fred. Olsen
Oslo, Norway
Email: gaute.tjensvoll@fredolsen.no

Marta Molinas
Norwegian University of
Science and Technology
Trondheim, Norway
Email: marta.molinas@ntnu.no

***Abstract*—*Wave Energy Converters* (WECs) with direct electric Power Take Off systems have large fluctuations in output power, and have a peak to average power ratio far above most other energy producers. Moreover, the typical average power production from a WEC is lower than that of other power plants, typically less than 1 MW. Array connection of several WECs can mitigate these shortcomings by increasing both the power output and quality. The focus of this paper is to analyze Fred. Olsen designed WEC system Bolt2Wavehub and the effect of expanding to a small array. The required specifications for the array geometry, the electrical configuration and the overall system are discussed and a specific array design consisting of 7 WECs is suggested as a solution and analyzed in detail. The results show that the peak to average power ratio can be reduced by a factor of 4 if the array covers a full wave length.**

I. Introduction

Wave energy producers are different from most other energy producers in that the prime mover operates with a sinusoidal velocity. When such a producer is directly connected to its generator, the power output will be continuously fluctuating with zero crossings in every wave. This behavior can be seen in Fig. 2 which shows the simulated power output from Fred Olsen's (FO) *Wave Energy Converter* (WEC) Bolt2. The Bolt2 power plant is pictured in an early stage of design in Fig. 1.

A power flow with such a high level of distortion is unsuitable for direct export to the grid, mainly because of the poor utilization of installed conversion and transmission capacity. For instance, in the example of Bolt2, as will be shown later, the required installed capacity would have to be around twenty times the average exported power. In addition, with such a high level of distortion, fulfilling the grid code requirements could prove difficult.

WEC systems based on the point absorber principle have an inherent limitation on installed power. When the absorber size approaches the wavelength, the vertical movement and hence the absorbed power decay towards zero. This limitation is often referred to as Budal's upper boundary [1]. The practical maximum power limit for these devices is estimated to be in the range 30-600 kW, with passively damped systems in the low end and systems based on advanced reactive control in the high end.

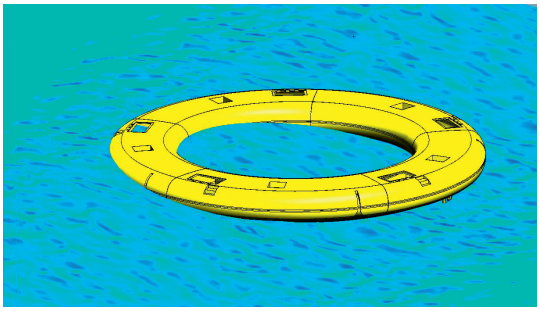

Fig. 1. Artistic impression of Bolt2

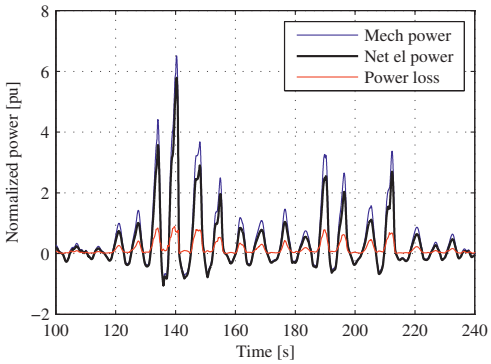

Fig. 2. Simulated power for Bolt2

The obvious approach to deal with these issues and meet the requirements on both power level and power quality is to rely on array systems. By installing additional WECs, the output power can be added up, and by electrically connecting the array elements together on a common bus the power can

Fig. 3. FO's Wave Energy Converter Bolt® located outside Risør, Norway, was launched in June 2009, and is still in operation.

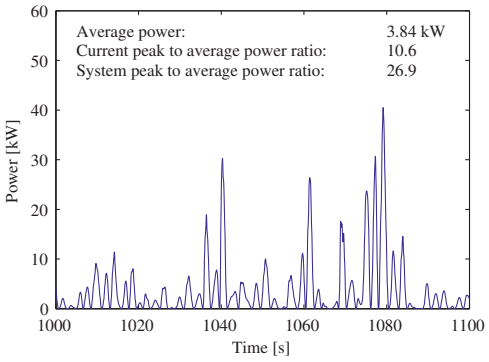

Fig. 4. Typical power output from Bolt® in low waves

be effectively shared to reduce the peak to average ratio. Many studies have been performed earlier on farm solutions showing a favorable outcome [2], [3]. The focus of this paper is to analyze the case of the Fred. Olsen Wave Energy Project on how to create an array system based on the new Bolt2 prototype built within the Bolt2Wavehub project.

A. Fred. Olsen Wave Energy Project

FO started with Wave Energy in 2000, leading to the first Wave Energy Converter prototype *Buldra*®, built as multiple point absorber platform and launched in 2004. Since then FO has tested out various concepts and built several different prototypes, all based on the point absorber principle. The series of experiences have led to the single body point absorber system Bolt® as pictured on site in Fig. 3. Even though the point absorber principle may not be the most efficient absorber type, it has shown to be successful in terms of total performance and cost of energy. Bolt® has been in operation outside Risør in Norway since June 2009 and has till date performed very well with only minor issues and incidents. As on December 22, 2010 she had produced 3 360 kWh [4], and is expected to exceed 6 000 kWh during 2012.

Based on the success with Bolt®, FO has decided to use the knowledge and experience gained so far to proceed with the next generation design. An agreement with several UK companies was made with funding from the UK *Technology Strategy Board* (TSB). The goal of the project is to improve the Bolt® concept to a commercial level where it can be launched at Wavehub [5], and hence the project name *Bolt2Wavehub*.

The first prototype WEC built within the project, referred to as *Bolt2*, is designed with five individual all-electric *Power Take Off* (PTO) systems. The PTOs are tightly moored to the sea floor by a winch and drum system, which directly ties surface movements to the generator through a custom designed transmission system. Thus, the generator moves with a sinusoidal velocity pattern with zero crossings in every wave. Since the winch system will require active power for pull-back during downward movement the generator is ran in motoring mode with a low pull-back torque during half the wave cycle. This accounts for the periods of active power consumption indicated in Fig. 2. The exact configuration and mode of operation of the device is explained in detail in earlier publications [4], [6]–[9] and is not within the scope of this paper.

II. Array configuration

When designing the array, several properties have to be taken into consideration. The following list is a suggestion of the aspects that should be prioritized, and is mainly based on the experience gained from single WEC systems in the FO Wave Energy Project.

- **Power smoothing**
  Ensuring the highest possible power quality from the array is one of the key factors. This is achieved by distributing the absorbers over a distance along the wave direction so that the incoming wave crest hits one absorber at a time.
- **Shadowing**
  To ensure maximum energy capture, the absorbers should be placed so that the shadowing effects from nearby absorbers are minimized. This is achieved by placing the absorbers on a line perpendicular to the incoming wave direction, which contradicts the preceding item.
- **Easy access**
  The array must be designed so that all the absorbers are easily accessible for installation, maintenance and repair. This generally points towards one-dimensional arrays as opposed to two-dimensional arrays.
- **Mooring configuration**
  The mooring system is one of the major cost drivers in wave energy power plants, and care should be taken during the array design so that this can be efficiently utilized and shared between the absorbers.
- **Small and simple**
  As wave energy is still in early development and little experience has been gained, focus should be put towards

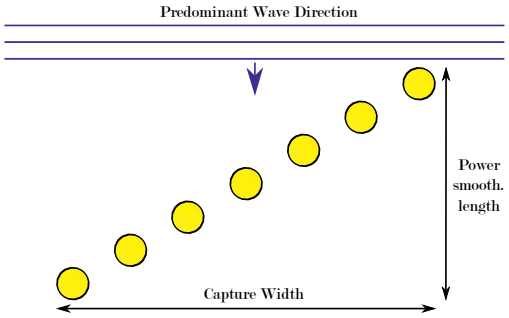

Fig. 5. Proposed configuration for small array of Bolt2 WECs

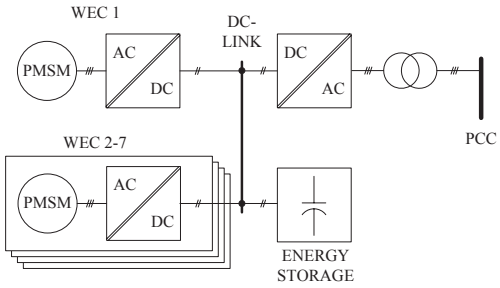

Fig. 6. Electrical configuration of the array

small and simple array systems with few absorbers. Array concepts that require large number of absorbers and/or a high level of complexity to be successful should be postponed until wave energy production has reached a mature level.

- **Common electrical bus**
  To ensure effective balancing of power through the array the WECs should be interconnected on a common electrical bus. This will allow the power to float freely between the devices so that the grid connection point will see the array as a single power producer.

Based on these considerations FO has designed the array illustrated in Fig. 5 as a first step for further study and simulation. The array consists of seven absorbers of the Bolt2 type, as indicated by the yellow circles, and has an angle of 45° with the predominant wave direction, which is expected to give the best compromise between power smoothing and capture efficiency. Further, the simple one-dimensional design with all the absorbers in one row allows for easy access and possibly an efficient mooring system. With the proposed number of seven absorbers, the array covers a full wavelength in the important wave states, which is essential for Bolt2 as it produces positive power only during half the wave cycle.

The proposed power system for the array is an extension of the Bolt2 multi-PTO concept, where all production units are connected on a common DC-Link. This is made possible by the 3-phase AC/DC inverters that control each generator of the *Permanent Magnet Synchronous Machine* (PMSM) type. Full converter configuration is required for continuous generator operation in the heavily varying speed specter induced by the waves. The generator is controlled as a linear damper with torque saturation on upwards movement of the WEC and as with constant wind-in torque on downwards movement. This causes the bi-directional power flow described in Fig. 2.

The common DC-Link coupling allows the produced power to be balanced out between the WECs without additional transmission or conversion equipment. The grid side inverter harvests the produced power from the DC-Link, and the power is further transformed and transferred to the *point of common coupling* (PCC). All the components in the grid connection chain have to be sized according to the array peak power, and because of the improvement in power quality, there can be substantial cost reductions. As sketched in Fig. 6 the power quality can be improved further by introducing an energy storage before the grid converter, however this is not within the scope of this work, but is currently being investigated.

III. Simulation Model

The model used for the array simulation is based on the single absorber model for Bolt2 [10], [11]. The simulation model solves Equation (1) for $\zeta(t)$ in the time domain. The index denotes the mode of motion, given by the six *degrees of freedom* (DOF) of motion for the floater. The excitation force matrix $F_{e,i}$ is the time dependent force due to incident waves, and M denotes the mass of the system.

$$F_{e,i}(t) - F_{D,i}(t) = M\frac{d^2\zeta(t)}{dt^2} \quad (1)$$

$$F_{D,i}(t) = F_{r,i}(t) + F_{d,i}(t) + C_i \cdot \zeta_i(t) + F_{PTO}(t) \quad (2)$$

$F_{D,i}$ accounts for the sum of all the damping forces in Equation (2). Here, $F_{r,i}$ accounts for the time dependent forces on the floater due to radiation of waves. The term $F_{d,i}$ accounts for non linear damping terms, mainly the drag forces. ζ_i is the time dependent motion of the floater, C_i is the restoring force matrix accounting for the hydrostatic pressure acting on the floater, and F_{PTO} is the time dependent force applied from the PTO. The PTO is modeled as a rope and winch system that is tightly moored to the sea floor.

Since the simulation is based on a detailed 6DOF model for Bolt2, FO keeps the simulation model confidential. However, the high level of complexity is not essential for this study and a simplified 1DOF model would produce much the same result. It is therefore possible for a third party to verify the results published here without detailed knowledge about the simulation model used.

To simulate a wave state, a 20-minute time series of irregular waves is generated based on the Wavehub spectrum. The subsequent excitation forces are then calculated and

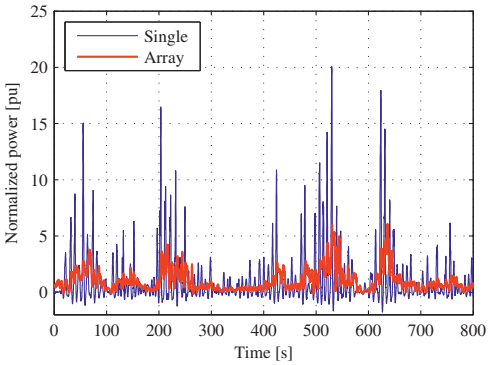

Fig. 7. Peak to average power ratio for array versus single absorber

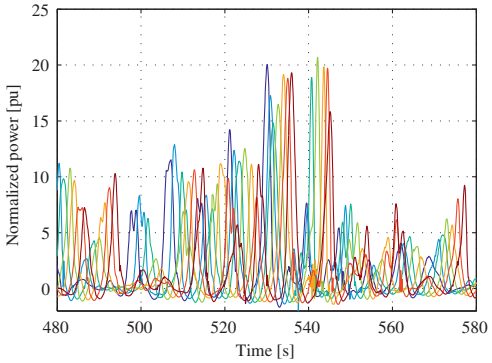

Fig. 8. Individual instantaneous power from array absorbers

the simulation is performed for the full length of the time series. The simulation model also takes into account PTO and generator losses, and the model outputs a 20-minute time series of exported electrical power from the WEC. The simulation model has undergone many years of development and testing and is verified against real production data from several prototypes, including Bolt.

Array simulations are performed by running the simulation model separately for each absorber in the array. All absorbers are simulated for the same wave, and the expected wave propagation through the array is taken into account. However, since there is no interaction between the absorbers in the model, each absorber output is given without shadow effects, as if the absorber was producing alone. This is expected to exaggerate the the simulated produced power. A method to compensate the shadowing effects is under development to address this shortcoming. However, the simulation in its current form is believed to give a good indication of the power smoothing effects and the peak to average ratio of the array.

IV. Results

The resulting output power from the array is plotted in Fig. 7, where the ordinate is normalized to the average output power, which equals the peak to average ratio. The benefit of the array configuration is clearly demonstrated, as seen in the reduction of the peak to average ratio from 20 to 5. In Fig. 8, the power is plotted individually for all the absorbers in the array. Upon close study of Fig. 8, it can be seen how the waveform changes as the wave propagates through the array.

To explore further the power properties and the sensitivity on array configurations, simulations with varying numbers of absorbers in the array were performed, following the same design principle. The resulting peak to average ratios for arrays consisting of 1-20 and 20-101 absorbers are plotted in Fig. 9 and Fig. 10 respectively. The latter configuration is unrealistic as will be argued later, but gives an impression of the power quality that could be obtained from larger systems.

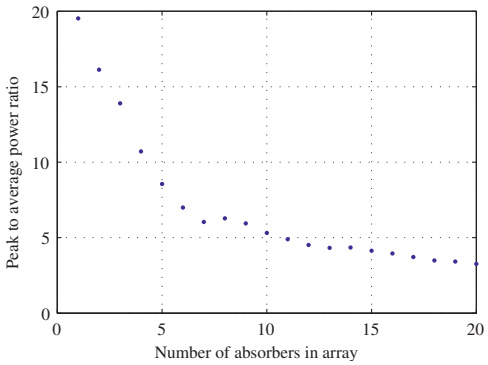

Fig. 9. Peak to average ratio for small arrays

As can be seen from the 1-20 array analysis, there is a quick drop in the peak to average ratio as the first few devices are added. When the array covers approximately one full wavelength at around 7 WECs, the peak to average ratio level out at around 5. The jump seen at WEC number 8 is probably related to the transition of covering more than one wavelength, thus encountering higher harmonic disturbance. These effects are related to specific wave states and are expected to be canceled out when all the wave states are taken into account. However, cases must be expected in all the wave states where adding a new WEC will increase, instead of reducing the peak to average ratio. This should be analyzed and optimized for the specific location of the farm.

It can be seen from the result of the 20-101 analysis that the peak to average ratio i still descending, but at a lower rate. While the effect observed in the previous case was mainly related to smoothing within a single wave, the effect seen here is related to smoothing between successive waves. Earlier studies and experience from other systems have shown that the power must be smoothed over 100-200 seconds [3] to be

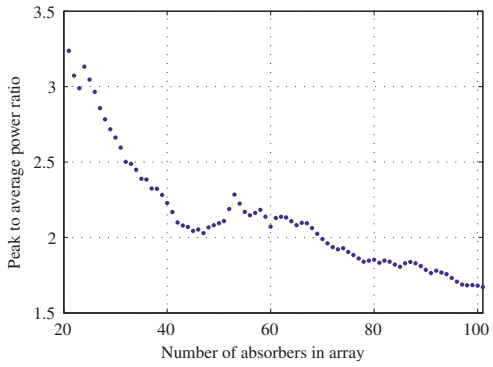

Fig. 10. Peak to average ratio for large arrays

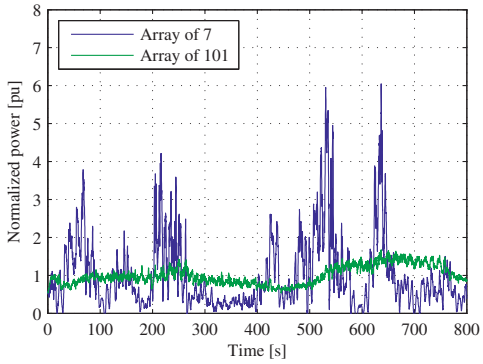

Fig. 11. Instantaneous power from large array versus small array

suitable for direct injection to grid. This can be done either by energy storage or by covering an area that corresponds to the required smoothing time.

$$\lambda = \frac{g \cdot T^2}{2\pi} \tag{3}$$

$$\lambda = c \cdot t \tag{4}$$

$$c = \frac{g \cdot T}{2\pi} \tag{5}$$

$$L = \frac{g \cdot T}{2\pi} t_{avg} \tag{6}$$

The basic behavior for ocean waves are governed by Equations (3)-(5) [12], where λ denotes the wave length, g is the gravity, T is the wave period and c is the wave velocity. From these, Equation (6) can be derived which gives the required array length, L, to smooth the absorbed power over an average time t_{avg}. The wave state with hs=2.75 m and Tz=6.5 s, where hs is the significant wave height and Tz is the zero crossing time period, is defined by FO as the benchmark wave state for production optimization. For this wave state the required array length is 1-2km. This corresponds to 80-160 units of the Bolt2 type if the approach specified earlier is followed, alternatively the required area could be covered by several smaller arrays.

V. Discussion

Even though the large array analysis indicates that the peak to average can be brought close to unity, this solution seems less practical. As the PTOs are equipped with industrial 400 VAC electrical machinery, the voltage level on the common DC-Link will be around 600 VDC. On this voltage level, there are practical limits to the amount of power that can be transferred, and also limits on how large distances that can be tolerated. Since the system is also likely to require flexible cable systems to handle the absorber motion, nominal current capabilities above 1000 A seems less likely, and so this level is used as a limit. If the grid side inverter is placed in the middle of the array, this limits the total array power to 1.2 MW without intermediate conversion. Also the length of the cables poses a limitation, especially if the cables are brought down to the seabed between the absorbers, as the voltage drop ratio will be significant.

Intermediate voltage conversion could be implemented on the DC-link to increase the voltage level, but the required converters would only benefit from the improved power quality provided by the subordinate array branch. Thus, the converter must be designed with a higher peak to average rating than provided by the full array. Even if the limitations on transmission are ignored, the concept of having one large line array with more than twenty absorbers seems less favorable. In an optimized array design, the mooring systems and electrical systems are likely to be designed so that there exists some level of dependence between the absorbers. This could cause the entire array to go off-line upon failure of a single absorber, during repair, or during regular maintenance. This could be acceptable for small arrays, but would require fail-safe systems to be implemented on larger array systems. Based on this it could be interpreted that the arrays should be designed smaller with around ten absorbers. Larger farms should consist of several independent smaller arrays. The array power systems should handle the peak to average ratio of around five. Several steps can be taken to further improve the power quality such as energy storage, and production capping. This will be the subject of further study.

VI. Conclusion

This analysis shows that connecting the Bolt2Wavehub system in a small array successfully brings the peak to average ratio down from 20 to 5. This is the result of power smoothing within a single wave, and requires the array to cover at least one wavelength. Further power smoothing by increasing the array is possible, but looks less favorable because of large geographical area that needs to be covered. Thus, it seems reasonable that the peak to average power ratio of 5 should

be tolerated, and that the grid power export system must be designed accordingly.

ACKNOWLEDGMENT

The authors would like to thank Johannes Falnes for sharing his vast experience and knowledge within the field of wave energy research, and Vijay Vadlamudi for his help on linguistic questions.

REFERENCES

[1] J. Falnes and J. Hals, "Heaving buoys, point absorbers and arrays," *Philosophical Transactions of the Royal Society A: Mathematical, Physical and Engineering Sciences*, vol. 370, no. 1959, pp. 246–277, 2012. [Online]. Available: http://rsta.royalsocietypublishing.org/content/370/1959/246.abstract

[2] M. Molinas, O. Skjervheim, B. Sørby, P. Andreasen, S. Lundberg, and T. Undeland, "Power smoothing by aggregation of wave energy converters for minimizing electrical energy storage requirements," *Power*, no. xx, pp. 3–8, 2007.

[3] S. H. Salter, "World progress in wave energy 1988," *International Journal of Ambient Energy*, vol. 10, no. 1, pp. 3–24, 1989. [Online]. Available: http://www.tandfonline.com/doi/abs/10.1080/01430750.1989.9675119

[4] I.Bjerke, E.Hjetland, G.Tjensvoll, and J.Sjolte, "Experiences from field testing with the bolt wave energy converter," in *European Wave and Tidal Energy Conference (EWTEC11)*, 2011.

[5] "The wave power climate at the wave hub site," November 2006, journal: Applied Wave Research Review of Wave Power Climate.

[6] J.Sjolte, I.Bjerke, E.Hjetland, and G.Tjensvoll, "All-electric wave energy power take off generator optimized by high overspeed," in *European Wave and Tidal Energy Conference (EWTEC11)*, 2011.

[7] J. Sjolte, I. Bjerke, A. Crozier, G. Tjensvoll, and M. Molinas, "All-electric wave energy power take off system with improved power quality at the grid connection point," in *2012 IEEE PES Transmission and Distribution Conference and Exposition*, 2012, In press.

[8] ——, "All-electric wave energy converter with stand-alone 600vdc power system and ultracapacitor bank," in *2012 EVER International Conference and Exhibition on Ecological Vehicles and Renewable Energies*, 2012, In press.

[9] E.Hjetland, I.Bjerke, G.Tjensvoll, and J.Sjolte, "A brief introduction to the bolt-2-wave project," in *European Wave and Tidal Energy Conference (EWTEC11)*, 2011.

[10] M.Molinas, O.Skjervheim, P.Andreasen, T.Undeland, J.Hals, T.Moan, and B.Sorby, "Power electroncis as grid interface for actively controlled wave energy converters," International Conf. on Clean Energy Power (ICCEP07), Tech. Rep., 2007.

[11] O.Skjervheim, B.Sorby, and M.Molinas, "All electric power take off for a direct coupled point absorber," Proceedings of the 2nd International Converence on Ocean Energy (ICOE2008), Tech. Rep., 2008.

[12] J. Falnes, *Ocean Waves and Oscillating Systems: Linear Interactions Including Wave-Energy Extraction*. Cambridge University Press, 2002.

Appendix E

Conference paper 5

Title: Annual Energy and Power Quality from an All-Electric Wave Energy Converter Array

Conference/Journal: Power Electronics and Motion Control Conference (IEEE/EPE/PEMC)

Date: 4.-6. September 2012

Location/Publisher: Novi Sad, Serbia

Annual Energy and Power Quality from an All-Electric Wave Energy Converter Array

Jonas Sjolte*, Bernt Sørby†, Gaute Tjensvoll‡ and Marta Molinas§
*Fred. Olsen / Norwegian University of Science and Technology, E-mail: jonas.sjolte@fredolsen.no
†NYAC, E-mail: bernt.sorby@nyac.no
‡Fred. Olsen, Fred Olsens Gate 2, N0152 Oslo, gaute.tjensvoll@fredolsen.no
§Norwegian University of Science and Technology, E-mail: marta.molinas@ntnu.no

***Abstract*—Power electronics and advanced motion control has allowed for creating *Wave Energy Converters* (WECs) with the generator directly coupled to the sinusoidal motions of the prime mover. However, this gives large fluctuations in output power, and the resulting peak to average power ratio exceeds most other energy producers. Moreover, the typical average power production from a WEC is lower than that of other power plants, typically less than 1 MW. Array connection of several WECs can mitigate these shortcomings by improving both the power output and power quality. Earlier studies performed on arrays by *Fred. Olsen* has shown a favorable outcome, and has demonstrated a reduction factor of four in the peak to average ratio for a small array. These results were obtained by simulating for the design wave state at the optimum wave direction. To obtain a complete power profile this work focus in simulating a full year of production by implementing the full scatter including wave directions for the Wavehub site. Also the previously ignored interaction forces within the array are taken into account. This allows for mapping annual load hours, installed power and the expected power quality at grid connection point.**

I. Introduction

Wave Energy Converters (WECs) are different from most other energy producers in that the prime mover operates with a sinusoidal velocity. When such a producer is directly connected to its generator, the power output is continuously fluctuating with zero crossings in every wave. This behavior can be seen in Fig. 2 for the single absorber case, which shows the simulated power output from Fred Olsen's (FO) WEC Bolt2. The Bolt2 power plant is pictured in an arrayed configuration in Fig. 1.

A power flow with such a high level of distortion is unsuitable for direct export to the grid, mainly because of the poor utilization of installed conversion and transmission capacity. For instance, in the example of Bolt2, as can be seen from Fig. 2, the required installed capacity would have to be approximately twenty times the average exported power. In addition, with such a high level of distortion, fulfilling the grid code requirements could prove difficult.

WEC systems based on the point absorber principle also have an inherent limitation on installed power. When the absorber size approaches the wavelength, the vertical movement and hence the absorbed power decay towards zero. This limitation is often referred to as Budal's upper boundary [1]. The practical maximum power limit for these devices is estimated to be in the range 30-600 kW, with passively damped

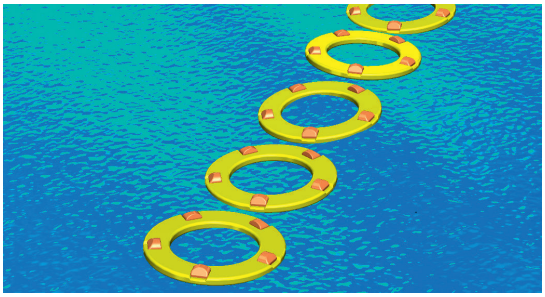

Fig. 1. Artistic impression of Bolt2 array at Wavehub

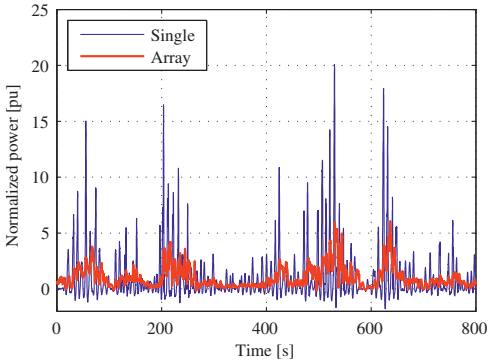

Fig. 2. Peak to average power ratio for array versus single absorber

systems in the low end and systems based on advanced reactive control in the high end.

In an endeavor to improve the export power quality, FO has undertaken a study of arrayed systems. The first step of the work was presented in our paper [2], and investigated the basic geometrical properties of the array, and the potential for power quality improvements. The analysis was performed for one specific wave state, on one wave direction only, and was based on the geometry shown in Fig. 8. The results are plotted in Fig. 2 and demonstrates a favorable outcome on power quality, reducing the peak to average ratio by a factor of four. This was

Fig. 3. FO's Wave Energy Converter Bolt® located outside Risør, Norway, was launched in June 2009, and is still in operation.

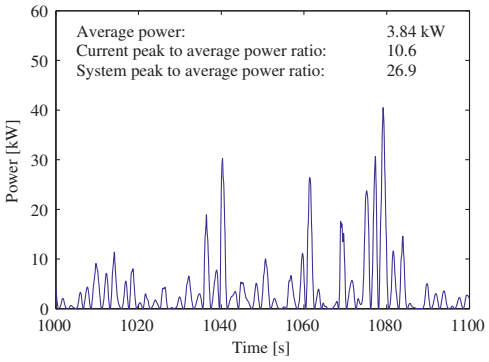

Fig. 4. Typical power output from Bolt® in low waves

achieved by orienting the array so that the incoming wave crest only interacts with one absorber at the time. The simulation was performed for the design wave state, hs=2.75m / Tz=6.5s, where hs is the significant wave height and Tz is the zero crossing time period. The analysis was of qualitative nature only, not taking into account the changing nature of a real site. Also, the simulation ignored the interaction forces between the absorbers, referred to as the *shadowing effects*.

To continue the study, the goal of this paper is to quantify the annual performance of the array by analyzing the array for each specific wave state. The annual produced energy can then be calculated by summing up all the wave states. A full year of power production will be simulated based on the Wavehub climate. Shadowing effects are taken into account by a separate hydrodynamic study, and the subsequent power correction is imported into the simulation model. All the work is based on the seven WEC array showed in Fig. 8.

A. Fred. Olsen Wave Energy Project

FO started with Wave Energy in 2000, leading to the first Wave Energy Converter prototype *Buldra*®, built as multiple point absorber platform and launched in 2004. Since then FO has tested out various concepts and built several different prototypes, all based on the point absorber principle. The series of experiences have led to the single body point absorber system Bolt® as pictured on site in Fig. 3. A typical production curve from a low wave state is plotted in Fig. 4. Even though the point absorber principle may not be the most efficient absorber type, it has shown to be successful in terms of total performance and cost of energy. Bolt® has been in operation outside Risør in Norway since June 2009 and has till date performed very well with only minor issues and incidents. As on December 22, 2010 she had produced 3 360 kWh [3], and is expected to exceed 6 000 kWh during 2012.

Based on the success with Bolt®, FO has decided to use the knowledge and experience gained so far to proceed with the next generation design. An agreement with several UK companies was made with funding from the UK *Technology Strategy Board* (TSB). The goal of the project is to improve the Bolt® concept to a commercial level where it can be launched at Wavehub [4], and hence the project name *Bolt2Wavehub*. The project is currently in progress with the new Bolt2 prototype already launched early in April 2012.

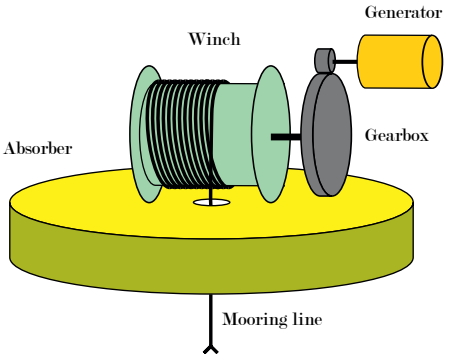

Fig. 5. PTO principal sketch for Bolt2

II. System description

The array is based on the WEC Bolt2 which is a toroidal absorber with five individual all-electric *Power Take Off* (PTO) units. The PTOs are tightly moored to the sea floor by a winch and drum system, which directly ties surface movements to the generator through a custom designed transmission system. The wave to wire coupling is illustrated in Fig. 5. Since the winch system requires active power for pull-back during downward movement, the generator is ran in motoring mode with a low pull-back torque for this part of the wave cycle. This accounts for the negative power intervals seen for the single absorber case in Fig. 2.

The absorbed power from a point absorber is greatly influenced by the control strategy applied by the PTO. In general the optimal energy extraction is achieved when the

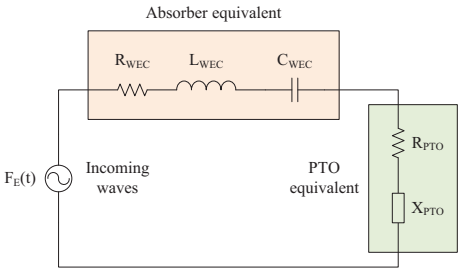

Fig. 6. RLC equivalent circuit of the PTO and WEC system

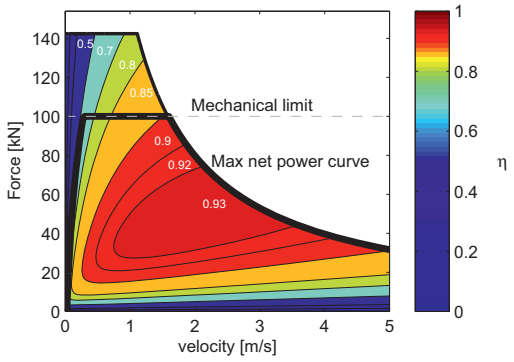

Fig. 7. Efficiency plot for the generator used at Bolt2Wavehub. The thick line shows the torque that result in maximum exported power from the generator. The thin line shows maximum available torque from the generator. The dashed line shows the mechanical limit for the gearbox.

point absorber is moving with a 90° phase shift to the waves [5]. Several methods of approaching this production mode are described, the best known being *reactive control* [6], [7] and *latching control* [8]. Figure 6 shows an electrical equivalent circuit for the WEC where the dynamic behavior of the WEC is modeled as an RLC circuit. The PTO is modeled as a power extraction element (resistance) in series with a reactive element (impedance). The goal of reactive control is to tune the reactive element of the PTO so that it compensates for the reactive elements of the WEC as a whole and thus maximize power extraction.

With the current design of Bolt2 the PTO force is too low to have significant impact by reactive control. This is mainly caused by the large area of the absorber that leads to a high spring constant and a high resonance frequency. Passive damping is therefore selected as the primary production model. In the lowest sea states however, advanced control algorithms may improve output [9], but is not implemented yet. The large and flat absorber shape is selected as a result of economical optimization and FO acquired viewpoint that the absorber

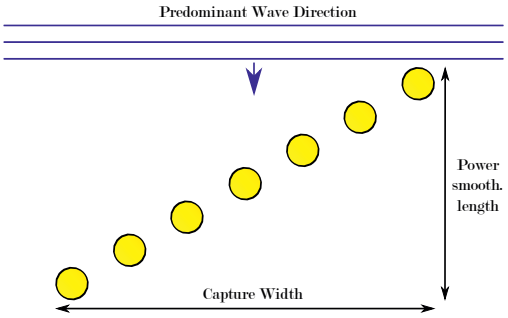

Fig. 8. Proposed configuration for small array of Bolt2 WECs

should be large enough to push the PTO into saturation already in moderate wave states.

$$\tau = -B \cdot \omega \tag{1}$$

Passive damping is defined by Equation (1). The damping coefficient B is optimized to produce the highest possible net power output. τ is the generator torque and ω is the generator speed. Fig. 7 shows the torque and speed characteristics for the generator used on Bolt2. The thick line shows the optimal torque that maximizes the generated electrical power. Two important saturation mechanisms are present; the first is the mechanical force limit of the gearbox. This is reached already at 0.27 m/s. The second is the power limit of the generator that is reached at 1.55 m/s. The linear region from 0 - 0.27 m/s corresponds to a damping coefficient of ca 350 kNs/m, which is the chosen value for B on Bolt2. The system is described in more detail in earlier publications [3], [10]–[13].

The array is created by installing seven of the Bolt2 WEC in a row as illustrated in Fig.8 and Fig. 1. The array angle to the dominating wave direction is initially $45°$, but will be optimized as a part of this work. The covered length along the incoming wave direction ensures that an incoming wave crest only interact with one absorber at the time, thus ensuring smoother output power. Spacing perpendicular to the wave direction is necessary to ensure good energy capture, thus the angle of $45°$ seems to be a good compromise.

The proposed power system for the array is an extension of the Bolt2 multi-PTO concept, where all production units are connected on a common DC-Link. This is made possible by the 3-phase AC/DC inverters that control each generator of the *Permanent Magnet Synchronous Machine* (PMSM) type. Full converter configuration is required for continuous generator operation in the heavily varying speed specter induced by the waves. The generator is controlled as a linear damper with torque saturation on upwards movement of the WEC and with constant wind-in torque on downwards movement, which causes the bi-directional power flow as discussed earlier.

The common DC-Link coupling allows the produced power to be balanced out between the WECs without additional transmission or conversion equipment. The grid side inverter

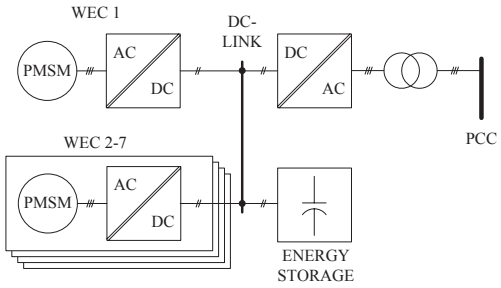

Fig. 9. Electrical configuration of the array

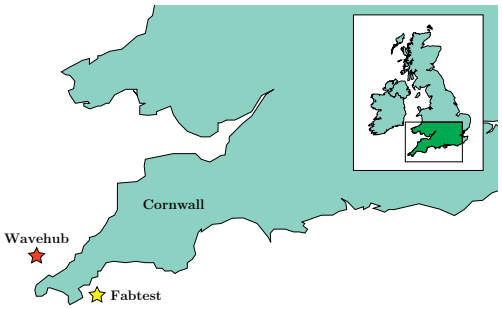

Fig. 10. Location of the UK test sites *Wavehub* and *Fabtest*

harvests the produced power from the DC-Link, and the power is further transformed and transferred to the *point of common coupling* (PCC). All the components in the grid connection chain have to be sized according to the array peak power, and because of the improvement in power quality, there can be substantial cost reductions. As indicated in Fig. 9 the power quality can be improved further by introducing an energy storage before the grid converter, however this is not within the scope of this paper, but is currently being investigated.

III. Simulation model

The simulations are performed with focus on the WEC prototype test site *Wavehub* located west of Cornwall, England as shown in Fig. 10. This is a joint project funded and supported by a renewable energy program administrated by the British government. The site includes a sub-sea power substation that allows for electrically connecting the WECs to grid. Wavehub has been surveyed and monitored for an extensive period and work is still ongoing to calculate true statistical wave data for the site. In this paper preliminary data are used which are expected to give a good impression of the power quality, but should be updated for an accurate estimate for annual energy production. The directional spectrum is heavily influenced by waves from west and the directional plot plotted in Fig. 11 had to be plotted on a logarithmic scale to show all directions observed.

The model used for the array simulation is based on the single absorber model for Bolt2 [14], [15]. The simulation model solves Equation (2) for $\zeta(t)$ in the time domain. The index denotes the mode of motion, given by the six *degrees of freedom* (DOF) of motion for the floater. The excitation force matrix $F_{e,i}$ is the time dependent force due to incident waves, and M denotes the mass of the system.

$$F_{e,i}(t) - F_{D,i}(t) = M\frac{d^2\zeta(t)}{dt^2} \tag{2}$$

$$F_{D,i}(t) = F_{r,i}(t) + F_{d,i}(t) + C_i \cdot \zeta_i(t) + F_{PTO}(t) \tag{3}$$

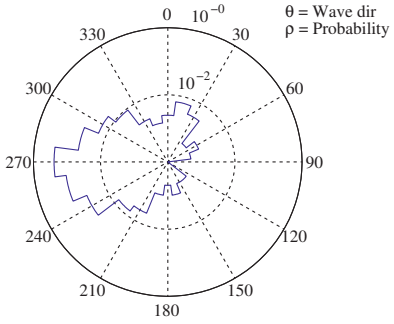

Fig. 11. Probability distribution of wave direction on Wavehub. The plot is a logarithmic polar plot defined by the angle θ and radi ρ.

$F_{D,i}$ accounts for the sum of all the damping forces in Equation (3). Here, $F_{r,i}$ accounts for the time dependent forces on the floater due to radiation of waves. The term $F_{d,i}$ accounts for non linear damping terms, mainly the drag forces. ζ_i is the time dependent motion of the floater, C_i is the restoring force matrix accounting for the hydrostatic pressure acting on the floater, and F_{PTO} is the time dependent force applied from the PTO. The PTO is modeled as a rope and winch system that is tightly moored to the sea floor.

Since the simulation is based on a detailed 6DOF model for Bolt2, FO keeps the simulation model confidential. However, the high level of complexity is not essential for this study and a simplified 1DOF model would produce much the same result. It is therefore possible for a third party to verify the results published here without detailed knowledge about the simulation model used.

To simulate a wave state, a 20-minute time series of irregular waves is generated based on the Wavehub spectrum. The subsequent excitation forces are then calculated and the simulation is performed for the full length of the time series. The simulation model also takes into account PTO

Significant wave height Hs [m]	Wave period Tz [sec]								
	3,5	4,5	5,5	6,5	7,5	8,5	9,5	10,5	11,5
0,25	26	79	44	18	0	0	0	0	0
0,75	499	832	491	140	18	0	0	0	0
1,25	184	1051	604	307	70	26	9	0	0
1,75	0	587	701	333	149	53	26	0	9
2,25	0	96	534	254	123	44	9	0	0
2,75	0	0	237	228	105	26	9	9	0
3,25	0	0	26	175	123	44	9	0	0
3,75	0	0	0	79	96	35	18	0	0
4,25	0	0	0	9	44	26	9	9	0
4,75	0	0	0	0	26	18	9	0	0
5,25	0	0	0	0	18	26	18	0	0
5,75	0	0	0	0	0	18	9	0	0
6,25	0	0	0	0	0	9	0	0	0

TABLE I
WAVEHUB SCATTER DIAGRAM

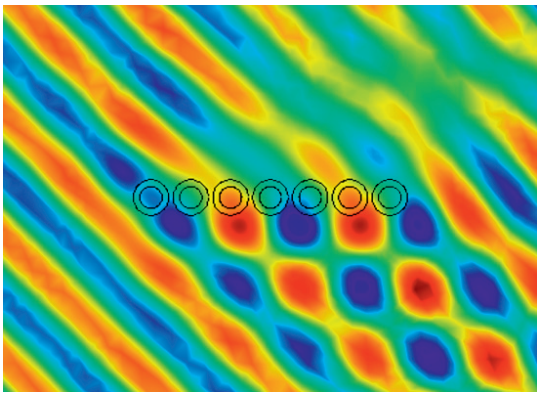

Fig. 12. Illustration of the wave interaction with the array. The wave direction is from southwest and thus causes amplification on the southern side of the array and attenuation on the northern side.

and generator losses, and the model outputs a 20-minute time series of exported electrical power from the WEC. The simulation model has undergone many years of development and testing and is verified against real production data from several prototypes, including Bolt.

Array simulations are performed by running the simulation model separately for each absorber in the array. All absorbers are simulated for the same wave, and the expected wave propagation through the array is taken into account.

A. Hydrodynamic interactions within the array

The hydrodynamical problem is solved within the framework of linear potential theory, specifically Laplaces' equation, resulting in the interaction field illustrated in Fig. 12. In this paper the theoretical basis is only gone through briefly. A number of books have been written on the subject of linear potential theory, among other J.N Newman's "Marine Hydrodynamics" [16].

Since the velocity potential is linear, all contributions to forces and motions are linear. As a result the principle of superposition applies. Therefore it is convenient to split the complex problem into a set of simpler problems. The full solution is thus the sum of several simpler solutions. The potential arising from N absorbers placed in a string can thus be described as the sum of the following contributions.

$$\phi = \phi_0 + \phi_D + \phi_R \tag{4}$$

The total velocity potential ϕ due to the interaction of N absorbers on a string is the sum of the excitation potential due to incident waves ϕ_0, the diffraction potential due to the interaction of the incident potential with all absorbers at rest ϕ_D, and the radiation potential ϕ_R due to the independent motion of every absorber in every mode of motion with no incident waves present.

The diffraction problem and the radiation problem is solved independently. Thus there are $N + 1$ independent problems to solve. Further the radiation potential from each absorber is separated in 6 independent modes of motion. The total potential ϕ_N^i acting on absorber N in mode i of motion is thus the sum of every other absorbers' radiation and diffraction potential in addition to the diffraction and radiation potential from absorber N acting on itself in mode i of motion. Combining the 6 modes of motions for each absorber allowing for all absorbers to interact results in a total of $N \times 6$ independent linear equations to be solved for each wave frequency.

With a full description of the velocity potential it is possible to integrate solutions in the frequency domain on specific wave climates and optimize the array energy output with respect to array layout angle and power take off damping coefficient.

In order to represent the interactions within the array in the time domain model a set of correction factors is applied to the power output from a time domain model of an array without interactions. These are plotted individually for each WEC in the array as a function of array angle in Fig. 13. The method is only meant as a first step but is expected to give reasonable results with respect to yearly average energy output and is therefore regarded as valid within the scope of this paper.

IV. RESULTS

The simulation returns accurate power time series for all observed wave states at Wavehub. By weighing the time series according to the scatter, it is possible to create a continuous time series for the exported power with high resolution that covers a full year. By sorting the samples in descending order the resulting dataset plotted in Fig. 14 emerges. This is probably the most important plot for evaluating the utilization of installed power as it gives a clear picture of the power distribution from the array. It is important to note that the plot is given with sub-second resolution and must be viewed as an instantaneous power analysis. It does not give a good impression of how the power is distributed through a day or a year. But it shows in detail how the installed converter and the grid connection are utilized.

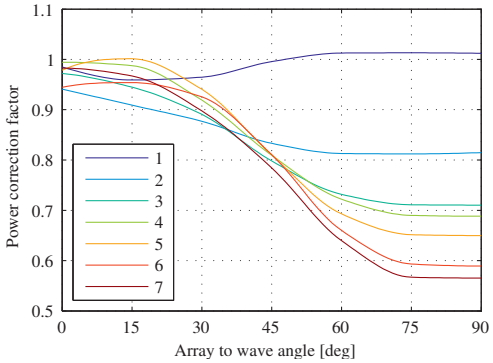

Fig. 13. Power correction factors for absorbers in array calculated from shadowing effects

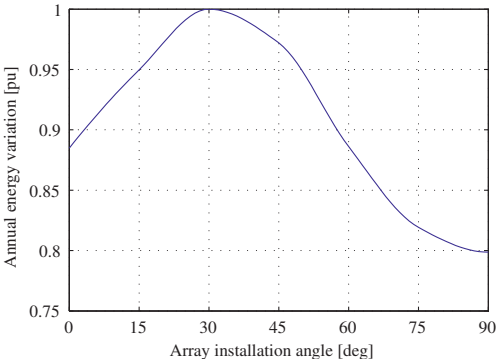

Fig. 15. Annual energy produced with different installation angles

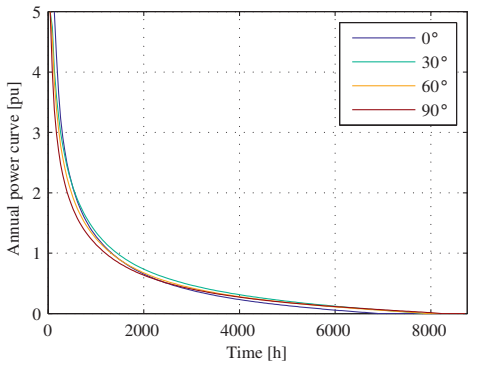

Fig. 14. Annual power hours produced by array on Wavehub for different installation directions.

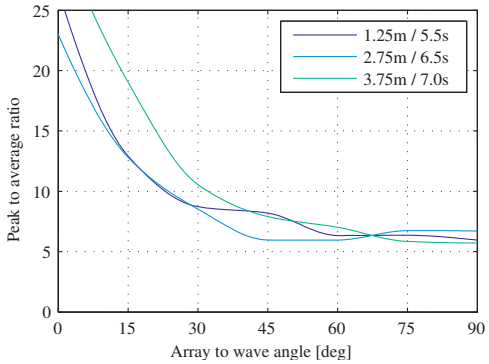

Fig. 16. Array peak to average factor as function of installation angle

Based on the findings in the initial array study [2], the power is capped at five times the average production in the design wave state, and the power curve is normalized to this average power. The variations between the different wave directions are not so distinct in Fig. 14, but becomes clearer in Fig. 15 and Fig. 16. These plots show the annual energy and the power quality as function of array angle. Both figures are linked and closely related to the result set presented in Fig. 14, as will be showed shortly.

To simplify the simulations, the array is only simulated for incoming wave directions over one quadrant. Since the array is symmetrical from right to left and from front to aft, this is valid. When the array operates with zero angle to the waves, the absorbed power is maximized. However, since the power quality is poor at this angle, significant energy is lost due to power capping. On the other hand, with 90° array angle significant energy is lost to the shadowing effect. Subsequently, the optimal array angle turns out to be 30° for this configuration. The optimal angle is expected to move towards higher numbers as the power system is further optimized with lower peak power ratings. The design angle of 45° therefore still seems to be a good choice, but must be verified when the electrical system design is complete.

By Fourier transforming the power time series the power output can also be evaluated in the frequency plane. Fig. 17 shows the frequency plot for the design wave state hs=2.75m / Tz=6.5s at different array angles. It clearly shows the effect of array smoothing at higher frequencies. However, at the low frequencies there is little effect as the corresponding wave travel distance becomes much larger than the array. The peak observed around 0.1 Hz coincides with the 7 s wave period. Except for this peak, there are no distinct points in the spectrum, which is related to the stochastic nature of ocean waves.

The annual energy is found by integrating the power curve in Fig. 14. By dividing the annual energy on the installed power, the *annual full load hours* are found. This is a benchmark figure used to quantify the utilization factor of installed transfer capacity, and is widely used for renewable energy

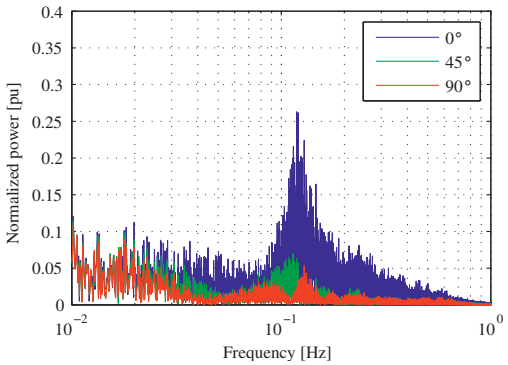

Fig. 17. Frequency plot of exported power from array

power plants. The resulting annual full load hours for this analysis turns out to be approximately 1 000 hours, which is quite low when compared to land based wind that is believed to average 2 000 hours. However, the system is still in an early stage of design and there are still several steps of optimization that has to be performed. For instance, it can be seen by visual inspection of Fig. 14 that the installed power capacity factor can be reduced from five to three without significant loss of annual energy. This would improve the annual load hours to approximately 1 500 hours. However, such an optimization must be performed for the complete system including energy storage and other measures, and this path is not pursued further in this work.

V. Conclusion

This analysis shows that the annual energy from the array installed at Wavehub is mostly in accordance with expectations, and in accordance with earlier analysis. Some reduction is observed in both annual energy and in availability as the shadowing effects are accounted for. The reduction in availability is believed to be caused by the shadowing effects impacting stronger on the low wave states. The array achieves approximately 1 000 annual load hours in the current configuration, and must undergo further improvements to reach the preferred range of 1 500 - 3 000 load hours. Several steps of optimization can be utilized, including active power capping and introduction of intermediate energy storage. These measures will be subject to further study.

Acknowledgment

Thanks to Even Hjetland for help with graphical design and thanks to www.freemaps.no for making vectorized open source maps freely available.

References

[1] J. Falnes and J. Hals, "Heaving buoys, point absorbers and arrays," *Philosophical Transactions of the Royal Society A: Mathematical, Physical and Engineering Sciences*, vol. 370, no. 1959, pp. 246–277, 2012. [Online]. Available: http://rsta.royalsocietypublishing.org/content/370/1959/246.abstract

[2] J. Sjolte, G. Tjensvoll, and M. Molinas, "All-Electric wave energy converter connected in array with common DC-Link for improved power quality," in *3rd International Symposium on Power Electronics for Distributed Generation Systems (PEDG'12)*, Aalborg, Denmark, Jun. 2012.

[3] I.Bjerke, E.Hjetland, G.Tjensvoll, and J.Sjolte, "Experiences from field testing with the bolt wave energy converter," in *European Wave and Tidal Energy Conference (EWTEC11)*, 2011.

[4] "The wave power climate at the wave hub site," November 2006, journal: Applied Wave Research Review of Wave Power Climate.

[5] J. Falnes, *Ocean Waves and Oscillating Systems: Linear Interactions Including Wave-Energy Extraction*. Cambridge University Press, 2002.

[6] E.Tedeschi and M.Molinas, "Effect of control strategies and power take-off efficiency on the power capture from sea waves," in *IEEE Transactions on Energy Conversion*, 2011, in Press.

[7] E. Tedeschi, M. Molinas, M. Carraro, and P. Mattavelli, "Analysis of power extraction from irregular waves by all-electric power take off," in *Energy Conversion Congress and Exposition (ECCE), 2010 IEEE*, sept. 2010, pp. 2370 –2377.

[8] J.Falnes, "Principles for capturie of energy from ocean waves: phase control and optimum oscillation," NTNU, Tech. Rep., 1997, http://folk.ntnu.no/falnes/w_e/index-e.html\#RAPPORTAR.

[9] E. Tedeschi and M. Molinas, "Impact of control strategies on the rating of electric power take off for wave energy conversion," in *Industrial Electronics (ISIE), 2010 IEEE International Symposium on*, july 2010, pp. 2406 –2411.

[10] J.Sjolte, I.Bjerke, E.Hjetland, and G.Tjensvoll, "All-electric wave energy power take off generator optimized by high overspeed," in *European Wave and Tidal Energy Conference (EWTEC11)*, 2011.

[11] J. Sjolte, I. Bjerke, A. Crozier, G. Tjensvoll, and M. Molinas, "All-electric wave energy power take off system with improved power quality at the grid connection point," in *2012 IEEE PES Transmission and Distribution Conference and Exposition*, 2012, In press.

[12] ——, "All-electric wave energy converter with stand-alone 600vdc power system and ultracapacitor bank," in *2012 EVER International Conference and Exhibition on Ecological Vehicles and Renewable Energies*, 2012, In press.

[13] E.Hjetland, I.Bjerke, G.Tjensvoll, and J.Sjolte, "A brief introduction to the bolt-2-wave project," in *European Wave and Tidal Energy Conference (EWTEC11)*, 2011.

[14] M.Molinas, O.Skjervheim, P.Andreasen, T.Undeland, J.Hals, T.Moan, and B.Sorby, "Power electroncis as grid interface for actively controlled wave energy converters," International Conf. on Clean Energy Power (ICCEP07), Tech. Rep., 2007.

[15] O.Skjervheim, B.Sorby, and M.Molinas, "All electric power take off for a direct coupled point absorber," Proceedings of the 2nd International Converence on Ocean Energy (ICOE2008), Tech. Rep., 2008.

[16] J. Newman, *Marine Hydrodynamics*. Mit Press, 1977. [Online]. Available: http://books.google.no/books?id=nj-k_lAmaBYC

Appendix F

Conference paper 6

Title: All-Electric Wave Energy Converter Array with Energy Storage and Reactive Power Compensation for Improved Power Quality

Conference/Journal: Energy Conversion Congress and Exposition (IEEE/ECCE)

Date: 15.-20. September 2012

Location/Publisher: Raleigh, NC, USA

All-Electric Wave Energy Converter Array with Energy Storage and Reactive Power Compensation for Improved Power Quality

Jonas Sjolte
Fred. Olsen / NTNU
Norwegian University of
Science and Technology
Email: jonas.sjolte@fredolsen.no

Gaute Tjensvoll
Fred. Olsen
Oslo, Norway
Email: gaute.tjensvoll@fredolsen.no

Marta Molinas
Norwegian University of
Science and Technology
Trondheim, Norway
Email: marta.molinas@ntnu.no

***Abstract*—Power electronics and advanced motion control has allowed for creating *Wave Energy Converters* (WECs) with the generator directly coupled to the sinusoidal motions of the prime mover. However, this results in large fluctuations in output power, and the resulting peak to average power ratio exceeds most other energy producers. Moreover, the typical average power production from a WEC is lower than that of other power plants, and array connection of several WECs is necessary to help mitigate these shortcomings. Earlier studies performed on arrays by *Fred. Olsen* (FO) has shown a favorable outcome, and has demonstrated a reduction factor of four in the peak to average ratio for a small array. These results were obtained without further power conditioning and resulted in poor utilization of installed capacity. In an endeavor to fully optimize the WEC system for grid connection, this study investigates three possibilities for power quality improvements: Introduction of energy storage, implementation of controlled power capping and implementation of reactive power compensation. By simulation of annual production for a specific production site, the resulting power quality improvements are estimated, and demonstrates that the WEC system can obtain a power quality level close to wind power. Reactive power compensation demonstrate the ability to increase the power quality and to improve the local power balance by optimizing the grid utilization during no production periods.**

I. Introduction

Wave Energy Converters (WECs) are different from most other energy producers in that the prime mover operates with a sinusoidal velocity. When such a producer is directly connected to its generator, the power output is continuously fluctuating with zero crossings in every wave, resulting in a high peak to average ratio. This behavior can be seen in Fig. 2 which shows the power output from Fred Olsen's (FO) *Lifesaver* power plant, pictured on site in Fig. 1. Since the performance of FO's systems are measured and simulated to a high level of detail, only normalized results are presented in this paper to protect the intellectual property of FO. However, this is not believed to reduce the value of the results as they should be valid for this type of WEC in general. Unity power in the normalization is defined as the average exported power in the design wave state, hs = 2.75m / Tz = 6.5s, where hs is the significant wave height and Tz is the wave period. This is regarded as the installed production capacity.

In an endeavor to improve the export power quality, FO has undertaken a study on arrayed systems. The first step of the work was presented in our paper [1] and investigated the basic geometrical properties of the array and the potential for power quality improvements. The analysis was performed for the design wave state with a wave direction of 45° to the array, and concluded on the geometry illustrated in Fig. 3. The resulting array power is compared to the single WEC power and plotted in Fig. 4. The power is normalized to the average design production for both configurations, and

Fig. 1. *Lifesaver* on site outside Falmouth

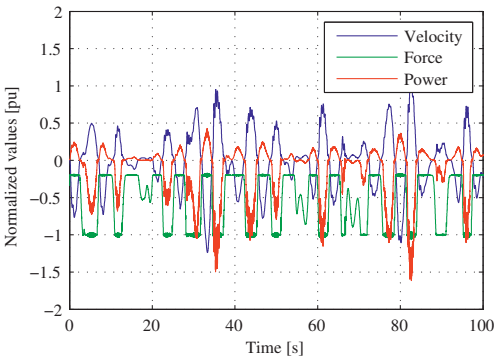

Fig. 2. Actual production and system operation measured on Lifesaver

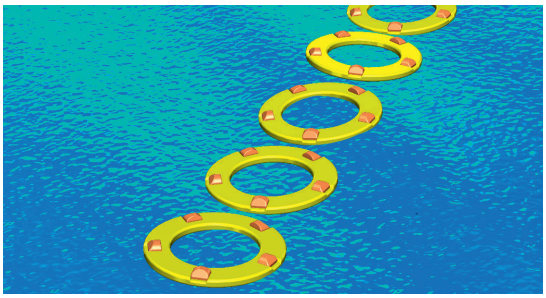

Fig. 3. Artistic impression of array at Wavehub based on Lifesaver

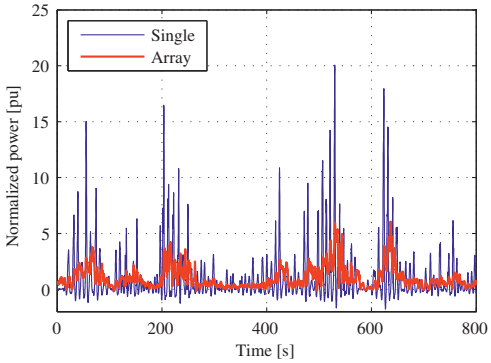

Fig. 4. Peak to average power ratio for array versus single absorber

effectively demonstrates the improvement in power quality, reducing the peak to average ratio by a factor of four. This is mainly the result of the orientation of the array which causes the incoming wave crest to interact with one absorber at the time. This analysis was of qualitative nature only, not taking into account the changing nature of the real sea. Also, the simulation ignored the interaction forces between the absorbers, referred to as the *shadowing effects*.

The next step in the array study, presented in our paper [2], investigated the total performance of such an array system for real sea conditions with focus on annual energy production. The simulations are performed for the WEC prototype test site *Wavehub* located west of Cornwall, England, as illustrated in Fig. 5. Wavehub is a joint project funded and supported by a renewable energy program administrated by the British government. The site includes a sub-sea power substation that allows for electrically connecting prototype WECs to grid. Wavehub has been surveyed and monitored for an extensive period, and work is still ongoing to calculate true statistical wave data for the site. For the study undertaken here, preliminary data were used, which are expected to give a good impression of the power quality, but should be updated for an accurate estimate for annual energy production.

The simulation also took into account the interaction forces between the absorbers in the array by the application of a sep-

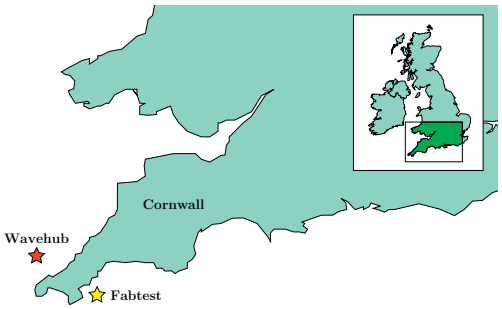

Fig. 5. Location of the UK test sites *Wavehub* and *Fabtest*

arate hydrodynamical model. This model was not integrated into the main simulation model, but produced a lookup table of power correction factors for the array for all encountered wave states and wave directions. The full power production simulation was performed for the full wave scatter diagram for Wavehub, and the annual power distribution and total energy production was calculated. Until this point the installed electrical transfer capacity has been unconstrained, which leads to poor power utilization and only 1 000 annual full load hours for this case.

To continue the array study the goal of this work is to investigate how the installed electrical power can be optimized. Three methods are to be applied:

- Power capping
- Energy storage
- Reactive power compensation

The first two methods will improve the availability by reducing the installed power. The last method is a possibility to use the spare conversion capacity to improve the power quality at PCC by reactive power compensation. This may improve the power balance at PCC also during no load periods, allowing the WEC to supply some base load capacity.

This work is based on earlier presented simulation methods and results, and takes the raw output power from these as input. The simulation is not elaborated here, but is described in detail in our earlier publications [1]–[3].

A. Fred. Olsen Wave Energy Project

FO started with Wave Energy in 2000, leading to the first Wave Energy Converter prototype *Buldra*®, built as multiple point absorber platform and launched in 2004. Since then FO has tested out various concepts and built several different prototypes, all based on the point absorber principle. The series of experiences have led to the single body point absorber system Bolt® as pictured on site in Fig. 6. Even though the point absorber principle may not be the most efficient absorber type, it has shown to be successful in terms of total performance and cost of energy. Bolt® has been in operation outside Risør in Norway since June 2009 and has till date performed very well with only minor issues and incidents. As

Fig. 6. FO's Wave Energy Converter Bolt® located outside Risør, Norway, was launched in June 2009, and is still in operation.

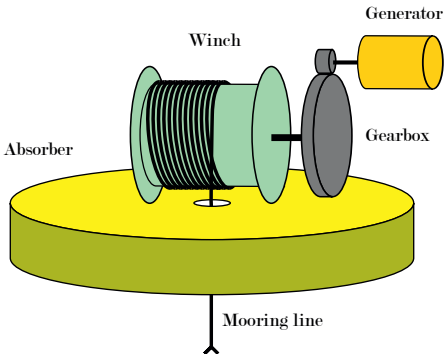

Fig. 7. Principal sketch of FO's WEC system

on December 22, 2010 she had produced 3 360 kWh [4], and is expected to exceed 6 000 kWh during 2012.

Based on the success with Bolt®, FO decided to use the knowledge and experience gained so far to proceed with the next generation design. An agreement with several UK companies was made with funding from the UK *Technology Strategy Board* (TSB). The goal of the project is to improve the Bolt® concept to a commercial level where it can be launched at Wavehub [5], and hence the project name *Bolt2Wavehub*. The project resulted in the full scale WEC *Lifesaver* pictured in Fig. 1, which was launched early in April 2012. The name is inspired by the shape of the buoy which is similar to a rescue buoy. Lifesaver is situated outside Falmouth, UK on the marine research test site *Fabtest*, see Fig. 5. Lifesaver has not been in operation long enough for a comprehensive statistical analysis, but preliminar results indicate that the system operates close to expectations. An example of the device in production is shown in Fig. 2 which shows speed, torque and power from one of its generators during normal production.

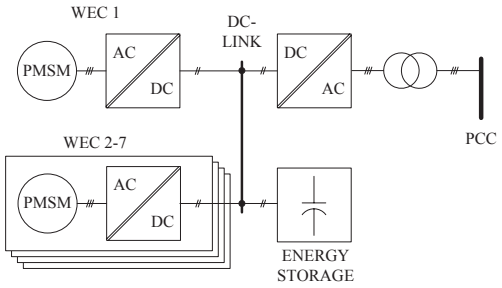

Fig. 8. Electrical configuration of the array

II. System description

The array is based on the WEC Lifesaver which is a toroidal absorber with five individual all-electric *Power Take Off* (PTO) units. The PTOs are tightly moored to the sea floor by a winch and drum system, which directly ties surface movements to the generator through a custom designed transmission system. The wave to wire coupling is illustrated in Fig. 7. Since the winch system requires active power for pull-back during downward movement, the generator is ran in motoring mode with a low pull-back torque for this part of the wave cycle. This accounts for the positive power intervals seen in the production output from Lifesaver in Fig. 2.

The array is created by installing seven of the Lifesaver WEC in a row as illustrated in Fig. 3, with an array angle to the dominating wave direction of $45°$. The covered length along the incoming wave direction ensures that an incoming wave crest only interacts with one absorber at the time, thus ensuring smoother output power. Spacing perpendicular to the wave direction is necessary to ensure good energy capture, and the angle of $45°$ has proved to be a good compromise.

The proposed electrical power system for the array is an extension of the Lifesaver multi-PTO concept, where all production units are connected on a common DC-Link [6]. This is made possible by the 3-phase AC/DC inverters that control each generator of the *Permanent Magnet Synchronous Machine* (PMSM) type. Full converter configuration is required for continuous generator operation in the heavily varying speed specter induced by the waves. The generator is controlled as a linear damper with torque saturation on upwards movement and with constant wind-in torque on downwards movement, causing the bi-directional power flow discussed earlier.

The common DC-Link coupling allows the produced power to be balanced out between the WECs without additional transmission or conversion equipment. The grid side inverter harvests the produced power from the DC-Link, and the power is further transformed and transferred to the *point of common coupling* (PCC). Since all the components in the grid connection chain, from the DC-Link to the PCC, have to be sized according to the array peak power, there can be substantial cost reductions from lowering the peak to average ratio.

Fig. 9. 48V balanced ultracapacitor module by Maxwell Technologies.

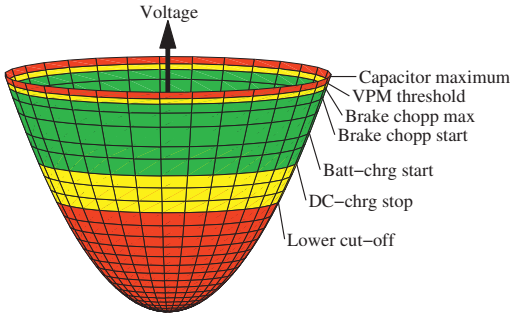

Fig. 10. Illustration of energy storage capacity at Lifesaver. The power management system is controlled based on the capacitor voltage.

By closer study of Fig. 4 it can be seen that the output power peaks are short in time. These peaks can be filtered out either by absorbing the energy in an energy storage or by reducing the power production during these high waves to comply with a lower level of installed power. The former method is more costly, but will retain the annual production, whilst the latter method is free, but sacrifices some of the annual production. The optimal solution is likely to be a combination of the two methods and should be decided based on economical optimization. This work will explore the effects of these two methods and give a qualitative impression on how the system should be sized.

The energy storage is regarded as ideal with respect to efficiency, power capacity and lifetime, and only the energy capacity is taken into consideration. Based on experience form earlier systems, and Lifesaver in particular, ultracapacitors are believed to be the most suitable technology for this kind of application. They offer high efficiency, high power, good power density and reasonable lifetime in this power regime. One important design parameter which greatly affects the ultracapacitor system is whether it is directly connected on the DC-Link or connected behind a intermediate converter. A direct connected system will have almost no practical power limit, but will require large voltage fluctuations on the DC-Link. During normal operation, ultracapacitors should only be cycled between the nominal voltage V_{nom} and $\frac{1}{2}V_{nom}$. If the power converters of the WEC can operate within this window, the ultracapacitor energy can be fully utilized. Lifesaver utilizes this possibility and has a 1 MJ ultracapacitor bank connected directly to the DC-Link. The energy storage consists of 17 modules in series of the Maxwell module pictured in Fig. 9. These modules are internally balanced and can handle the maximum DC-Link voltage of 830V. The control of the DC-Link and energy storage for Lifesaver is illustrated in Fig. 10.

However, for a larger system, like a complete wave farm, it is likely that the system would suffer from other adverse effects caused by the fluctuating DC-Link, such as reduced inverter efficiency and reduced power quality at PCC due to DC-Link undervoltage, and subsequent hijacking by the diode rectifier. This can be avoided by introducing an intermediate converter between the DC-Link and the ultracapacitor bank, which allows the DC-Link voltage to be constant, but introduces the installed conversion capacity as a new boundary condition to the energy storage. As stated initially, the energy storage is simplified and regarded as ideal to simplify the model and reduce the parameters that influence on the results. Based on the experience with Lifesaver this simplification does not significantly affect the results.

Design of the control method used for the energy storage is a study on its own. It should be controlled so that the exported power follows the smoothest possible curve, whilst ensuring maximum possible energy export. These are conflicting interests as the attempt to smooth the output power may result in the energy storage being unnecessarily full when a large wave train is passing by, thus resulting in unwanted power shedding. In this work, this problem is simply solved by running the export converter at full capacity whenever there is energy in the storage. This will guarantee maximized power export, but will also generate an unnecessarily distorted output power.

III. Active Power Analysis

The simulation model for the energy storage takes the raw production data output from the array simulation as input and calculates the amount of stored energy and the resulting export power. The simulation output is plotted in Fig. 11 which shows the energy and power for a system with 2 pu installed power capacity and 10 pu·s installed energy storage in the design wave state. The figure also illustrate the crudeness of the current control, which causes abrupt changes in output power when the energy storage clearly could have been exploited to produce a smoother output.

The output power from the array simulation is feed into the energy storage model and scanned through several parameter pairs for installed energy and power. The resulting annual energy outputs are listed as pu-hours in Table I. The table clearly shows the effect of the energy storage, but also demonstrates the need to sacrifice some of the annual energy to avoid unrealistic system ratings. An annual production of 4 600 pu·h is considered for further investigation. This amounts

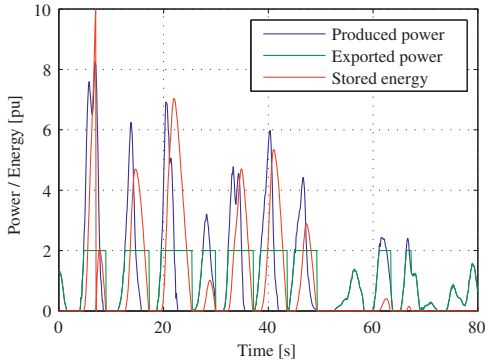

Fig. 11. Power balance with energy storage in design wave state

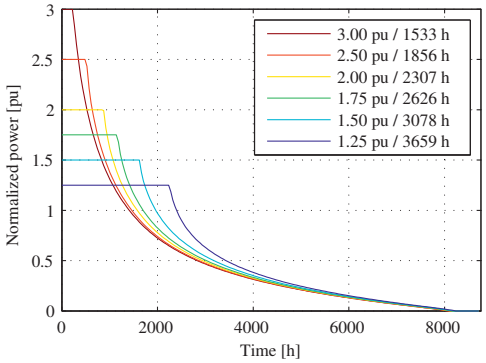

Fig. 12. Annual power distribution for the energy/power pairs highlighted in Table I

Energy capacity [pu·s]	Power capacity [pu] 1.25	1.5	1.75	2	2.5	3	∞
0	3676	3911	4096	4243	4457	**4599**	4950
5	4045	4238	4380	4490	**4641**	4736	4950
10	4197	4380	4514	**4613**	4736	4810	4950
15	4291	4473	**4595**	4683	4795	4854	4950
20	4356	4531	4650	4728	4830	4884	4950
30	4454	**4616**	4726	4791	4869	4915	4950
45	4530	4686	4779	4845	4913	4934	4950
60	**4574**	4725	4823	4881	4928	4944	4950
90	4624	4768	4860	4913	4944	4950	4950
120	4646	4794	4886	4922	4950	4950	4950

TABLE I
ANNUAL ENERGY [PU·H], FOR VARIOUS CONFIGURATIONS

to 7% reduction from the theoretical maximum of 4 950 pu·h. The corresponding values are highlighted in Table I, and the annual power distribution is plotted for each of the cases resulting in the plots shown in Fig. 12. The figure demonstrate a significant improvement from the starting point of 1 000 load hours, and shows that WEC systems can be grid intergrated with relatively simple measures.

The analysis is based on instantaneous power export on a sub-second scale. This is believed to be valid for the solid state based inverters which have limited overload capacity. However, it could be expected that the remaining part of the grid connection chain, mainly the transformer and the cable to PCC, could have a higher overload capacity based on its high thermal mass. This could for instance allow for a system with 2 pu inverter capacity to have only 1.5 pu of installed transfer capacity, which would further improve the system availability. The availability must be calculated for each specific configuration for each specific site, but in general this analysis shows that with these steps wave energy can achieve an annual availability comparable to wind energy.

IV. REACTIVE POWER ANALYSIS

The calculations in the preceding section demonstrates promising numbers for availability, but it also shows that there is free capacity in the grid inverter for most of the time. Depending on the technology used in the grid inverter, this spare capacity could be exploited for reactive power compensation. With the size of the current WEC system, an IGBT based inverter is likely, which gives great flexibility for alternative compensation methods. For this work, an IGBT based system is assumed.

Reactive power compensation can be performed by many methods, and to different levels of sophistication, the simplest being power factor correction by optimizing the phase shift angle φ between voltage and current. Since this can be compensated by simpler and cheaper methods, it seems sensible to focus on more complex forms of distortion. With the increasing use of power electronics, such distortions are also becoming more common, raising the need for compensation.

This work will be based on the work and methods presented by Akagi et al [7]. They present two general methods to quantify and isolate distortions, the p-q method which is based on Clarke-transformation to the $\alpha\beta 0$ reference frame, and a second method referred to as the abc method that can be applied directly on the abc phase voltages and phase currents. This analysis will be based on the abc method.

In instantaneous reactive power compensation one of the key elements is to identify the current components that does not contribute to active power transfer and that should be compensated. The abc method identifies this directly through application of Equation (1) and (2), where i_k is the load current, v_k is the phase voltage, $p_{3\phi}$ is the three phase instantaneous power, i_{qk} is the resulting compensation current and the index k refers to the three phases ($k \in \{a, b, c\}$). The abc method only deals with instantaneous power and reactive power.

$$\begin{bmatrix} i_{qa} \\ i_{qb} \\ i_{qc} \end{bmatrix} = \begin{bmatrix} i_a \\ i_b \\ i_c \end{bmatrix} - \frac{p_{3\phi}}{{v_a}^2 + {v_b}^2 + {v_c}^2} \begin{bmatrix} v_a \\ v_b \\ v_c \end{bmatrix} \quad (1)$$

$$p_{3\phi} = v_a i_a + v_b i_b + v_c i_c \quad (2)$$

A secondary effect which may cause sub-optimal energy transfer is fluctuations in active power, which is not addressed

by the abc method. However, a similar method, referred to as *Generalized Fryze Currents* presented by Fryze in 1932 [8] deals with this by introducing the average power in the calculation. The Fryze method is based on the constant evaluation of the actual admittance of the load. The method is based on Equation (3) and (4) where $i_{\bar{q}k}$ is the Fryze current and g_e is the admittance. The Fryze method must be tuned with a corresponding time constant to decide the duration of the power smoothing. This must be matched to the available energy storage and the expected load fluctuations. In this simulation a time constant of 6π is chosen, which corresponds to three full periods at 50Hz.

$$\begin{bmatrix} i_{\bar{q}a} \\ i_{\bar{q}b} \\ i_{\bar{q}c} \end{bmatrix} = \begin{bmatrix} i_a \\ i_b \\ i_c \end{bmatrix} - G_e \begin{bmatrix} v_a \\ v_b \\ v_c \end{bmatrix} \tag{3}$$

$$G_e = \frac{1}{T}\int_0^T g_e(t)\,\mathrm{d}t = \frac{1}{T}\int_0^T \left(\frac{v_a i_a + v_b i_b + v_c i_c}{{v_a}^2 + {v_b}^2 + {v_c}^2}\right)\mathrm{d}t \tag{4}$$

In this work the goal of the compensation is better utilization of the power transmission lines to the central grid as WEC systems are most likely to be placed in remote locations along the coast line with weak connections. A relevant WEC application could be to improve the power balance in coastal towns by installing small WEC farms, thus avoiding expensive power line upgrades. However, renewable energy producers cannot guarantee production at peak load demand, thus adding little improvement to the power balance.

$$I_S = \sqrt{{I_p}^2 + {I_q}^2} \tag{5}$$

Nevertheless, it may be that by performing reactive power compensation in periods of no or little active power production, the power line apparent power could be improved sufficiently to guarantee the peak load demand. This can be evaluated analytically by the orthogonal vector sum of RMS values, as given in Equation (5), where the line current I_S is evaluated based on the active current I_p and the reactive current I_q. Even though the compensation currents $i_{qk}, k \in \{a, b, c\}$ are not necessarily sinusoidal, the principle of orthogonality is still valid as the average product of i_{qk} and i_{pk} is zero. For this case study the following system properties are defined:

- Load with semi-weak connection to grid. $Z_{line} = 0.012 + j0.19$ pu which gives a short circuit capacity of 5 pu
- Installed electrical WEC capacity is 0.10 pu of the power line capacity
- At peak load demand the distortion current is at least 0.10 pu
- Power line utilization is 1.0 pu at peak load demand

Based on this example it will be investigated how the WEC can utilize reactive compensation to improve the load balance, also during no production periods. During peak load, I_S equals 1 pu, and I_q equals 0.1 pu in the worst case scenario. By complete compensation of I_q, I_S can be reduced to I_p. This result in approximately 0.50% reduction of I_S. The small

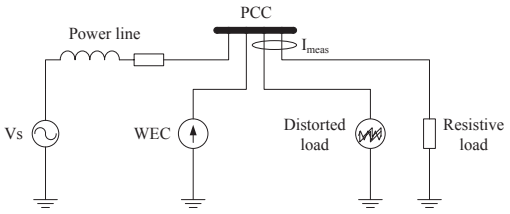

Fig. 13. Simulation model for instantaneous power quality analysis

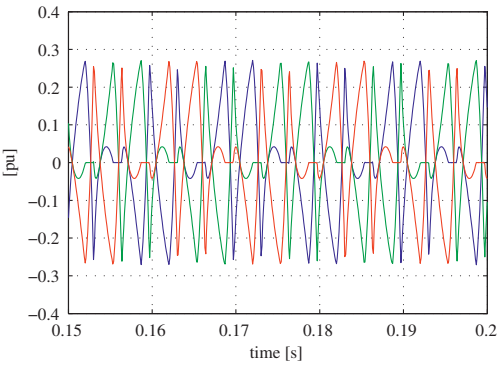

Fig. 14. Compensation current calculated by the ABC method

effect is caused by the square relationship of I_S, which weigh the higher values heavier. If instead the distortion current is intitially 0.3, and is reduced to 0.2, the reduction in I_S improves to 2.5%. This evaluation becomes more difficult for the Fryze method, as the compensation current may also contain active current parts, I_p. However, this may also lead to better results from the Fryze method, as reducing the I_p current will have higher impact on I_S.

To investigate further on these issues, a simulation model is created based on the earlier stated assumptions. The simulation model is defined as illustrated in Fig. 13, and is based on the case parameters listed above. The distorted load is implemented as a current source connected on the DC side of a 3-phase rectifier. The active load is realized by a 3-phase resistor. The resulting total load current is measured as indicated in Fig. 13, and the compensation factors for the Fryze case and abc case are calculated. The resulting i_{qk} and $i_{\bar{q}k}$ currents are plotted in Fig. 14 and 15 respectively.

The two compensation currents look very similar, the only significant difference being the sinusoidal-like curve sections with approximately 0.05 pu amplitude. The flat sections in the i_q currents in Fig. 14 coincide with the short-circuit between the two opposite phases during rectifier commutation, and are caused by the instant change in power during this interval. The average power based Fryze method is not affected by this. Fig. 17 shows the resulting harmonic distortion for the three simulated cases. The effect of compensation is well demonstrated, and is also supported by the calculated *Total*

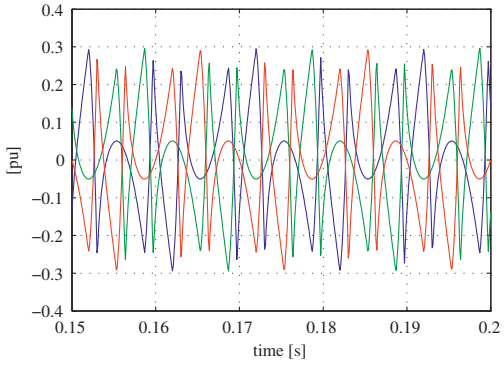

Fig. 15. Compensation current calculated by the Generalized Fryze method

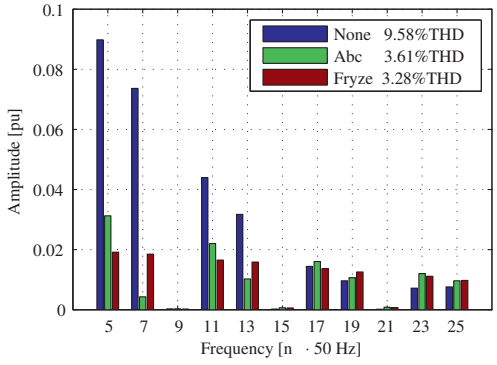

Fig. 17. Frequency analysis of PCC voltage. Higher harmonics.

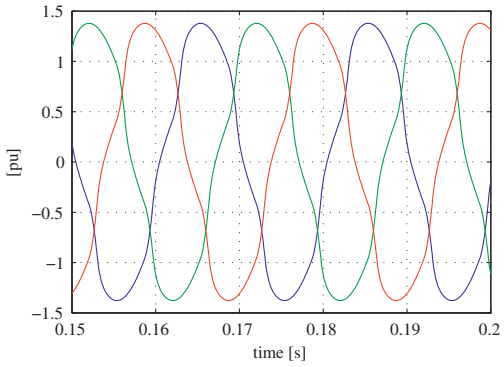

Fig. 16. Current measured at PCC without reactive compensation

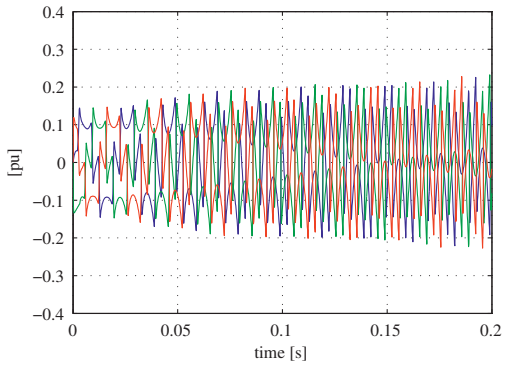

Fig. 18. WEC export current during linear sweep from maximum active power production to maximum reactive power compensation

Harmonic Distortion (THD) for these cases. In the cases were the WEC compensation current was unconstrained, the harmonic distortion was almost completely canceled out, and the remaining harmonic distortion is mainly due to the limited rating of the WEC inverter.

The WEC inverter is also constrained by a 10 kHz first order filter to simulate the natural restrictions in a real system. This is to high as a realistic system probably would operate at a switching frequency around 2 kHz. In addition, the required feedback current control loop for the *Voltage Source Inverter* (VSI) would limit the ability to compensate the higher harmonics from 20 and upwards. Since most of the distortion in this simulation occurs at lower frequencies, this error is not expected to significantly impact on the results.

To investigate further on the possibility of the Fryze method to also compensate active current instabilities, a second load case is defined where the current source load behind the rectifier fluctuates with 75 Hz. The resulting line current is plotted in Fig. 19 and shows how the phase currents are unbalanced. Fig. 20 shows the results from simulating both load cases for the three compensation cases. The difference between the two compensation methods is well demonstrated for the two load cases. For the first load case they perform almost equally good, but for the second load case the Fryze method outperforms the abc method. Also, if the two load cases are compared to the uncompensated case, it can be seen that the Fryze method obtains a reduction in line current of 1.6% for the second load case compared to 0.8% reduction for the first load case.

The final step to verify the system operation is to investigate how the system behaves when combining active power production from the WEC array and reactive power compensation. The system is modeled so that the active power production dictates the power export, and the remaining current capacity is used for reactive compensation. The actual compensation current is obtained by linearly scaling the reference compensation current to match the free RMS current capacity. To demonstrate the dynamic shift between active and reactive power production, a sweep method was used where the converter starts at maximum active power export and gradually shifts to reactive power export. Fig. 18 shows the resulting WEC

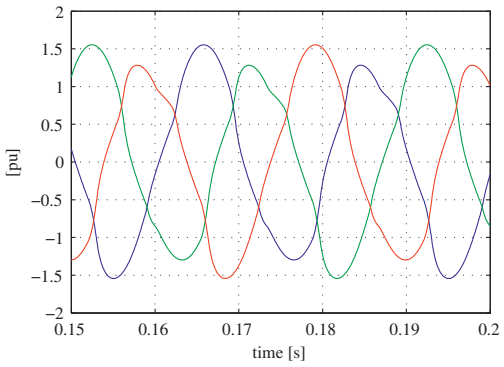

Fig. 19. Special case with rectifier load fluctuating at 75 Hz.

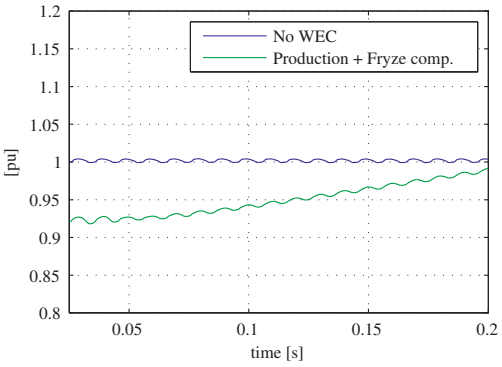

Fig. 21. Line RMS current during active to reactive power sweeps

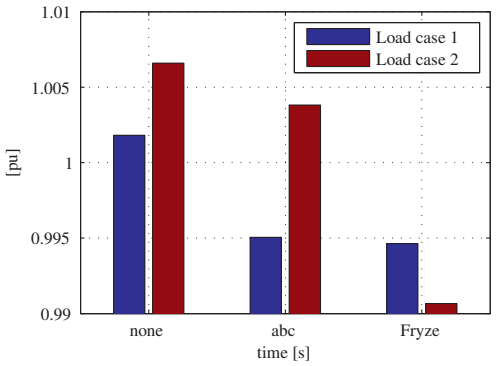

Fig. 20. Resulting line current RMS values for the two load cases.

output current during the sweep. Although it is difficult to see from the figure, the output current is purely sinusoidal at t=0. The high level of distortion in the compensation current quickly distorts the sinusoidal waveform when it is phased in. Fig. 21 shows the resulting RMS line current for the two load cases during the sweep. The initial 0.025 seconds are taken out as they are distorted due to RMS calculation ramp-up. The figure shows the expected 10% drop in line current at full active power export, and the remaining 1% when only reactive compensation is performed. In general, the combined operation works fine, the WEC converter always stays within its nominal rating, all active power is transferred and the reactive power compensation operates in a stable mode in spite of the changing amplitude.

V. Conclusion

This analysis shows that the availability of the WEC array can be greatly improved by a small amount of production shedding and a small energy storage. The initial unconstrained case produced only 1 000 annual load hours, but by shedding 7% of the annual production, and by introduction of a 10 s energy storage, the availability was increased to 2 300 annual load hours. By increasing the energy storage to 30 s the availability is raised to 3 000 annual load hours without further production shedding. Most of the production shedding occurs in wave states above the design wave state. The analyzis is performed based on preliminary data for Wavehub, and must be repeated when the Wavehub study is complete. Utilization of the free export capacity for reactive power compensation showed good effect with great impact on harmonic distortion up to the 19. harmonic. Some improvement of peak load capacity can also be expected, but is very system specific and must be investigated for a specific configuration. For the systems modelled here, improvements in transfer capacity of 0.5% - 2.5% was demonstrated without energy production from the WEC.

References

[1] J. Sjolte, G. Tjensvoll, and M. Molinas, "All-Electric wave energy converter connected in array with common DC-Link for improved power quality," in *3rd International Symposium on Power Electronics for Distributed Generation Systems (PEDG'12)*, Aalborg, Denmark, Jun. 2012.

[2] ——, "Annual energy and power quality from an All-Electric wave energy converter array," in *European Power Electronics and Motion Control and Applications Conference (EPE-PEMC'12)*, Novi Sad, Serbia, Sep. 2012.

[3] J. Sjolte, I. Bjerke, A. Crozier, G. Tjensvoll, and M. Molinas, "All-electric wave energy power take off system with improved power quality at the grid connection point," in *2012 IEEE PES Transmission and Distribution Conference and Exposition*, 2012, In press.

[4] I.Bjerke, E.Hjetland, G.Tjensvoll, and J.Sjolte, "Experiences from field testing with the bolt wave energy converter," in *European Wave and Tidal Energy Conference (EWTEC11)*, 2011.

[5] "The wave power climate at the wave hub site," November 2006, journal: Applied Wave Research Review of Wave Power Climate.

[6] J. Sjolte, I. Bjerke, A. Crozier, G. Tjensvoll, and M. Molinas, "All-electric wave energy converter with stand-alone 600vdc power system and ultracapacitor bank," in *2012 EVER International Conference and Exhibition on Ecological Vehicles and Renewable Energies*, 2012, In press.

[7] H. Akagi, E. Watanabe, and M. Aredes, *Instantaneous power theory and applications to power conditioning*, ser. IEEE Press series on power engineering. Wiley, 2007. [Online]. Available: http://books.google.no/books?id=tyZTAAAAMAAJ

[8] S. Fryze, "Wirk-, blind- und scheinleistung in elektrischen stromkreisen mit nicht-sinusfrmigem verlauf von strom und spannung," in *ETZ-Arch. Electrotech.*, vol. 53, 1932, pp. 596–599, 625–627, 700–702.

Appendix G

Conference paper 7

Title: Summary of Performance After One Year of Operation with the Lifesaver Wave Energy Converter System

Conference/Journal: European Wave and Tidal Energy Conference (EWTEC)

Date: 2.-5. September 2013

Location/Publisher: Aalborg, Denmark

Summary of Performance After One Year of Operation with the Lifesaver Wave Energy Converter System

Jonas Sjolte*†, Ida Kathrine Bjerke*, Gaute Tjensvoll* and Marta Molinas†
*Fred. Olsen, Fred Olsens Gate 2, N-0152 Oslo, E-mail: firstname.lastname@fredolsen.no
†Norwegian University of Science and Technology, Department of Electric Power Engineering,
O. S. Bragstads plass 2E, N-7034 Trondheim, Norway E-mail: jonas.sjolte@ntnu.no / marta.molinas@ntnu.no

***Abstract*—Fred. Olsen has operated the Wave Energy Converter *Lifesaver* at the *FaB Test* wave energy test site since April 2012. After one year of operation, significant experience has been gained, and a large amount of test data has been acquired. This paper presents the key performance data gathered through this test period, and compares the actual production with the expected figures obtained through theoretical simulation. The practical aspect of operating a WEC is also discussed, and figures for availability, uptime and accessibility for maintenance is presented. In general, the actual results show good correlation with the simulation models. Through the test period, Lifesaver has performed very well without major incidents, and has demonstrated a moderate reliability acceptable for pre-commercial testing.**

I. Introduction

Lifesaver, pictured in Fig. 1, is a *Wave Energy Converter* (WEC) system developed by *Fred. Olsen* (FO). She is an electro-mechanical system for producing electricity from ocean waves for grid export. The system consists of a 16 m wide toroidal floater, three production machines and one electrical conversion package. She was installed at sea on 31. March 2012 for commissioning and sea trials, and has currently been in continuous service for one year. Lifesaver is currently not grid connected, and is equipped with a sophisticated stand-alone power system to emulate the grid connection functions to allow normal operation of the electrical machinery [1].

Lifesaver is operated at *FaB Test*, which is a UK test site for pre-commercial WEC concepts located in Falmouth bay outside Cornwall, England. The exact location of FaB Test is shown in Fig. 3. FaB Test is envisioned to be a preparation site for WECs planned for commercial operation at the Wavehub site [2], and has a moderate wave climate with good balance between production hours and availability for maintenance. Lifesaver is designed with focus on modularity, maintainability and reliability. All mechanical and electrical parts are placed above surface for easy access, and the modular and autonomous *Power Take-Off* (PTO) configuration allows for maintaining system operation and power export with one or more PTOs out of service. Fig. 2 shows an example of maintenance work at Lifesaver, where one of the PTOs were lifted off for on-shore repairs.

Fig. 1. *Lifesaver* on site outside Falmouth, England.

Fig. 2. Lifesaver during PTO lifting operation

A. The FO Wave Energy Project

FO started with Wave Energy in 2000, and in 2004 the Wave Energy Converter *Buldra*, built as a platform with multiple point absorbers [3], was launched. Since then, FO has tested out various concepts and built several different prototypes, all based on the point absorber principle. The series of experiences have led to the single body point absorber

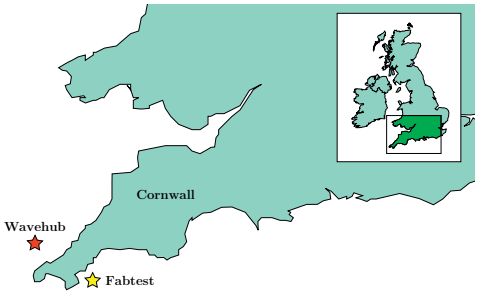

Fig. 3. Location of the UK test sites *Wavehub* and *FaB Test*

concept, as realized by our latest prototype *Lifesaver*. Point absorbers are not necessarily the most efficient type of WEC measured in terms of captured energy, but have shown to be successful on total performance and cost of energy.

Until now, FO has operated four WECs based on the single body point absorber in real sea conditions. The first, named *B33*, was a small proof-of-concept device that was operated outside Risør, Norway during the autumn of 2007 and the winter of 2008. B33 showed good results, leading to the second device, named *B22*, which was equipped with a full-scale control, communication and production system. B22 was operated outside Risør, Norway from the summer of 2008 until the spring of 2009. Based on these experiences, FO started the next development phase in collaboration with a selected few European companies and universities through the *SEEWEC* project. This work led to the full-scale system *Bolt*® that was installed outside Risør, Norway in June 2009. Bolt has, as on December 22, 2010, produced 3 360 kWh of energy (Bjerke et al.) [4].

Based on the success with Bolt®, FO decided to use the knowledge and experience gained so far to proceed to the next generation design. An agreement with several UK companies was made with funding from the UK *Technology Strategy Board* (TSB). The goal of the project was to improve the Bolt® concept towards a commercial level where it can be launched at Wavehub [2], and hence the project name *Bolt2Wavehub*. The project resulted in the Lifesaver system and is planned to stay in operation at FaB Test until October 2013.

Until now, FO has not had a single serious event with any of the WEC systems, which has allowed for continuous long term testing in real sea conditions. This has proved invaluable for building experience with wave energy converters. Based on our experience, the problems and issues that arise in real sea conditions are multifaceted and goes beyond the scope of the tests undertaken.

II. System description

Lifesaver is based on the point absorber principle, which has been extensively researched and is well described in literature (Falnes et al., 2003, 2012) [5], [6]. Several companies and academic institutions have explored point absorbers for energy production. The Swedish based company *Seabased*, that works in close collaboration with Uppsala University, has developed a point absorber system with high resemblance to the FO system, except for that the production machinery is placed at the sea floor [7]. US based *Ocean Power Technologies* has developed the *PowerBuoy*, which is a slack moored dual body point absorber [8]. Similar systems have been researched and tested by the Oregon State University program *SeaBeavl* [9], and has also been realized in systems as *IPS* and *Wavebob* [10]. Common for all these systems is that they endeavor to maximize the power absorption from the sea by tuning the system to resonate with the waves. FO pursued this control principle on our first devices, but has later dropped this approach as it was found to costly to implement on the FO systems.

FO has designed the Lifesaver floater structure towards high surface area and low mass to obtain a cost efficient system with respect to absorbed power. This geometry results in a high resonance frequency and thus leads to a *Response Amplitude Operator* (RAO) (Falnes, 2002) [11] close to unity for most of the relevant wave states. The system is therefore quite stiff and well suited for power production by passive damping control. The absorber is tightly moored to the sea floor with a PTO system that produces power from heaving, pitching and rolling motion. The point absorber system is independent of wave direction, which may simplify the mooring system and makes the system robust against mixed directional waves. Table I lists the general system properties of Lifesaver.

TABLE I
LIFESAVER KEY PARAMETERS

Floater outer diameter	16	m
Floater inner diameter	10	m
Floater height	1.0	m
Mass	55	tons
Water depth	55	m
Number of PTO slots	5	
Currently installed number of PTOs	3	
Damping force per PTO	100	kN
WEC rated export power	70	kW
Total installed generator capacity	400	kW

The PTOs are realized as winch and rope systems, as illustrated in Fig. 4. The generator can only produce power during upwards motion, and has to operate in motoring mode during downwards motion to maintain rope tension. The control principle utilized on Lifesaver is based on passive damping, but is heavily influenced by saturation on both torque and power, as indicated by the maximum net power curve in Fig. 6. The control principle is described in more detail in our previous publications [1], [12]. The generator used on Lifesaver is a high performance permanent magnet machine manufactured by Siemens® and is designed for industrial servo applications. It has high torque output and low inertia, and is suitable for direct-drive applications with low gear ratio or entirely without gearbox. The machine also has high efficiency, as demonstrated by the efficiency map plotted

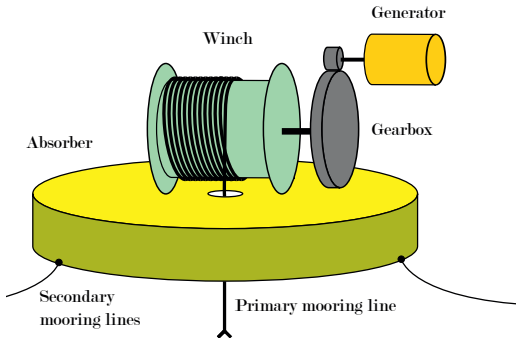

Fig. 4. Principal sketch of the WEC, showing one PTO. Lifesaver is designed for five individual PTOs, but is currently installed with three individual PTOs.

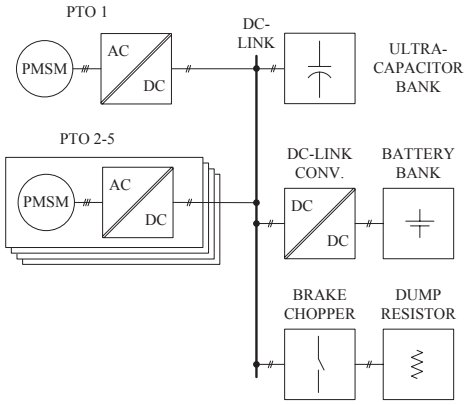

Fig. 5. Electrical system configuration on Lifesaver

in Fig. 6. The generator is powered through a full bridge converter, which gives full control of the generator torque with high precision and quick response. In total, this gives a very powerful package with high performance that is well suited for the reciprocal wave motions. The electrical configuration of the WEC and the PTOs can be seen in Fig. 5, which is quite similar to other WEC concepts (Boström, 2011) [13] and (Rahm, 2010) [14], but is somewhat more advanced since the FO system also includes the full-bridge converter on the generator side.

WECs are different from most other power plants in that the prime mover operates with a sinusoidal-based velocity pattern. However, due to the irregularities caused by the random nature of ocean waves, and their varying frequency components, the peak to average power ratio will typically be around ten for a converter system like Lifesaver [15]. This is mainly due to the wave to wave variations that results in groups of waves referred to as *wave trains* [16]. This behavior results in high peak to average power ratios and poor power quality. FO has researched extensively on this issue and found that the power quality can be enhanced to an exportable level by clever system design without adding significant costs. This work has been published in a series of articles [12], [17]–[20].

III. Simulation Model

The simulation model used for Lifesaver is based on the work done at NTNU for the Buldra® platform (Molinas et al., 2007, Skjervheim et al., 2008) [21], [22]. The model solves Equation (1) for $\zeta(t)$ in the time domain, where the index i denotes the mode of motion, given by the six *degrees of freedom* (DOF), for the floater. The excitation force matrix $F_{e,i}$ contains the time dependent forces due to incident waves, and M denotes the mass of the system.

$$F_{e,i}(t) - F_{D,i}(t) = M\frac{d^2\zeta(t)}{dt^2} \quad (1)$$

$$F_{D,i}(t) = F_{r,i}(t) + F_{d,i}(t) + C_i \cdot \zeta_i(t) + F_{PTO}(t) \quad (2)$$

$F_{D,i}$ accounts for the sum of all the damping forces in Equation (2), where $F_{r,i}$ accounts for the time dependent forces on the floater due to radiation of waves. The term $F_{d,i}$ accounts for non-linear damping terms, mainly the drag forces. ζ_i is the time dependent motion of the floater, C_i is the restoring force matrix accounting for the hydrostatic pressure acting on the floater, and F_{PTO} is the time dependent force applied from the PTO. The PTO is modeled as a rope and winch system that is tightly moored to the sea floor. Detailed performance curves for Lifesaver is presented in our article [23].

Since the simulation is based on a detailed 6DOF model of Lifesaver, FO keeps the simulation model confidential. However, the high level of complexity is not essential to verify the basic principles presented in this work. It is possible for a third party to qualitatively verify the published results without detailed knowledge of the Lifesaver simulation model. Depending on the simulation at hand the model may be simplified by locking out some degrees of freedom, or by using simplified functions for parts of the system. For the power simulations presented here, the model was run in 3DOF mode with only *heave*, *surge* and *pitch motion*.

To simulate a wave state, a 20-minute time series of irregular waves is generated based on the JONSWAP wave spectrum [24]. The wave state is defined by the significant wave height H_s, the zero crossing period T_z and the wave direction θ. The subsequent excitation forces are then calculated and the simulation is performed for the full length of the time series. The simulation model also takes into account PTO and generator losses, and the model outputs a 20-minute time series of exported electrical power from the WEC. The simulation model has undergone many years of development and testing, and is verified against real production data from several prototypes, including Bolt and Lifesaver.

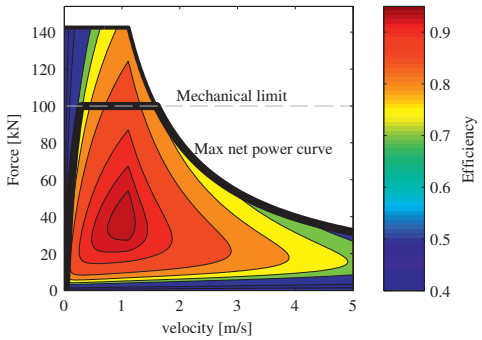

Fig. 6. Efficiency map for the generator used on Lifesaver

The simulation model also estimates the conversion efficiency so that accurate figures for exportable electrical power can be calculated. Most of the energy conversion loss occurs in the generator, and in the design wave state, the generator operates with an efficiency of around 80 %. This is the result of economical optimization of the system, and the relatively low system efficiency is the result of the large speed fluctuations enocountered at the generator shaft. The details of this optimization are explained in our publications [1], [12], [23]. A detailed efficiency map for the generator was produced by Siemens and is the basis for the efficiency plot presented in Fig. 6. This allows for calculating the generator power loss to a high level of precision. The mechanical efficiency of the winch and gearbox is estimated based on actual tests during PTO commissioning, where two PTOs were connected in a back-to-back configuration.

IV. Results

Over the past year a large amount of operational data has been acquired. All signals and measurements are logged continuously at 200 Hz while in operation, and gives a comprehensive database for analysis. Together with the advanced simulation model, this helps build a detailed understanding of the system, and complements the theoretical model of the system. The theoretical production from Lifesaver is listed in Table II and shows the simulated exportable power for all relevant wave states. This simulation is performed with the current control parameter setting at Lifesaver, which is somewhat conservative. Thus, the presented figures in Table II are about 30 % lower than the theoretical production potential with optimal control parameters.

Wavehub has been used as the design base for sizing the power system on Lifesaver. The wave state that produces most energy annually at Wavehub is H_s = 2.75 m / T_z = 6.5 s, and is chosen as the design wave state for Lifesaver. The estimated production potential in this wave state is 70 kW on average, and this figure is selected as the name plate rating for Lifesaver. Defining rated power from a WEC is not straight forward as there usually is no clear and practical limit to how much power the WEC can produce. This is illustrated by the Lifesaver production scatter in Table II, which shows that the output is increasing with wave height, even though the power system is optimized for the design wave state. The method for defining rated power proposed by FO is site dependent and will vary with with the site case. However, it gives a good impression of the practical power that can be expected from the device, and that can be comparable to other renewable energy sources.

A. Measured power production

The actual measured power production from Lifesaver for the entire test period is plotted against the wave state in Fig. 7. The wave measurements are taken from a wave measurement buoy situated 1 km from the location of Lifesaver. Qualitatively, the measured response shows good correlation to the simulated results, and shows performance equal to similar tests performed by others [25]. However, when comparing directly to the simulated results presented in Table II, it can be seen that the measured power production is somewhat lower, and also that there is a large spread in output power for the the same wave state. There are several reasons for these power differences, some are related to the selected control parameters and some are related to the system:

- **Number of PTOs**
  The simulations are performed on a system consisting of

TABLE II
Simulated exportable power [kW] from Lifesaver with five PTOs and current control settings

Wave height (hs) - [m] \ Wave period (Tz) - [s]	2	3	3.5	4	4.5	5	5.5	6	6.5	7	7.5	8	9	10	11	12	14	16	18	20	22
0.25																					
0.5	0.3	0.8	1.2	1.4	1.5	1.6	1.6	1.4	1.3	1.1	1.0	0.9	0.7	0.6	0.4	0.4	0.1	0.0			
0.75		2.7	3.6	4.0	4.2	4.5	4.4	4.0	3.8	3.3	3.1	2.9	2.4	2.1	1.7	1.5	0.9	0.7	0.5	0.3	0.2
1		5.3	6.9	7.6	8.0	8.5	8.3	7.7	7.3	6.5	6.1	5.7	4.8	4.2	3.3	2.9	2.1	1.7	1.3	1.0	0.8
1.25		8.9	11.4	12.4	12.9	13.6	13.5	12.4	11.8	10.5	9.9	9.2	7.8	6.4	5.4	4.4	3.6	3.0	2.4	1.9	1.6
1.5			16.9	18.1	18.8	19.7	19.7	18.0	17.1	15.4	14.4	13.3	11.0	9.1	7.7	6.5	5.7	4.6	3.7	3.0	2.6
2			30.9	31.8	32.7	34.0	33.2	31.3	29.5	26.6	24.7	22.9	19.5	15.8	13.8	12.3	10.7	8.9	7.2	5.9	5.1
2.5				47.9	48.3	49.5	48.5	45.6	42.9	38.7	36.4	33.5	28.3	23.5	21.0	20.3	17.3	13.9	11.8	9.6	8.4
3					63.9	65.3	63.0	59.9	56.5	51.1	48.2	44.8	37.3	33.6	30.2	28.6	23.6	19.7	16.6	13.7	12.3
3.5						80.0	76.8	72.8	69.1	62.7	59.6	56.1	48.3	45.1	41.4	37.7	30.7	25.9	21.7	18.3	16.4
4						92.9	89.2	84.4	80.3	73.7	70.2	66.3	58.9	54.9	49.6	46.3	37.7	31.6	26.8	22.8	21.0
5							109	104	98.9	92.9	88.5	84.8	78.3	72.7	67.1	61.6	51.1	43.3	37.5	32.3	29.4
6									113	107	103	99.4	93.5	86.7	81.4	75.6	63.7	54.4	47.6	41.9	38.5
7									123	119	115	111	105	98.2	93.2	86.5	74.7	64.9	57.5	51.0	47.4
8										127	124	119	114	107	103	96.3	83.7	74.7	66.9	60.2	56.1
9											129	126	121	114	110	103	91.5	83.1	75.0	69.1	65.1
10												130	125	120	116	109	98.1	90.0	82.3	76.5	73.0

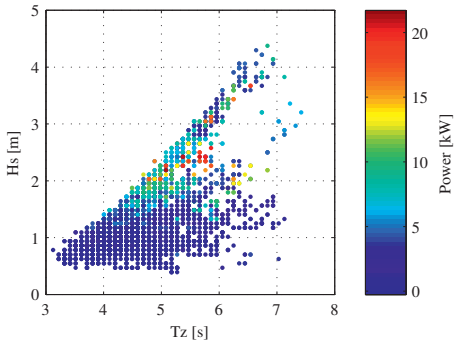

Fig. 7. Exportable electrical power for various sea states measured through one year on FaB Test

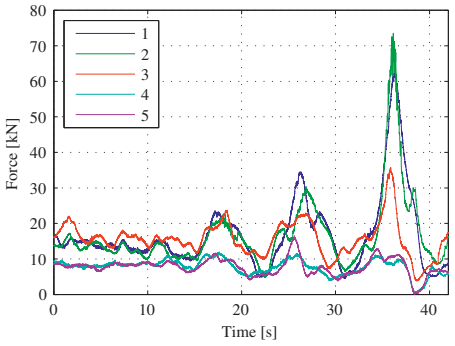

Fig. 9. Forces encountered in secondary moorings during normal production in a high sea state. The mooring lines are evenly distributed along the floater circumference in counter-clockwise order.

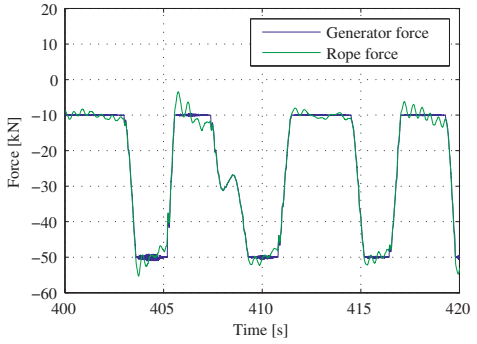

Fig. 8. Oscillations encountered in primary moorings due to system dynamics

five PTOs, while Lifesaver currently only has three PTOs installed.

- **Sub-optimal control parameters**
  After installation, much time was spent on verifying system operation through stepwise parameter changes. This has caused a large amount of production data with sub-optimal parameter settings, and is the cause of many of the poor production series close to the design wave state.
- **Unwanted system behavior**
  In higher production states, the winch and floater system occasionally showed rapid vibrations in the primary mooring force, as plotted in Fig. 8. This is believed to be caused by the dynamic response of the primary mooring, which results in an unforeseen aggregate system response. Similar behavior has been described in related systems (Vicente et al, 2013) [26], and pose a challenge to tight moored WEC systems. On Lifesaver, the oscillations are mainly excited as the generator shifts from damping control to saturation control, and can be reduced by smoothing this shift. Initial results indicate that the primary moorings have strong non-linear components, this will be verified by practical tests of the moorings during the Autumn 2013. Until the issue with oscillations is managed, conservative control parameters are set for the high wave states. This is the cause for the low production in the high wave states.
- **Secondary mooring system**
  Due to the strict regulations on FaB Test, Lifesaver is equipped with a strong five-point catenary mooring system, in addition to the regular production moorings. This is undesired from an energy point of view and is expected to cause some reduction in production. An example of the mooring forces experienced in the secondary mooring lines is plotted in Fig. 9. The effects of the moorings are currently not taken into consideration in the simulation model. To get a better understanding this should be included in the model, and could for instance be implemented as described by (Fitzgerald and Bergdahl, 2008) [27].
- **Floater height**
  The floater was intentionally designed shallow to reduce the system cost and the horizontal forces, and to gain experience with required height and draft in an optimized system. Data from on-board draft sensors show that the waves are frequently over-topping the device already in the design wave state. Some power production is believed to be lost to this due to reduced buoyancy and stability. In the simulation model, the buoy is modeled with infinite height. The effect of over-topping is difficult to model and the impact of this on production output is unknown.

To investigate further on these effects, the simulation model was adjusted to match the number of PTOs and the control parameters used in the measured production series. Fig. 10 shows the difference between simulated produced power and actual produced power for all production series. The figure shows a good correlation between measured production and simulated

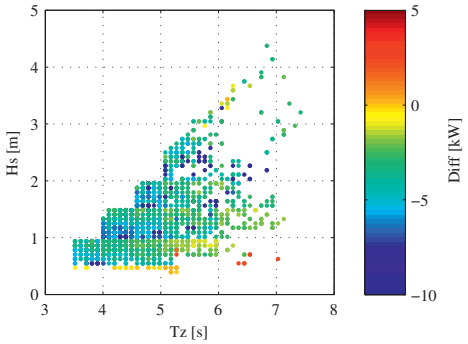

Fig. 10. Difference between actual produced power and simulated produced power for various sea states. Simulations are performed with actual parameters and configuration used at FaB Test.

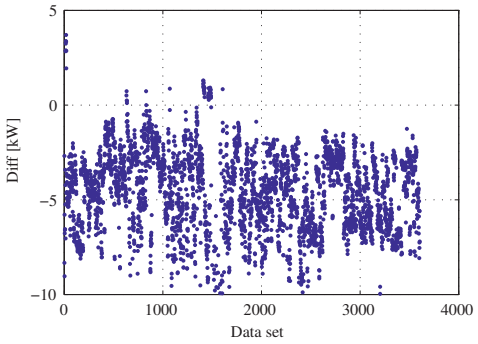

Fig. 11. Difference between actual produced power and simulated produced power for all logged data sets. Each data set lasts for 20 min. Simulations are performed with actual parameters and configuration used at FaB Test.

production, but with a clear tendency of the measured production being lower than the simulated production. This is most likely caused by the combination of the secondary mooring damping and the unwanted over-topping of the device.

Upon close study of Fig. 10, several properties points out. The steps observed to the left in the plot are caused by wave states that where not simulated, and that has been taken out. The horizontal lines are caused by merging the observed wave states into the simulated windows of wave height and period, and there is an obvious trend of improved production towards the top of the wave height window. There is also a trend towards lower power deficit at higher periods, but the cause of this is currently not identified. Some groups of data points show large deviations from the general trend, mainly the lower row of orange to red dots and the band of dark blue dots between 2 and 3 m H_s. The former is believed to caused by a measurement error in the wave rider buoy where long swells with high period and low amplitude is sometimes missed in mixed wave patterns. The latter group is probably caused by manual startup and shutdown, which will lead to a low average power for the measurement series. In an attempt to investigate further on the deviation between simulated and measured production, Fig. 11 was produced, and shows all production series up to date in chronological order. The figure could reveal time dependent effects on the measured production, but the figure does not give any clear trend towards this.

The generator system at Lifesaver estimates the actual torque on the generator shaft with high precision, and also measures the exported electrical power. This allows for accurate measurement of the generator efficiency and can be used to verify the figures obtained through simulations. The actual conversion efficiency is calculated and presented in Fig. 12, and includes the measured generator and inverter loss, in addition to the estimated mechanical loss. The figure shows that there is a strong dependency between system efficiency and wave height, which is supported by the theoretical work,

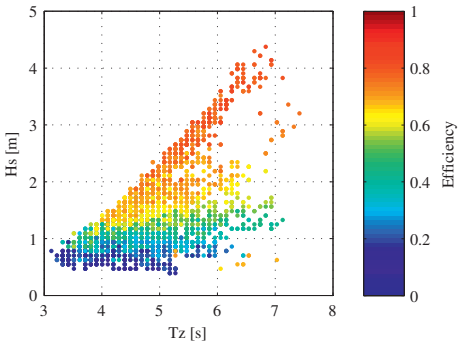

Fig. 12. Conversion efficiency: Ratio between actual exported electrical power and actual absorbed mechanical energy for various sea states experienced at FaB Test.

and is mainly linked to the generator speed. As the damping force follows the thick black line drawn in Fig. 6, it can be seen that the speed has to go beyond the 0.3 m/s threshold to enter force saturation before the efficiency starts to move towards a reasonable level.

As Lifesaver is currently not grid connected, the system has to produce net positive power to remain in operation. When the net production drops below zero, the system automatically shuts down and enters a power save mode with minimum power consumption. Shutdown typically occurs between 0.5 m and 0.6 m H_s, but has been measured as low as 0.4 m H_s for higher periods. This ability to maintain net power production at such low levels is unique for Lifesaver when compared to our earlier devices, and is made possible by the electro-mechanical PTO configuration, as opposed to the earlier systems that relied on hydraulics, either directly or indirectly. This allows for high uptime, and may result in continuous production on high energy sites. High uptime results in more load hours and is

good for the energy balance as the WEC will always consume some power for monitoring purposes.

B. System operation and availability

Lifesaver has been in operation for more than one year as this paper is being written, and has given significant experience on how to operate and maintain a WEC system over time. The key performance indicators up to date are listed in Table III and shows that the system has been available for production for the majority of the deployment time. A graphical presentation of the KPI is plotted in Fig. 13 and gives an impression of the time line of accessibility of the device, and the WEC production state. As experience with the system was gained, it was discovered that Lifesaver could maintain net positive power production down to H_s = 0.5 m, and subsequently the wave height threshold for production startup was lowered in September 2012. This contributed to a significant share of the increased production availability seen in Fig. 13 after this date, together with rougher weather as the autumn season set in. The accumulated energy production for the test period is plotted in Fig. 14.

TABLE III
KEY PERFORMANCE INDICATORS

Production hours	1 468	h
Electrical energy produced	4 644	kWh
Mechanical energy absorbed	7 192	kWh
Overall efficiency	64.6	%
Average power during production	3.2	kW
Time on site	376	days
One or more PTOs ready for production	234	days
All PTOs ready for production	23	days
Longest continuous production period	24	days
Time available for maintenance	211	days
Availability hull	100	%
Availability communication	98	%
Availability scientific instrumentation	79	%
Availability control dependent instrumentation	100	%
Availability storm moorings	100	%
Availability cooling system	99	%

It is important to note that the goal of the Bolt2Wavehub project is not to maximize power output, but to gain experience with all the operational aspects of operating a wave energy power plant. The FaB Test site was selected for its high availability for maintenance and moderate wave climate. This allows for close monitoring of the device, which is crucial for providing practical feedback into the design process, and to understand the operational expenditures (OpEx) of operating the device. Moreover, the device has been used as a test bench for testing out different maintenance methods. For instance, when some mechanical components had to be replaced in all the PTOs early in the test period, two different maintenance approaches were tested out. The first PTO was lifted off and brought ashore for maintenance, as shown in Fig. 2, while the second PTO was serviced on site. It became clear that heavy-lift operations between two moving objects demanded much calmer weather than on-board maintenance, and the latter method has been adopted as the preferred approach. Except for the heavy-lift trial, all maintenance during the test period has been performed on site.

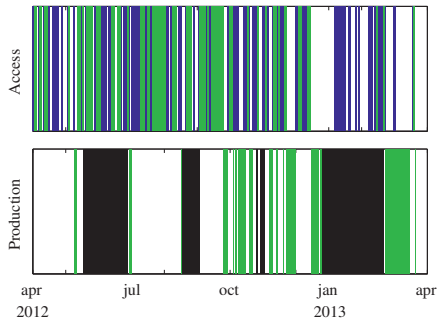

Fig. 13. **Upper plot:** Lifesaver accessibility (Green = accessible for heavy lift, Blue = accessible for maintenance). **Lower plot:** Lifesaver production state (Green = production, White = ready for production, Black = Planned or unexpected downtime).

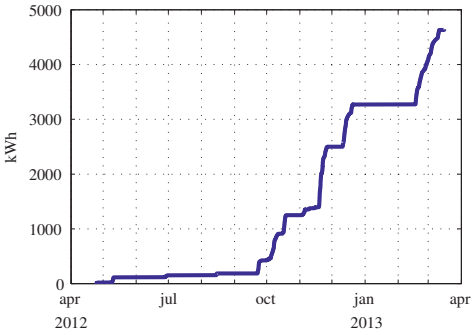

Fig. 14. Accumulated electrical energy produced at Lifesaver

The most critical component on Lifesaver for reliable power production is the production mooring, usually referred to as *primary mooring*, due to the high wear on the winch. FO has put serious effort on investigating alternative line types and winch mechanisms. Most of the downtime on Lifesaver is related to the primary moorings, either due to planned maintenance for switching winch components, or due to unexpected failures in the primary mooring. In case of a failure, the other PTOs will still be operating as before, due to the independence of the individual PTOs. The winch concept currently pursued is a high performance system with high potential lifetime, but is more fragile to abnormal loads and wear mechanisms, which has caused problems in the early stages of testing. The issues with the primary moorings are not yet solved, but significant steps have been taken towards a reliable system in close collaboration with with the manufacturer, and we have reason to believe that the reliability will be improved to a level suitable for commercial operation within the remainder of the Bolt2Wavehub project. However, an increased level of

maintenance and monitoring must be expected for a prolonged period, also in commercial operation, and makes high energy sites like Wavehub less attractive in the near future due to the difficult maintenance regime.

V. Conclusion

Lifesaver has showed good performance at FaB Test with no major incidents or problems, and has demonstrated acceptable power production and reliability. The FaB Test test site has a moderate wave climate with good availability for maintenance, and has proved to be a valuable test site for gaining operational experience and testing out various maintenance methods. The practical work has shown a clear advantage towards on-board maintenance, as opposed to bringing heavy equipment ashore. The main failure mode causing downtime on Lifesaver is failing primary moorings. This is a well known challenge with this kind of device, and FO is pursuing several paths towards solving this issue. Although the primary moorings are not yet performing flawlessly, significant steps have been taken in the right direction, and there is reason to believe that the problem will be solved within the remainder for the test period. Thus, Lifesaver should soon be ready to operate on a commercial level, although elevated monitoring and maintenance must be expected for still some time. Operation on high energy sites is therefore less likely in the near future.

Acknowledgment

We would like to thank Fred. Olsen for funding and supporting the Wave Energy Project. We would also like to thank the Norwegian Research Council for funding the industrial PhD program for Jonas Sjolte, which made it possible to publish this work.

References

[1] J. Sjolte, I. Bjerke, A. Crozier, G. Tjensvoll, and M. Molinas, "All-electric wave energy converter with stand-alone 600vdc power system and ultracapacitor bank," in *2012 EVER International Conference and Exhibition on Ecological Vehicles and Renewable Energies*, march 2012.

[2] "The wave power climate at the wave hub site," Nov 2006, journal: Applied Wave Research Review of Wave Power Climate.

[3] R. Taghipour and T. Moan, "Efficient frequency-domain analysis of dynamic response for the multi-body wave energy converter in multi-directional waves," in *Proceedings of the Eighteenth International Offshore and Polar Engineering Conference*, 2008.

[4] I.Bjerke, E.Hjetland, G.Tjensvoll, and J.Sjolte, "Experiences from field testing with the bolt wave energy converter," in *Submitted to the European Wave and Tidal Energy Conference (EWTEC11)*, september 2011.

[5] J.Falnes and P.M.Lillebrekken, "Budal's latching-controlled-buoy type wave-power plant," in *5th European Wave Energy Conference*, 2003.

[6] J. Falnes and J. Hals, "Heaving buoys, point absorbers and arrays," *Philosophical Transactions of the Royal Society A: Mathematical, Physical and Engineering Sciences*, vol. 370, no. 1959, pp. 246–277, 2012. [Online]. Available: http://rsta.royalsocietypublishing.org/content/370/1959/246.abstract

[7] J. Engström, "Hydrodynamic modelling for a point absorbing wave energy converter," Ph.D. dissertation, Uppsala University, Electricity, 2011.

[8] "Ocean power technologies," http://www.oceanpowertechnologies.com/.

[9] D. Elwood, S. C. Yim, J. Prudell, C. Stillinger, A. von Jouanne, T. Brekken, A. Brown, and R. Paasch, "Design, construction, and ocean testing of a taut-moored dual-body wave energy converter with a linear generator power take-off," *Renewable Energy*, vol. 35, no. 2, pp. 348 – 354, 2010. [Online]. Available: http://www.sciencedirect.com/science/article/pii/S0960148109002237

[10] A. F. Falco, J. J. Cndido, P. A. Justino, and J. C. Henriques, "Hydrodynamics of the {IPS} buoy wave energy converter including the effect of non-uniform acceleration tube cross section," *Renewable Energy*, vol. 41, no. 0, pp. 105 – 114, 2012. [Online]. Available: http://www.sciencedirect.com/science/article/pii/S0960148111005702

[11] J. Falnes, *Ocean Waves and Oscillating Systems: Linear Interactions Including Wave-Energy Extraction*. Cambridge University Press, 2002.

[12] J. Sjolte, I. Bjerke, A. Crozier, G. Tjensvoll, and M. Molinas, "All-electric wave energy power take off system with improved power quality at the grid connection point," in *Transmission and Distribution Conference and Exposition (T D), 2012 IEEE PES*, may 2012, pp. 1 –7.

[13] C. Boström, "Electrical systems for wave energy conversion," Ph.D. dissertation, Uppsala University, Electricity, 2011, felaktigt tryckt som Digital Comprehensive Summaries of Uppsala Dissertations from the Faculty of Science and Technology 727.

[14] M. Rahm, "Ocean wave energy : Underwater substation system for wave energy converters," Ph.D. dissertation, Uppsala University, Electricity, 2010.

[15] E. Tedeschi and M. Molinas, "Tunable control strategy for wave energy converters with limited power takeoff rating," *IEEE Transactions on Industrial Electronics*, vol. 59, no. 10, pp. 3838–3846, 2012. [Online]. Available: http://www.scopus.com/inward/record.url?eid=2-s2.0-84860439180\&partnerID=40\&md5=6c9b62f38538f73809c8838d19b8663a

[16] S. H. Salter, "World progress in wave energy 1988," *International Journal of Ambient Energy*, vol. 10, no. 1, pp. 3–24, 1989. [Online]. Available: http://www.tandfonline.com/doi/abs/10.1080/01430750.1989.9675119

[17] J. Sjolte, G. Tjensvoll, and M. Molinas, "All-electric wave energy converter connected in array with common dc-link for improved power quality," in *Power Electronics for Distributed Generation Systems (PEDG), 2012 3rd IEEE International Symposium on*, june 2012, pp. 431 –436.

[18] ——, "Annual energy and power quality from an All-Electric wave energy converter array," in *European Power Electronics and Motion Control and Applications Conference (EPE-PEMC'12)*, Novi Sad, Serbia, Sep 2012.

[19] ——, "All-electric wave energy converter array with energy storage and reactive power compensation for improved power quality," in *Energy Conversion Congress and Exposition (ECCE), 2012 IEEE*, sept. 2012, pp. 954 –961.

[20] E. Tedeschi, J. Sjolte, M. Molinas, and M. Santos, "Stochastic rating of storage systems in isolated networks with increasing wave energy penetration," *Energies*, vol. 6, no. 5, pp. 2481–2500, 2013. [Online]. Available: http://www.mdpi.com/1996-1073/6/5/2481

[21] M.Molinas, O.Skjervheim, P.Andreasen, T.Undeland, J.Hals, T.Moan, and B.Sorby, "Power electroncis as grid interface for actively controlled wave energy converters," International Conf. on Clean Energy Power (ICCEP07), Tech. Rep., 2007.

[22] O.Skjervheim, B.Sorby, and M.Molinas, "All electric power take off for a direct coupled point absorber," Proceedings of the 2nd International Converence on Ocean Energy (ICOE2008), Tech. Rep., 2008.

[23] J.Sjolte, I.Bjerke, E.Hjetland, and G.Tjensvoll, "All-electric wave energy power take off generator optimized by high overspeed," in *Submitted to the European Wave and Tidal Energy Conference (EWTEC11)*, september 2011.

[24] "Joint north sea wave observation project (jonswap)@ONLINE," http://www.wikiwaves.org/Ocean-Wave_Spectra.

[25] R. Waters, M. Rahm, M. Eriksson, O. Svensson, E. Strmstedt, C. Bostrm, J. Sundberg, and M. Leijon, "Ocean wave energy absorption in response to wave period and amplitude - offshore experiments on a wave energy converter," *IET Renewable Power Generation*, vol. 5, no. 6, pp. 465–469, 2011. [Online]. Available: www.scopus.com

[26] P. C. Vicente, A. F. Falco, and P. A. Justino, "Nonlinear dynamics of a tightly moored point-absorber wave energy converter," *Ocean Engineering*, vol. 59, no. 0, pp. 20 – 36, 2013. [Online]. Available: http://www.sciencedirect.com/science/article/pii/S0029801812004179

[27] J. Fitzgerald and L. Bergdahl, "Including moorings in the assessment of a generic offshore wave energy converter: A frequency domain approach," *Marine Structures*, vol. 21, no. 1, pp. 23 – 46, 2008. [Online]. Available: http://www.sciencedirect.com/science/article/pii/S0951833907000500

Appendix H

Conference paper 8

Title: Reliability Analysis of IGBT Inverter for Wave Energy Converter with Focus on Thermal Cycling

Conference/Journal: Electric Vehicles and Renewable Energy conference (IEEE/EVER)

Date: 25.-28. March 2014

Location/Publisher: Monte Carlo, Monaco

Reliability Analysis of IGBT Inverter for Wave Energy Converter with Focus on Thermal Cycling

Jonas Sjolte
Fred. Olsen / Norwegian University of Science and Technology
Email: jonas.sjolte@ntnu.no

Gaute Tjensvoll
Fred. Olsen
Oslo, Norway
Email: gaute.tjensvoll@fredolsen.no

Marta Molinas
Norwegian University of Science and Technology
Trondheim, Norway
Email: marta.molinas@ntnu.no

***Abstract*—Power electronics and advanced motion control has allowed for creating *Wave Energy Converters* (WECs) with the generator directly coupled to the sinusoidal motions of the prime mover. However, this gives large fluctuations in output power, and the resulting peak to average power ratio exceeds most other energy producers. The typical cycle time of ocean waves is 5-7 seconds with subharmonic wave train fluctuations of 30-200 sec. These slow power fluctuations may cause significant thermal cycling of the IGBT powered inverter, with reduction in lifetime as result. In this work the Fred Olsen WEC system is used as a staring point, and a detailed thermal model for the inverter is implemented and simulated. Based on the study of earlier publications on IGBT reliability the resulting lifetime of the system is estimated. This study indicate that thermal cycling may impact on the system lifetime and that some oversizing is required.**

I. Introduction

Wave Energy Converters (WECs) are different from most other energy producers in that the prime mover operates with a reciprocating velocity. With modern power electronic based variable speed drives the producer can be connected directly to the generator, however this leads to a constantly fluctuating output power that touches zero in every incoming ocean wave. This behavior can be seen in Fig. 2, which shows the actual power output from Fred Olsen's (FO) WEC Bolt shown in Fig. 1. The heavily distorted output power poses a great challenge for the conversion system to grid. This has been addressed and explored in several earlier publications by FO [1], [2]. Another important effect of the fluctuating power is the reduction in power component lifetime. One of the crucial parameters for lifetime estimation for IGBTs is the thermal environment and the number of thermal cycles the device undergo. This paper will investigate how the IGBT based inverter system specified for the FO concept is affected and what lifetime can be expected.

A. Fred. Olsen Wave Energy Project

FO started with Wave Energy in 2000, leading to the first Wave Energy Converter prototype *Buldra*®, built as multiple point absorber platform and launched in 2004. Since then FO has tested out various concepts and built several different prototypes, all based on the point absorber principle. The series of experiences have led to the single body point absorber system Bolt® as pictured on site in Fig. 1. Even though the point absorber principle may not be the most efficient absorber type, it has shown to be successful in terms of total performance and cost of energy [3]. Bolt® has been in operation outside Risør in Norway since June 2009 and has till date performed very well with only minor issues and incidents. As on December 22, 2010 she had produced 3 360 kWh [4].

Based on the success with Bolt®, FO has decided to use the knowledge and experience gained so far to proceed with the next generation design. An agreement with several UK

Fig. 1. FO's Wave Energy Converter Bolt® located outside Risør, Norway, was launched in June 2009, and is still in operation.

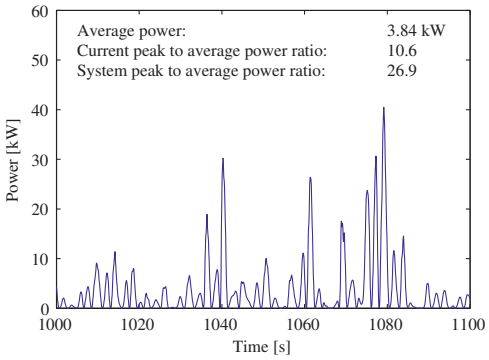

Fig. 2. Typical power output from Bolt® in low waves

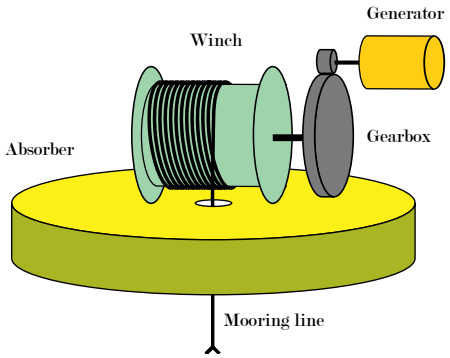

Fig. 3. PTO principal sketch for Bolt2

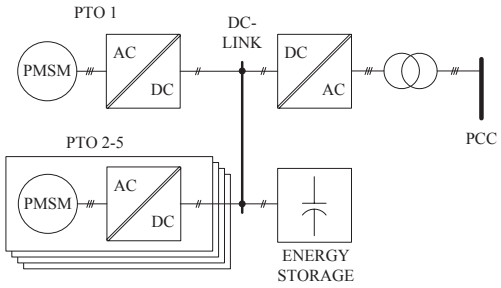

Fig. 4. WEC electrical system schematics

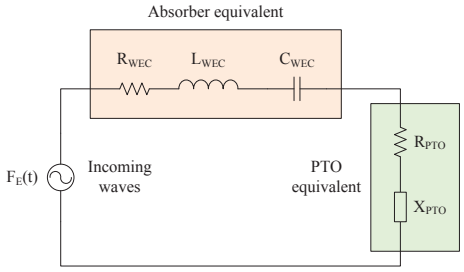

Fig. 5. RLC equivalent circuit of the PTO and WEC system

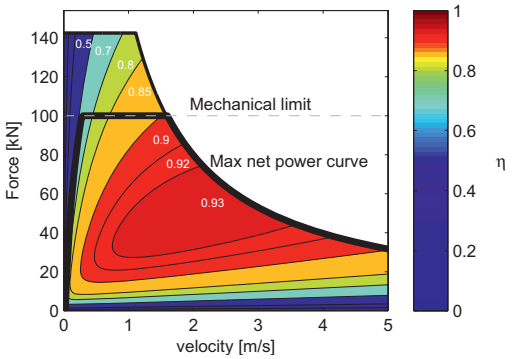

Fig. 6. Efficiency plot for the generator used at Bolt2Wavehub. The thick line shows the torque that result in maximum exported power from the generator. The thin line shows maximum available torque from the generator. The dashed line shows the mechanical limit for the gearbox.

companies was made with funding from the UK *Technology Strategy Board* (TSB). The goal of the project is to improve the Bolt® concept to a commercial level where it can be launched at Wavehub [5], and hence the project name *Bolt2Wavehub*. The project is currently in progress with the new Bolt2 prototype already launched early in April 2012.

II. System description

The *Power Take Off* (PTO) units are tightly moored to the sea floor by a winch and drum system, which directly ties surface movements to the generator through a custom designed transmission system. The wave to wire coupling is illustrated in Fig. 3. Since the winch system requires active power for pull-back during downward movement the generator is ran in motoring mode with a low pull-back torque for this part of the wave cycle.

The power system for the WEC is shown in Fig. 4. Several PTO units are connected together on a common DC-Link. This is made possible by the 3-phase AC/DC inverters that control each generator of the *Permanent Magnet Synchronous Machine* (PMSM) type. Full converter configuration is required for continuous generator operation in the heavily varying speed specter induced by the waves. The generator is controlled as a linear damper with torque saturation on upwards WEC movement, and with constant wind-in torque on downwards movement.

The common DC-Link coupling allows the produced power to be balanced out between the PTOs without additional transmission or conversion equipment. The grid side inverter harvests the produced power from the DC-Link, and the power is further transformed and transferred to the *point of common coupling* (PCC).

The absorbed power from a point absorber is greatly influenced by the control strategy applied by the PTO. In general the optimal energy extraction is achieved when the point absorber is moving with a 90° phase shift to the waves [6]. Several methods of approaching this production mode are described, the best known being *reactive control* [7], [8] and *latching control* [9]. Figure 5 shows an electrical equivalent circuit for the WEC where the dynamic behavior of the WEC is modeled as an RLC circuit. The PTO is modeled as a power extraction element (resistance) in series with a reactive element. The goal of reactive control is to tune the reactive element of the PTO so that it compensates for the reactive elements of the WEC as a whole and thus maximize power

extraction.

With the current design of Bolt2 the PTO force is too low to have significant impact by reactive control. This is mainly caused by the large area of the absorber that leads to a high spring constant and a high resonance frequency. Passive damping is therefore selected as the primary production model. In the lowest sea states however, advanced control algorithms may improve output [10], but is not implemented yet. The large and flat absorber shape is selected because of economical optimization and FO's acquired viewpoint that the absorber should be large enough to push the PTO into saturation already in moderate wave states.

$$\tau = -B \cdot \omega \tag{1}$$

Passive damping is defined by Equation (1). The damping coefficient B is optimized to produce the highest possible net power output. τ is the generator torque and ω is the generator speed. Fig. 6 shows the torque and speed characteristics for the generator used on Bolt2. The thick line shows the optimal torque that maximizes the generated electrical power. Two important saturation mechanisms are present; the first is the mechanical force limit of the gearbox. This is reached already at 0.27 m/s. The second is the power limit of the generator that is reached at 1.55 m/s. The linear region from 0 - 0.27 m/s corresponds to a damping coefficient of ca 350 kNs/m, which is the chosen value for B on Bolt2. This control method results in the operation characteristic plotted in Fig. 7 and the typical output time series as shown in Fig. 8. The system is described in more detail in earlier publications [2], [4], [11]–[13].

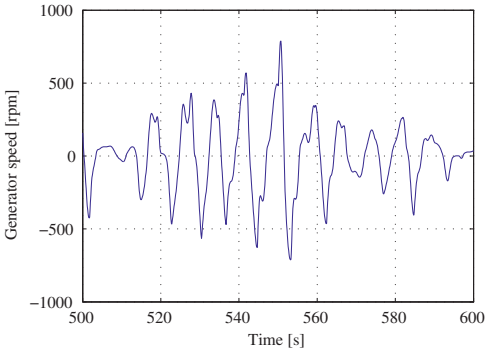

(a) Speed

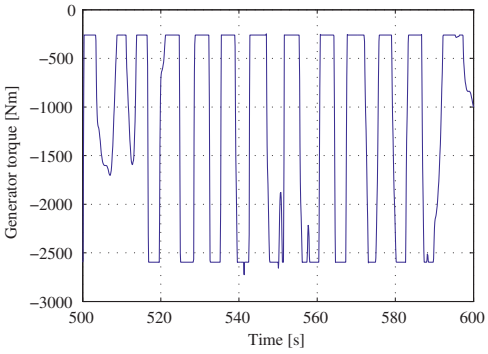

(b) Torque

Fig. 7. Normal generator operation

III. IGBT RELIABILITY

Solid-state devices have in general good reliability and long lifetime as there are no moving parts involved that may wear out. However, the devices are fragile to excessive voltage and currents, and can be damaged even by very short duration shocks above maximum ratings. In well-designed systems, the solid-state devices are well protected from such events with little threat to lifetime. The second mechanism of importance that may wear down the transistor over time is thermal stress. Fig. 9 illustrates the common sandwich structure of common IGBT devices with several boundary layers of different materials. As these materials have different coefficients of thermal expansion, there will be exerted a mechanical stress on the interface between the layers. Over time this stress may cause reduced thermal and/or electrical conductivity [14], [15] which may degrade the device and eventually cause a positive feedback effect which worsens the issue an breaks the device.

The most common failure mode is referred to as *bond lift off* which is caused by fatigue in the electrical connections to the chip. The cause of failure is usually detachment of the solder between the chip and the bond wire. There is continuous progress in mitigating these negative effects, and newer devices suffer less from these problems, but they are still present.

Fatigue as a result of thermal stress is directly linked to the number of thermal cycles the device undergo. Numbers vary for cycle lifetime, but may be as low as 1 000 extreme load cycles from minimum rating to maximum rating (typically $-40°\mathrm{C} - 120°\mathrm{C}$). In the paper by Ciappa et al [16], empirical results indicate a logarithmic relationship between lifetime and the magnitude of the thermal cycles. ΔT=40°C has a specified lifetime of $5 \cdot 10^6$ cycles while an increase to ΔT=80°C results in a lifetime of 10^5 cycles.

Several publications describe methods on how to estimate the thermal cycling lifetime [17], but they all are based on detailed knowledge about the exact physical structure of the device and the thermal flux inside. To estimate the lifetime the following work will focus on creating an accurate thermal model of the device that simulates the actual temperature in the different parts of the device experienced under normal operation.

Several mechanisms may cause thermal cycling, the most obvious being startup and shutdown of the system. Also, modes of operation that involves power fluctuation or low frequency may cause thermal cycling of the IGBTs. Typical examples of applications that undergo thermal cycling are trains, lifts, arc welding, automotive, renewable energy, wave

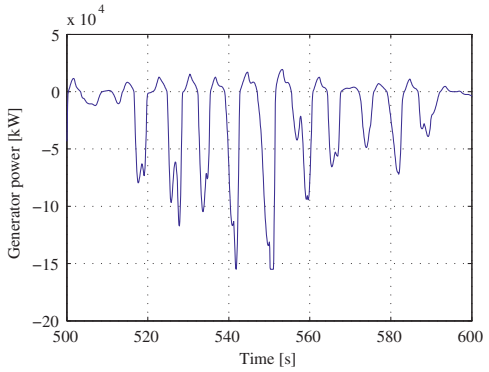

(a) Wave to wave power fluctuations

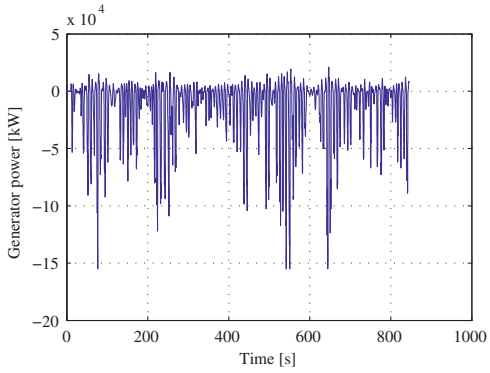

(b) Wave train power fluctuations

Fig. 8. WEC short term power fluctuations

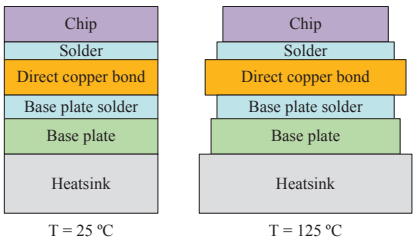

Fig. 9. Illustration of thermal stress in module

energy. For wave energy, the problem is mostly linked to power fluctuations. The lowest output frequency at nominal current is 15 Hz, and frequency cycling is therefore of less concern.

In general, there are two frequency domains for the power fluctuation. One caused by the wave-to-wave movement with a period of 4-10 seconds. The second is the wave train fluctuation that consist of groups of waves with close to the same energy content, which fluctuates in a 20-200 second pattern [18]. These two frequency domains are also visible in Fig. 8, which shows the simulated output power from Bolt2.

IV. Simulation model

The simulation model consists of two parts, one model for the thermal behavior of the device and one model that estimates the transistor and diode loss based on generator torque and speed profiles. Earlier simulations have shown that a wave state must be simulated for at least 20 minutes to become statistically stable. Since this is very high in contrast to the fast switching speed of the transistors, the discrete switching model that simulates the exact transistor operation is abandoned.

Instead, a continuous linear model is implemented that estimates the average losses based on stationary RMS values for voltage, current and phase shift. The stationary values are calculated from time series data for generator speed and torque, as shown in Fig. 7, by solving the motor equations illustrated by the phase plot in Fig. 11. The total equivalent circuit for the inverter and generator is shown in Fig. 10. The model is based on *Pulse With Modulation* (PWM) control of the IGBTs, and since the difference between the switching frequency and the wave frequency is so large, dynamic effects from the feedback control are neglected.

The transistor duty cycle D defined as the transistor on to off ratio can be calculated by Equation (2) where v_s is the instant generator voltage, V_d is the DC-Link voltage and V_S is the generator RMS voltage given with the phase shift φ to the current. All the calculations are evaluated for one electrical cycle of ωt.

$$D(\omega t) = \frac{v_s(\omega t)}{2V_d} = \frac{V_S\sqrt{2}}{2V_d}\sin(\omega t + \varphi) \tag{2}$$

Based on the duty cycle it is possible to estimate the continuous diode and transistor conduction loss P_{cd} and P_{ct} from the instantaneous current i_S and the equivalent on resistance and on voltage R_{d0} / R_{t0} and V_{d0} / V_{t0}, as given in Equations (3) - (6).

$$p_{cd}(\omega t) = i(\omega t)\{i(\omega t)\cdot R_{d0} + V_{d0}\} \tag{3}$$

$$p_{ct}(\omega t) = i(\omega t)\{i(\omega t)\cdot R_{t0} + V_{t0}\} \tag{4}$$

$$P_{cd} = \frac{1}{2\pi}\int_0^{\pi} p_{cd}(\omega t)\cdot\{1 - D(\omega t)\}\,\mathrm{d}\omega t \tag{5}$$

$$P_{ct} = \frac{1}{2\pi}\int_0^{\pi} p_{ct}(\omega t)\cdot D(\omega t)\,\mathrm{d}\omega t \tag{6}$$

The calculation for continuous switching loss is based on the simplified estimate that the dissipated energy for one switching operation can be estimated by the power transferred by the IGBT multiplied with a constant switching time T_{sw}. The constant PWM switching frequency of the inverter is f_s. The resulting continuous switching loss is given by Equation (7).

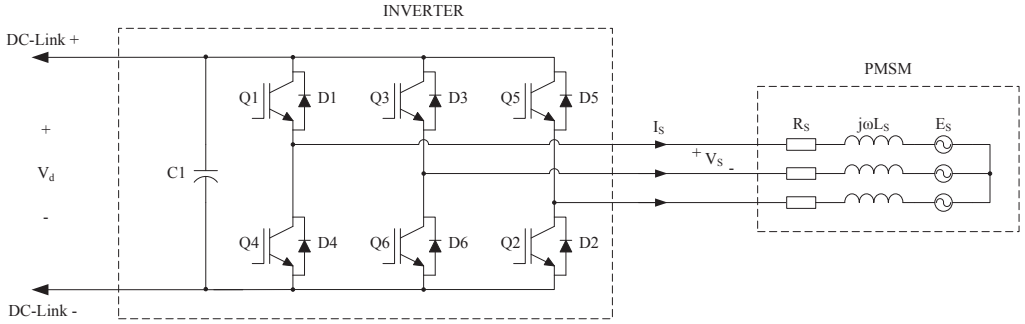

Fig. 10. Inverter and generator equivalent circuit

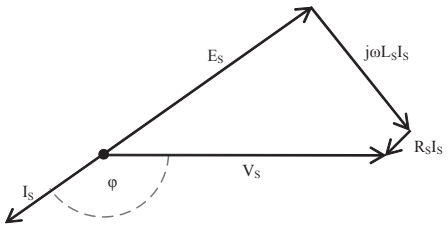

Fig. 11. PMSM phasor diagram in generator mode

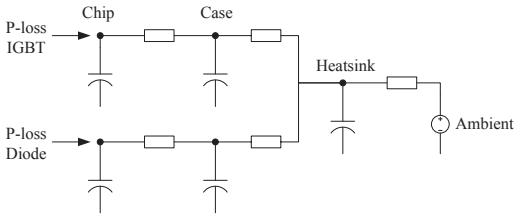

Fig. 12. Thermal model for IGBT/Diode module

Diode chip heat capacity	0.156	J/K
Diode case heat capacity	0.36	J/K
Diode chip/case resistivity	0.0843	K/W
Diode case/hsink resistivity	0.241	K/W
Transistor chip heat capacity	0.268	J/K
Transistor case heat capacity	0.7	J/K
Transistor chip/case resistivity	0.027	K/W
Transistor case/hsink resistivity	0.123	K/W
Heat sink heat capacity	50	J/K
Heat sink to ambient resistivity	0.5	K/W
Ambient temp	40	°C

TABLE I
THERMAL PARAMETERS

Switching frequency	2	kHz
Switch time	100	ns
DC-Link voltage (V_d)	600	V
Generator torque/current ratio	10.8	Nm/A
Generator speed/voltage ratio	6.59	Vs/rad
Generator resistance (R_S)	0.038	Ω
Generator inductance (L_S)	0.0014	H

TABLE II
ELECTRICAL PARAMETERS

$$P_{st} = \frac{1}{2\pi} \int_0^{\pi} V_d \cdot i\left(\omega t\right) \cdot T_{sw} \cdot f_s \, \mathrm{d}\omega t \tag{7}$$

The thermal model used is drawn in Fig. 12 and implements the heat capacity of the chip, case and heat sink, and the thermal conductivity between these elements. This is modeled for both the diode and the transistor.

The exact parameters for the thermal model are listed in in Table I. The values are taken from a datasheet for a similar system. The electrical parameters for the generator and inverter listed in Table II are taken from the Bolt2 system, and are fully accurate.

The simulations were ran for approximately 15 minutes in the design wave state and the temperature data series was collected for all measured elements of the solid state device.

V. RESULTS

From the results plotted in Fig. 13, 14 and 15 it immediately becomes clear that the diode takes most of the burden, and that the IGBT sees little thermal stress. This is likely to be caused by the mode of operation with the PMSM in generating mode, requiring low one time duty cycle from the IGBT and thus low conduction loss. The resulting conduction loss in the diode is equally higher. The PMSM in generator mode operates much like an active front-end device and the inverter should have been optimized with IGBT modules matched for this, instead of the typical motor mode configuration.

From the IGBT chip parameters it can be seen that the device has much better thermal properties for thermal transfer than the diode. This is because the device is designed for motoring mode. Devices for active front-end converters are

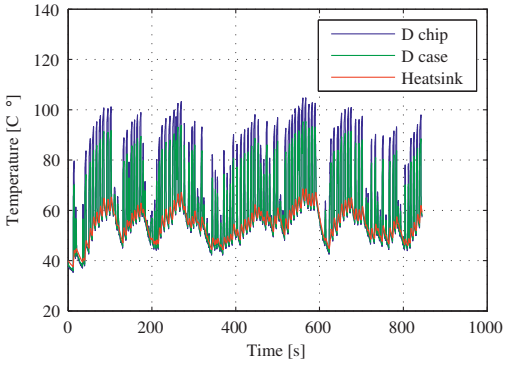

Fig. 13. Diode temperature

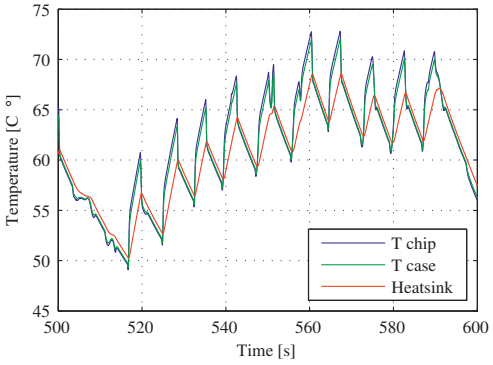

Fig. 15. Transistor temperature, wave to wave fluctuations

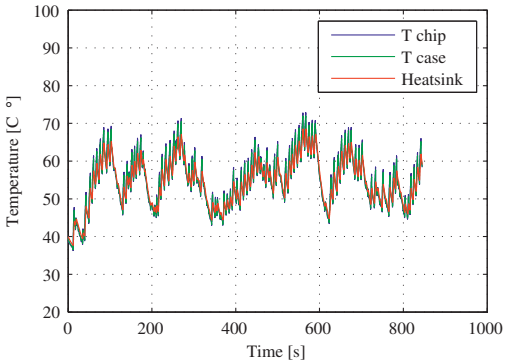

Fig. 14. Transistor temperature

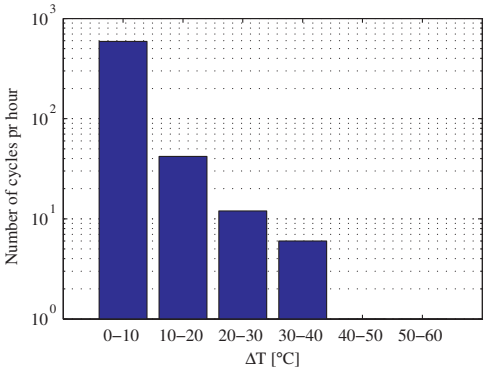

Fig. 16. Transistor cycle count

usually balanced more in favor of the diode.

It is not straightforward to calculate the annual thermal cycles for this system. To get an accurate result all load cases for the entire year should be simulated individually. FO has performed such simulations earlier to estimate annual energy production, but they are very time consuming. To simplify the case it is estimated that the full year of production corresponds to 1 500 hours of production at the design wave state. The number of cycles per hour is thus only simulated for the design wave state, and is plotted in Fig. 16. By multiplying these results with the annual production, the annual number of cycles with $\Delta T = 40°$ C becomes 9 000. By calculating for all thermal cycle levels, and by using the results obtained by Gappa and Fichtner [16] the resulting cycle lifetime is estimated to be 500 years.

It therefore seems like thermal cycles does not influence the IGBT lifetime in its current configuration. However, if the IGBTs are reduced and optimized so that ΔT increases by 40 °C in Fig. 16, estimated lifetime drops to 10 years, and immediately becomes the limiting factor for the system lifetime. Thus, it becomes clear that the system must be designed with a significant margin, and that thermal cycles must be taken into consideration during design. The effect of thermal cycling of diodes is not studied in this paper, but the same issues and effects must be expected here. The diode is cycled heavily compared to the IGBT, and a significant reduction in lifetime must be expected. The system should therefore be designed with more focus on diode performance.

VI. Conclusion

The analysis shows that the lifetime does not seem to be heavily influenced by thermal cycling in the current configuration for this Wave Energy Converter application. However, it is clear that balance between the IGBT and the anti-parallel diode in the chip is poor. Also, the IGBT is significantly oversized for the application, however if it was to be matched exactly to its load case, thermal cycling would pose a threat. It therefore seems like the system should be optimized by using IGBT modules for front-end devices to improve the internal chip balance between the diode and the IGBT, and that the system

in general should be oversized with some margin to ensure adequate lifetime.

REFERENCES

[1] J. Sjolte, G. Tjensvoll, and M. Molinas, "All-electric wave energy converter connected in array with common dc-link for improved power quality," in *Power Electronics for Distributed Generation Systems (PEDG), 2012 3rd IEEE International Symposium on*, june 2012, pp. 431 –436.

[2] J. Sjolte, I. Bjerke, A. Crozier, G. Tjensvoll, and M. Molinas, "All-electric wave energy power take off system with improved power quality at the grid connection point," in *Transmission and Distribution Conference and Exposition (T D), 2012 IEEE PES*, may 2012, pp. 1 –7.

[3] J.Sjolte, I.Bjerke, , G.Tjensvoll, and M.Molinas, "Summary of performance after one year of operation with the lifesaver wave energy converter system," in *Submitted to the European Wave and Tidal Energy Conference (EWTEC13)*, September 2013.

[4] I.Bjerke, E.Hjetland, G.Tjensvoll, and J.Sjolte, "Experiences from field testing with the bolt wave energy converter," in *Submitted to the European Wave and Tidal Energy Conference (EWTEC11)*, september 2011.

[5] "The wave power climate at the wave hub site," Nov 2006, journal: Applied Wave Research Review of Wave Power Climate.

[6] J. Falnes, *Ocean Waves and Oscillating Systems: Linear Interactions Including Wave-Energy Extraction*. Cambridge University Press, 2002.

[7] E. Tedeschi, M. Carraro, M. Molinas, and P. Mattavelli, "Effect of control strategies and power take-off efficiency on the power capture from sea waves," *IEEE Transactions on Energy Conversion*, vol. 26, no. 4, pp. 1088–1098, 2011. [Online]. Available: http://www.scopus.com/inward/record.url?eid=2-s2.0-82155162473\&partnerID=40\&md5=8154812c8af086cfd9453f02ec99ee8d

[8] E. Tedeschi and M. Molinas, "Impact of control strategies on the rating of electric power take off for wave energy conversion," in *IEEE International Symposium on Industrial Electronics*, 2010, pp. 2406–2411. [Online]. Available: http://www.scopus.com/inward/record.url?eid=2-s2.0-78650351853\&partnerID=40\&md5=a82865e32786f6209031b80a5811868a

[9] J.Falnes, "Principles for capturie of energy from ocean waves: phase control and optimum oscillation," NTNU, Tech. Rep., 1997, http://folk.ntnu.no/falnes/w_e/index-e.html\#RAPPORTAR.

[10] J. Ulvin, M. Molinas, and J. Sjolte, "Analysis of the power extraction capability for the wave energy converter bolt," *Energy Procedia*, vol. 20, pp. 156–169, 2012.

[11] J.Sjolte, I.Bjerke, E.Hjetland, and G.Tjensvoll, "All-electric wave energy power take off generator optimized by high overspeed," in *Submitted to the European Wave and Tidal Energy Conference (EWTEC11)*, september 2011.

[12] J. Sjolte, I. Bjerke, A. Crozier, G. Tjensvoll, and M. Molinas, "All-electric wave energy converter with stand-alone 600vdc power system and ultracapacitor bank," in *2012 EVER International Conference and Exhibition on Ecological Vehicles and Renewable Energies*, march 2012.

[13] E.Hjetland, I.Bjerke, G.Tjensvoll, and J.Sjolte, "A brief introduction to the bolt-2-wave project," in *Submitted to the European Wave and Tidal Energy Conference (EWTEC11)*, september 2011.

[14] W. Wu, G. Gao, L. Dong, Z. Wang, M. Held, P. Jacob, and P. Scacco, "Thermal reliability of power insulated gate bipolar transistor (igbt) modules," in *Semiconductor Thermal Measurement and Management Symposium, 1996. SEMI-THERM XII. Proceedings., Twelfth Annual IEEE*, Mar 1996, pp. 136–141.

[15] A.Hamidi, N.Beck, K.Thomas, and E.Herr, "Reliability and lifetime evaluation of different wire bonding technologies for high power igbt modules," in *Microelectronics Reliability 01*, 1999.

[16] M. Ciappa and W. Fichtner, "Lifetime prediction of igbt modules for traction applications," in *Reliability Physics Symposium, 2000. Proceedings. 38th Annual 2000 IEEE International*, 2000, pp. 210–216.

[17] T. Poller, M. Feller, I. Hoyer, and J. Lutz, "Thermal mechanical behavior of solder layers im power modules," in *International Exhibition and Conference for POWER ELECTRONICS INTELLIGENT MOTION POWER QUALITY*, 2009.

[18] S. H. Salter, "World progress in wave energy 1988," *International Journal of Ambient Energy*, vol. 10, no. 1, pp. 3–24, 1989. [Online]. Available: http://www.tandfonline.com/doi/abs/10.1080/01430750.1989.9675119

Appendix I

Journal paper 1

Title: Power Collection from Wave Energy Farms

Conference/Journal: International Journal of Applied Sciences

Date: 2. April 2013

Location/Publisher: MDPI, Open access

Appl. Sci. **2013**, *3*, 1-x; doi:10.3390/——

OPEN ACCESS

applied sciences

ISSN 2076-3417

www.mdpi.com/journal/applsci

Article

Power Collection from Wave Energy Farms

Jonas Sjolte [1,*], Gaute Tjensvoll [1] and Marta Molinas [2]

[1] Fred. Olsen / Norwegian University of Science and Technology, Fred. Olsens Gate 2, N0152 Oslo, Norway; E-Mail: gaute.tjensvoll@fredolsen.no

[2] Department of Electric Power Engineering, Norwegian University of Science and Technology, O. S. Bragstads plass 2E, N-7034 Trondheim, Norway; E-Mail: marta.molinas@ntnu.no

* Author to whom correspondence should be addressed; E-Mail: jonas.sjolte@ntnu.no; Tel.: +47-22341145 or +47-97688440; Fax: +47-22341141.

Received: 7 January 2013; in revised form: 12 March 2013 / Accepted: 13 March 2013 / Published: xx

Abstract: Most *Wave Energy Converters* (WECs) produce highly distorted power due to the reciprocal motion induced by ocean waves. Some WEC systems have integrated energy storage that overcomes this limitation, but add significant expenses to an already costly system. As an alternative approach, this article investigates the direct export option that relies on aggregate smoothing among several WECs. By optimizing the positioning of the WEC devices with respect to the incoming waves, fluctuations may be mutually canceled out between the devices. This work is based on *Fred. Olsen's* WEC system *Lifesaver*, and a WEC farm consisting of 48 devices is designed in detail and simulated. The major cost driver for the electrical export system is the required oversize factor necessary for transfer of the average power output. Due to the low power quality, this number can be as high as 20 at the entry point of the electrical system, and it is thus crucial to quickly improve the power quality so that the downstream power system is efficiently utilized. The simulations undertaken in this work indicate that a high quality power output can be achieved at the farm level, but that a significant oversize factor will be required in the intermediate power system within the farm.

Keywords: wave; energy; array; farm; power; quality; peak; average; ratio

1. Introduction

Wave Energy Converters (WECs) are different from most other energy producers in that the prime mover operates with a sinusoidal velocity. When such a producer is directly connected to its generator, the output power is continuously fluctuating with zero crossings in every wave, resulting in a high peak-to-average power ratio. *Fred. Olsen's* (FO) power plant *Lifesaver*, pictured in Figure 1, illustrates this typical behavior, as plotted in Figure 2. This level of power distortion is unlikely to be suitable for export to the grid as the utilization of installed power capacity is very low. In this article, the method of aggregate power smoothing from multiple WECs in order to improve the power quality will be investigated. As the incoming wave energy is close to constant when averaged over longer periods of time, the power production can be equally averaged by covering a large distance of the incoming wave. Substantial work has previously been performed within this topic, and the articles (Tissandier *et al*., 2008) [1], (Kavanagh *et al*., 2011) [2] and (Blavette *et al*., 2012) [3] demonstrate successful integration of WECs into a farm system. The focus of this work is the specific integration of Lifesaver into a WEC farm system, and the potential for economical optimization of the power transfer chain from wave to wire.

Figure 1. *Lifesaver* on site outside Falmouth, England.

The power quality is very poor when the wave energy enters the WEC, mainly due to two factors. Firstly, the sinusoidal shape of the incoming wave causes a sinusoidal movement of the *power take-off* (PTO) system, and does not allow the PTO to run constantly at rated speed. Secondly, waves tend to group into *wave trains* that consist of series of waves with similar amplitude (Salter, 1988) [4]. This adds subharmonic fluctuations with respect to the incoming wave period and further reduces the utilization factor of installed PTO power. Moreover, WEC systems that utilize the mooring line as a production force can only extract power during the upwards motion. This unidirectional production pattern adds another doubling to the peak-to-average ratio. This can subsequently add up to a total peak-to-average ratio in the high tens, depending on the system configuration.

Figure 2. Actual production and system operation measured with Lifesaver.

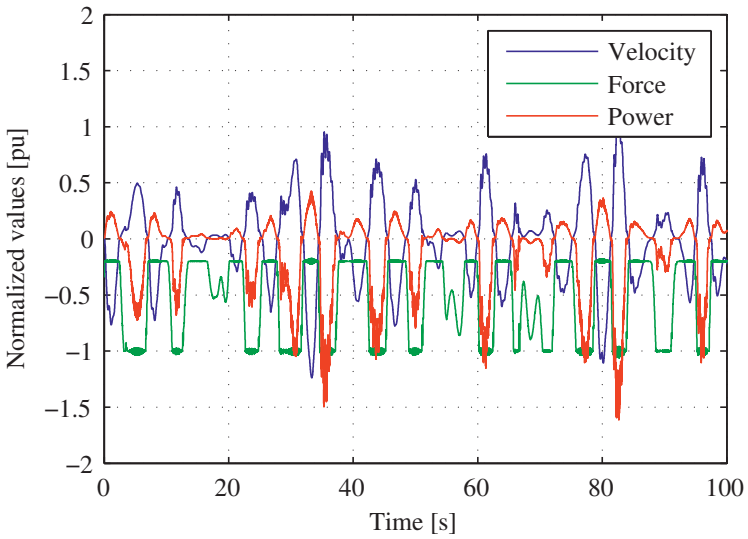

Figure 3. Illustration of the improved power quality through the power transfer chain. The power quality is given as the peak-to-average ratio and illustrated with orange bars. The nominal oversize factor is denoted with parentheses (*i.e.*, the name plate rating on the generator divided by the average produced power).

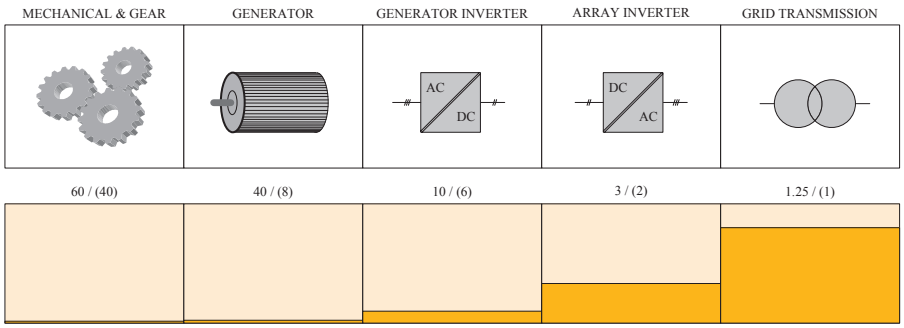

Lifesaver has a peak-to-average ratio of approximately 60 on the entry point of mechanical wave power. Thus, in the design wave state, the PTO is designed for power peaks up to 60 *per unit* (pu), while only 1 pu is transferred on average. If the PTO was constantly operated at rated speed and rated force, on average 60 pu of power could be transferred. This exceptionally low utilization factor is a major challenge for the profitability of WECs and must be managed carefully. Moreover, it is important to

quickly reduce the peak-to-average ratio in the downstream power system towards the grid. The poor mechanical utilization factor is not necessarily an issue in and of itself, as the mechanical transmission cost can be low compared to the cost of the total system. However, it is important that this poor utilization factor not be carried forward to the rest of the system. Figure 3 illustrates the gradual increase in power quality that is required from an economical point of view, and is the focus of this work. The underlying details of the figure will be explained and analyzed in detail in the following sections.

1.1. The FO Wave Energy Project

FO started with Wave Energy in 2000, and, in 2004, the Wave Energy Converter *Buldra*, built as a platform with multiple point absorbers, was launched. Since then, FO has tested out various concepts and built several different prototypes, all based on the point absorber concept. The series of experiments have led to the single body point absorber concept, as realized by our latest prototype *Lifesaver*. Point absorbers are not the most efficient when measured in terms of captured energy, but have nonetheless proven to be successful on total performance and energy costs.

Until now, FO has operated four WECs based on the single body point absorber in real sea conditions. The first, named *B33*, was a small proof-of-concept device that was operated outside Akland, Norway during the autumn of 2007 and the winter of 2008. B33 showed good results, leading to the second device, named *B22*, which was equipped with a full-scale control, communication and production system. B22 was operated outside Risør, Norway from the summer of 2008 until the spring of 2009. Based on these experiences, FO started the next development phase in collaboration with a selected few European companies and universities through the Sustainable Economically Efficient Wave Energy Converter (SEEWEC) project. This work led to the full-scale system Bolt®Bolt that was installed outside Risør, Norway in June 2009. Bolt is pictured in Figure 4 on site and has, since 22 December 2010, produced 3360 kWh of energy (Bjerke *et al.*) [5].

Figure 4. FO's Wave Energy Converter *Bolt*®, located outside Risør, Norway has been in operation since June 2009.

Based on the success of Bolt®, FO decided to use the knowledge and experience gained so far to proceed to the next generation of design. An agreement with several UK companies was made with funding from the UK Technology Strategy Board (TSB). The goal of the project was to improve the Bolt® concept towards a commercial level where it can be launched at Wavehub [6], and hence the project name *Bolt2Wavehub*. The project resulted in the full-scale system Lifesaver, consisting of a 16 m toroidal floater with five individual all-electric PTO systems. Lifesaver was installed on the test site *Fabtest* in April 2012 and is planned to be in operation until March 2013, when it has to be brought ashore due to the strict UK regulations. Fabtest is a UK test site for pre-commercial WEC concepts located in Falmouth Bay outside of Cornwall, England. The exact location of Fabtest is shown in Figure 5.

Figure 5. Location of the UK test sites *Wavehub* and *Fabtest*.

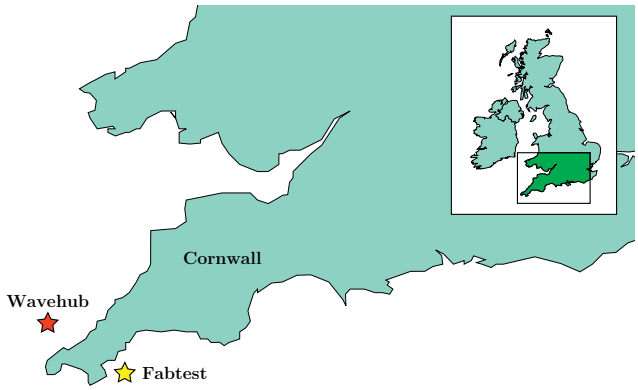

Thus far, FO has not had a single serious event with any of the WEC systems, which has allowed for continuous long-term testing in real sea conditions. This has proved invaluable for building a knowledge base with wave energy. However, the problems and issues that arise in real sea conditions are multifaceted and thus exceed the scope of the undertaken tests.

2. System Description

FO's WEC concept is based on the point absorber principle, which is well described in the literature (Falnes *et al*., 2003, 2012) [7,8] and has been extensively researched. FO has designed a floater structure with high surface area and low mass that is cost efficient with respect to absorbed power. This geometry results in a high resonance frequency and thus leads to a Response Amplitude Operator (RAO) (Falnes, 2002) [9] close to unity for most of the relevant wave states. The system is therefore quite rigid and well suited for power production by passive damping control. The absorber is tightly moored to the sea floor with a PTO system that produces power from the heaving motion. The point absorber system is independent of wave direction, which simplifies the mooring system and makes the system robust in mixed directional waves.

2.1. Power Take-Off (PTO)

The PTO system is realized as a winch and rope system, as illustrated in Figure 6. The generator can only produce power during upwards motion, and has to operate in motoring mode during downwards motion to maintain rope tension. The detailed control principle utilized by FO is described in our previous publications [10,11]. The generator is a high performance permanent magnet machine manufactured by Siemens® and is designed for industrial servo applications. It has high torque output and low inertia, and is suitable for direct-drive applications with low gear ratio or entirely without a gearbox. The generator is powered through a full bridge converter that gives full control of the generator torque with high precision and quick response, which in total gives a very powerful package with high performance that is well suited for the reciprocal wave motions. The electrical configuration of the generator and converter can be seen in Figure 7(b).

Figure 6. Principal sketch of the WEC.

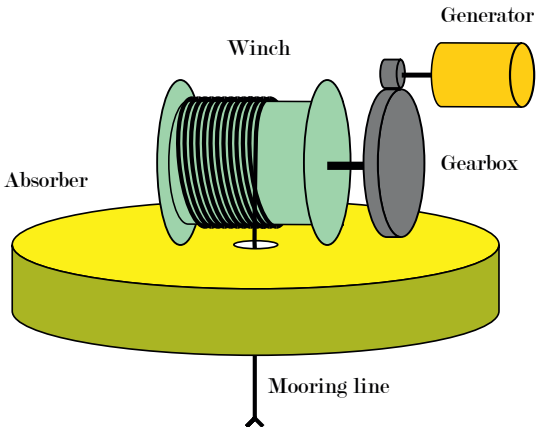

Figure 7. Array design. (**a**) Array configuration; (**b**) Electrical configuration.

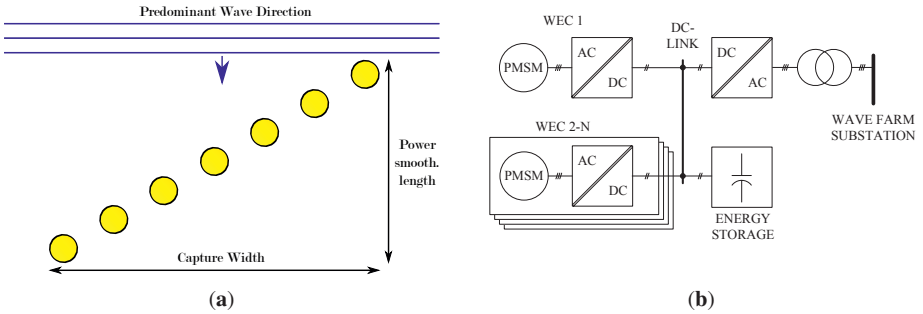

As discussed earlier, the unidirectional production principle increases the peak-to-average ratio with a factor of two as the production becomes asymmetrical. The consequent reduction in power quality transfers to the generator and the converter, reducing the utilization factor on these components to 50%. Symmetrical production may be achieved by implementing a separate spring system that produces enough pre-tension to tense the rope and also pull the generator at full power during the downward motion. As this will be an expensive and powerful system, the costs must be carefully weighed against the increased generator and converter costs of the asymmetrical system. Our earlier prototype Bolt®, shown in Figure 4 is designed with the symmetrical option based on a hydraulic spring system.

When cost-optimizing the PTO, the rated production force turns out to be the design property with the highest cost impact, since it governs the strength and the physical size for most of the mechanical components. The rated power has the second highest cost impact and influences mostly the generator and the converter. There is also a high potential for cost savings on the inverter by extensive utilization of field weakening control, as described in our previous work [11]. The third driving cost parameter is the ability to handle mechanical inertia by the implemented control system. As the system has to follow the reciprocal motion of the waves, the dynamical drive train response is very important. Also, a high inertia will cause high power fluctuations due to change in kinetic energy. The inertia is dominated by the generator and can be reduced by moving towards more expensive direct drive generators with high torque and low speed. Thus, there will be a cost balance between good control and low inertia on the generator. Hence, it is important to keep in mind that the power rating of a PTO alone is not sufficient to give a clear picture of the PTO cost. However, to simplify further analysis, power rating is used as the key performance indicator in the following sections.

2.2. Array

To increase the output power, and to improve the output power quality, several WECs may be linked together into an array. Figure 7(a) shows the proposed layout that was put forward in our previous study described in [12,13]. The fundamentals behind this design is the need to space the WECs along the incoming wave direction to gain power quality from intermediate wave smoothing, while simultaneously achieving a good capture ratio, which requires spacing perpendicular to the incoming wave direction. Thus, a 45° angle to the incoming wave direction was found to be optimal. Also, the array design should endeavor to cover a full wave length along the predominant wave direction to maximize the effect of power smoothing. With Lifesaver as the basis, this amounts to around seven absorbers per array.

It is FO's point of view that the devices within the array should be positioned close together and interconnected so that the array can be viewed and operated as a single system. Furthermore, this allows for sharing a common mooring system and simplifies the electrical connections between the devices as the cable can run along the floater topside. The exact configuration of the mechanical interfaces is not yet decided, but preliminary studies indicate that a combination of strong moorings pulling the devices apart and flexible bumper connections between the devices can maintain the mechanical integrity of the array within reasonable cost. In this work, a spacing of 2 m is chosen between the devices to account for the interface structure. Figure 8 illustrates an array based on Lifesaver with this configuration.

Figure 8. Artistic impression of array based on Lifesaver.

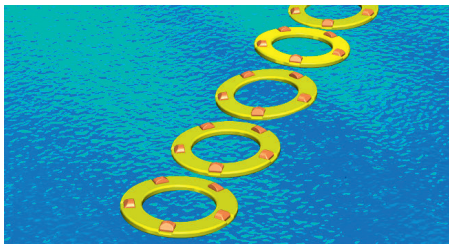

The array is electrically connected to DC by coupling the DC-Link on the inverters. The configuration is illustrated in Figure 7(b), and shows how the power can flow freely between the WECs without additional conversion or transmission equipment. This allows a producing WEC to directly transfer power to a consuming WEC that is running in pull-back, and allows the sum of WEC powers to be directly transferred. However, the low DC-link voltage poses a practical limit to the size of the array due to the sea cables that have to run between the WECs. As a rule of thumb, 1000 A is used as a current limit for low voltage sea cables. This limits the number of WECs in the array to around ten, and supports the earlier stated figure of seven absorbers in the array. Thus, this array size is adopted for the following simulation work.

As the allowed current transfer capacity is fully utilized within the array, the array output must be transformed to a higher voltage before export from the array. The middle WEC should act as a *mother WEC* and house the electrical conversion equipment and connect to the export cable. Since the aggregated array power is low voltage DC, an active front-end inverter and a transformer is required to convert the output to medium voltage AC. The cost of this equipment is directly influenced by the peak power requirement and power quality at this point. In our earlier publication [13], we showed that the peak to average ratio would be directly reduced by a factor of 3–5 due to natural power smoothing between the devices. The peak-to-average ratio could be further improved towards 1.5 by implementing a small energy storage, as shown in our work [14]. As will be demonstrated in the following, the peak power rating for the current configuration is close to three, which will require a rated installed converter capacity of about twice the average exported power. This is illustrated in Figure 3 on page 3.

2.3. Farm

The array could be directly connected to the grid as it outputs standard AC power. However, since the power utilization is only about 50%, it will be beneficial to further improve the power quality by creating a WEC farm that consists of several arrays. The arrays must be positioned in the farm according to the same principles of the WEC placement in the array. Hence, no array must shield another array from the predominant wave direction. Also, for effective power smoothing, the incoming wave along the predominant wave direction should only interfere with one WEC at a time. A proposed farm configuration consisting of six arrays that complies with this is shown in Figure 9(a), and implemented in the following simulation work. Some interference is expected between the absorbers, which in general

reduces the power output from the rear WECs. The wedge-shaped layout could compensate some of this by amplifying the incoming wave, but this has not yet been verified by hydrodynamical analysis, and must be treated with care.

Figure 9. Wave farm design. (**a**) Farm configuration; (**b**) Electrical configuration.

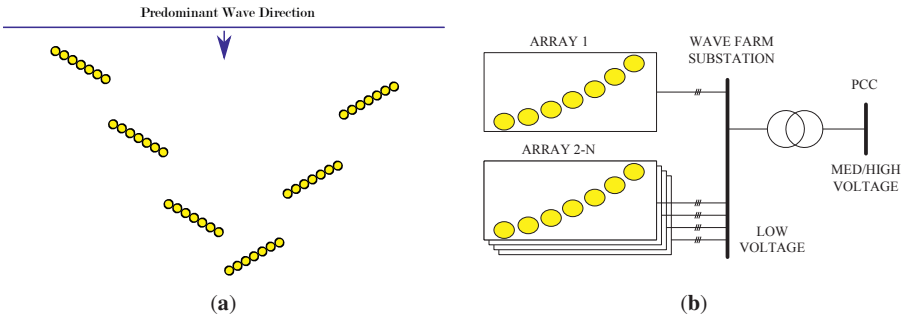

While the smoothing effect of the array mainly comes from evening out the power fluctuations within a single wave, the smoothing effect for the farm comes from balancing out the differences between waves in an incoming wave train. As demonstrated by Stephen Salter (Salter, 1988) [4], smoothing of about 100–200 seconds is required to effectively smooth out wave train fluctuations. This corresponds to a fetch of 1–2 km and is far greater than the farm configuration suggested here. Some cyclical power fluctuations must therefore be expected also on the farm output, and a peak-to-average ratio of approximately 1.25 is expected. The proposed electrical configuration for the farm is shown in Figure 9(b) and shows how the medium voltage power from each array is collected for export. A second step-up transformer may be included to further increase the output voltage. The main benefit of the improved power quality from the farm is better utilization of the shore cable connecting to the grid.

3. Simulation Model

The simulations are performed on the basis of the WEC prototype test site *Wavehub* located west of Cornwall, England as shown in Figure 5. The test site is funded and supported by the renewable energy program administrated by the British government. The site includes a sub-sea power substation that allows for electrically connecting the WECs to the grid. Wavehub has been surveyed and monitored for an extensive period and work is still ongoing to calculate true statistical wave data for the site. The wave scatter diagram and the directional spectrum for Wavehub is plotted in Figure10(a) and Figure 10(b), respectively. The directional scatter is heavily dominated by waves from the west, and the directional plot must be logarithmically scaled to show all the directions observed.

The model used for the farm simulation is based on the single absorber model for Lifesaver (Molinas *et al*., 2007, Skjervheim *et al*., 2008) [15,16]. The simulation model solves Equation (1) for $\zeta(t)$ in the time domain. The index denotes the mode of motion, given by the six *degrees of freedom*

(DOF) of motion for the floater. The excitation force matrix $F_{e,i}$ is the time-dependent force due to incident waves, and M denotes the mass of the system.

$$F_{e,i}(t) - F_{D,i}(t) = M\frac{d^2\zeta(t)}{dt^2} \tag{1}$$

$$F_{D,i}(t) = F_{r,i}(t) + F_{d,i}(t) + C_i \cdot \zeta_i(t) + F_{PTO}(t) \tag{2}$$

$F_{D,i}$ accounts for the sum of all the damping forces in Equation (2), where $F_{r,i}$ accounts for the time-dependent forces on the floater due to radiation of waves. The term $F_{d,i}$ accounts for non-linear damping terms, mainly the drag forces. ζ_i is the time-dependent motion of the floater, C_i is the restoring force matrix accounting for the hydrostatic pressure acting on the floater, and F_{PTO} is the time-dependent force applied from the PTO. The PTO is modeled as a rope and winch system that is tightly moored to the sea floor. Detailed performance curves for Lifesaver are presented in our previous article [17].

Figure 10. Wave climate at Wavehub. (**a**) Wavehub scatter diagram. Hours per wave state; (**b**) Probability distribution of wave direction on Wavehub. The plot is a logarithmic polar plot defined by the angle θ and radi ρ.

Significant wave height hs [m] \ Wave period Tz [sec]	3,5	4,5	5,5	6,5	7,5	8,5	9,5	10,5	11,5
0,25	26	79	44	18	0	0	0	0	0
0,75	499	832	491	140	18	0	0	0	0
1,25	184	1051	604	307	70	26	9	0	0
1,75	0	587	701	333	149	53	26	0	9
2,25	0	96	534	254	123	44	9	0	0
2,75	0	0	237	228	105	26	9	9	0
3,25	0	0	26	175	123	44	9	0	0
3,75	0	0	0	79	96	35	18	0	0
4,25	0	0	0	9	44	26	9	9	0
4,75	0	0	0	0	26	18	9	0	0
5,25	0	0	0	0	18	26	18	0	0
5,75	0	0	0	0	0	18	9	0	0
6,25	0	0	0	0	0	9	0	0	0

(**a**)

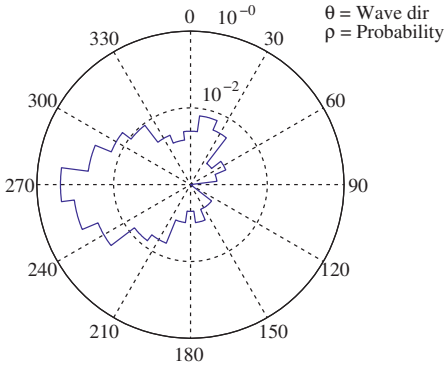

(**b**)

Since the simulation is based on a detailed 6DOF model for Lifesaver, FO keeps the simulation model confidential. However, such high level of complexity is not essential for this study, and a simplified 1DOF model would produce almost the same result. It is therefore possible for a third party to qualitatively verify the results published here without detailed knowledge of the simulation model used.

To simulate a wave state, a 20-minute time series of irregular waves is generated based on the JONSWAP wave spectrum [18]. The wave state is defined by the significant wave height h_s, the zero crossing period t_z, and the wave direction θ. The subsequent excitation forces are then calculated and the simulation is performed for the full length of the time series. The simulation model also takes into account PTO and generator losses, and the model outputs a 20-minute time series of exported electrical power from the WEC. The simulation model has undergone many years of development and testing, and is verified against real production data from several prototypes, including Bolt® and Lifesaver.

Array and farm simulations are performed by running the simulation model separately for each absorber in the array/farm. All absorbers are simulated for the same wave scenario, and the wave propagation through the array is modeled in detail to produce an authentic result. The simulation model does not take interference between the WECs into consideration. This is handled by separate modeling work and is described in the next section.

3.1. Hydrodynamic Interactions within the Array

The hydrodynamical problem is solved within the framework of linear potential theory, specifically the Laplace equation, resulting in the interaction field illustrated in Figure 11(a). In this paper, the theoretical basis is only covered briefly. The work of J.N Newman's *Marine Hydrodynamics* [19] is used as basis for this simulation work.

Figure 11. Hydrodynamical interference between absorbers. (**a**) Illustration of the wave interaction with the array. The wave direction is from southwest and thus causes amplification on the southern side of the array and attenuation on the northern side; (**b**) Power correction factors for absorbers in array calculated from shadowing effects ($Tz = 6.5\ s$).

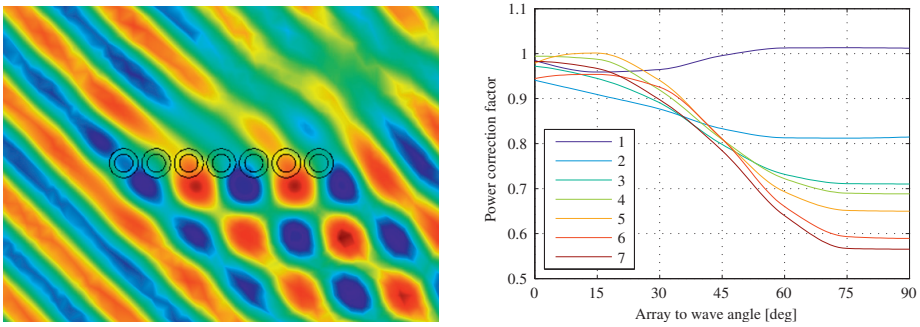

(**a**) (**b**)

Since the velocity potential is linear, all contributions to forces and motions are linear. As a result, the principle of superposition applies. Therefore, it is convenient to split the complex problem into a set of simpler problems. The full solution is thus the sum of several simpler solutions. The potential arising from N absorbers placed in a string can thus be described as the sum of the following contributions.

$$\phi = \phi_0 + \phi_D + \phi_R \tag{3}$$

The total velocity potential ϕ due to the interaction of N absorbers on a string is the sum of the excitation potential due to incident waves ϕ_0, the diffraction potential due to the interaction of the incident potential with all absorbers at rest ϕ_D, and the radiation potential ϕ_R due to the independent motion of every absorber in every mode of motion with no incident waves present.

The diffraction problem and the radiation problem are solved independently. Thus, there are $N + 1$ independent problems to solve. Furthermore, the radiation potential from each absorber is separated

in 6 independent modes of motion. The total potential ϕ_N^i acting on absorber N in mode i of motion is the sum of every other absorber's radiation and diffraction potential, in addition to the diffraction and radiation potential from absorber N acting on itself in mode i of motion. Combining the six modes of motions for each absorber, and allowing for all absorbers to interact, results in a total of $N \times 6$ independent linear equations to be solved for each wave frequency. With a full description of the velocity potential, it is possible to integrate solutions in the frequency domain on specific wave climates and optimize the array energy output with respect to array layout angle and power take off damping coefficient.

In order to represent the interactions within the array in the time domain model, a set of correction factors is applied to the power output from a time domain model of an array without interactions. Correction factors are calculated individually for each wave direction and wave period encountered. The correction factor for the individual WECs are plotted as a function of the array angle in Figure 11(b) for the design wave period ($Tz = 6.5\ s$). Currently, only interactions within arrays are taken into consideration, and the hydrodynamical effect of the wave farm is not modeled. A detailed farm study will be required to produce an accurate figure for annual energy production, but based on experience with similar modeling, the interactions are not believed to have significant impact on the simulated power quality. The results presented here are therefore believed to be accurate and valid for evaluating power quality.

4. Results

The wave energy farm is simulated for the WEC design wave state, which is defined as 2.75 m significant wave height hs and 6.5 s zero-crossing period Tz. Production from each of the 48 WECs is simulated for the same 20 minute window, and the actual power output from each WEC is stored. Figure 12(a) shows the simulated raw output power from each of the 48 WECs. The power from each absorber is individually colored with a rainbow color map, and the power scale is normalized to rated average output power for one WEC. The plot illustrates the time-shifting effect of the power peaks as the waves propagate through the array. It also clearly shows the lack of power smoothing as the wave trains passes through the farm in that the power peaks do not reach maximum power for some portion of the time.

By adding up the power from each WEC according to the array and farm configuration, the aggregated power from each of the six arrays is calculated and plotted in Figure 12(b) by applying the same plot method as in the previous figure. The plot demonstrates the improvement in power quality as the power fluctuations within a single wave is smoothed out with a reduction in peak-to-average ratio from ten to three. As the rated capacity of an inverter may be exceeded for short periods, an array inverter with double power capacity of the rated power is likely to suffice. Still, this will require a converter with twice the cost compared to an average exported power, and measures to further improve the power quality should be kept in mind. Our previously published paper [14] indicates a final peak-to-average ratio for the array between 1.5 and 3 after energy storage is included, the exact figure being a result of economic optimization.

Figure 12. Simulation results. All values are normalized to the average output power of the unit (WEC/array/farm). (**a**) Individual power output from all 48 WECs; (**b**) Aggregated power output from each of the six arrays; (**c**) Aggregated power output from the entire wave farm. The red curve shows the output power smoothed with a 10-second low pass filter; (**d**) Illustration of the power quality improvement as the power is aggregated in the farm; (**e**) Output power in frequency domain; (**f**) Output power distribution.

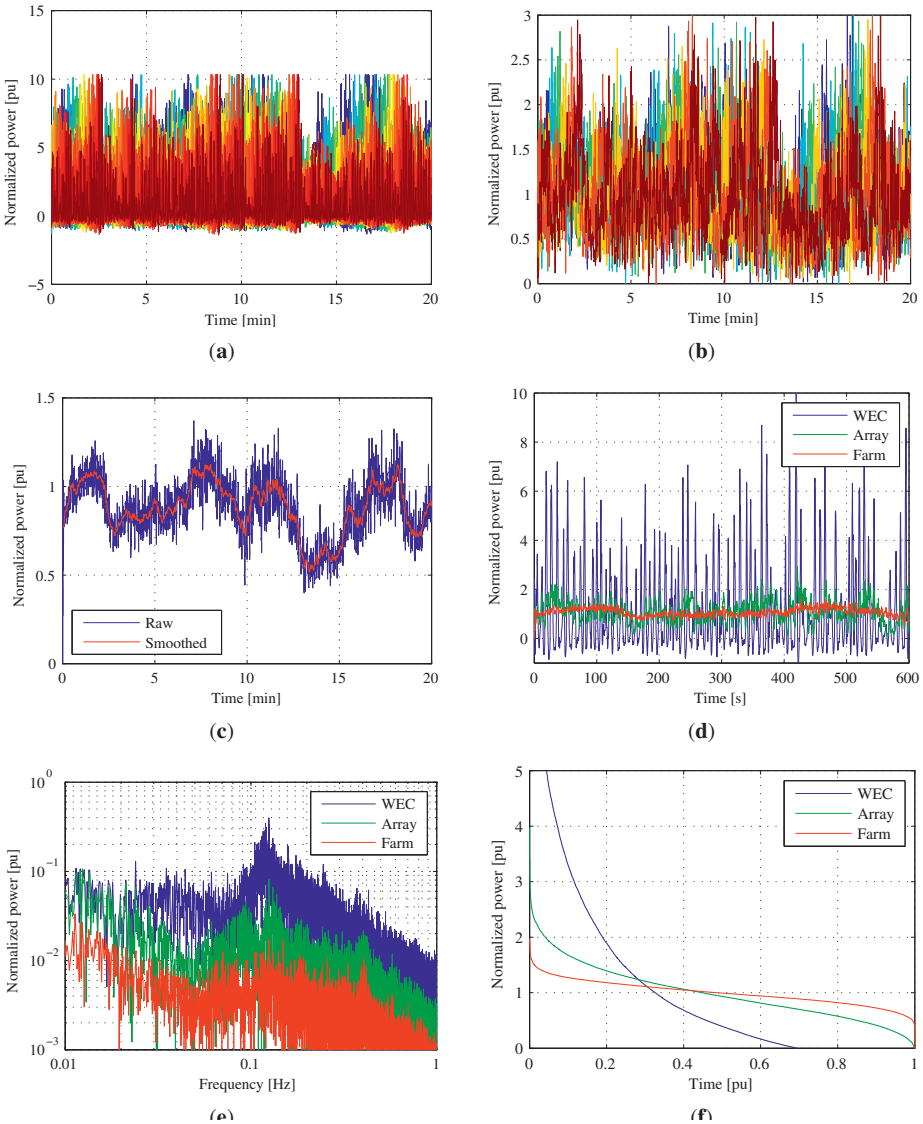

The total aggregate wave farm power is calculated by adding up the six array outputs. The result is plotted in Figure 12(c) and shows a further improvement of power quality. The resulting peak-to-average power ratio is 1.56 in this case, which is higher than the target of 1.25. However, it can be seen that there is a high frequency distortion on the power signal that seems to relate directly to the wave fluctuations from the WECs. These rapid fluctuations can be filtered down quite easily with a small energy storage, and the red curve in Figure 12(c) shows the total farm output power smoothed with a 10-second filter. In this case, the peak-to-average ratio is reduced to a healthy 1.28, which is regarded as satisfactory. At this level, almost the whole of the installed conversion and transfer capacity can be utilized with negligible cost impact due to reduced power quality. The calculated rms value of the output power is only 1.63% higher than the average power.

In Figure 12(d) a power time series from WEC, array and farm are plotted together to illustrate the power quality improvement as power is aggregated. The power in each case is normalized to the rated power of the unit. A small energy storage seems favorable given the high fluctuations still present on the farm power output, but it is not necessarily required to be located in the farm connection point. If distributed energy storages were instead installed on each of the arrays, and controlled or tuned to compensate the aggregated fluctuations on the farm output, the energy storage could serve dual purposes by also reducing the array peak-to-average power, which would further improve the power quality before transformation to AC. This may save the expensive converter capacity and must be subjected to detailed economical investigation.

To investigate further the frequency components causing the fluctuations, a frequency analysis of the output power was performed. Figure12(e) shows the result of a fast Fourier transform (FFT) analysis during the different power stages. Power is normalized to rated output for each stage. In general, the figure shows the expected characteristics with a decreasing level of distortion as power is aggregated. The peak of the spectrum coincides well with the wave period, and it can be seen how the farm has high attenuation at 0.1 Hz and significantly lower attenuation at 0.01 Hz in comparison with the WEC. The local minimum observed at 0.05 Hz on both the farm output and the array output is expected to be caused by low excitation in combination with good attenuation at this frequency. The frequency plot can serve as a powerful tool when optimizing the farm layout.

As an illustration of the utilization of installed power capacity, Figure 12(f) shows the power/time distributions at the three farm levels. The plot is created by sorting all the points in Figure 12(d) in descending order. This plot is an effective tool for optimizing the the power components in the power transfer chain as it visualizes the energy that is produced on various power levels. For instance, it shows that both the array and the farm output have steep inclines close to the y-axis. The allowed peak power of the power transfer equipment can be drawn as horizontal lines on the plot. The area between output power line and the horizontal line will then represent lost power due to the transfer capacity deficit, while the area below the horizontal line represents the power that can be transferred. For instance, it can be seen directly from the figure that the array peak-to-average transfer capacity can be reduced from 2.5 to 2.0 with only a small energy sacrifice. As these curves currently represent only one wave state, they should be used with care. When a complete analysis is performed, these data serve as valuable inputs to the economical cost model.

Thus far, the analysis has only been performed for the design wave state, and for the optimal wave direction. A complete analysis should be performed, taking into account all sea states and directions encountered throughout a year to find the annual produced energy with the given system configuration. The smoothing effects will be less efficient from unfavorable wave directions and will cause higher peak production than the installed capacity. This is not a problem in and of itself, but will force the WECs to hold back production and exporting less power due to the downstream restrictions. A thorough analysis with annual data will show the exact amount of power shedding and give a good basis for detailed scaling of the power components. However, based on experience from our previous work [13], and given the strong directionality at the Wavehub site, which is the basis of this work, it is believed that the current findings are realistic and only require minor adjustments after a comprehensive analysis.

5. Conclusions

This work shows that a wave energy farm can be grid connected with adequate power quality and good utilization of installed transfer capacity without major power conditioning components. The power transfer chain is believed to be economically efficient, although some components within the wave farm require significant over-capacity. Earlier studies of annual power have shown annual full-load export capacity of approximately 3500 hours per year [14], and with the improvements that the farm configuration brings, it is believed that an annual full-load export capacity of more than 4000 hours per year will be attainable. This is better than land-based wind turbines which, on average, provide approximately 2500 full-load hours per year [20], and is believed to be competitive with offshore wind farms. This analysis has been performed only on the most dominant wave state, and therefore future work should involve a complete study based on the annual wave climate.

Acknowledgment

We would like to thank the Norwegian Research Council, whose funding for the industrial PhD project of Jonas Sjolte made it possible to publish this work.

References

1. Tissandier, J.; Babarit, A.; Clement, A. Study of the Smoothing Effect on the Power Production in an Array of SEAREV Wave Energy Converters. In Proceedings of the International Offshore and Polar Engineering Conference, Vancouver, Canada, 6 July 2008.
2. Kavanagh, D.; Keane, A.; Flynn, D. Challenges Posed by the Integration of Wave Power onto the Irish Power System. In Proceedings of the EWTEC11 Conference, Southampton, England, 5 Sept 2011.
3. Blavette, A.; O'Sullivan, D.; Lewis, A.; Egan, M. Impact of a wave farm on its local grid: Voltage limits, flicker level and power fluctuations. In Proceedings of the OCEANS Conference, Virginia, USA, 14 Oct 2011.
4. Salter, S.H. World progress in wave energy 1988. *Int. J. Ambient Energy* **1989**, *10*, 3–24.

5. Bjerke, I.; Hjetland, E.; Tjensvoll, G.; Sjolte, J. Experiences from Field Testing with the BOLT Wave Energy Converter. In Proceedings of the European Wave and Tidal Energy Conference (EWTEC11), Southampton, England, 5 Sept 2011.
6. Pitt, E. G. The wave power climate at the Wave Hub site. *Appl. Wave Res. Rev. Wave Power Clim.* **2006** @ONLINE. Available online: http://ebookbrowse.com/november-2006-applied-wave-research-review-of-wave-power-climate-pdf-d256126921. (accessed on 26 Mar 2013).
7. Falnes, J.; Lillebrekken, P.M. Budal's Latching-controlled-buoy Type Wave-power Plant. In Proceedings of the 5th European Wave Energy Conference, Cork, Ireland, 17 Sept 2003.
8. Falnes, J.; Hals, J. Heaving buoys, point absorbers and arrays. *Philos. Trans. R. Soc. Math. Phys. Eng. Sci.* **2012**, *370*, 246–277.
9. Falnes, J. *Ocean Waves and Oscillating Systems: Linear Interactions Including Wave-Energy Extraction*; Cambridge University Press: Cambridge, UK, 2002.
10. Sjolte, J.; Bjerke, I.; Crozier, A.; Tjensvoll, G.; Molinas, M. All-Electric Wave Energy Converter with Stand-alone 600VDC Power System and Ultracapacitor Bank. In Proceedings of the 2012 EVER International Conference and Exhibition on Ecological Vehicles and Renewable Energies, Monte Carlo, Monaco, 22 Mar 2012.
11. Sjolte, J.; Bjerke, I.; Crozier, A.; Tjensvoll, G.; Molinas, M. All-electric Wave Energy Power Take Off System with Improved Power Quality at the Grid Connection Point. In Proceedings of the Transmission and Distribution Conference and Exposition (T D), 2012 IEEE PES, Orlando, USA, 7 May; Publisher: IEEE 2012; pp. 1–7.
12. Sjolte, J.; Tjensvoll, G.; Molinas, M. All-electric Wave Energy Converter Connected in Array with Common DC-link for Improved Power Quality. In Proceedings of the Power Electronics for Distributed Generation Systems (PEDG), 2012 3rd IEEE International Symposium on, Ålborg, Denmark, 25 June 2012; pp. 431–436.
13. Sjolte, J.; Tjensvoll, G.; Molinas, M. Annual Energy and Power Quality from an All-Electric Wave Energy Converter Array. In Proceedings of the European Power Electronics and Motion Control and Applications Conference (EPE-PEMC'12), Novi Sad, Serbia, 4 Sept 2012.
14. Sjolte, J.; Tjensvoll, G.; Molinas, M. All-electric Wave Energy Converter Array with Energy Storage and Reactive Power Compensation for Improved Power Quality. In Proceedings of the Energy Conversion Congress and Exposition (ECCE), 2012 IEEE, Raleigh, USA, 15 Sept; Publisher: IEEE 2012; pp. 954–961.
15. Molinas, M.; Skjervheim, O.; Andreasen, P.; Undeland, T.; Hals, J.; Moan, T.; Sorby, B. Power Electroncis as Grid Interface for Actively Controlled Wave Energy Converters. In Proceedings of the Technical Report, International Conference on Clean Energy Power (ICCEP07), Capri, Italy, 21 May 2007.
16. Skjervheim, O.; Sorby, B.; Molinas, M. All Electric Power Take Off for a Direct Coupled Point Absorber. In Technical Report, Proceedings of the 2nd International Converence on Ocean Energy (ICOE2008), France, Brest, 15 Oct 2008.
17. Sjolte, J.; Bjerke, I.; Hjetland, E.; Tjensvoll, G. All-Electric Wave Energy Power Take Off Generator Optimized by High Overspeed. In Proceedings of the Submitted to the European Wave and Tidal Energy Conference (EWTEC11), Southampton, England, 5 Sept 2011.

18. Joint North Sea Wave Observation Project (JONSWAP)@ONLINE. Available online: http://www.wikiwaves.org/Ocean-Wave_Spectra (accessed on 26 Mar 2013).
19. Newman, J. *Marine Hydrodynamics*; MIT Press: Cambridge, MA, USA, 1977.
20. Table of capacity factors for various sources of power generation. Available online: http://en.wikipedia.org/wiki/Capacity_factor (accessed on 26 Mar 2013).

Appendix J

Journal paper 2

Title: Exploring the Potential for Increased Production from the Wave Energy Converter Lifesaver by Reactive Control

Conference/Journal: International Journal on Energies

Date: 25. July 2013

Location/Publisher: MDPI, Open access

Energies **2013**, *xx*, 1-x; doi:10.3390/——

OPEN ACCESS

energies

ISSN 1996-1073

www.mdpi.com/journal/energies

Article

Exploring the Potential for Increased Production from the Wave Energy Converter Lifesaver by Reactive Control

Jonas Sjolte [1,2,*], Christian McLisky Sandvik [2], Elisabetta Tedeschi [3] and Marta Molinas [2]

[1] Fred. Olsen, Fred. Olsens Gate 2, N0152 Oslo, Norway

[2] Department of Electric Power Engineering, Norwegian University of Science and Technology, O.S. Bragstads plass 2E, N-7034 Trondheim, Norway; E-Mails: mcliskysandvik@gmail.com (C.M.S.); marta.molinas@ntnu.no (M.M.)

[3] SINTEF Energy Research, Postbox 4761 Sluppen, Trondheim 7465, Norway. Email: tedeschi@ieee.org

* Author to whom correspondence should be addressed; E-Mail: jonas.sjolte@ntnu.no; Tel.: +47-223-411-45; Fax.: +47-223-424-15.

Received: 5 March 2013; in revised form: 22 May 2013 / Accepted: 23 June 2013 / Published: xx

Abstract: Fred Olsen is currently testing their latest wave energy converter (WEC), Lifesaver, outside of Falmouth Bay in England, preparing it for commercial operation at the Wavehub test site. Previous studies, mostly focusing on hydrodynamics and peak to average power reduction, have shown that this device has potential for increased power extraction using reactive control. This article extends those analyses, adding a detailed model of the all-electric power take-off (PTO) system, consisting of a permanent magnet synchronous generator, inverter and DC-link. Time domain simulations are performed to evaluate the PTO capabilities of the modeled WEC. However, when tuned towards reactive control, the generator losses become large, giving a very low overall system efficiency. Optimal control with respect to electrical output power is found to occur with low added mass, and when compared to pure passive loading, a 1% increase in annual energy production is estimated. The main factor reducing the effect of reactive control is found to be the minimum load-force constraint of the device. These results suggest that the Lifesaver has limited potential for increased production by reactive control. This analysis is nevertheless valuable, as it demonstrates how a wave-to-wire model can be used for investigation of PTO potential, annual energy production estimations and evaluations of different control techniques for a given WEC device.

Keywords: wave energy; reactive control; lifesaver; wave-to-wire model; power take-off; point absorber

1. Introduction With increasing oil prices and the consequent focus on shifting the world energy-dependency towards renewable resources, wave energy has regained increased attention. It is estimated that when today's technology is fully matured, around 140–750 TWh will be commercially exploitable annually [1]. If all potential technology is realized, this number can be greatly increased, with some scenarios as large as 2,000 TWh, corresponding to approximately 10% of the global electricity consumption in 2008 [2]. One of such technologies, developed by the Fred Olsen Wave Energy Project *Bolt2Wavehub*, named *Lifesaver*, was deployed in early 2012 as a stand-alone system at Falmouth Bay, England. The next step is to make it commercially ready and launch it at Wavehub [3].

The control method used on the *wave energy converter* (WEC) greatly affects the output power, and the selection and optimization of control method for the Lifesaver system will be the focus of this work. The theoretical control method for optimal power extraction is well-established, thanks to the pioneering work of Falnes [4,5]. He shows that the optimal power extraction occurs when the system is controlled with a 90° phase-shift between wave motion and absorber motion, a method referred to as *complex-conjugate* control or *reactive* control. Due to the irregular nature of ocean waves, such a production mode can only be maintained by active control of the power extraction system and requires the real-time phase and frequency information of the incoming waves. Falnes and his team have suggested practical solutions and optimization methods toward this [6,7], but attaining accurate real-time wave information has proven difficult, and several methods of sub-optimal control have been suggested to make up for this [8].

During the current deployment, the performance of the Lifesaver *power take-off* (PTO) and the impact of the control strategy on the PTO is of great interest. The design process of Lifesaver has shown that the production machines are by far the most expensive component in the system and that the absorber hull is relatively cheap in comparison. This forces a major shift in control strategy from the traditional control method that focuses on maximizing the absorber output. Instead, Lifesaver is optimized towards maximizing the PTO utilization, which leads to a control method based on damping, where the production force is proportional to the absorber speed. In this control mode, the production force are in phase with the production speed and are referred to as *active forces*, as opposed to a complex-conjugate control that requires *reactive forces*, which reduce the PTO utilization [9]. The damping control selected at Lifesaver also avoids the need of real-time wave information and allows for a simple and robust time-invariant control.

However, initial investigations indicate that Lifesaver might have potential for increased power extraction with reactive control during calmer sea states [10], by utilizing free production capacity. These investigations have so far focused on the hydrodynamic model of the WEC and on optimizing average power while reducing the peak-to-average power ratio, while less attention has been paid to the physical limitations of the generator, switchgear and the rest of the PTO system. The purpose of this

study is therefore to develop a full wave-to-wire model of Lifesaver with an all-electric PTO system. The model is used to evaluate the effect of different control strategies on the PTO capabilities under different sea state conditions. Such a study is interesting, since the power extraction capabilities of a WEC device will be strongly dependent on the impact of the control strategy implemented. Depending on the WEC device, parameters and physical constraints of the PTO system, a control strategy with a reactive component can potentially increase the energy production and, therefore, be an important factor for the commercial exploitation possibilities of the WEC concept.

1.1. Description of the Investigated System

Lifesaver consists of five point absorbers with individual PTO systems connected together on a toroid shaped device. The PTOs are all-electric systems sharing a common DC-Link and uses an electric energy storage to power the generators and to maintain continuous rope tension. This means that each generator will have to operate in motoring mode and wind in the rope on downward movement of the device, meaning that some energy will have to be supplied to the system in this part of the oscillatory cycle. Having the PTOs on a common platform gives obvious economical advantages and allows, among other things, to utilize the pitching motion created on the device by the sea. Lifesaver is pictured on site outside Falmouth, England, in Figure 1. Figure 2 illustrates the function of the PTO and WEC system.

Figure 1. *Lifesaver* on site outside Falmouth, England.

For the purpose of this study, a simplified representation of the system is defined, which consists of a single point absorber coupled to an all-electric PTO system (generator and inverter including the DC-link). This module is defined as the basis for the design of the wave-to-wire model in this paper. To model the full Lifesaver system, several modules are employed in parallel to simulate multiple PTOs. Lifesaver is prepared for operation with five PTOs, which is the basis for this work, but currently only operates with three PTOs.

Figure 2. Lifesaver power take-off (PTO) function.

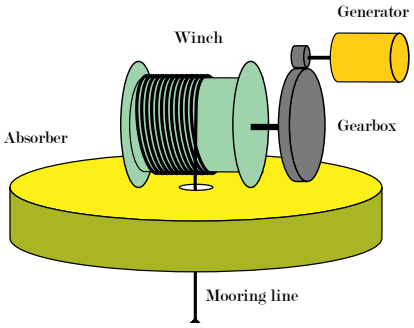

2. Hydrodynamic Model

The hydrodynamic model of Lifesaver has the following input:

- Wave elevation time-series;
- Load force, F_L, given by the load force parameters, damping, B_L, and added mass, M_L.

The output of the model is the velocity, $\dot{\eta}$, and acceleration, $\ddot{\eta}$, of the device. In this work, the hydrodynamic model is realized as a one *degrees of freedom* (DOF) model and only models heaving motion. In simulation work that demands high accuracy, we use a more complex three-DOF model that takes into account heaving, surging and pitching motion. However, as this work focus on the electrical performance, with a relative comparison of the output result, we believe that the simplified one-DOF model is sufficient for this work.

2.1. Generation of Wave Elevation Time Series

A common way to model the sea is by using an energy spectrum. There are various mathematical models that are used for defining such spectra, and the most widely known is the two-parameter Bretschneider spectrum [11]. The preferred analytical form of the frequency spectrum, $S(\omega)$, is given in Equation (1).

$$S_{(\omega)} = \frac{5}{16} H_s^2 \frac{\omega_0^4}{\omega^5} e^{-\frac{5\omega_0^4}{4\omega^4}} \tag{1}$$

here, H_s is the significant height of the sea state; and ω_0 is the peak frequency. Figure 3 shows the Bretschneider spectra for different values of the peak frequency. The time-domain wave elevation of the real sea waves can be regarded as the super-position of different frequency sinusoidal waves. Thus, the energy spectrum can be used to represent the sea by summing a large, but finite, number of different frequency components of infinitesimal height and random phase. The elevation due to each such wave components can be expressed by Equation (2) [12].

$$\zeta_n(t) = \sqrt{2S(\omega_n)d\omega}\sin(\omega_n t + \phi_n) \tag{2}$$

here, ϕ_n is the randomly generated offset angle for each wave component; n. By summing these waves, the wave elevation time-series is created as described by Equation (3). A typical output time-series is plotted in Figure 4.

Figure 3. Bretschneider spectra for different values of the peak period, $T_p[s]$.

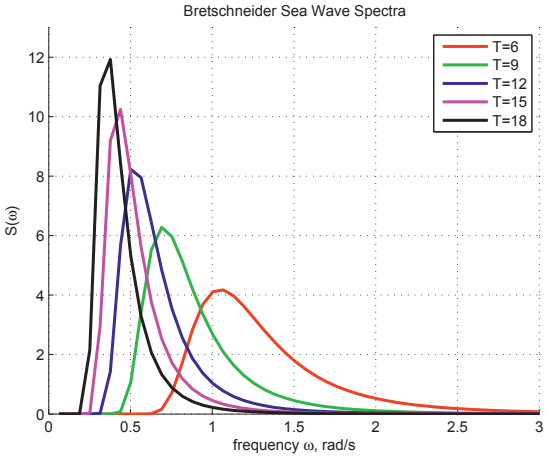

$$\zeta(t) = \sum_{n=1}^{N} \sqrt{2S(\omega_n)d\omega}\sin\left(\omega_n t + \phi_n\right) \tag{3}$$

Figure 4. Time-series of a Bretschneider spectrum, $H_s = 7m$ and $T_p = 11s$.

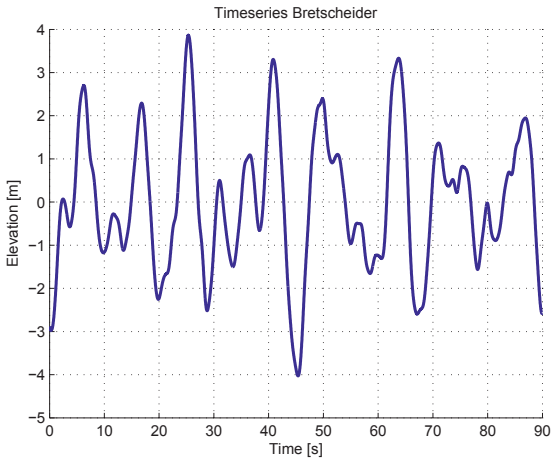

2.2. Forces Acting on the WEC System

$$M\ddot{\eta} = f_e(t) + f_s(t) + f_r(t) + f_m(t) \tag{4}$$

Equation (4) calculates the force balance for a buoy excited by an incoming wave, where η is the device position with respect to the equilibrium position; and M is the equivalent mass of the WEC system, consisting of the mass of the WEC and the inertia of the power take off system [13]. f_e is the excitation force; f_r is the radiation force; f_m is the machinery force, or the force related to the power take off system; and f_s represents the hydrostatic force. In this model, the mooring forces, viscous forces and environmental forces are disregarded.

2.2.1. Hydrostatic Force

The hydrostatic force is the resultant force of gravitational forces and forces acting on the buoy due to displaced water and is calculated with Equation (5), where k_s represents the hydrostatic stiffness. Commonly, the stiffness is considered a constant value, and thus, the force is proportional to device displacement, η [8].

$$f_s = k_s\eta \tag{5}$$

2.2.2. Radiation Force

An oscillating device will create a diffraction wave, and the force acting on the device due to this wave is referred to as the radiation force. In the frequency domain, it is typically expressed by Equation (6), where m_r is the added mass of the water oscillating with the device and R_r is the radiation resistance. As these parameters are frequency dependent, the time domain expression of the radiation resistance can be described by Equation (7) [14].

$$\hat{F}_R(\omega) = m_r(\omega)\ddot{\eta} + R_r(\omega)\dot{\eta} \tag{6}$$

$$F_r(t) = m_r(\infty)\ddot{\eta} + \int_0^t k(t-\tau)\dot{\eta}(\tau)d\tau \tag{7}$$

In the first term of the right-hand side of this expression, $m_r(\infty)$ is the added mass at infinite frequency. The second term is a convolution integral, where the convolution kernel, k, can be considered the radiation force impulse response. As discussed by Hals [8], a good approximation is to replace this convolution term by the state-space equivalent represented by Equations (8) and (9).

$$F_r(t) = \mathbf{C}_k\mathbf{z}(t) + \mathbf{D}_k\dot{\eta}(t) \tag{8}$$

$$\dot{\mathbf{z}}(t) = \mathbf{A}_k\mathbf{z}(t) + \mathbf{B}_k\dot{\eta}(t) \tag{9}$$

Taghipour, Perez and Moan show in [15] how the *Realization Theory* can be used in order to identify the state-space parameters, $\mathbf{A}_k$, $\mathbf{B}_k$, $\mathbf{C}_k$ and $\mathbf{D}_k$. By identifying the discrete radiation impulse response

through inverse Fourier transform of $k(\omega)$, as shown in Equation (10), a state-space system with a corresponding impulse response is generated.

$$k(\omega) = i\omega\{m_r(\omega) - m_r(\infty)\delta(\omega)\} + R_r(\omega) \tag{10}$$

The values for radiation resistance and the added mass of Lifesaver in the frequency domain are known and supplied by Fred Olsen for a range of frequencies. This impulse response fitting is realized using the Matlab Robust Toolbox function *imp2ss*, which is based on the Hankel Singular value decomposition proposed by Kung [16]. Using this, a state-space system is generated and a good representation of the radiation force is obtained. A more thorough explanation of how the radiation force is modeled for Lifesaver is given in [10].

2.2.3. Excitation Force

The force that the incident wave exerts on the WEC body is called the excitation force. It is given by the elevation of the sea, ζ, and the excitation force coefficient, $H_{F\zeta}$, as defined in Equation (11).

$$F_{e,c}(\omega) = H_{F,\zeta}(\omega)\zeta(\omega) \tag{11}$$

this coefficient is known and supplied by Fred Olsen for a range of frequencies. In a similar way, as for the radiation force, the time domain expression of the excitation force becomes a convolution term [8], as described by Equation (12).

$$F_{e,c}(t) = \int_0^t h_{F\zeta}(t - \tau_c)\zeta(\tau)d\tau \tag{12}$$

A state space representation of the convolution term is then found in the same manner as outlined for the radiation force; by impulse response fitting with the discrete excitation force impulse response extracted from the excitation force coefficients.

2.2.4. Load Force

The load force, F_L, or machinery force, is the force applied to the system by the PTO. The magnitude of this force, and how this force is applied, greatly influences the power extraction capabilities of the WEC. Typically, the load force is represented by one component proportional to the device velocity and a second component proportional to the device acceleration, as stated by Equation (13). B_L is considered the machinery damping; while M_L is the machinery added mass. Input into the wave-to-wire model is therefore either the load force or the load force parameters.

$$F_L = B_L\dot{\eta} + M_L\ddot{\eta} \tag{13}$$

3. Electric Power Take-off System

The Lifesaver PTO system, which is the basis for the model developed in this article, is all-electric. The stand-alone system, currently deployed outside the coast of England, consists of the following components:

- Permanent Magnet Synchronous Machine;
- Inverter/Rectifiers;
- Ultra-capacitor Bank;
- DC-link Charger;
- Battery Charger;
- Brake Charger and Dump Resistor.

In Lifesaver, all the PTO rectifiers are coupled in a common DC-link, as illustrated in Figure 5. The point absorber with PMSMand an inverter/rectifier is considered a complete system, which only needs to connect to a DC-link to operate. The scope of this section is to model one such module and to consider the DC-link as a constant voltage of 600 V. The electric system considered for the model is shown in Figure 6. The main specifications of the PTO, as defined by Fred Olsen, are given in Table 1.

Figure 5. Current topology of the stand-alone system for Lifesaver.

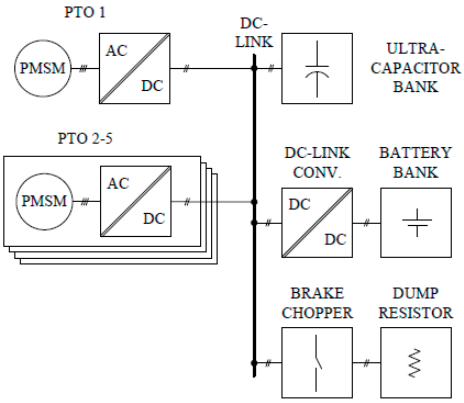

Figure 6. Schematic representation of the all-electric PTO system.

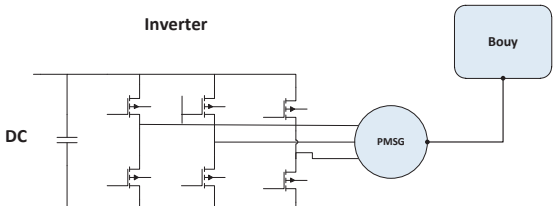

Table 1. Lifesaver PTO characteristics.

Property	**Value**	**Unit**
Generator nominal speed	400	rpm
Generator maximum torque	3700	Nm
DC-bus voltage	600	V
Angular to linear gear ratio	38.5	1/m
PTO maximum force	100	kN
PTO minimum force	10	kN
PTO nominal speed	1.1	m/s

3.1. PWM Converter Modeling

The PWMconverter is modeled with a time constant equal to unity in the comparably slow wave energy system. This implies that the voltage applied by the converter is considered to follow the reference voltage perfectly and instantly. This approach has the following advantages:

- Simulation time is significantly reduced. Even for low switching frequencies in the converter bridge, the simulation time becomes tenfold times longer than with the unity block solution;
- No filter is needed in the system in order to evaluate voltage measurements, as the harmonic distortion due to the high frequency switching is not present.

For the simulations that are being performed in this article, there are two important attributes to consider for the PWM converter. One is the maximum value of the voltage, which is set by the constant value of the DC-bus, and the other is the losses that occur in the converter. The first condition is handled by direct saturation of the voltage in the current controller and by advanced field-weakening control, as explained later. The losses are more difficult to evaluate, since not enough data is available of the converter used in the Lifesaver system. However, the inverter efficiency is included in the efficiency model provided in Section 3.3, so that a complete figure for the mechanical to electrical conversion efficiency is produced. The inverter losses are small compared to the generator and contributes with 3%–10% of the total losses.

3.2. Modeling and Control of the Permanent Magnet Synchronous Generator

In this model of the Lifesaver PTO, the generator is considered a 28 pole surface-mounted PMSM. The generator characteristics used for the model are given in Table 2.

For given voltages, u_q and u_d, on the generator terminals, the current equations for the PMSM are commonly expressed as stated by Equations (14) and (15) [17].

$$\frac{di_d}{dt} = -\frac{R_S}{L} i_d + \omega_e i_q + \frac{1}{L} u_d \tag{14}$$

$$\frac{di_q}{dt} = -\frac{R_S}{L} i_q - \omega_e \left(i_d + \frac{\Psi_{PM}}{L} \right) + \frac{1}{L} u_q \tag{15}$$

here, ω_e is the electric angular frequency of the generator; i_d and i_q are the d- and q-axis current; Ψ_{PM} is the rotor permanent magnet flux; while R_s and L are the stator resistance and inductance, as defined in Table 2. For a surface mounted PMSM, the inductance in the d- and q-axis can be considered equal.

Table 2. Generator characteristics.

Property	**Value**	**Unit**
Rated Power, P_n	83.7	kW
Rated Voltage, V_n	400	V
Number of Poles, n_p	28	
Torque Constant, k_T	10.8	Nm/A
Winding Resistance, R_s	0.038	Ω
Inductance, L	1.4	mH
Inertia, J_{gen}	1.31	kgm^2
Permanent Magnet Flux,Ψ_{PM}	0.257	Wb

3.2.1. Current Control

As is known from d-q reference frame analysis [17], there is a cross coupling between the q-axis and the d-axis in Equations (14) and (15). This can be avoided by feed-forward technique, defining a reference voltage, $v_d = u_d + \omega_e L i_q$ and $v_q = u_q - \omega_e L i_d - e_q$. This gives two independent first-order equations in the d-q frame, as given by Equations (16) and (17). The transfer functions from current, i; to voltage, v, can thus be written as stated by Equation (18).

$$v_d = R_s i_d + L_s \frac{di_d}{dt} \tag{16}$$

$$v_q = R_s i_q + L_s \frac{di_q}{dt} \tag{17}$$

$$\frac{i(s)}{u(s)} = \frac{\frac{1}{R_s}}{1 + \frac{L_s}{R_s} s} \tag{18}$$

These current loops are controlled using PIregulators. Figure 7 shows the block diagram with the PI-controller, PWM and converter bridge included. As discussed earlier, the transfer block of the PWM and converter bridge is set to be unity.

Figure 7. Block diagram of current control loop. Notably, the PWM + converter block is represented by a unity gain.

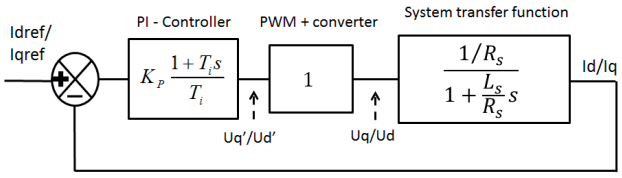

The parameters of these PI regulators are tuned according to the modulus optimum [18], canceling out the electrical time constant, $T_i = \frac{L_s}{R_s}$. This results in the open-loop transfer function expressed in Equation (19). Determination of gain, K_p, is done through evaluating the term for the closed loop transfer function. As it is desirable to have a closed loop transfer function gain equal to unity, a value for K_p can be approximated.

$$G_{OL} = K_p \frac{1 + T_i s}{T_i s} \frac{\frac{1}{R_s}}{1 + \frac{L_s}{R_s} s} = K_p \frac{\frac{1}{R_s}}{\frac{L_s}{R_s} s} = K_p \frac{1}{L_s s} \tag{19}$$

$$M(\omega) = \frac{G_{OL}}{1 + G_{OL}} = \frac{K_p}{L_s j\omega + K_p} = 1 \tag{20}$$

To obtain unity closed-loop gain, $K_p >> L_s\omega$, as shown in Equation (20). As the value for $L_s = 1.4$ mH and $\omega_{e,max} < n_{max} \frac{2\pi}{60} n_{pp} \approx 5,000$, it is considered that $K_p = 25$ is sufficiently large for all operation areas. In Figure 8, the current control with de-coupling and PI controllers is shown implemented in the Simulink block, named *current control*.

Figure 8. Current control implemented in Simulink.

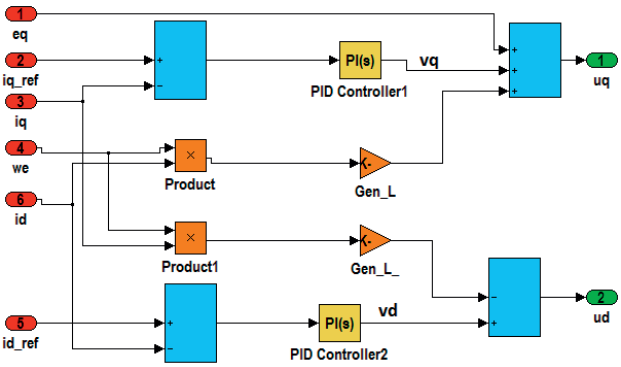

3.2.2. Torque Control

In order to make sure that the limitations of the electric PTOs are not exceeded, torque control is required. For low-speed operation, this is realized by maintaining a constant damping, B_L, and added mass, M_L. However, control is required to saturate the load-force at its maximum value, as well as to implement the field weakening control reference current-values. Initially, the torque control method over the entire range of operation speeds is designed to function as described in Figure 9. Here, I_{min} refers to the minimum torque constraint to keep tension in the rope.

The input into the torque-control flowchart in Figure 9 is the i_q reference current and the generator speed, ω_e. The reference current is obtained based on the reference torque from Equation (21). The reference torque is calculated from the mechanical model of the wave energy converter in Equation (22),

where ρ_g is the total gear ratio, including the linear-to-rotational radius, thus having the unit, $[\frac{1}{m}]$. The generator speed is also calculated from the mechanical model and is given by Equation (23).

$$i_{q,ref} = \frac{T_{e,ref}}{\frac{3}{2} n_p \Psi_{PM}} \tag{21}$$

$$T_{e,ref} = \frac{1}{\rho_g} (B\dot{\eta} + M_L \ddot{\eta}) \tag{22}$$

$$\omega_e = n_p \rho_g \dot{\eta} \tag{23}$$

Figure 9. Flowchart representing the idea behind the determination of current reference for the torque control.

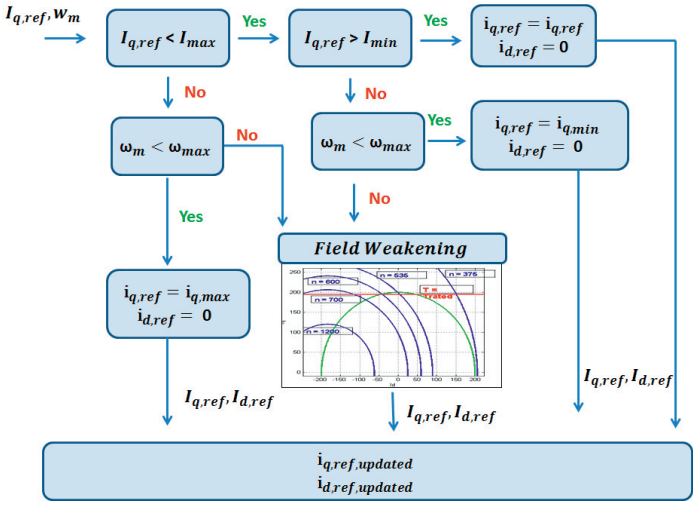

The speed at which field weakening begins, $\omega_{max} = \omega_{fw}$, can be expressed by the generator characteristics, as seen in Equation (24). The method used for determining the field weakening reference d- and q-axis currents is based on the robust field weakening control strategy described by (Pan and Liaw, 2005) [19].

$$\omega_{fw} = \frac{-2R_s I_{max} \Psi_{PM} + \sqrt{(2R_s I_{max} \Psi_{PM})^2 - 4(\Psi_{PM}^2 + L I_{max}^2)(R_s^2 I_{max}^2 - V_{max}^2)}}{2(\Psi_{PM}^2 + L^2 I_{max}^2)} \tag{24}$$

3.3. Generator Efficiency

As the detailed properties of the generator and converter are not known, it is not possible to make an accurate model of the system losses based on theoretical analysis. However, from the manufacturer of the generator and converter module, the efficiency at a number of operating points have been provided to Fred Olsen. This has been used to develop a polynomial expression for the combined generator and

converter losses as a function of generator torque, T_e; and speed, ω_e, as given by Equation (25). Due to a confidentiality agreement with the manufacturer, the actual figures cannot be disclosed. However, the resulting efficiency map plotted in Figure 10 gives a good understanding of the system performance.

$$P_{loss} = a_1 T_e^4 + a_2 T_e^2 + a_3|\omega_e| + a_4\omega_e^2 + a_5|\omega_e||T_e| + a_6|\omega_e|T_e^2 \tag{25}$$

Figure 10. Generator and converter efficiency map.

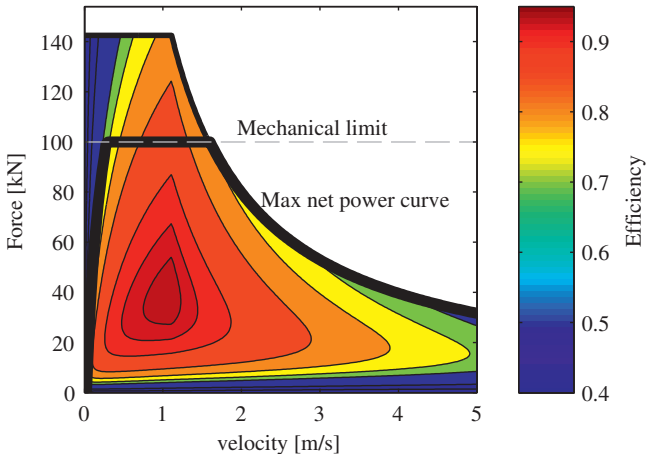

4. Wave-to-Wire Modeling

The complete wave-to-wire Simulink model of the WEC system of Lifesaver is shown in Figure 11. Previous investigations [10] show a large increase in average generated power when complex conjugate control is applied to the Lifesaver buoy. To further investigate this potential, full wave-to-wire simulations will be performed, where the physical limitations and efficiency of the all-electric PTO system are also included. When the control is being referred to as *complex conjugate*, it is meant that the load parameters are being tuned according to complex conjugate control equations [9] in the non-saturated mode of operation.

4.1. Simulation Results for a Passive Loaded System

The system is simulated for a low wave state with $H_s = 0.5\,m$ and $T_p = 6.5\,s$. The load coefficient is calculated as explained in [10] and results in damping, $B_L = 90$ kNs/m. In Figures 12 and 13, the input wave elevation and the corresponding generator speed is plotted. Notably, the generator speed is well below the torque saturation speed for the entire simulation time. The d-axis current, q-axis current and generator torque are shown in Figure 14, and in accordance with the generator speed plot, these plots show that torque saturation does not occur for this simulation. The constant zero d-axis current

also indicates that field weakening does not occur. The mechanical extracted power, generator losses and output electrical power is plotted in Figures 15 and 16.

Figure 11. Simulink wave-to-wire model of the wave energy converter (WEC), Lifesaver.

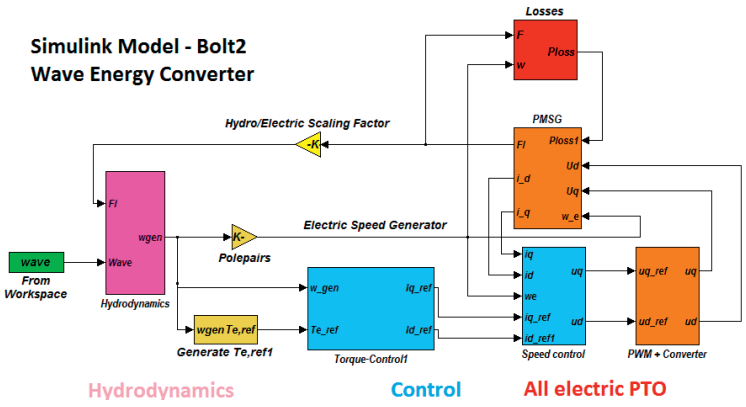

The average extracted mechanical power for this simulation is found to be 1.75 kW, and the generator losses are 0.56 kW. This gives an average efficiency of 66.85% and an electrical output power of 1.17 kW. The low efficiency is typical in low wave states, where the generator has to operate with high torque and low speed.

Figure 12. Plot showing input wave elevation time series. $H_s = 0.5\,m$ and $T_p = 6.5\,s$.

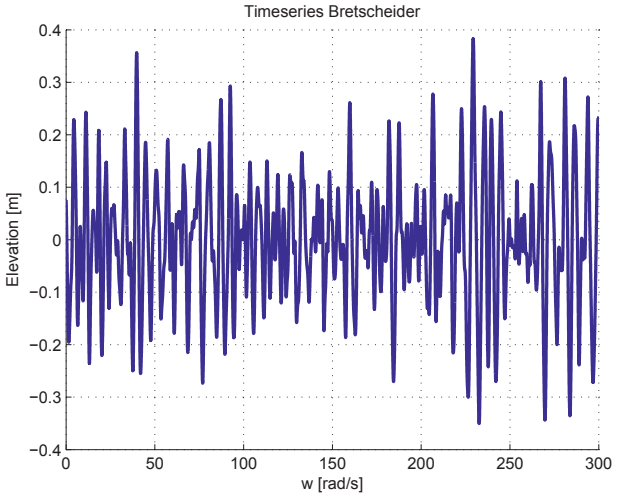

Figure 13. Generator speed for the input wave elevation shown in Figure 12. The red line indicates torque saturation speed; the black line indicates field weakening speed. The system is passively loaded.

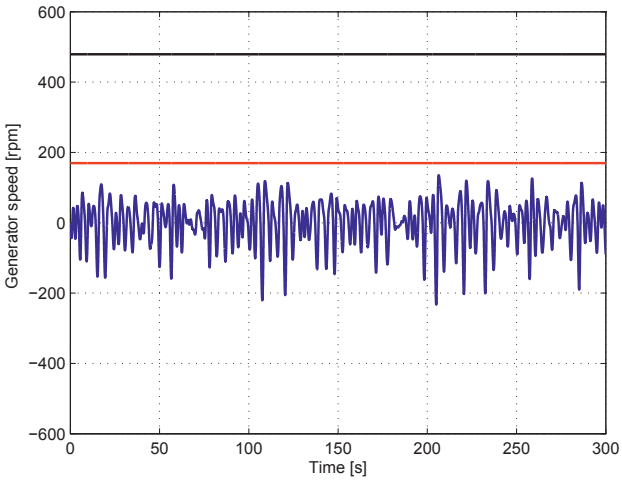

Figure 14. Converter operation for the passively loaded case.

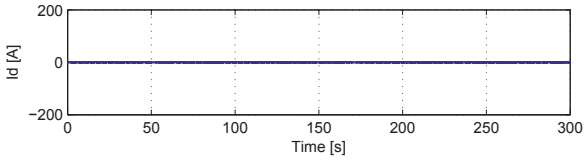

(a) D-axis current

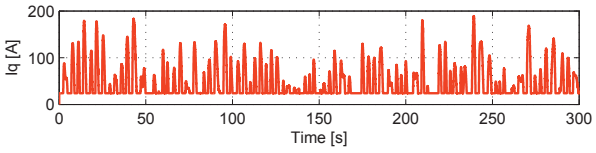

(b) Q-axis current

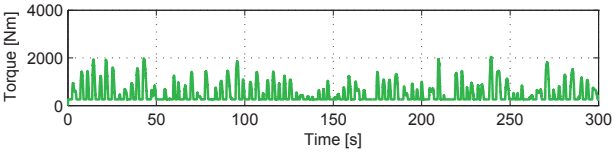

(c) Generator torque

Figure 15. Generator operation for the passively loaded case.

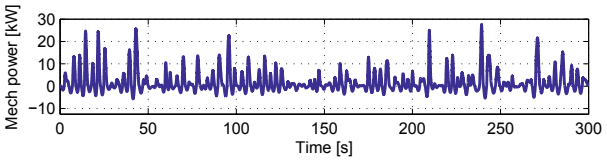

(a) Mechanical extracted power

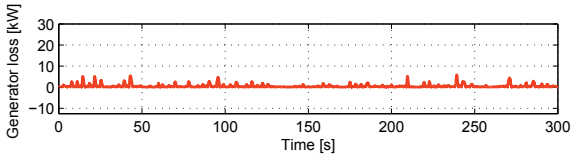

(b) Generator losses

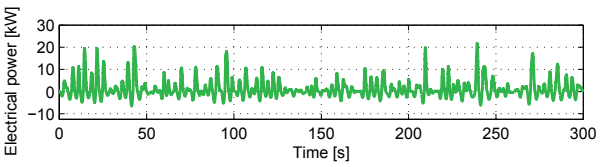

(c) Electrical output power

Figure 16. Mechanical extracted power (blue), generator losses (red) and electrical output power (green). The WEC system is passively loaded.

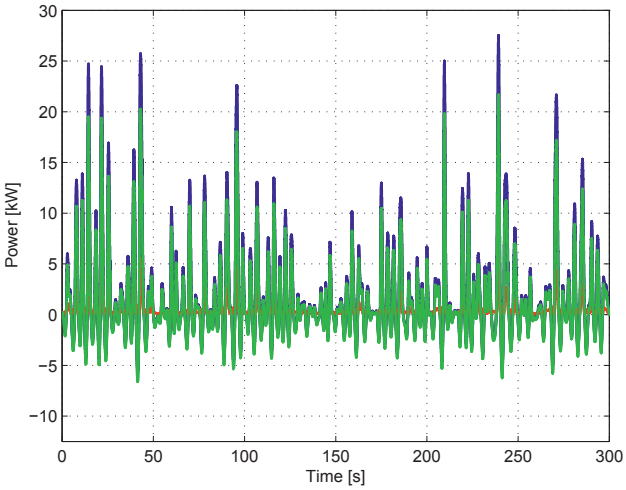

4.2. Simulation Results for a Reactive Controlled System

Now, a wave-to-wire simulation is performed for a similar wave elevation input as seen in Figure 12. The load parameters are tuned according to [10]. This gives a damping, $B_L = 22.1\ kNs/m$, and an added mass, $M_L = 84.4$ tons. The generator speed for such a controlled system can be seen in Figure 17, and as expected, the generator speed is significantly increased when compared to the reference case of passive loading shown in Figure 13. When the generator speed increases above 190.5 rpm, the q-axis current and the torque saturate, as is seen in Figure 18. In Figure 19, the generator speed and torque are plotted in the same normalized figure. In this case, in contrast to the passively loaded system, the torque is not in phase with the generator speed.

Figure 17. Generator speed for the input wave elevation shown in Figure 12. The red line indicates torque saturation speed; the black line indicates field weakening speed. The WEC system is reactively controlled.

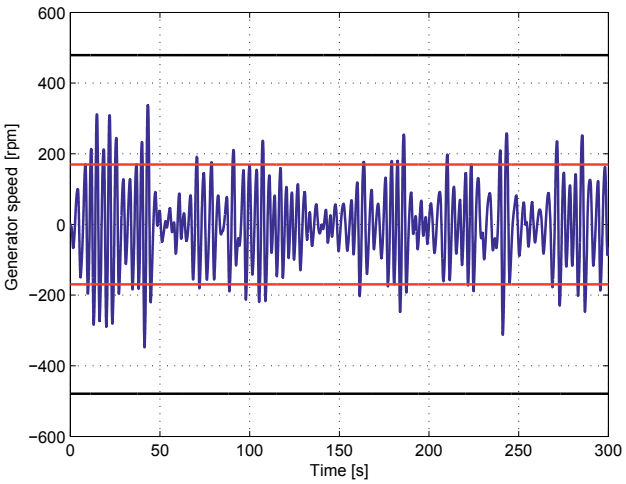

From linear control analysis, it is demonstrated that when a reactive component is added to the applied force, negative power-flow will occur [9]. This can also be understood from the plot of generator speed and force, as seen in Figure 19, where there is a phase difference between these two values. When dealing with the changing direction of the power flow, it is important to evaluate the losses correctly. In the Simulink model, the absolute value of the losses is calculated. The electrical output power is then found by Equation (26). This means that the electrical power will have lower magnitude than the mechanical power in the positive power sequence, but larger magnitude than the mechanical power when the electrical power is negative. The time domain plots for these values are plotted in Figures 20 and 21.

Figure 22 shows in a more detailed way how these powers compare to each other between 135 and 145 seconds.

$$P_{el} = P_{mech} - |P_{loss}| \tag{26}$$

Figure 18. Converter operation for the reactively loaded case.

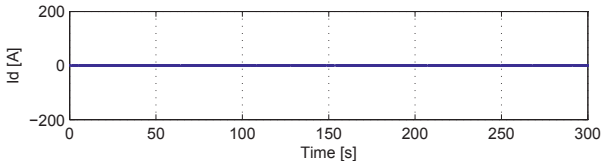

(a) D-axis current

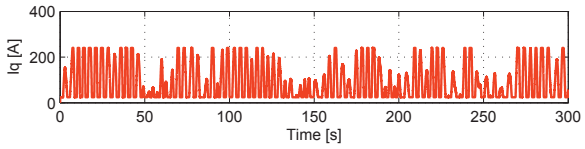

(b) Q-axis current

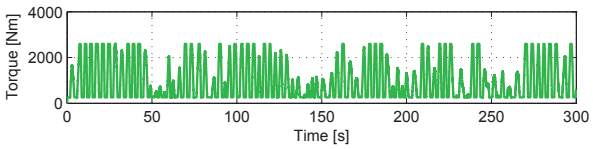

(c) Generator torque

Figure 19. Zoomed-in generator speed (blue) and generator force (red) plotted together and normalized. The WEC system is reactively controlled.

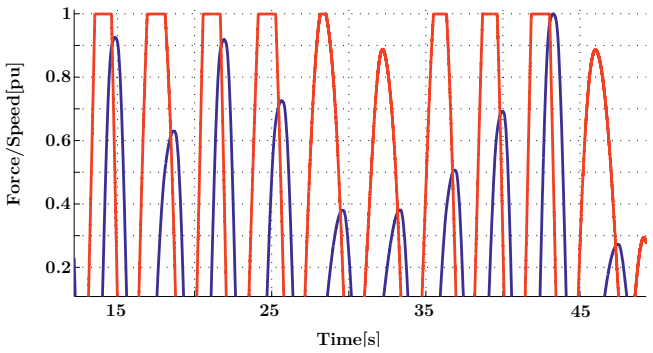

Figure 20. Generator operation for the reactively loaded case.

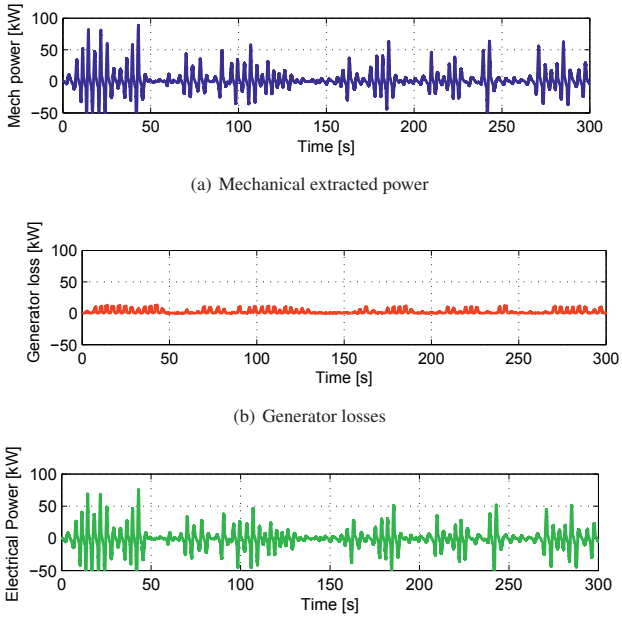

(a) Mechanical extracted power

(b) Generator losses

(c) Electrical output power

Figure 21. Mechanical extracted power (blue), generator losses (red) and electrical output power (green). The system is reactively controlled.

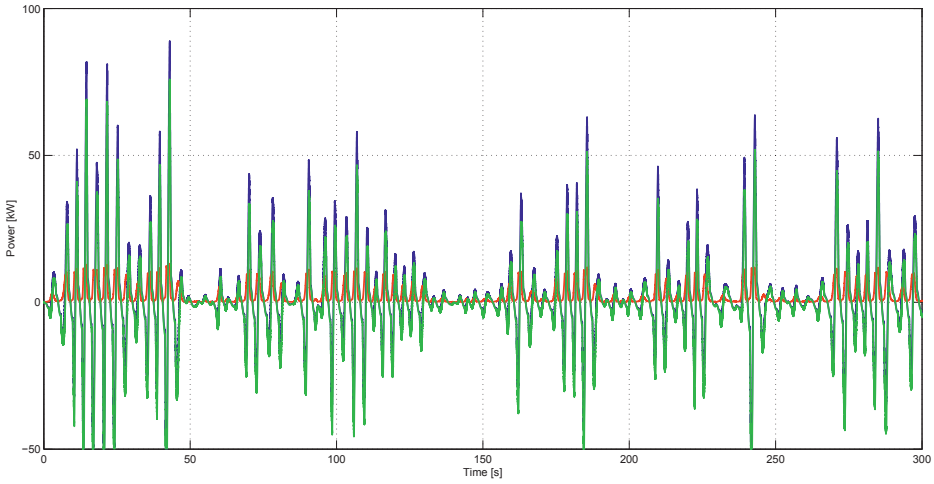

Figure 22. Close-up of mechanical extracted power (blue), generator losses (red) and electrical output power (green). The WEC system is reactively controlled.

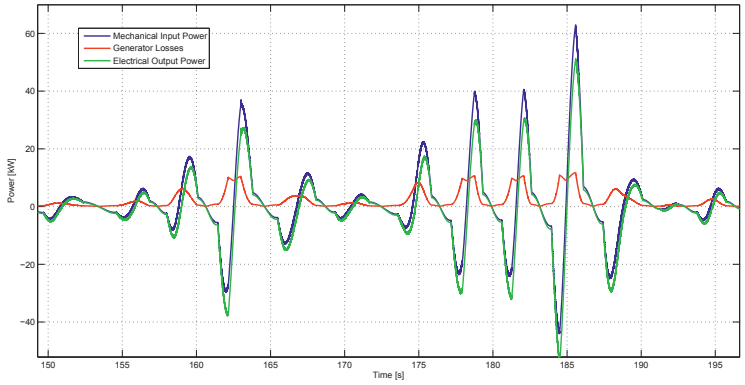

It is important to keep in mind the fact that losses do not behave bidirectionally [20] and that the accumulated average of the losses can become even larger than the average extracted mechanical power. The performed simulation is an example of this; the average extracted mechanical power is 2.57 kW, while the average losses are 2.72 kW. This means that the average output electrical power is -0.15 kW, and the permanent magnet machine consumes more power due to losses than it produces.

4.2.1. Performance of Passive Loading *vs*. Reactive Control

The key result from these simulations is that when taking generator losses into account, the performance of reactive control close to complex conjugate control is not satisfactory [9]. In fact, average delivered power to the grid is negative, meaning that in average power flows from the grid to the ocean. In order to understand why such conditions occur, a few properties about reactive control has to recognized. In order to achieve reactive control, the machinery that supplies the load force not only receives energy, but also has to return some energy. We recognize that by the increased bi-directional power flow, which results in high peaks of received power and lower peaks in returned power. On average, the power is therefore positive. However, as J. Falnes comments in [4], this calls for an energy conversion efficiency preferably close to unity, which is not the case for the Lifesaver generator. The above observations lead to the following conclusions:

- Approximate complex conjugate control leads to increased mechanical power extraction;
- However, the generator efficiency becomes more important, as the bi-directional power peaks both contribute to the average losses;
- As Lifesaver has an average generator efficiency of around 80% in the design wave state and lower efficiency in the lower wave states, the losses can become very large;
- Due to this, approximate complex conjugate control does *not* give maximum electrical power output.

In the following sections, a simulation trial for determining the optimal control parameters for a given sea state will be outlined.

4.3. Maximizing Electrical Output Power-Table for Sub-Optimal Operation Parameters

Optimal control of a wave energy converter is often thought of as the control that gives maximum power extraction or maximum energy absorbed from the sea. However, a practical definition should be the set of control parameters, which gives the maximum electrical power delivered to the grid respecting the physical limits of the WEC device. From now on, the term *optimal control* (or sub-optimal) is used with this definition in mind. It has been shown that linear control theory is not a suitable approach to identify these optimal control parameters for irregular waves. Instead, an analytical solution to the problem can be attempted from the expression of the average extracted power in Equation (27) and the loss approximation expression in Equation (25).

$$P_{opt,el}(R_l, L_L) = max\left(P_M - |P_{loss}|\right) \tag{27}$$

This expression becomes a non-trivial equation to solve as the generator losses is a fourth-order expression dependent on the control parameters, as well as the generator speed. A simplified approach is therefore pursued by running a number of simulations with different load parameters to identify optimal control for each sea state by trial and error. The goal of these simulations is, however, to make a map of optimal control parameters for different sea states.

4.3.1. Example Identification of Optimal Control Parameters for a Low Wave State

The identification of optimal control parameters is performed by scanning step-wise through all values for B_L and M_L. The resulting output is illustrated in Table 3 with some values listed. Notably, the leftmost column corresponds to the purely damped system.

The losses are listed in Table 4. Notably, it is observed that maximum generator losses occur when the system is complex conjugate-controlled. This is due to the accumulated average losses of the high bidirectional peaks in power. The losses are lowest for the upper left corner of the table, where the control parameters go towards zero. This is natural as it corresponds to a no-load operation of the generator, and the losses are purely rotational losses.

Combining the two tables, the corresponding electric output table can be seen in Table 5. As seen from the map, an optimal set of control parameters is identified for this sea state with an added damping, $B_L = 120\,kNs/m$, and an added mass of $M_L = 40$ tons. Notably, the average electric output power is increased by 11.9% compared with the optimal passive load case.

Table 3. Average extracted mechanical power [kW].

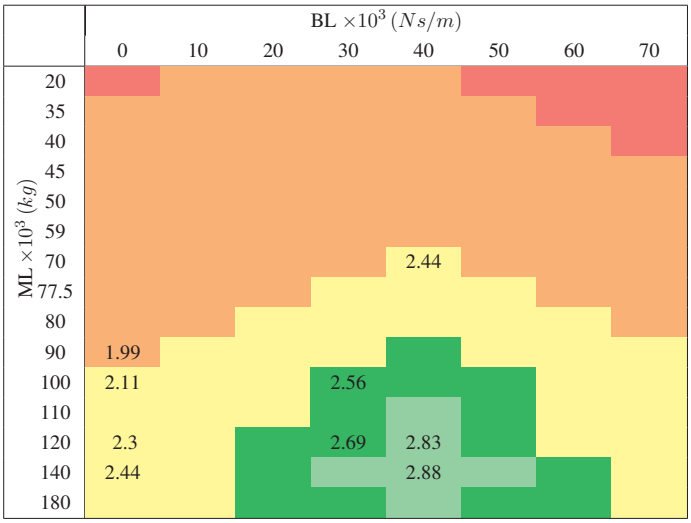

Table 4. Average losses [kW].

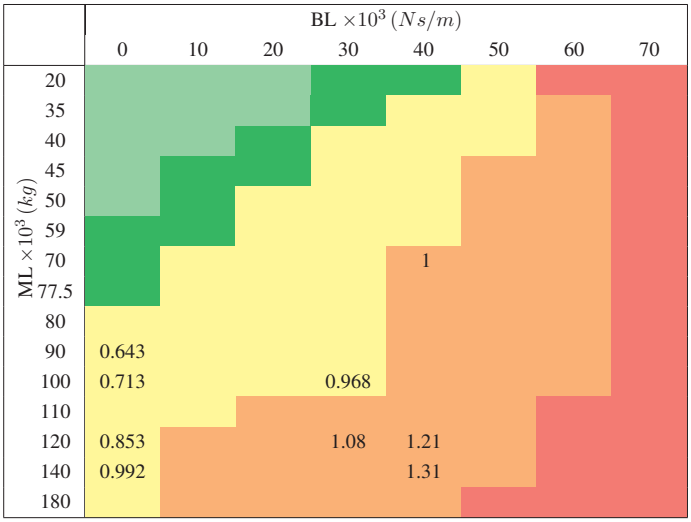

Table 5. Output electric power [kW].

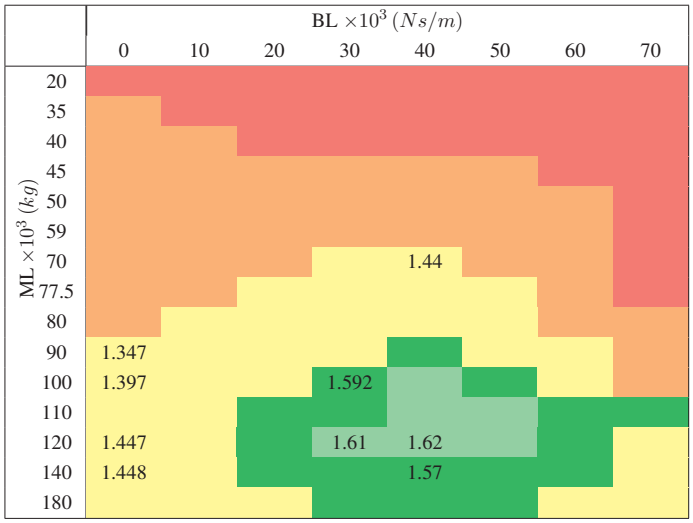

4.3.2. Observations from Mapping of Control Parameters

From a number of simulation results for the different sea states, some general observations can be made from the optimal control parameter mapping.

- Combining the maps of output mechanical power and generator losses, a map of optimal control parameters with respect to electrical output power is made;
- For sea states with low significant wave height, the optimal control parameters have a larger component of added mass and smaller component of added damping;
- For the sea states with low significant height, the average power is increased by a significant factor, *i.e.*, 10% for $H_s = 0.5$;
- When the significant wave height increases, the optimal control parameters shift towards a larger factor of added damping;
- For the sea states with a higher significant wave height, the increase in average power compared with the reference case of passive loading goes towards zero;
- For a sea state with lower peak periods, the optimal control parameters have a larger damping factor;
- For increasing peak periods, the optimal control parameters have larger fraction of added damping. This means that the optimal control moves towards complex conjugate control;
- Average power extraction decreases with increasing peak period of the sea. This is caused by the reduced generator speed and the subsequent generator performance reduction [21,22].

4.4. Energy Calculations-Potential Increase in Annual Energy Production with Optimal Control

By using sea-state statistics, estimations of annual energy production can be made. Previous estimations have been made for the Lifesaver concept [23], and some preliminary investigations have also been performed into a potential increase in annual energy production using reactive control. However, the latter paper does not take into account the generator force limitation or generator losses, and these factors become very significant under reactive control in particular [24]. This means that an investigation into increased energy production using reactive control with generator limitations is a very interesting and novel addition to the former research.

Identification of the optimal control parameters for all sea-states has not been performed. Only selected sea-states were used as a representation of the whole spectra. From the wave scatter diagram in Table 6, one can define the following three sea states:

- $H_s = 0.75\,m$ and $T_p = 4.5\,s$ are the sea states that represents the low energy sea states;
- $H_s = 1.75\,m$ and $T_p = 5.5\,s$ represent the medium energy sea states;
- $H_s = 3.25\,m$ and $T_p = 6.5\,s$ represent the high energy sea states.

Table 6. Wave scatter diagram for Wavehub location. Blue area represents low-energy sea-states, green represents medium energy sea-states and red represents high energy sea-states.

		Wave period Tz [sec]								
		3,5	4,5	5,5	6,5	7,5	8,5	9,5	10,5	11,5
Significant wave height hs [m]	0,25	26	79	44	18	0	0	0	0	0
	0,75	499	832	491	140	18	0	0	0	0
	1,25	184	1051	604	307	70	26	9	0	0
	1,75	0	587	701	333	149	53	26	0	9
	2,25	0	96	534	254	123	44	9	0	0
	2,75	0	0	237	228	105	26	9	9	0
	3,25	0	0	26	175	123	44	9	0	0
	3,75	0	0	0	79	96	35	18	0	0
	4,25	0	0	0	9	44	26	9	9	0
	4,75	0	0	0	0	26	18	9	0	0
	5,25	0	0	0	0	18	26	18	0	0
	5,75	0	0	0	0	0	18	9	0	0
	6,25	0	0	0	0	0	9	0	0	0

Defining the different sea states in Table 6 as one of these three and summing the total annual hours results in Table 7. Using the similar approach, as seen in the previous section, Table 7 lists the average power extraction for each of the three defined sea states for both optimal passive loading and optimal control parameters from an electrical output perspective. The results show that an annual energy production increase of 1% is a fair estimation for Lifesaver if optimal reactive control is implemented.

Table 7. Power and energy calculations for the representative sea states

	Low energy	**Medium energy**	**High energy**	**Total**
Hours per wave state	2182	4370	2468	8760
Av. Pow. Pass.(kW)	6.70	19.04	31.40	-
Av. Pow. Opt. (kW)	7.02	19.24	31.47	-
Diff (%)	4.78	1.4	0.22	-
Ener. Pass.(MWh)	14.62	83.22	77.53	175.37
Ener. Opt.(MWh)	15.32	84.10	77.70	177.12
Difference (%)	4.78	1.40	0.22	1.0

5. Discussion

The main motivation of this article was to develop a full wave-to-wire model of the Lifesaver WEC and to use this model to investigate how to control the device in order to extract maximum power under given physical constraints. Based on this, the key observations are summarized below:

- A full wave-to-wire model of Lifesaver point absorber with all-electric power take off system has been made in Matlab and Simulink;
- The main characteristics of the Lifesaver generator and power take off system have been modeled using classical representation of a Permanent Magnet Synchronous Machine complete with field weakening operation and a simplified model of the inverter and DC-link;
- A control method has been demonstrated that enforces the force, voltages and currents within the different rating constraints of the power take-off system, even for the sea states with high significant wave height;
- Wave-to-wire simulations show that Lifesaver has limited potential for increased power extraction using reactive control, due to the force and efficiency limitations of the generator; Analysis shows that the if the device is optimally controlled, only a 1% increase in annual energy production can be expected compared to the reference case of passive loading.

5.1. Aspects of Practical Implementation in Lifesaver

As Lifesaver is currently deployed in the ocean for an extensive testing period, the results reported in this article can also be experimentally verified. There is naturally some degree of uncertainty regarding how realistic the developed model is of the real-life Lifesaver WEC. This is especially due to the following factors:

- Hydrodynamic model of Lifesaver is not completely accurate;
- The validity and accuracy of the simplified PMSM model used;
- The damping coefficients used by Lifesaver in the sea are not the same found to give optimal power extraction in the model.

Still, it is interesting to investigate the effect of reactive control on the physical device. A control strategy can be suggested for a preliminary test of Lifesaver's response to reactive control based on the observations done in this model. As a rule of thumb, the results in this investigation finds that optimal control of Lifesaver occurs with an added mass of approximately 10% of the added damping. However, undertaking such an investigation might not be desirable if the theoretical maximum annual increase in energy is only 1%. It is therefore important to analyze the initial test in detail in order to evaluate if the limited potential described in this article could be valid also in reality.

5.2. Implications for a Generic WEC

Several of the observations in this article could be very useful for a generic point absorber and can thus be implemented in the planning and research of future wave energy devices. Primarily, this is true regarding how to develop a wave-to-wire model based on hydrodynamic measurement data of the device and on the electric power take-off ratings. Perhaps the most interesting point is that such a wave-to-wire model can be used to investigate control techniques and decide on favorable power electronics and generator ratings at an early stage of the concept development. In order to do this, one would need hydrodynamic parameters, like the excitation force coefficient, radiation resistance and the mass of the device for a range of different frequencies. These can either be obtained by model testing of a prototype or by some software analysis (using WAMITand ACQUA).

6. Conclusions

Wave-to-wire simulations show that implementing reactive control with load parameters close to approximate conjugate control does not give increased electrical output power. This is because the high peak-average ratio of approximate complex conjugate control gives large accumulated average losses, and in the extreme examples these, losses can be larger than the average extracted mechanical power, meaning electric power is, on average, extracted from the grid. An intermediate control strategy based on a smaller component of added mass is found to be the optimal control strategy from an electrical output power point of view, and the optimal control parameters for a set of representative sea states is identified. Annual energy estimations are performed based on a set of representative sea states. Compared to the reference case of passive loading, the optimally controlled Lifesaver shows an annual increase in energy production of 1%. This indicates that Lifesaver has low potential for increased power extraction using reactive control, and it is recognized that this is due to the non-negative minimum force restriction of the power take-off system and the limited efficiency of the generator. These results should be verified by practical implementation on Lifesaver, but must be weighed against the cost of updating the control software, as the expected production gain is marginal.

The limited effect of reactive control on Lifesaver has been demonstrated through a series of wave-to-wire simulations. This analysis of the power take-off capability of the Lifesaver WEC is nonetheless valuable, especially for future development of point absorber wave energy devices. In addition to demonstrating the development of a wave-to-wire model of a WEC, perhaps the most important contribution of this investigation is in highlighting some of the major advantages, properties and drawbacks of the PTO capabilities of all electric direct-driven point absorbers.

Acknowledgments

We would like to thank Fred. Olsen for funding the Wave Energy Project. The work of Elisabetta Tedeschi was supported by a Marie Curie Intra-European Fellowship within the 7th European Community Framework Programme (FP7-PEOPLE-2010-IEF n.272571). The work of Jonas Sjolte was supported by the Norwegian Research Council under the program *NæringsPhd*.

References

1. Thorpe, T. *2010 Survey of Energy Resources.* Technical Report, World Energy Council: London, United Kingdom, 2010.
2. IEA. *Electricity in the World* Technical Report, International Energy Agency, Paris, France, 2008.
3. Wave Hub. Available online: www.wavehub.co.uk (accessed on 12 Jul 2013).
4. Falnes, J. *Ocean Waves and Oscillating Systems, Linear Interaction Including Wave-Energy Extraction*; Cambridge University Press: Cambridge, United Kingdom, 2002.
5. Falnes, J. *Principles for capturie of energy from ocean waves: Phase control and optimum oscillation.* Technical Report, NTNU, 1997. Available online: http://folk.ntnu.no/falnes/w_e/index.html (accessed on 12 Jul 2013).
6. Falnes, J.; Hals, J. Heaving buoys, point absorbers and arrays. *Philos. Trans. R. Soc. A Math. Phys. Eng. Sci.* **2012**, *370*, 246–277.
7. Falnes, J.; Lillebrekken, P.M. Budal's Latching-Controlled-Buoy Type Wave-Power Plant. In Proceedings of the 5th European Wave Energy Conference, Cork, Ireland, 1720 September 2003.
8. Hals, J. Modelling and Phase Control of Wave-Energy Converters. Doctor thesis, Norwegian University of Science and Technology, Trondheim, May 2010.
9. Tedeschi, E.; Molinas, M. Tunable control strategy for wave energy converters with limited power takeoff rating. *IEEE Trans. Ind. Electron.* **2012**, *59*, 3838–3846.
10. Sandvik, C.; Molinas, M.; Sjolte, J. Time Domain Modelling of the Wave-to-Wire Energy Convert Bolt. In Proceedings of the 7th International Conference and Exhibition on Ecological Vehicles and Renewable Energies, EVER12, Monte Carlo, Monaco, 2225 March 2012.
11. Mitchell, W.H. Sea spectra revisited. *Marine Technol.* **1999**, *4*, 211–227.
12. Dean, R.; Dalrymple, R. *Water Wave Mechanics for Engineers and Scientists*; Prentice Hall: New Jersey, USA, Volume 2, 1984.
13. Newman, J. *Marine Hydrodynamics*; Mit Press: Cambridge, USA, 1977.
14. Cummins, W.E. The impulse response functions and ship motions. *Schiffstechnik* **1962**, Report (Department of the Navy, David Taylor Model Basin), http://books.google.no/books?id=GLLANwAACAAJ (accessed on 12 Jul 2013).
15. Taghipour, R.; Perez, T.; Moan, T. Hybrid frequencytime domain models for dynamic response analysis of marine structures. *Ocean Eng.* **2008**, *35*, 685–705.
16. Kung, S. A New Identification and Model Reduction Algorithm via Singular Value Decompositions. In Proceedings of the 12th Aslilomar Conf. on Circuits, Systems and Computers, Pacific Grove, California, 6-8 November 1978; pp. 705–714.

17. Mohan, N. *Advanced Electric Drives Analysis, Control and Modeling Using Simulink*; Mnpere, Minnesota, USA 2001.
18. Umland, J.; Safiuddin, M. Magnitude and Symmetric Optimum Criterion for the Design of Linear Control Systems-what is it and does it Compare with the others? In Proceedings of the IEEE Industry Applications Society Annual Meeting, Salt Lake City, USA2-7 Oct 1988; pp. 1796 –1802.
19. Pan, C.T.; Liaw, J.H. A robust field-weakening control strategy for surface-mounted permanent-magnet motor drives. *Energy Conver. IEEE Trans.* **2005**, *20*, 701–709.
20. Tedeschi, E.; Molinas, M.; Carraro, M.; Mattavelli, P. Analysis of Power Extraction from Irregular Waves by All-Electric Power Take off. In Proceedings of the IEEE Energy Conversion Congress and Exposition (ECCE), Phoenix, Arizona, 12-16 Sep 2010; pp. 2370–2377.
21. Sjolte, J.; Bjerke, I.; Hjetland, E.; Tjensvoll, G. All-Electric Wave Energy Power Take off Generator Optimized by High Overspeed. In Proceedings of the Submitted to the European Wave and Tidal Energy Conference (EWTEC11), Southampton, UK, 59 September 2011.
22. Molinas, M.; Skjervheim, O.; Sørby, B.; Andreasen, P.; Lundberg, S.; Undeland, T. Power smoothing by aggregation of wave energy converters for minimizing electrical energy storage requirements. In Proceedings of the Submitted to the European Wave and Tidal Energy Conference (EWTEC07), Porto, Portugal, 1113 September 2007.
23. Sjolte, J.; Tjensvoll, G.; Molinas, M. All-electric Wave Energy Converter array with Energy Storage and Reactive Power Compensation for Improved Power Quality. In Proceedings of the IEEE Energy Conversion Congress and Exposition (ECCE),Raleigh, NC, USA, 1520 September 2012; pp. 954 –961.
24. Tedeschi, E.; Molinas, M. Impact of Control Strategies on the Rating of Electric Power take off for Wave Energy Conversion. In Proceedings of the IEEE International Symposium on Industrial Electronics, Bari, Italy, 4-7 Jul 2010; pp. 2406–2411.

Appendix K

Journal paper 3

Title: Self-Sustained All-Electric Wave Energy Converter System

Conference/Journal: The International Journal for Computation and Mathematics in Electrical and Electronic Engineering.

Date: Accepted for publication on 9. January 2014, *In Press*

Location/Publisher: EMRALD

Self-Sustained All-Electric Wave Energy Converter System

Jonas Sjolte, Gaute Tjensvoll and Marta Molinas

Fred. Olsen/NTNU, jonas.sjolte@fredolsen.no
Fred. Olsen, gaute.tjensvoll@fredolsen.no
Norwegian University of Science and Technology, marta.molinas@ntnu.no

Abstract:

Purpose - This paper describes the design and function of Fred. Olsens Wave Energy Converter system *Lifesaver* with special focus on the stand-alone electrical system that is implemented for operation without grid-connection.

Design/methodology/approach - The paper focus on the detailed design of the DC-Link system that drives the industrial 400 VAC inverters and generators for the production system. The DC-Link is stabilized by an ultracapacitor bank and has no external source or grid-connection.

Findings - The system has been tested through extensive sea trials since April 2012 and has proved its function. Some results from real sea testing are presented.

Practical implications - This paper proves the viability of the specified design and may serve as a basis for the design if similar systems in the future.

Originality/value - This paper presents a Wave Energy Converter system that has proven successful operation through practical tests, and is therefore regarded as a high value paper as there is limited experience on this subject.

Keywords Wave Energy Converter, All-electric, Prototype, Fabtest, Lifesaver, Fred Olsen

Paper type Research paper

1 Introduction

Fred. Olsen (FO) has endeavored on developing a commercial *Wave Energy Converter* (WEC) that can convert ocean wave energy into electricity suitable for grid injection. Ocean Wave Energy shows a great potential for power extraction with high power density and good availability. However, after more than 100 years of development, trial and error, wave energy has not yet reached a commercial level. The greatest challenges seems in FO's point of view to be mainly two issues: Designing a system with high reliability that can tackle the harsh ocean environment, and handling the large fluctuations in incoming power that demands heavily oversized mechanical and electrical conversion capacity. Both issues can be handled through good engineering, however the challenge is to achieve this within a reasonable cost.

Figure 1: FO's Wave Energy Converter *Lifesaver*, located in Falmouth Bay, England, was launched in April 2012.

The FO team has been working steadily toward the goal of commercial wave power through several years of development, and our latest WEC named *Lifesaver*, was installed in *Falmouth Bay test area* (FABTEST) outside Cornwall, England in April 2012 (Hjetland et al) [1]. Lifesaver has three individual *Power Take-Off* units that produce electricity from an electro-mechanic winch drive, and is equipped with a complete power production system. Lifesaver is pictured in on site Fig. 1 and the actual power output from the three PTOs in normal production is plotted in Fig. 2. The power level is normalized to the rated output power for the device, and the plot demonstrates the poor power quality typical for wave energy converters. However, as shown in our series of articles [2, 3, 4, 5], this issue can be handled effectively in a larger WEC farm, and the power quality does not seem to be a threat to effective grid export.

During the first test phase at FABTEST grid connection is not available, thus Lifesaver is designed as a dual option system that can operate both in stand-alone and grid connected configuration. Since the on-board electrical conversion system is based on 400 VAC industrial drives and machinery, an advanced power system was designed to supply the required on-board power. There are no auxiliary power sources (i.e. diesel generator, wind turbines, PV cells) in the system and all power for on-board systems are drawn from the produced wave energy. This is realized with an ultracapacitor bank that is connected directly on the common DC-Link,

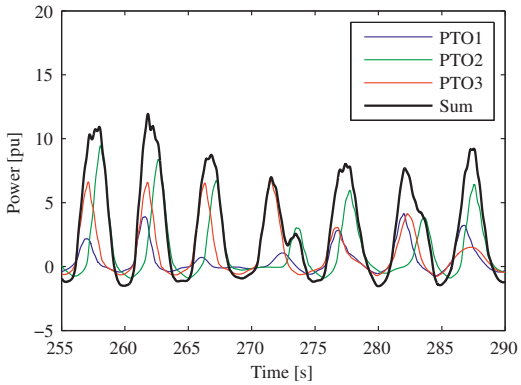

Figure 2: Typical power output from *Lifesaver*, as produced at FABTEST. The output power is normalized to the rated output power for the power plant.

and can be viewed as the corner stone in the system. The system also relies on a battery bank with bi-directional DC/DC converters to handle startup and service modes, and a power dump system is installed to handle excess energy during production. This article focus on the stand-alone power system designed for Lifesaver and describes the requirements, design and development. Some results from the on-going sea trials are also presented.

1.1 Fred. Olsen's Wave Energy Project

FO started with Wave Energy in 2000 and in 2004 the Wave Energy Converter *Buldra*, built as a platform with multiple point absorbers, was launched. Since then FO has tested out various concepts and built several different prototypes, all based on the point absorber concept. The series of experiences have led to the single body point absorber concept, as realized by our latest prototype Lifesaver. Point absorbers are not the most efficient absorber type measured in captured energy, but has shown to be successful on total performance and cost of energy.

Up to date FO has operated four WECs based on the single body point absorber in real sea conditions. The first, named *B33*, was a small proof-of-concept device that was operated outside Akland, Norway during the autumn 2007 and winter 2008. B33 showed good results, leading to the second device, named *B22*, that was equipped with a full-scale control, communication and production system. B22 was operated outside Risør, Norway from the summer 2008 until spring 2009. Based on these experiences FO started the next development phase in collaboration with a few selected European companies and universities through the *SEEWEC* project. This work lead to the full-scale system *Bolt* that was installed outside Risør, Norway in June 2009. Bolt is pictured in Fig. 3 on site and has per December 22, 2010 produced 3 360 kWh of energy (Bjerke et al) [6].

Figure 3: FO's Wave Energy Converter *Bolt*, located outside Risør, Norway has been in operation since June 2009.

Based on the success with Bolt, FO decided to use the knowledge and experience gained so far to proceed to the next generation design. An agreement with several UK companies was made with funding from the UK *Technology Strategy Board* (TSB). The goal of the project was to improve the Bolt® concept towards a commercial level where it can be launched at Wavehub [7], thus the project name *Bolt2Wavehub*. The project resulted in the full-scale system Lifesaver, which consists of a 16 m toroidal floater with five individual all-electric PTO systems. Lifesaver was installed on FABTEST in April 2012 and is planned to be in operation until March 2013, when she has to be brought ashore due to strict UK regulations.

Up to date FO has not has not had a single serious event with any of the WEC systems, which has allowed for continuous long term testing in real sea conditions. This has proved invaluable for building experience with wave energy. Based on our experience the problems and issues that arise in real sea conditions are multifaceted and outreaches far beyond the scope of the tests undertaken.

2 System description

Lifesaver is an all electric WEC system based on direct electric winch drives that are moored to the sea floor. The PTO principle is sketched in Fig. 4 and demonstrates the mechanical simplicity of the system. To keep tension in the winch system upon downwards movement, the generator is operated in motoring mode, effectively winding the rope back in on the drum. This causes the negative power periods that can be seen in Fig. 2.

On the electrical side, all PTOs are connected to a common DC-bus that serves as the backbone for the power system. This allows for natural power exchange between the PTOs and the power components, and ensures a natural balance in the power flow. As can be seen in Fig. 5 this configuration is the same for both the stand-alone and the grid connected solution.

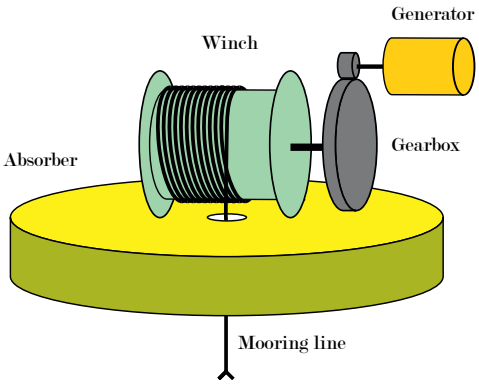

Figure 4: PTO principal sketch for Lifesaver

In the grid connected option the available power surplus on the DC-Link is converted to AC and transformed to grid. The capacitor bank indicated on the schematics could serve as an intermediate energy storage before transfer to grid, however recent studies have shown that this is not required and that capacitor bank only needs to be sized for the control stability of the inverters.

In the stand-alone solution on the other hand, a significant energy storage is required to make up for the negative power periods caused by pull-back. Several options were considered, pointing towards the ultracapacitor bank as the most suitable solution for our system. The ultracapacitor bank is connected directly on the DC-link, and is backed by a battery bank through a bi-directional DC/DC converter. In addition, a power dump system is required to handle excess energy. Fig. 5(b) shows the detailed schematics for the stand-alone system, and the specific system components and solutions are explained in detail in the following sections.

2.1 Power Take-Off system

Property	Value	
Maximum production force	100	kN
Nominal generator speed	400	rpm
Maximum generator speed	1 800	rpm
PTO nominal production power	15	kW
Generator nominal power	80	kW
Inverter nominal power	120	kW

Table 1: PTO specifications

The purpose of the *Power Take-Off* (PTO) system, is to convert mechanical motion imposed by the waves to electrical energy. The main PTO components are the winch system, the gen-

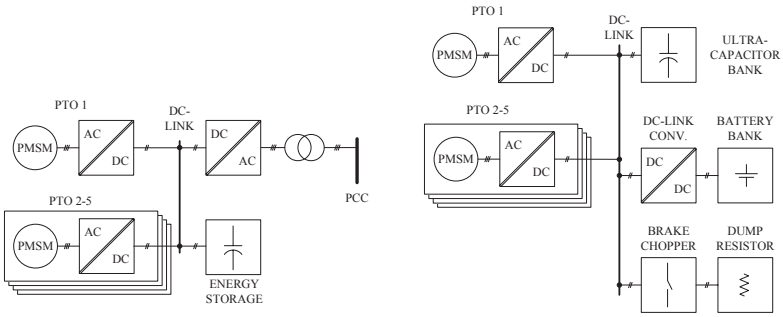

(a) Topology for grid connected system (b) Topology for stand-alone system

Figure 5: Lifesaver topology

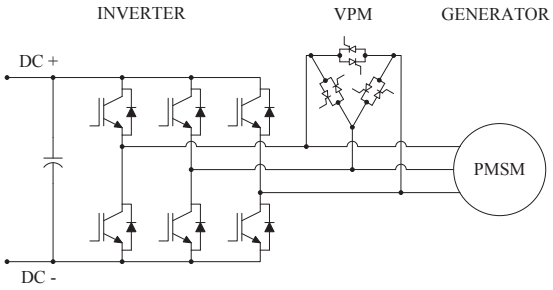

Figure 6: Electrical power take off system with *Voltage Protection Module* (VPM).

erator and the inverter. The mechanical configuration is shown in Fig. 4. A high-performance permanent magnet servo machine manufactured by Siemens is selected as generator for the system. These machines are characterized by low inertia, high torque density and high efficiency, which are important properties for a direct coupled wave energy device with a constantly changing speed. The machine is custom built after FO specifications to meet the requirements for Lifesaver. One of the most important characteristics of the machine is the high ratio between nominal and maximum speed, as listed in Table 1. This allow for early power saturation and results in reduced cost on the inverter and power transfer system. The effect of this on cost and performance is described in detail in previously published articles [2],[8].

A permanent magnet machine that is driven by an external uncontrollable force, such as the case for a wave power plant, can be vulnerable to overspeed. If the machine is forced to exceed nominal speed while the inverter is not in operation, the system may be electrically damaged by overvoltage, even though the machine can handle the speed mechanically. Therefore, each PTO is fitted with a *Voltage Protection Module* (VPM), which will automatically short-circuit the generator in the event of uncontrolled overspeed. This will ensure that no harmful energy is allowed to enter the inverter or the downstream power system. The VPM used is a standard product supplied by Siemens and fires at 830V, which is the maximum allowed voltage for the inverter used. This defines the upper limit of the operational range of the capacitor bank as illustrated in Fig. 15 on page 16.

The PTO is designed as a complete system, and only requires a DC-Link connection and a field bus control connection to operate. This leads to a flexible system where PTOs may be swapped, serviced and rebuilt without any changes to the WEC itself.

2.2 Capacitor bank

The energy storage is the corner stones in the stand-alone system. Initially, two solutions were explored: A flywheel based system and a capacitor based system. The flywheel could be implemented as an extra PTO system that rotates a mass instead of driving a winch. However, the performance and modularity offered by the off-the-shelf ultracapacitor system was thought to outperform the flywheel solution, as this would have to be custom designed.

The requirement for the capacitor bank is to supply the required energy for winding in 10 m of rope on each PTO with 10 kN of pull force. It must also handle wind-in speeds of several meters per second. With a system efficiency of 0.8, and taking into account all five PTOs, the required energy can be calculated to 625 kJ by Equation 1. W_m is the mechanical energy, F is the mechanical force and s is the distance of motion parallel to the direction of force. Equation 2 is the time derivative of equation 1 where energy and distance becomes power and speed, and indicates a required power of several hundred kilowatts. Equation 3 shows the energy storage capacity W_e of a capacitor based on capacitance C and nominal voltage V_n.

$$W_m = F \cdot s \tag{1}$$

$$P_m = F \cdot v \tag{2}$$

Figure 7: Maxwell technologies® 48V ultracapacitor bank module with active cell balancing

$$W_e = \frac{1}{2} C \cdot {V_n}^2 \tag{3}$$

A third requirement for the capacitor bank is that it must handle peak voltages up to 830 V. A configuration of 17 serial connected modules of the Maxwell technologies® 48 V module [9] fulfill all these requirements, and is the selected configuration. The module is shown in Fig. 7. Each module contain 18 serial connected ultracapacitors that are conditioned by an active balancing network. The balancing network allows for bypassing some of the charging current on each cell and is controlled so that all the cells are at equal voltage. If the nominal voltage on the entire module is exceeded, some current is by-passed through the entire module to ensure module balance. The technical data for the capacitor bank is given in Table 2.

A drawback with direct connection to the DC-Link is that capacitor voltage will have to stay within the operational limits of the DC-Link components. Thus the full energy potential for the capacitor cannot be utilized as it cannot be allowed to fluctuate between zero and nominal voltage. However, for the ultracapacitors to maintain the specified lifetime they are not allowed to be charged below $\frac{1}{2}V_{nom}$ during normal operation. Since the Siemens inverters used allow for high fluctuations on the DC-Link, this problem can be mitigated somewhat. On Lifesaver the system is allowed to fluctuate between 500 V and 760 V in normal operation, which corresponds to 65% of the available energy. Hence, 35% more energy could cycled through the energy storage if a separate converter were used for the ultracapacitor bank.

The capacitor module has a specified cycle life of 10^6 cycles. If every charge/discharge cycle during production is counted this number will be reached in less than one year of operation due to the wave frequency. However, most of the cycles are caused by low waves with low energy. Maxwell technologies® offered to simulate the expected life time of the system specifically based on the expected energy profile of Lifesaver. The input for the simulation is given in Fig.

Property	Value	
Nominal voltage	816	V
Capacitance	4.88	F
Nominal energy	1.63	MJ
Useful energy (400V-776V)	1.08	MJ
Max continuous current	100	A
Max peak current	1 100	A
Short circuit current	4 800	A
Nominal power at 600V	60	kW
Peak power at 600V	660	kW
Modules in bank	17	
Cells per module	18	
Cell capacitance	1.5	kF
Cell voltage	2.70	V
Cycle life	10^6	

Table 2: Ultracapacitor bank specifications

8 and shows capacitor bank voltage profiles from three different wave states, low, high and extreme. The three wave states have a defined probability of 0.4, 0.1 and 1/365 respectively. The remaining probability of approximately 0.5 is the down time expected during calm weather. The high down time expected is due to the sheltered conditions on the first test site. Based on these inputs Maxwell technologies® has ensured a lifetime significantly above the base case.

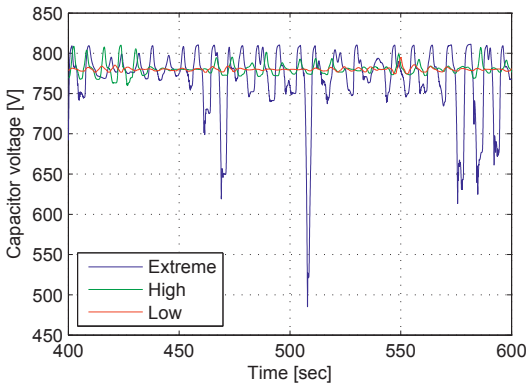

Figure 8: Capacitor voltage in three wave states, Low: hs=1.25 m / Tz=5.5 sec, High: hs=2.75 m / Tz=6.5 sec and Extreme: hs=8.0 m / tz=10.0 sec

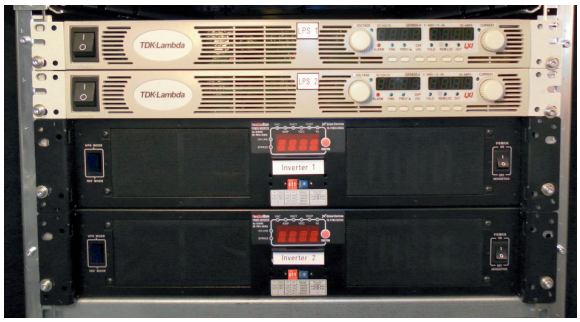

Figure 9: DC-Link charger: Inverters and laboratory power supplies in 19" rack configuration.

2.3 DC-Link charger

The DC-Link charger converts energy from the battery bank to the capacitor bank. This is mainly required for three purposes:

- During startup when the capacitor bank have to be pre-charged and the PTOs have to pull in and tension the production ropes.
- During service when the PTO winches have to be maneuvered.
- In extreme wave states when the required pullback energy might exceed the available energy in the capacitor bank. The pullback process and energy balance is described in section 3.1.

The specifications for the DC-Link charger are as follows:

- Supply up to 5kW of power
- Supply output voltage in the range 0-600VDC
- Handle output voltage in the range 0-830VDC
- Handle input voltage in the range 22.0-29.0VDC
- Allow for current limited operation
- Controllable over LAN
- Serviceable
- Reliable with MTTF $> 20\,000$h

From a power electronics point of view the best solution would be to use a DC/DC boost converter that directly converts the battery voltage to 600VDC. An even more interesting solution would be to merge the DC-charger and the battery charger, that will be described in the next section, into a single bi-directional converter. A possible solution for this is the *Reduced Matrix Converter*, which is based on bi-directional RB-IGBTs. This concept has been explored in detail and has for instance been proposed for off-shore wind turbines [10]. However, no converters based on these topologies that meet all the requirements could be found. Development of such a system from scratch is costly and time consuming, especially when taking into account the required support for maintenance and service. This approach was therefore rejected.

Instead a modular two step solution based on a standard 24VDC to 230VAC inverter and a 230VAC to 600VDC laboratory power supply is selected. This takes the power via 230VAC, which is a drawback, but greatly increases the number of off-the-shelf components available. The power supply selected is controllable by LAN, it can supply any voltage in the range 0-630VDC and can operate in current limited mode with set currents in the range 0-4.2A. This leads to a maximum supply power of 2650W. However, it cannot handle more than 660VDC on the output terminals and have to be shield from the voltages on the DC-Link by a reverse blocking diode. The inverter and power supplies are 19" rack modules and can be seen in Fig. 9.

2.4 Battery charger

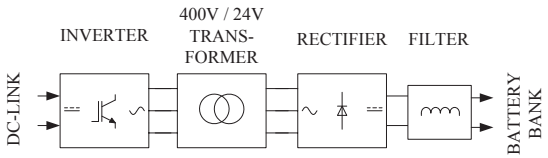

Figure 10: Battery charger topology

On board systems such as communication, data logging and monitoring equipment consume a considerable amount of power from the 24V battery bank. This power must be generated by some means, and the obvious solution is to use the generated wave energy. This is not straightforward however, given the high- and fluctuating voltage level on the DC-Link. A solution based on off-the-shelf wind turbines or PV cells would seem easier to implement. Nonetheless, FO decided that it was worth the extra effort to develop the system, as the purpose of the prototype is to prove the viability of wave energy. Moreover, an external power system with the required power rating would be large and potentially fragile to the extreme weather conditions experienced at sea.The battery charger has the following requirement specification:

- Handle input voltage in the range 0-830VDC
- Operate with input voltage in the range 600-830VDC

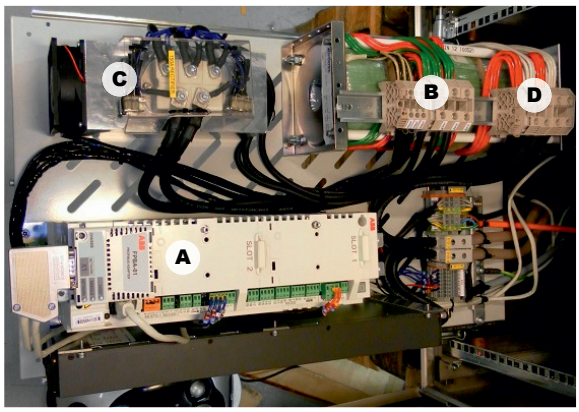

Figure 11: Implemented battery charger configuration: A) Inverter, B) Transformer, C) Rectifier, D) Choke

- Supply output voltage in the range 20-29VDC
- Supply up to 125A of charging current
- Control charging current based on input voltage
- Comply with 3-stage battery charging principle
- Controllable by field bus

FO decided that the easiest approach to meet these requirements was to base the battery charger on the same motor drive inverter that powers the PTO generators. They can naturally handle the input voltage range, they are programmable, they natively support closed-loop control and FO already has the required knowledge to operate and program them.

The concept is described in Fig. 10. The inverter drives a three-phase 400V/24V transformer that supplies to a 3-phase bridge rectifier. Finally, the output power is smoothed through an inductive filter and fed into the battery bank. To simplify the configuration, the transformer and chokes are designed with the same cores and fixed in a common frame. The actual implemented system can be seen in figure 11.

The inverter is operated in scalar mode, which allows for controlling the output frequency directly. The output voltage is regulated proportional to the output frequency to keep the motor impedance constant. This principle is directly transferable to the transformer and gives a system where the output voltage of the transformer can be controlled without risk of excessive magnetizing currents. The nominal output frequency of the inverter is set to 200Hz as this reduces the transformer size, while still allowing for standard 50/60 Hz transformer design methods to be applied.

The charger program is implemented as a closed-loop feedback control with an inner current control loop and an outer voltage control loop as shown in Fig. 12. The current loop uses the inverter output current as feedback while the voltage loop regulates on the actual battery voltage. This is measured by an external sensor. The three-stage battery charger program is implemented by controlling the current and voltage references. The maximum allowed charging current is set to 125 A, the maximum charging voltage is set to 28.8 V and the trickle charging voltage is set to 27.6 V. The trickle charging stage triggers when the charging current falls below 10% of the nominal charging current.

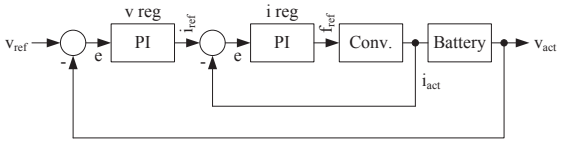

Figure 12: Battery charger control principle

The battery charger must adjust the charger power to the DC-Link voltage to allow for stable steady-state conditions for all production levels. This is implemented by setting maximum allowed charging current as a linear function with zero power at 650 VDC and full power at 720 VDC. This prevents the battery charger from draining the capacitor bank at low production levels.

2.5 Brake chopper

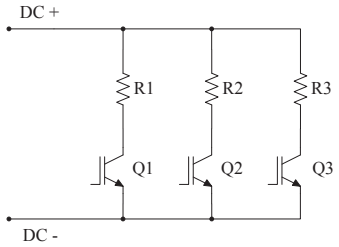

Figure 13: Brake chopper system

The WEC is expected to produce a power surplus, except for in the lowest wave states close to cut-off. This excess energy will cause the DC-Link voltage to rise and must be taken away to balance the system. This is normally done by switching in a resistor that dissipates the excess energy. For good controllability, the system is typically controlled by *Pulse Width Modulation* (PWM) at around 1 kHz. This setup is usually referred to as a *brake chopper* and is very common in motor drive systems.

On Lifesaver a standard brake chopper system supplied by Siemens is used which will start dumping energy at 776 V. The brake chopper has a linear PWM region where the duty cycle is increased proportional to the voltage until saturation occurs around 790 V and the resistor bank is constantly switched on. The resistor bank is a large array of air-cooled heating elements that is placed on top of the power system box on Lifesaver. It is visible on Fig. 1 on page 2 as the gray structure to the upper-right. Air-cooling was selected in favor of water-cooling for simplified access and maintenance.

The brake choppers operate as stand-alone units and only monitor the DC-Link voltage. They do not require any external regulation or control. Three brake choppers are installed in parallel with individual resistors as shown in Fig. 13. Each brake chopper has a nominal power of 50 kW and a peak power of 250 kW. This leads to a total braking power of 150 kW nominal and 750 kW in peak, and a fully redundant system.

Lifesaver is not expected to go beyond the nominal power on average as the production will be curtailed in high to extreme wave states. However, the peak power limit of 750kW may occasionally be breached by single large waves appearing in high sea states. This requires active production control and is described in the next section. Fig. 14 shows the actual response of the DC-Link system during brake chopper operation. The rapid fluctuation around 760 V is caused by the startup and shutdown of the brake chopper and not the actual PWM during operation. The issue is believed to be caused by inaccurate control of the brake chopper at low power levels and could be eliminated by improved control. Since this does not cause problems for the general operation, and since the voltage fluctuations are relatively low, it has been decided to leave it as it is.

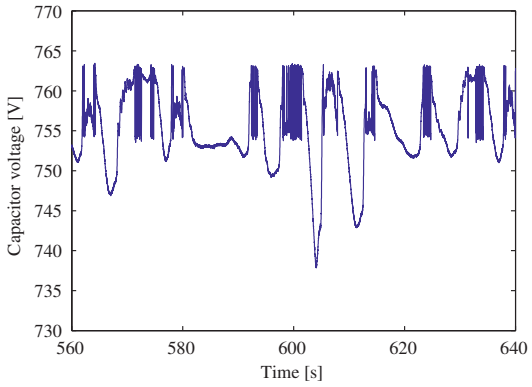

Figure 14: DC-Link voltage during brake chopper operation

3 Control

Three layers of control are implemented to operate the system:

1. Top-level control of the WEC
2. Mid-level control of the DC-Link voltage
3. Low-level control of the PTO inverter

The top-level control mainly holds the state machine functions for the WEC and is only discussed briefly. The mid-level and low-level control is discussed in the subsequent sections.

3.1 DC-Link control

The purpose of the DC-Link control is to keep the capacitor bank and the DC-Link voltage within the allowed range, and to ensure the required energy for pullback. The DC-Link control is not a centralized control function, but is accomplished as the sum of several components and functions operating together. The DC-Link conditioning can be divided into three levels, green, yellow and red, as illustrated in Fig. 15. Within the green region, the capacitor bank voltage is conditioned by the DC-charger in the low voltage end and the brake chopper in the high voltage end. The PTOs are allowed to operate with optimal generation and motoring force. If the production exceeds the brake chopper capacity or the consumption exceeds the DC-charger capacity the yellow region is entered. Operation of all PTOs is then constrained to counteract further aggravation. In the unlikely event that the absolute limits are breached and the DC-Link voltage enters the red region, all PTOs immediately shut down. For the high voltage case, the VPMs also fires to protect the DC-system and to bring the generators to a controlled stop. Since the rope tension will be lost in this case, no further extreme movements on the PTOs are to be expected.

The battery charger will start charging the batteries at 650V and will ramp up to full charging power of 125A / 3.6kW at 720V. These thresholds are set to optimize for production in low waves to maintain an untouched reserve of pullback energy between 650V and 540V. In the higher wave states, the capacitor bank is expected to maintain a close to fully charged condition with voltage above 720V most of the time. It is also important to maintain blanking voltage between the DC-charger shutdown threshold and the battery charger startup threshold to avoid circulation of power between the two converters. The DC-charger can supply a maximum voltage of 630VDC and the startup threshold of 650VDC ensures adequate safety margin.

In the extreme wave states it is possible that the capacitor bank is completely cycled in each wave, which can be seen in Fig. 8 at 510 sec. This will cause cyclic charging between the battery bank and capacitor bank as the missing pullback energy must be borrowed from the battery bank. This is only expected occasionally during worst-case conditions and should not significantly affect battery life.

The DC-Link charger will normally operate whenever the DC-Link voltage is below 540V. However, if the WEC is in a low production state, the 540V level is instead used as a trigger

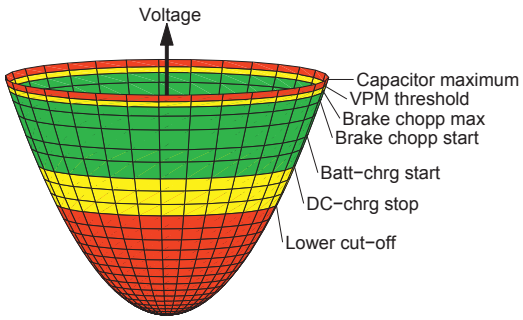

Figure 15: Capacitor bank capacity illustrated as a volume of energy. The energy is proportional to the square of the voltage, which correlates to a paraboloid

for cut-off and causes the entire WEC to shutdown. The WEC will then go into power save mode and measure the waves periodically to determine when production can start up again. This is handled by the top-level WEC control.

3.2 PTO Control

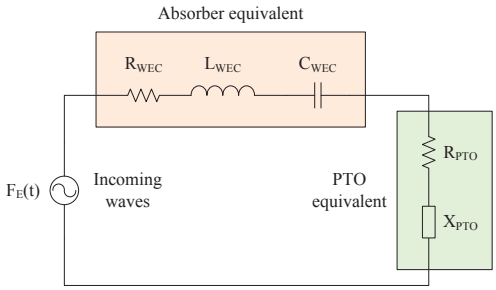

Figure 16: RLC equivalent circuit of the PTO and WEC system

The absorbed power form a point absorber is greatly influenced by the control strategy applied by the PTO. In general the optimal energy extraction is achieved when the point absorber is moving with a 90° phase shift to the waves [11]. Several methods of approaching this production mode are described, the best known being *reactive control* (Tedeschi et al, 2010-2011) [12, 13, 14] and *latching control* (Falnes, 2002) [15]. Fig. 16 shows an electrical

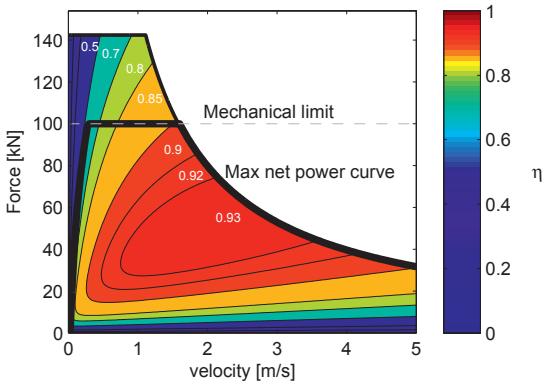

Figure 17: Efficiency plot for the generator used at Lifesaver. The thick line shows the torque that result in maximum exported power from the generator. The thin line shows maximum available torque from the generator. The dashed line shows the mechanical limit for the gearbox.

equivalent circuit for the WEC where the dynamic behavior of the WEC is modeled as an RLC circuit. The PTO is modeled as a power extraction element (resistance) in series with a reactive element (impedance). The goal of reactive control is to tune the reactive element of the PTO so that it compensates for the reactive elements of the WEC as a whole and thus maximize power extraction.

With the current design of Lifesaver the PTO force is too low to have significant impact by reactive control. This is mainly caused by the large area of the absorber that leads to a high spring constant and a high resonance frequency. Passive damping is therefore selected as the primary production model. In the lowest sea states however, advanced control algorithms may improve output (Tedeschi and Molinas, 2012) [16], but is not implemented yet. A recent study by NTNU that specifically investigates the Bolt project indicates that a production boost can be expected from reactive control in wave states with low amplitude and high frequency (Ulvin, 2012) [17]. The large and flat absorber shape is selected as a result of economical optimization and FO's acquired viewpoint that the absorber should be large enough to push the PTO into saturation already in moderate wave states.

$$\tau = -B \cdot \omega \tag{4}$$

Passive damping is defined by Equation 4. The damping coefficient B is optimized to produce the highest possible net power output. τ is the generator torque and ω is the generator speed. Fig. 17 shows the torque and speed characteristics for the generator used on Lifesaver. The thick line shows the optimal torque that maximizes the generated electrical power. Two important saturation mechanisms are present; the first is the mechanical force limit of the gearbox. This is reached already at 0.27 m/s. The second is the power limit of the generator that is reached at 1.55 m/s. The linear region from 0 - 0.27 m/s corresponds to a damping

coefficient of ca 350 kNs/m, which is the chosen value for B on Lifesaver.

4 Discussion

The stand-alone system design presented has demonstrated its function at FABTEST, and had operated for six months without any issues when this article was written. Most of the solutions that are known to be sub-optimal are specific for this test phase and will not be required in a grid connected, commercial power plant. The ultracapacitor bank has performed very well in the system, and could potentially be continued on a grid connected system to smooth the produced power before transfer. However, it is important to note the special solution chosen on Lifesaver where the capacitor bank is directly connected on the DC-Link. This forces all the inverters to follow the capacitor fluctuations as energy is moved in and out of the energy storage. This may reduce the inverter and generator efficiency as they will be operating outside their optimal voltage, and will distort the generator control by shifting the field-weakening point which complicates high speed regulation. It therefore seems like the energy storage should be decoupled from the DC-Link with a separate converter for better utilization of both the capacitor bank and the inverters in a commercial system.

5 Conclusion

A stand-alone power system based on ultracapacitors has been designed and built for the wave energy converter Lifesaver. After six months of continuous sea trials the system has shown no operational issues, and rated energy and power seems to be well sized. The energy transfer system between the capacitor bank and the battery bank operates well within the safe operating area, and a long lifetime for the system can be expected. The system is fully operational and has not yet had any need for service or replacement.

References

[1] E.Hjetland, I.Bjerke, G.Tjensvoll, and J.Sjolte, "A brief introduction to the bolt-2-wave project," in *Submitted to the European Wave and Tidal Energy Conference (EWTEC11)*, september 2011.

[2] J. Sjolte, I. Bjerke, A. Crozier, G. Tjensvoll, and M. Molinas, "All-electric wave energy power take off system with improved power quality at the grid connection point," in *Transmission and Distribution Conference and Exposition (T D), 2012 IEEE PES*, may 2012, pp. 1 –7.

[3] J. Sjolte, G. Tjensvoll, and M. Molinas, "All-electric wave energy converter connected in array with common dc-link for improved power quality," in *Power Electronics for Distributed Generation Systems (PEDG), 2012 3rd IEEE International Symposium on*, june 2012, pp. 431 –436.

[4] ——, "Annual energy and power quality from an All-Electric wave energy converter array," in *European Power Electronics and Motion Control and Applications Conference (EPE-PEMC'12)*, Novi Sad, Serbia, Sep. 2012.

[5] ——, "All-electric wave energy converter array with energy storage and reactive power compensation for improved power quality," in *Energy Conversion Congress and Exposition (ECCE), 2012 IEEE*, sept. 2012, pp. 954 –961.

[6] I.Bjerke, E.Hjetland, G.Tjensvoll, and J.Sjolte, "Experiences from field testing with the bolt wave energy converter," in *Submitted to the European Wave and Tidal Energy Conference (EWTEC11)*, september 2011.

[7] "The wave power climate at the wave hub site," November 2006, journal: Applied Wave Research Review of Wave Power Climate.

[8] J.Sjolte, I.Bjerke, E.Hjetland, and G.Tjensvoll, "All-electric wave energy power take off generator optimized by high overspeed," in *Submitted to the European Wave and Tidal Energy Conference (EWTEC11)*, september 2011.

[9] "Maxwell technologies," http://www.maxwell.com.

[10] A. Garces, E. Tedeschi, G. Verez, and M. Molinas, "Power collection array for improved wave farm output based on reduced matrix converters," in *Control and Modeling for Power Electronics (COMPEL), 2010 IEEE 12th Workshop on*, june 2010, pp. 1 –6.

[11] J. Falnes, *Ocean Waves and Oscillating Systems: Linear Interactions Including Wave-Energy Extraction*. Cambridge University Press, 2002.

[12] E. Tedeschi, M. Carraro, M. Molinas, and P. Mattavelli, "Effect of control strategies and power take-off efficiency on the power capture from sea waves," *IEEE Transactions on Energy Conversion*, vol. 26, no. 4, pp. 1088–1098, 2011. [Online]. Available: http://www.scopus.com/inward/record.url?eid=2-s2.0-82155162473&partnerID=40&md5=8154812c8af086cfd9453f02ec99ee8d

[13] E. Tedeschi, M. Molinas, M. Carraro, and P. Mattavelli, "Analysis of power extraction from irregular waves by all-electric power take off," in *2010 IEEE Energy Conversion Congress and Exposition, ECCE 2010 - Proceedings*, 2010, pp. 2370–2377. [Online]. Available: http://www.scopus.com/inward/record.url?eid=2-s2.0-78650080836&partnerID=40&md5=8c61000510e8fb13d631995a5d32b4c4

[14] E. Tedeschi and M. Molinas, "Impact of control strategies on the rating of electric power take off for wave energy conversion," in *IEEE International Symposium on Industrial Electronics*, 2010, pp. 2406–2411. [Online]. Available: http://www.scopus.com/inward/record.url?eid=2-s2.0-78650351853&partnerID=40&md5=a82865e32786f6209031b80a5811868a

[15] J.Falnes, "Principles for capturie of energy from ocean waves: phase control and optimum oscillation," NTNU, Tech. Rep., 1997, http://folk.ntnu.no/falnes/w_e/index-e.html#RAPPORTAR.

[16] E. Tedeschi and M. Molinas, "Tunable control strategy for wave energy converters with limited power takeoff rating," *IEEE Transactions on Industrial Electronics*, vol. 59, no. 10, pp. 3838–3846, 2012. [Online]. Available: http://www.scopus.com/inward/record.url?eid=2-s2.0-84860439180&partnerID=40&md5=6c9b62f38538f73809c8838d19b8663a

[17] J. Ulvin, M. Molinas, and J. Sjolte, "Analysis of the power extraction capability for the wave energy converter bolt," *Energy Procedia*, vol. 20, pp. 156–169, 2012.

Author Biographies

Jonas Sjolte
is a project engineer with Fred Olsen and works on the Wave Energy Project and leads the design and development of the electrical power systems. He graduated from NTNU in 2007 and received the degree MSc in Electrical Engineering. He has also worked at CERN, Geneva for one year where he did his master thesis within the field of High voltage pulsed power. In 2011 he started on a PhD program in collaboration between NTNU and Fred Olsen on grid integration of Wave Energy with the goal of connecting Fred Olsen's Bolt concept to Wavehub.

Gaute Tjensvoll
is the development manager of the Fred Olsen Wave Energy project, Bolt. He got his masters degree in product development from NTNU (Norwegian University of Technology and Science) and DTU (Denmark Technical University) in 1997. He also has a master's degree in Technology Management from NTNU and MIT (Massachusetts Institute of Technology) from 2002. His professional career started in an entrepreneurial company called Think, developing an electric vehicle. His product development experience was further broadened through managerial positions in a product development consultancy called Kitron Development. For the last six years he has been dedicated to realizing wave energy concepts in Fred Olsen.

Marta Molinas (M'94)
received the Diploma of Electro-mechanical engineer from the National University of Asuncion, Paraguay in 1992; MSc from Ryukyu University, Japan, in 1997, and Doctor of Engineering from Tokyo Institute of Technology, Japan, in 2000. In 1998 she stayed at the University of Padova, Italy as a guest researcher. From 2004 to 2007 she was a Post Doctoral researcher at the Norwegian University of Science and Technology (NTNU) in Trondheim, Norway. In 2008 she became Professor at NTNU. From 2008-2009 she has been a JSPS Research Fellow at the Energy Technology Research Institute of AIST in Tsukuba, Japan. Her research interest is in wind/wave energy conversion systems, and power electronics and electrical machines in distributed energy systems. She is an active reviewer for IEEE Trans. of Industrial Electronics and Power Electronics. She is also AdCom member of IEEE Power Electronics Society and Associate editor of the IEEE Trans. of Power Electronics.

Acknowledgments

I would like to express my very great appreciation to my wife and family for the patience and support during this doctoral process, and for being able to move to Trondheim during the first year of research. I would also like to offer my special thanks to my supervisors Professor Marta Molinas and Gaute Tjensvoll for sharing their experience, and for supporting me when needed. My grateful thanks are also extended to the Fred. Olsen Wave Energy team for supporting my work and for helping out on my regular duties. I am particularly grateful for the assistance given by Bernt Sørby for his help and support on hydrodynamic theory. I would also like to offer my special thanks to the Fred. Olsen Company for supporting my PhD project, both financially and by sharing our data and experience. The support from the Norwegian Research Council has been greatly appreciated, both for their financial support and for supplying the framework necessary for a successful PhD process. Finally, I wish to acknowledge the support offered by the NTNU administration for being forthcoming and helpful in solving the practical details of this specialized PhD program.

Contents

List of Figures

List of Tables

Nomenclature

DOF	Degrees of Freedom
Fab Test	Falmouth Bay Test Area
FO	Fred. Olsen
IEA	International Energy Agency
IGBT	Insulated Gate Bipolar Transistor
IPCC	Intergovernmental Panel on Climate Change
IRR	Internal Rate of Return
KPI	Key Performance Indicator
LCoE	Levelized Cost of Energy
NPV	Net Present Value
NTNU	Norwegian University of Science and Technology
PCC	Point of Common Coupling
PMSM	Permanent Magnet Synchronous Machine
PTO	Power Take-Off
PV	Photo-Voltaic cells, solar panels
PWM	Pulse Width Modulation
R&D	Research and Development
RAO	Response Amplitude Operator
SOA	Safe Operating Area
THD	Total Harmonic Distortion
WEC	Wave Energy Converter